Unclassified
SECURITY CLASSIFICATION OF THIS PAGE (When Data Entered)

REPORT DOCUMENTATION PAGE

READ INSTRUCTIONS BEFORE COMPLETING FORM

1. REPORT NUMBER: IIHR Report No. 299
2. GOVT ACCESSION NO.
3. RECIPIENT'S CATALOG NUMBER

4. TITLE (and Subtitle): Development of a Two-Scale Turbulence Model and Its Application
5. TYPE OF REPORT & PERIOD COVERED: Technical Report, June 1985
6. PERFORMING ORG. REPORT NUMBER

7. AUTHOR(s): Ching-Jen CHEN and Kanwerdip Singh

8. CONTRACT OR GRANT NUMBER(s): N00014-84-0068

9. PERFORMING ORGANIZATION NAME AND ADDRESS: Department of Mechanical Engineering, The University of Iowa, Iowa City, IA 52242

10. PROGRAM ELEMENT, PROJECT, TASK AREA & WORK UNIT NUMBERS

11. CONTROLLING OFFICE NAME AND ADDRESS: DTNSRDC, Bethesda, MD 20084
12. REPORT DATE: June 1985
13. NUMBER OF PAGES: 251

14. MONITORING AGENCY NAME & ADDRESS (if different from Controlling Office): DTNSRDC, Bethesda, MD 20084
15. SECURITY CLASS. (of this report): Unclassified
15a. DECLASSIFICATION/DOWNGRADING SCHEDULE

16. DISTRIBUTION STATEMENT (of this Report): Unlimited Distribution

17. DISTRIBUTION STATEMENT (of the abstract entered in Block 20, if different from Report)

18. SUPPLEMENTARY NOTES: This research was partially supported by the Naval Sea Systems Command GHR Program administered by the David W. Taylor Naval Ship R&D Center, Code 1505, Bethesda, Maryland 20084

19. KEY WORDS (Continue on reverse side if necessary and identify by block number): Jet and Wake Flows, Turbulence Models, Computational Fluid Dynamics

20. ABSTRACT (Continue on reverse side if necessary and identify by block number)

The use of second order closure turbulence model in predicting turbulent flows is known to be more successful than the classical mixing length model. However, it is found that if the turbulence constants are not altered or modified, the second order closure turbulence model is unable to preduct satisfactorily for some flows such as round jet and wake flows. In order to improve the predictability of the second order closure model,

DD FORM 1 JAN 73 1473 EDITION OF 1 NOV 65 IS OBSOLETE

Unclassified
SECURITY CLASSIFICATION OF THIS PAGE (When Data Entered)

the present work proposes to consider two turbulent scales in the modelling of turbulent flows. One of these scales is based on using the turbulent kinetic energy, k, and its dissipation rate, ε, to characterize the large energy containing eddies. The other scale is based on the dissipation rate, ε, and the kinematic viscosity, ν, to characterize the small energy dissipating eddies. The second scale is based on the well known Kolmogorov hypothesis that dissipation of turbulent kinetic energy occurs primarily at small eddies. The turbulence model derived based on the concept of two different scales is called the two-scale turbulence model. The existing turbulence model which is modelled based on the one-scale concept of k and ε is called the one-scale turbulence model.

The two-scale turbulence model is then applied to predict turbulent free shear flows and recirculating flows. The calculations were done in three parts. The first test case was nonbuoyant free shear flows which included round and plane jets in stagnant and moving streams, plane wakes and mixing layer. In the second part, the model was tested for plane and round buoyant jets having different Froude numbers. Finally, some results were obtained for recirculating flows, namely, backward facing step and flow past an obstruction.

It is shown in the present study that the two-scale turbulence model performs significantly better than the one-scale turbulence model in all the cases concerned. The prediction capability of the two-scale turbulence model is shown since one does not need to alter or modify the turbulence constants as in the case of the one-scale turbulence model.

DEVELOPMENT OF A TWO-SCALE TURBULENCE MODEL AND ITS APPLICATIONS

by

Ching Jen Chen and Kanwerdip Singh

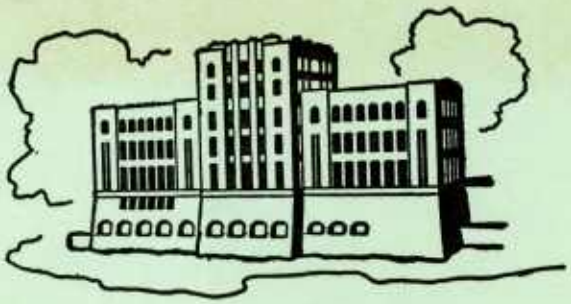

IIHR Report No. 299

Department of Mechanical Engineering and
Iowa Institute of Hydraulic Research
The University of Iowa
Iowa City, Iowa 52242-1585

October 1986

This research was partially supported by the Naval Sea Systems Command GHR Grant N00014-84-K-0068 administered by DTNSRDC

DEVELOPMENT OF A TWO-SCALE TURBULENCE MODEL AND ITS APPLICATIONS

by

Ching Jen Chen and Kanwerdip Singh

IIHR Report No. 299

Department of Mechanical Engineering and
Iowa Institute of Hydraulic Research
The University of Iowa
Iowa City, Iowa 52242-1585

October 1986

This research was partially supported by the Naval Sea Systems Command GHR Grant N00014-84-K-0068 administered by DTNSRDC

ABSTRACT

The use of second order closure turbulence model in predicting turbulent flows is known to be more successful than the classical mixing length model. However, it is found that if the turbulence constants are not altered or modified, the second order closure turbulence model is unable to predict satisfactorily for some flows such as round jet and wake flows. In order to improve the predictability of the second order closure model, the present work proposes to consider two turbulent scales in the modelling of turbulent flows. One of these scales is based on using the turbulent kinetic energy, k, and its dissipation rate, ε, to characterize the large energy containing eddies. The other scale is based on the dissipation rate, ε, and the kinematic viscosity, ν, to characterize the small energy dissipating eddies. The second scale is based on the well known Kolmogorov hypothesis that dissipation of turbulent kinetic energy occurs primarily at small eddies. The turbulence model derived based on the concept of two different scales is called the two-scale turbulence model. The existing turbulence model which is modelled based on the one-scale concept of k and ε is called the one-scale turbulence model.

The two-scale turbulence model is then applied to predict turbulent free shear flows and recirculating flows. The calculations were done in three parts. The first test case was nonbuoyant free shear

flows which included round and plane jets in stagnant and moving streams, plane wakes and mixing layer. In the second part, the model was tested for plane and round buoyant jets having different Froude numbers. Finally, some results were obtained for recirculating flows, namely, backward facing step and flow past an obstruction.

It is shown in the present study that the two-scale turbulence model performs significantly better than the one-scale turbulence model in all the cases concerned. The prediction capability of the two-scale turbulence model is shown since one does not need to alter or modify the turbulence constants as in the case of the one-scale turbulence model.

TABLE OF CONTENTS

LIST OF TABLES

LIST OF FIGURES

NOMENCLATURE

A	constant
C	C with subscripts are turbulent constants C_k, C_1, C_2, C_3, C_ε, $C_{\varepsilon 1}$, $C_{\varepsilon 2}$, C_T, C_{T1}, C_{T2}, C_{T3}, C_μ, $C_{\theta 1}$.
c or c_p	specific heat
D	spectral dissipation function; diameter of round jet
E	energy spectrum function
e	dissipation of turbulent kinetic energy
F	Froude number
G	modification function proposed by Rodi for $C_{\varepsilon 2}$;
g_i	body force in the ith direction
g	gravitational constant
g_i	acceleration due to gravity in the x_i direction
H	channel or step height
k	turbulent kinetic energy $\overline{u_i u_i}/2$; wave number $2\pi L/\lambda$
L	characteristic length
l	length scale $k^{3/2}/\varepsilon$ for energy containing eddies
M	grid spacing for isotropic flow
m_i	momentum equation for fluctuating component in x_i direction

N	number of data in ensemble average
n	frequency
P	pressure; production of k or $\overline{u_i u_j}$, e.g. P_{ij}, P_k.
p	pressure fluctuation
Pr	Prandtl number
q	heat flux
R_{ij}	velocity correlation function between i and j components
Re	Reynolds number based on characteristic length L and mean velocity U
Re_λ	Taylors's Reynolds number based on fluctuation u' and Taylor's microscale λ_g
r	radius vector
S(k)	spectral transfer function
T	mean temperature
t	time; time scale, k/ε, based on (k,ε) and $\sqrt{(\nu/\varepsilon)}$ on (ν,ε)
U	mean velocity in x-direction
u	velocity fluctuation in x-direction; characteristic velocity scale
V	mean velocity in y-direction
v	velocity fluctuation in y-direction
w	velocity fluctuation in z-direction
x	coordinate along direction of flow
y	coordinate along the direction normal to the flow
D/Dt	total or substantial derivative

[ ]	characteristic dimension
∇^2	Laplacian operator

Greek Symbols

α	thermal diffusivity
β	volumetric expansion coefficient
δ_{ij}	Kronicker delta $\delta=1$ if $i=j$ and $\delta=0$ if $i\neq j$
ν	kinematic viscosity
η	Kolmogorov length scale i.e.
λ_g	Taylor's microscale
ε	dissipation rate of turbulent kietic energy, k
μ	molecular viscosity
ρ	density
θ	temperature fluctuation
σ	turbulent constant for turbulent diffusion in turbulent transport equations
ϕ^*	instantaneous quantity;
ϕ	viscosity friction term; time or ensemble average of ϕ^*
τ	laminar stress τ_{ij}; turbulent stress τ_{ij}^t
ψ	mean stream function
π	constant 3.14159

Subscripts

a	ambient
b	buoyant quantity
L	centerline or axial location

d	energy dissipating eddy scale
E	free stream condition
e	energy containing eddies
i	x-dirction
j	y-direction
k	turbulent kinetic energy
l,m,n	dummy indices
N	nozzle condition
c	centerline condition
s	static state
T	temperature e.g. P_T
t	turbulent quantity e.g. τ_{ij}^t; total quantity e.g. P^t
μ	constant for eddy viscosity e.g. C_μ
λ	based on Taylor microscale
θ	temerature fluctuation e.g. ε_θ
0.5	half-width where $U=0.5U_o$ or $T=0.5T_o$

Superscripts

'	fluctuating quantities e.g. k',ϕ';
	dimensionless quantity e.g. x',k';
t	turbulent quantity e.g. q^t, τ_{ij}^t;
[ ]	average e.g. $\overline{u_i u_i}$;
*	instantaneous quantity e.g. U^*, τ^*;
→	vector e.g. r (space vector); k (wave vector)
j	j=0 for two-dimension case; j=1 for axisymmetric case

CHAPTER I

INTRODUCTION

1.1 Motivation of Research

Many fluid motions that occur in nature are turbulent, e.g. flow over aeroplanes, ships and cars, flow in jet engines and turbines, flow through pipes and ducts, weather patterns and ocean waves. Turbulent flow is a complex phenomena that plays an important role in many engineering designs. Therefore, it is important for engineers to study and understand this complex flow and be able to predict it. Equations for describing the fluid motions, known as the Navier-Stokes equations, have been postulated and derived for over a century. However, it is difficult to solve these equations for both laminar and turbulent flows mainly due to the nonlinearity of the equations. For turbulent flows, the problem is even more formidable because the turbulent fluid motion is irregular, random, time dependent and three dimensional. However, in most engineering applications, the detailed analysis of instantaneous turbulent motion is not necessary and the gross parameters like mean velocity, average pressure, mean temperature, wall shear stress and wall heat flux are often sufficient for engineering design.

In 1895, O. Reynolds [1] proposed an averaging technique by assuming that the variable ϕ^* at any instant consists of the mean quantity ϕ and a fluctuating part ϕ'. Hence,

$$\phi^{*} = \phi + \phi'$$

The time averaging process when applied to the Navier-Stokes equations, creates six additional unknowns. These unknowns, although called Reynolds stress, are created from the convective or non-linear terms of the Navier-Stokes equations. In order to solve the turbulent flow problem from the time averaged Navier-Stokes equations more equations or empirical relations are needed for Reynolds stress. Methods for deriving equations which specify a relation between the Reynolds stress and the mean flow quantities are called turbulence models. In other words, a turbulence model is needed to recover the information of turbulent motion that is lost in the averaging process. There are many turbulence models proposed to date. However, these models can predict accurately time averaged turbulent flows only for a certain class of problem. A more general model is needed if one expects a turbulence model to have a better prediction capability and a practical value for engineering applications.

The purpose of this research work is to introduce a new physical concept into the modelling of turbulent flows and to improve predictability of the model. The new model is developed for the second order turbulence correlation based on the concept of two turbulent scales, one for large or energy containing eddies and the other for small or energy dissipating eddies. The two-scale turbulence model is first tested and verified for a class of turbulent flows called 'Free

Turbulent Shear Flows'. In free turbulent shear flows, shear stress, heat flux and diffusion are significant in the directions perpendicular to the direction of flow and there is no solid wall in the flow domain. Some examples, shown in figure 1.1, are mixing layer, coaxial and plane jets, plumes, buoyant jets and wakes. The two-scale turbulence model is then used to predict some turbulent separation phenomena such as flow separation behind a step as shown in figure 1.2.

There are several reasons for selecting free turbulent shear flows to test the turbulence model. First, free shear flows, as shown in figure 1.1, have a weak pressure gradient so that the flow characteristic is largely controlled by turbulent shear motion which affects diffusion, production and dissipation of turbulent motion and not by pressure force. Therefore, the prediction of turbulent free shear flow is more sensitive to the turbulence model than flows with large pressure gradient. Secondly, abundant experimental data are available and comparison between predicted and experimental results can be made in detail. Thirdly, the complication of near wall turbulence is not present in free shear flows so that the accuracy of the two-scale turbulence model can be carefully examined without the interference of wall turbulence. Fourthly, turbulent shear flows have a number of practical applications and play an important role in various engineering design. Jet engines, chimney plumes, jet streams in atmosphere, wakes behind aeroplanes and ships and cooling water disposal in rivers are some of the examples. Though some of these flows have walls in their

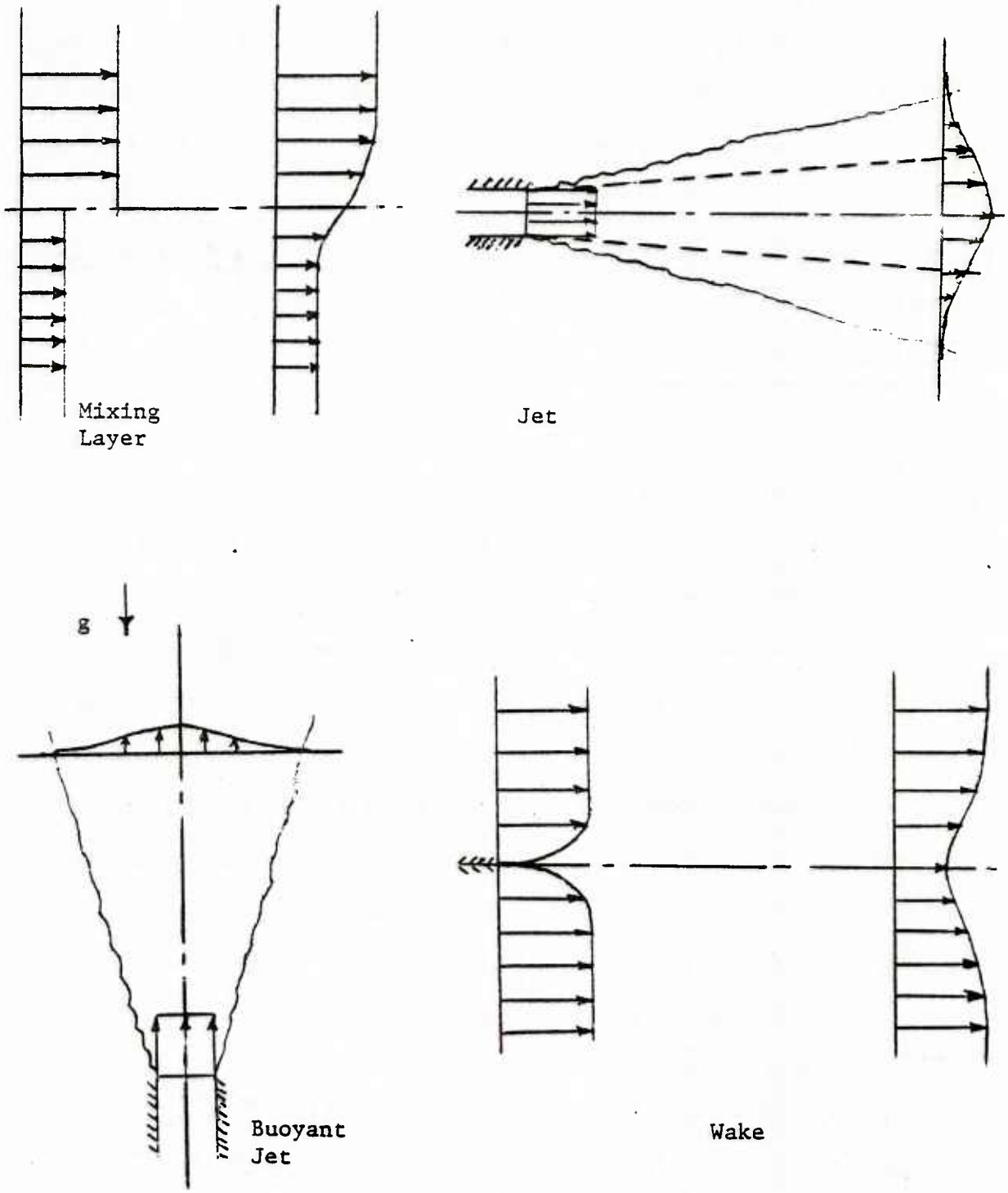

Figure 1.1. Examples of Free Shear Flows

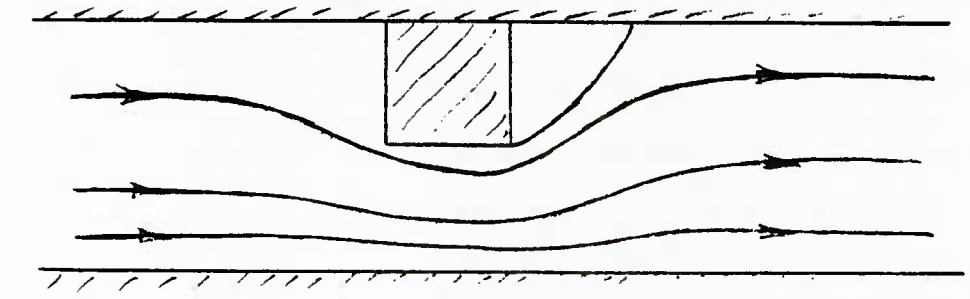

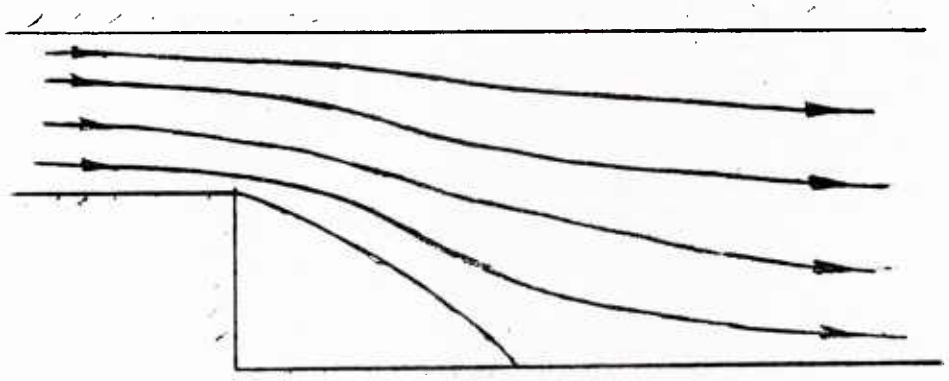

Figure 1.2. Examples of Separated Flow

vicinity, the study of free shear flows is, nevertheless, a first step in understanding problems and phenomena involved.

1.2 Historical Development of Turbulence Models

In this section, a brief historical review of turbulence modelling is made leading to a discussion of the problems in some of the models. In order to resolve the difficulties in the existing models, a new model is presented.

As mentioned earlier, the need of turbulence modelling arose when Reynolds [1] proposed the averaging process to obtain governing equations for turbulent flows. To faciltate the discussion, the Navier-Stokes equations and the energy equation for incompressible flow are written here as

$$\frac{\partial U_i^*}{\partial x_i} = 0 \tag{1.1}$$

$$\frac{DU_i^*}{Dt} = -\frac{\partial P^*}{\rho \partial x_i} + \nu \frac{\partial^2 U_i^*}{\partial x_j \partial x_j} \tag{1.2}$$

$$\rho c \frac{DT^*}{Dt} = \tau_{ij}^* \frac{\partial U_i^*}{\partial x_j} + K \frac{\partial^2 T^*}{\partial x_j \partial x_j} \tag{1.3}$$

The instantaneous quantities for velocity, pressure, stress and temperature U_i^*, P^*, τ_{ij}^*, T^* are denoted by

$$U_i^* = U_i + u_i; \quad P^* = P + p; \quad \tau_{ij}^* = \tau_{ij} + \tau_{ij}' \text{ and } T^* = T + \theta$$

where the quantities on the right are the mean, U_i, P, τ_{ij}, T , and fluctuation, u_i, p, τ_{ij}', θ, of velocity, pressure, stress and temperature. These are substituted in the Navier-Stokes equations and averaged by a short time average or ensemble average to give

$$\frac{\partial U_i^*}{\partial x_i} = 0 \tag{1.4}$$

$$\frac{DU_i}{Dt} = -\frac{\partial P}{\rho \partial x_i} + \nu \frac{\partial^2 U_i}{\partial x_j \partial x_j} - \frac{\partial \overline{u_i u_j}}{\partial x_j} \tag{1.5}$$

$$\rho c \frac{DT}{Dt} = \tau_{ij} \frac{\partial U_i}{\partial x_j} + K \frac{\partial^2 T}{\partial x_j \partial x_j} - \frac{\partial \overline{u_i \theta}}{\partial x_i} + \overline{\frac{\tau_{ij}' \partial u_i}{\rho c \partial x_j}} \tag{1.6}$$

These set of equations introduce additional unknowns $\overline{u_i u_j}$, $\overline{\tau_{ij}'(\partial u_i / \partial x_j)}$ and $u_i \theta$. Models proposed so far to evaluate these unknowns have them coupled to the mean quantities through either algebraic or differential equations. Some are based on empirical relation and others on postulations.

In 1877, Boussinesq [2] proposed the concept of eddy viscosity which assumes that, in analogy to the viscous stresses in laminar flows, turbulent stresses are proportional to the mean velocity gradients. For general flow situations, it is expressed as

$$-\overline{u_i u_j} = \nu_t \left[\frac{\partial U_i}{\partial x_j} + \frac{\partial U_j}{\partial x_i}\right] - \frac{2}{3} k \delta_{ij} \tag{1.7}$$

ν_t is the turbulent or eddy viscosity which, unlike molecular viscosity, is not a fluid property but depends on the state of turbulence. k represents the kinetic energy of the fluctuating motion or $\overline{u_i u_i}/2$. The above expression, however, does not close the problem of turbulent flows as ν_t and k are still unknowns. In 1925, Prandtl [3] proposed a turbulence model called the 'mixing length' model. This model provides a relation between the eddy viscosity, a length scale L characterizing the size of turbulent eddies and a suitable velocity scale, V. Thus

$$\nu_t \propto V*L$$

Both the turbulent velocity scale, V, and the mixing length scale, L, could be reasonably approximated for many flows. However, for such flows, empirical constants were needed to prescribe a length scale. In most of these flows, the constants were obtained by fitting the calculated results to experimental data of a particular flow under study. These mixing length model constants were found [4] to vary often from one flow to another. Consequently, the mixing length turbulence model is successful only in predicting turbulent flows in similar geometry and flow conditions but lacks the universality and predictability when the turbulent flow and geometry conditions are different. Other models [5,6], similar to the mixing length model, were shown to have success in a given flow but lacked generality when flow conditions and configuration changed.

To overcome the lack of predictability and generality, several more complex models [7,8] were developed during the 1940's and 1950's which employed differential transport equations for the turbulent quantities. However, these equations could not be solved directly as there were mathematical difficulties involved and numerical techniques and fast computers were not available. Alternatively, the governing partial differential equations for turbulent flows were often integrated and reduced to ordinary differential equations. These integral methods assumed some shape of mean profile and used some empirical relations for global behavior of turbulence. They lacked flexibility since the assumed profile must be approximately the same in the flow field and could not be applied for different flows.

Advances in computational facilities and numerical methods during the late 1960's and 1970's led to the use of more advanced models which solve complete partial differential equations for both mean flow and turbulent quantities. One of these models which solves the differential equation for k, the kinetic energy, is called the one-equation model as opposed to the zero-equation model where no differential equations are solved for turbulent quantities. With the kinetic energy known, the eddy viscosity can be written as

$$\nu_t = C_\mu k^{\frac{1}{2}} L \tag{1.8}$$

where $k^{\frac{1}{2}}$ represents a velocity scale, L the length scale and C_μ an empirical constant. The equation for k is

$$\frac{Dk}{Dt} = \frac{\partial}{\partial x_j}\left[\frac{\nu_t}{\sigma_k}\frac{\partial k}{\partial x_j}\right] - \overline{u_i u_j}\frac{\partial U_i}{\partial x_j} - C_D\frac{k^{1.5}}{L} \tag{1.9}$$

which is derived from the governing equation of fluctuating turbulent motion. Details of the derivation are given later. Here, C_D and σ_k are empirical constants. This one-equation model is not complete unless the length scale L is specified. In most cases, L is a variable and is obtained from simple empirical relations similar to those for the mixing layer.

Since one-equation models [9,10] account for the convective and diffusive transport of the turbulent kinetic energy, they are superior to the mixing length models in flows where the transport mechanism is important. Some examples are non-equilibrium boundary layers with rapidly changing free-stream conditions, boundary layers with free-stream turbulence and recirculating flows. However, in many flows it is difficult to specify the length scale empirically. The logical extension of the turbulence modelling is that the length scale be obtained from a differential transport equation.

Models which solve differential equations for both turbulent velocity scale or turbulent kinetic energy and length scale are known as two-equation models. Several different models [4,11] have been proposed which, in addition to the equation for k, solve an equation of the form $k^m L^n$ instead of L. The most popular one is the one suggested by Jones and Launder [11] which has m=1.5 and n=-1. The term $k^{1.5}L^{-1}$ which

appears in the last term of equation (1.9), has a physical significance as it has the same dimension as ε, the dissipation of turbulent energy. The dissipation function of turbulent kinetic energy, ε or $\overline{\nu(\partial u_i/\partial x_j)(\partial u_i/\partial x_j)}$ can be derived and modelled as

$$\frac{D\varepsilon}{Dt} = \frac{\partial}{\partial x_j}\left[C_\varepsilon \frac{k^2}{\varepsilon}\frac{\partial \varepsilon}{\partial x_j}\right] - C_{\varepsilon 1}\frac{\varepsilon}{k}\overline{u_i u_j}\frac{\partial U_i}{\partial x_j} - C_{\varepsilon 2}\frac{\varepsilon^2}{k} \qquad (1.10)$$

Details of the derivation of equation (1.10) are given later. Here, C_ε, $C_{\varepsilon 1}$ and $C_{\varepsilon 2}$ are empirical constants. The k-ε model with eddy viscosity from equation (1.7) now requires six emipirical constants C_μ, σ_k, C_D, C_ε, $C_{\varepsilon 1}$ and $C_{\varepsilon 2}$.

This k-ε model has been used in the calculation of boundary layer type of flows as well as recirculating flows. The model now can predict large number of different flow configurations and conditions and is certainly more general than the mixing length turbulence model. Though this model has a wider range of application in the past fifteen years, it still lacks universality as the coefficients need to be adjusted from one flow to another. As an example, the constant $C_{\varepsilon 2}$ in the ε-equation has a value between 1.90 and 1.92. Using this value of $C_{\varepsilon 2}$, a reasonably good prediction of plane jet flow can be made. However, if the value of this constant is slightly outside this range, the solution becomes sensitive to the constant and does not converge. Furthermore, the value of $C_{\varepsilon 2}$ between 1.90 and 1.92 which gives good prediction of plane jet flow cannot be used for a round jet since it produces a 30% error in the

spread of turbulent round jet. For a round jet, the value of $C_{\varepsilon 2}$ is found not to be a constant and is changed [4] to 1.92*(1-0.035G) where

$$G = [\frac{y_{\frac{1}{2}}}{U_L}(\frac{\partial U_c}{\partial x} - |\frac{\partial U_c}{\partial x}|)]^{0.2} \qquad (1.11)$$

Another problem is that, if these modified k-ε model equations (1.7), (1.8), (1.9), (1.10) and (1.11) were used for the calculation of plane wake flow, there is a 30% under-prediction in the growth or spread of the wake. This difficulty is further taken care of by making the constant C_μ in equation (1.7) a function of P/ε [4] where P is the production of turbulent kinetic energy $-\overline{u_i u_j}(\partial U_i/\partial x_j)$ and ε is the dissipation of this energy, $\overline{\nu(\partial u_i/\partial x_j)(\partial u_i/\partial x_j)}$.

It should be remarked here that these difficulties are mainly dealing with the generality or universality of the model. In general, the k-ε model has achieved a level of predictability which mixing length or one-equation turbulence models could not. In order to advance the predictability of turbulent flow motion further improvement in turbulence modelling must be made. This motivates the present investigation.

1.3 Scope of the Present Work

In this investigation, a fundamental change in turbulence modelling is made, that is, to introduce the two scale concept, one based on (k,ε) scale and the other (ε,ν) scale. In the present investigation, k and ε

are used to scale the turbulent phenomenon dominated by large scale motion such as diffusion term while the physical process associated with the dissipation of turbulent kinetic energy is modelled using ε and ν as the basic parameters, which is known as Kolmogorov scale. The Kolmogorov scale which is known since 1925 is more closely related to small eddy motion and has not been incorporated in the turbulence modelling so far. However, in the present investigation, this scale is used. The new turbulence model based on both (k,ε) and (ε,ν) scale is called the two-scale turbulence model.

In Chapter II, a description of the physics of turbulence and the theory behind the use of the two-scale model is given. Then, the detailed derivation of the two-scale turbulence model is shown. Chapter III gives the governing equations for buoyant flows. Chapter IV contains a review and collection of experimental data for free shear flows. In Chapters V and VI the prediction of several free shear flows is shown. Chapter VII shows the calculations for separated flows. Finally, chapter VIII contains several important observations about the model and possible areas of further work regarding multiple scale modelling.

CHAPTER II

TWO-SCALE SECOND ORDER TURBULENCE MODEL FOR INCOMPRESSIBLE FLOWS

This chapter gives a detailed derivation of the two-scale k-ε model for incompressible turbulent flows. The complete set of governing equations are presented which are then modelled based on a set of turbulent postulations.

2.1 Governing equations

The governing equations for incompressible turbulent flow are the averaged Navier-Stokes equations, namely, the continuity equation, the momentum equation and the energy equation. They are also known as the Reynolds equations since it was Reynolds [1] who first used the averaging technique. For a short time or ensemble average, the average value of an instantaneous quantity ϕ^* at a time t can be defined as

$$\phi = \frac{1}{N} \sum_{n=1}^{N} \phi^*(t,n)$$

where n denotes the n^{th} measurement of a total of N experiments. In cartesian tensor notations, the continuity equation is

$$\frac{\partial U_i}{\partial x_i} = 0 \tag{2.1}$$

The momentum equation is

$$\rho\frac{DU_i}{Dt} = -\rho G_i - \frac{\partial P}{\partial x_i} + \frac{\partial \tau_{ij}}{\partial x_j} + \frac{\partial \tau_{ij}^t}{\partial x_j} \tag{2.2}$$

where τ_{ij} and τ_{ij}^t are the laminar and turbulent stresses, G_i is the body force and P is the pressure. The stresses τ_{ij} and τ_{ij}^t are given by the relations

$$\tau = \mu\left[\frac{\partial U_i}{\partial x_j} + \frac{\partial U_j}{\partial x_i}\right] \quad \text{and} \quad \tau_{ij}^t = -\overline{\rho u_i u_j}$$

The term $-\rho u_i u_j$, known as Reynolds stress, is a result of averaging the convective acceleration. It is generally regarded as a turbulent stress in analogy with viscous stress, and is unknown. The energy equation, which too has additional unknown quantities, is given by

$$\rho c\frac{DT}{Dt} = \tau_{ij}\frac{\partial U_i}{\partial x_j} - \frac{\partial q_i}{\partial x_i} - \frac{\partial q_i^t}{\partial x_i} + \phi \tag{2.3}$$

where the laminar heat flux q_i and the turbulent heat flux q_i^t are given by the relations

$$q_i = -K\frac{\partial T}{\partial x_i} \quad \text{and} \quad q_i^t = -\rho c\overline{u_i\theta}$$

ϕ is the viscous dissipation due to the velocity fluctuation and is expressed as

$$\phi = \overline{\mu\left(\frac{\partial u_i}{\partial x_j} + \frac{\partial u_j}{\partial x_i}\right)\frac{\partial u_i}{\partial x_j}}$$

In the above five equations there are fifteen unknowns, namely, U_i, P, T, $u_i u_j$, $\overline{u_i \theta}$ and ϕ. Hence, it is necessary to obtain equations for $\overline{u_i u_j}$, $\overline{u_i \theta}$ and ϕ to complete the turbulence closure problem.

Equations for fluctuating velocity, u_i, and fluctuating temperature, θ, are obtained by subtracting the above averaged equations from the original Navier-Stokes equations. This gives the momentum equation denoted by (m_i) for the fluctuating velocity component, u_i,

$$\frac{Du_i}{Dt} + u_\ell \frac{\partial u_i}{\partial x_\ell} + u_\ell \frac{\partial u_i}{\partial x_\ell} - \frac{\partial \overline{u_i u_\ell}}{\partial x_\ell} = -\frac{1}{\rho}\frac{\partial p}{\partial x_i} + \nu \frac{\partial^2 u_i}{\partial x_\ell^2} \qquad (m_i)(2.4)$$

and the energy equation denoted by (θ) for fluctuating temperature, θ,

$$\frac{D\theta}{Dt} + u_\ell \frac{\partial T}{\partial x_\ell} + u_\ell \frac{\partial \theta}{\partial x_\ell} - \frac{\partial \overline{u_\ell \theta}}{\partial x_\ell} = \alpha \frac{\partial^2 \theta}{\partial x_\ell \partial x_\ell} + \frac{(\phi' - \phi)}{\rho c} \qquad (\theta)(2.5)$$

where

$$\phi' = \tau_{ij}\frac{\partial u_i}{\partial x_j} + \mu\left[\frac{\partial u_i}{\partial x_j} + \frac{\partial u_i}{\partial x_i}\right]\frac{\partial U_i}{\partial x_j} + \mu\left[\frac{\partial u_i}{\partial x_j} + \frac{\partial u_j}{\partial x_i}\right]\frac{\partial u_i}{\partial x_j}$$

From equation (2.4), the equation for $\overline{u_i u_j}$ is obtained using the relation $\overline{[(m_i)u_j + (m_j)u_i]}$. This results in

$$\frac{D\overline{u_i u_j}}{Dt} = \frac{\partial}{\partial x_l}[-\overline{u_i u_j u_l} - \overline{\frac{p}{\rho}(\delta_{ij}u_i + \delta_{il}u_j)} + \nu\frac{\partial \overline{u_i u_j}}{\partial x_l}]$$

$$-[\overline{u_i u_l}\frac{\partial U_j}{\partial x_l} + \overline{u_j u_l}\frac{\partial U_i}{\partial x_l}] - 2\nu\overline{\frac{\partial u_i}{\partial x_l}\frac{\partial u_i}{\partial x_l}} + \overline{\frac{p}{\rho}(\frac{\partial u_i}{\partial x_j} + \frac{\partial u_i}{\partial x_i})} \qquad (2.6)$$

In the above equation, the first term on the right hand side represents both the molecular and turbulent diffusion of the stress $\overline{u_i u_j}$. The next term is the product of the Reynolds stress and the strain rate which represents the interaction between fluctuating component and mean flow. It is often called the production. The third term is the dissipation. The last term in this equation represents the correlation between pressure and fluctuating velocity gradients. It is also called the pressure-strain term or the redistribution term. The above equation can be contracted to get the equation for turbulent kinetic energy k or $\overline{u_i u_i}/2$ by summing i=j and dividing it by 2. This gives with $\varepsilon = \nu\overline{[(\partial u_i/\partial x_\ell)(\partial u_i/\partial x_\ell)]}$

$$\frac{Dk}{Dt} = \frac{\partial}{\partial x_\ell}[-\overline{u_\ell(\frac{u_i u_i}{2} + \frac{p}{\rho})} + \nu\frac{\partial k}{\partial x_\ell}] - \overline{u_i u_\ell}\frac{\partial U_i}{\partial x_\ell} - \varepsilon \qquad (2.7)$$

where the term on the left side represents the time rate change of turbulent kinetic energy following the mean convection U_i. The first term on the right side is the diffusion of k. The second and third terms are the production and dissipation of the turbulent kinetic energy. The dissipation term, ε, represents the rate of dissipation of turbulent kinetic energy and is an unknown in the above equation. It should be

remarked that the dissipation term ε appears naturally in the k-equation. The variation of ε in the flow field has an important bearing of the distribution of the turbulent kinetic energy. Thus ε is an important turbulent transport property. The differential equation for ε is derived from the (m_i) equation by using the relation $\overline{2\nu[\partial(m_i)/\partial x_1][\partial u_i/\partial x_1]}$. This gives

$$\frac{D\varepsilon}{Dt} = \frac{\partial}{\partial x_\ell}[-\nu u_\ell \overline{\frac{\partial u_i \partial u_i}{\partial x_j \partial x_j}} - \overline{\frac{2\nu \partial u_\ell \partial p}{\rho \partial x_j \partial x_j}} + \nu\frac{\partial \varepsilon}{\partial x_\ell}] - 2\nu\frac{\partial U_i}{\partial x_j}[\overline{\frac{\partial u_\ell \partial u_\ell}{\partial x_i \partial x_j}} + \overline{\frac{\partial u_i \partial u_j}{\partial x_\ell \partial x_\ell}}]$$

$$-2\nu u_\ell \overline{\frac{\partial u_i \partial^2 U_i}{\partial x_\ell \partial x_\ell \partial x_j}} - 2\nu\overline{\frac{\partial u_i \partial u_i \partial u_j}{\partial x_j \partial x_\ell \partial x_\ell}} - 2[\nu\overline{\frac{\partial^2 u_i}{\partial x_\ell \partial x_\ell}}^2] \qquad (2.8)$$

It should be noted that although the above equation is exact but every term on the right side other than the viscous diffusion $\nu(\partial\varepsilon/\partial x_1)$, is an additional unknown quantity. The first term on the right side is the diffusion of ε while the second and third terms represent the production of ε. The last two terms are often called the destruction of ε. The modelling of these terms will be done in the next section.

Finally, the $\overline{u_i\theta}$-equation is obtained from equations (2.4) and (2.5) by using the relation $\overline{[\theta(m_i)+u_i(\theta)]}$ which results in

$$\frac{D\overline{u_i\theta}}{Dt} = \frac{\partial}{\partial x_\ell}[\overline{-u_\ell u_i \theta} - \overline{\delta_{i\ell}\frac{P\theta}{\rho}} + \alpha u_\ell \frac{\partial \theta}{\partial x_\ell} + \nu\overline{\frac{\theta \partial u_i}{\partial x_\ell}}]$$

$$-(\overline{u_i u_\ell}\frac{\partial T}{\partial x_\ell} + \overline{u_\ell \theta}\frac{\partial U_i}{\partial x_\ell}) - (\alpha+\nu)\overline{\frac{\partial u_i \partial \theta}{\partial x_\ell \partial x_\ell}} + \overline{\frac{P\partial\theta}{\rho \partial x_i}} + \frac{1}{\rho c}\overline{\phi' u_i} \qquad (2.9)$$

where

$$\phi' = \tau_{ij} \frac{\partial u_i}{\partial x_j} + \mu\left[\frac{\partial u_i}{\partial x_j} + \frac{\partial u_j}{\partial x_i}\right]\frac{\partial U_i}{\partial x_j} + \mu\left[\frac{\partial u_i}{\partial x_j} + \frac{\partial u_j}{\partial x_i}\right]\frac{\partial u_i}{\partial x_j}$$

In this equation, the terms on the right side are diffusion of $\overline{u_i\theta}$, the production of $\overline{u_i\theta}$, the dissipation, the pressure-temperature correlation and the frictional heating terms respectively. The unknown $\overline{\phi' u_i}$ in the $\overline{u_i\theta}$-equation represents the frictional heating generated by the fluctuating component and is usually considered to be smaller than the frictional heating generated by the mean flow motion $\tau_{ij}(\partial U_i/\partial x_j)$. Hence, it is often omitted in the mean energy equation. It should also be noted here that a part of the mean energy equation (1.6) $\overline{\mu[\partial u_i/\partial x_j + \partial u_j/\partial x_i][\partial u_i/\partial x_j]}$ is equal to ε which is derived in equation (2.8).

The four transport equations (2.6) to (2.8) derived above have several unknown terms on the right side most of which need to be modelled. This is discussed in the following section.

2.2 Concept of Two Turbulent Scales

Before attempting to model these equations, a brief discussion of turbulent flow structure is done and the concept of the two turbulent scales is introduced. In order to visualize the existence of two significantly different turbulent scales in a turbulent flow, it is instructive to consider a turbulent correlation function $R_{ij}(x;r)$ for velocity fluctuation, which is defined as

$$R_{ij}(x;r) = \overline{u_i(x)\, u_j(x+r)}$$

where $u_i(x)$ is the instantaneous value of the i^{th} component of the fluctuating velocity at the point of the position vector x and $u_j(x+r)$ the j^{th} component of the fluctuating velocity at (x+r). The average, with a bar over $u_i u_j$ may be considered either a time average or an ensemble average. If r=0 and i=j, the one point correlation $R_{ii}(x,0)$ is the Reynolds normal stress in the i^{th} direction. The correlation $R_{ij}(x,0)$ includes all possible turbulent eddy sizes at the position x. It is difficult to differentiate the scale that is significant in carrying out a turbulent process. One way to examine the behaviour of each turbulent eddy is to consider a spectral analysis of the correlation $R_{ij}(x,0)$, i.e.

$$\phi_{ij}(k) = \left(\frac{1}{2\pi}\right)^3 \int R_{ij}(x;r)\, \exp(-ik.r)\, dr$$

where $(\vec{k}.\vec{r})$ is the wave number vector, $\vec{k}$ dot the position vector at $\vec{r}$ distance from x. The wave number vector may be written as

$$\vec{k} = k_x i + k_y j + k_z k$$

The component wavenumber, k_i, is related to the fluctuating frequency n_i and the wavelength λ_i of an eddy in the x_i direction by

$$k_i = \frac{2\pi}{\lambda_i} = \frac{2\pi n_i}{U_i}$$

In fact $\phi_{ij}(k)$ is the Fourier transformation of $R_{ij}(\vec{x};\vec{r})$. The inverse Fourier transformation for recovering $R_{ij}(\vec{x};\vec{r})$ thus becomes

$$R_{ij}(\vec{x};\vec{r}) = \int_{-\infty}^{\infty} \phi_{ij}(k)\ \exp(\vec{ik}.\vec{r})dk$$

The reason for examining the spectral distribution ϕ_{ij} is that the transform is simply a method of representing the complex random wave form of turbulent eddy motion associated with R_{ij} by what is equivalent to a sum of sine or cosine waves of various amplitude or frequencies. The total sum of all sine and cosine waves is equivalent to the original wave form of $R_{ij}(\vec{x};\vec{r})$. Thus, one may think of $\phi_{ij}(\vec{k})$ as a fluctuating intensity of $R_{ij}(\vec{x};\vec{r})$ at a wave number, k_i, or frequency n_i. If the fluctuating intensity is large at a particular range of wave numbers, it means that the physical process of the turbulent phenomenon is intimately related to this range of wave number.

For the present analysis, the energy spectrum of a steady isotropic flow behind a wind tunnel grid at r=0 is considered. Then

$$R_{ij}(\vec{x};0) = \int_{-\infty}^{\infty} \phi_{ij}(\vec{k})d\vec{k}$$

The energy spectral $\phi_{ii}(\vec{k})$ is a function of the wave vector $\vec{k}$ or of a given point at $\vec{k}$ in wave space. An integrated energy spectrum $E_{ii}(k)$ which is a function of a scalar variable k can be obtained by integrating the energy spectrum $\phi_{ij}(k)$ over a spherical surface of radius $k=|\vec{k}|$ or

$$E_{ij}(k) = \int_s \phi_{ij}(k)ds(k)$$

Here, ds(k) is an element on the surface of the sphere of radius k. $E_{ij}(k)$ thus may be taken as the energy contribution from the eddy size with wave number k to the $\overline{u_i u_j}$ correlation. The energy spectrum function of turbulent kinetic energy in the wave space is

$$E(k) = \frac{1}{2}E_{ii}(k)$$

The total kinetic energy of the turbulent flow is then

$$\frac{1}{2}R_{ii} = \frac{\overline{u_i u_i}}{2} = \int_0^\infty E(k)dk$$

In particular, for isotropic flow the relation is

$$\int_0^\infty E(k)dk = \frac{3}{2}u^2$$

The spectrum equation of turbulent kinetic energy equation for isotropic turbulence can be written [12] as

$$\frac{\partial E(k)}{\partial t} = T(k) - D(k)$$

where T(k) is associated with the transfer of energy between wave numbers or eddy sizes. Its integral over all wave numbers is zero. It can thus be defined by a different transfer function

$$S(k) = -\int_0^k T(k)dk$$

which is the total energy transfered from eddies in the range from 0 to k to those in the range greater than k. In other words, S(k) is the flux of turbulent kinetic energy from a spherical volume of radius equal to wave number k. D(k) is the rate of dissipation of turbulent kinetic energy at the wave number k and is equal to

$$D(k) = 2\nu k^2 E(k)$$

Figure 2.1 shows the schematic energy spectrum E(k,t) and the dissipation spectrum D(k,t) for an isoptropic flow. The solid line shows a typical energy spectrum and the dashed line the dissipation of turbulent kinetic energy. Figure 2.2 gives the measured energy spectrum and the dissipation [12-14] in log-log scale for a steady flow behind a square grid screen with spacing of M in a wind tunnel. Here, the dimensionless wavenumber k is defined as $2\pi n\eta/U$ with n the frequency of a fluctuating component in turbulent flow, U the mean flow velocity and η is the Kolmogorov length scale or $(\nu^3/\varepsilon)^{\frac{1}{4}}$. t is a dimensionless time or the real time normalized by a characteristic time M/U. In figure 2.2, the Reynolds number Re_λ is $U\lambda_g/\nu$ where λ_g is Taylor's microscale [12]. The wavenumber, k, may be considered to be inversely proportional to the size of the eddies. In other words, the larger the size of the eddy, the smaller is its wavenumber. From figure 2.2, it can be seen that the measured energy and dissipation spectra are quite different and can be associated with different wavenumbers. For instance, a wavenumber characterized by k_d, in the order of 10^{-1} at Reynolds number Re_λ of 540

may be considered to be associated with the size of the small eddies that provide the main contribution to the dissipation of turbulent kinetic energy. This value k_d roughly corresponds to the maximum value of the dissipation curve. Similarly, there is a range of spectrum which corresponds to the energy containing large eddies. A wavenumber characterized by k_e, in the order of 10^{-4} at Re_λ of 540 may be considered to associate with this range which corresponds to the peak of the energy curve.

It has been shown both experimentally by Frieche et al. [13] and theoretically by Driscoll and Kennedy [14] that these energy and dissipation spectra change with Reynolds number. As given in figure 2.2, an increase in the Reynolds number causes the peaks of the energy and dissipation curves to separate further away.

In most of the spectral analysis, a turbulent Reynolds number is associated with the wavenumber, k_e. It has been shown [12] that

$$\frac{1}{k_e} = \ell_e = \frac{A}{15} Re_\lambda \lambda_g$$

where A is a constant and ℓ_e is the length of the eddy corresponding to the wavenumber, k_e. Re_λ is the Reynolds number based on Taylor microscale, λ_g or $U\lambda_g/\nu$. The Taylor microscale is a length scale associated with the curvature of the spatial velocity autocorrelations [15] and is related to the dissipation ε by the expression [12]

$$\varepsilon = 15\nu \frac{u'^2}{\lambda_g^2}$$

where u' is a velocity fluctuation.

Driscoll and Kennedy [14] obtained the energy and dissipation spectra for Re_λ ranging from 13 to 540 as shown in figure 2.2 The dimensionless wavenumber, k, is defined as $2\pi n\eta/U$ where η is the Kolmogorov length scale or $(\nu^3/\varepsilon)^{\frac{1}{2}}$. The energy spectra shows that when Re_λ increases $k_e\eta$ decreases. For a value of Re_λ=13, the peak wave number k_e is about 0.01 whereas for Re_λ=540, it is 0.0001. Hence, it can be said that the structure of turbulence is dependent on Reynolds number, whether it is the turbulent Reynolds number or the mean Reynolds number.

The quantity E(k) [12], used in Figures 2.1 and 2.2, is defined as

$$E(k) = 2\pi k^2 E_{ii}(k)$$

where $E_{ii}(k)$ is the Fourier Transformation of the correlation tensor $\overline{u_i u_i}$ or

$$E_{ii}(k) = \left(\frac{1}{2\pi}\right)^3 \int \overline{u_i u_i} \exp(-\vec{ik}.\vec{r})\, dr$$

Thus, the total energy contained by all the eddies is $1.5\overline{u^2}$,i.e.

$$E(k)dk = \frac{3}{2}\overline{u^2}$$

Therefore, figure 2.1 shows, conceptually, two distinguishing features of turbulence when one examines the turbulent spectra or turbulent eddies. The solid line gives the energy spectra from which it can be

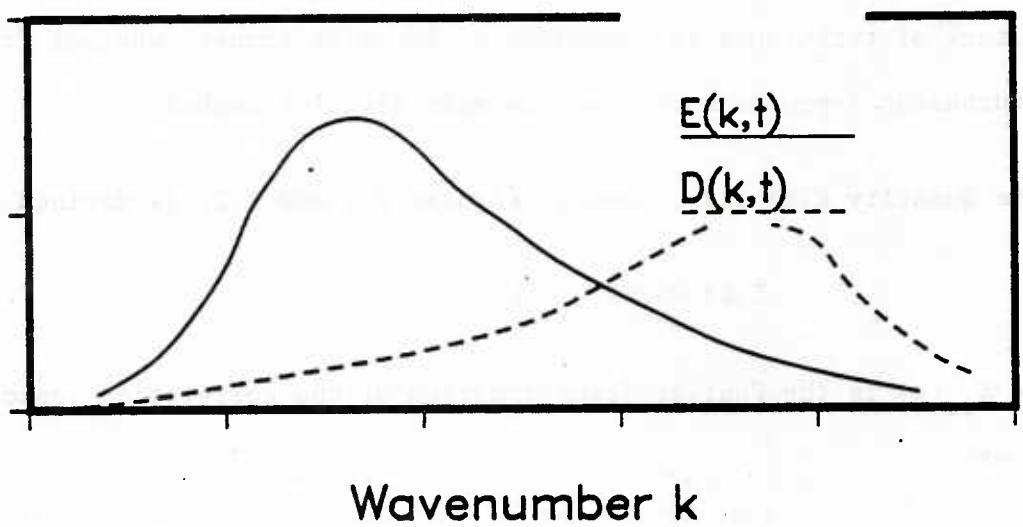

Figure 2.1. Energy and dissipation spectrum of an isotropic flow

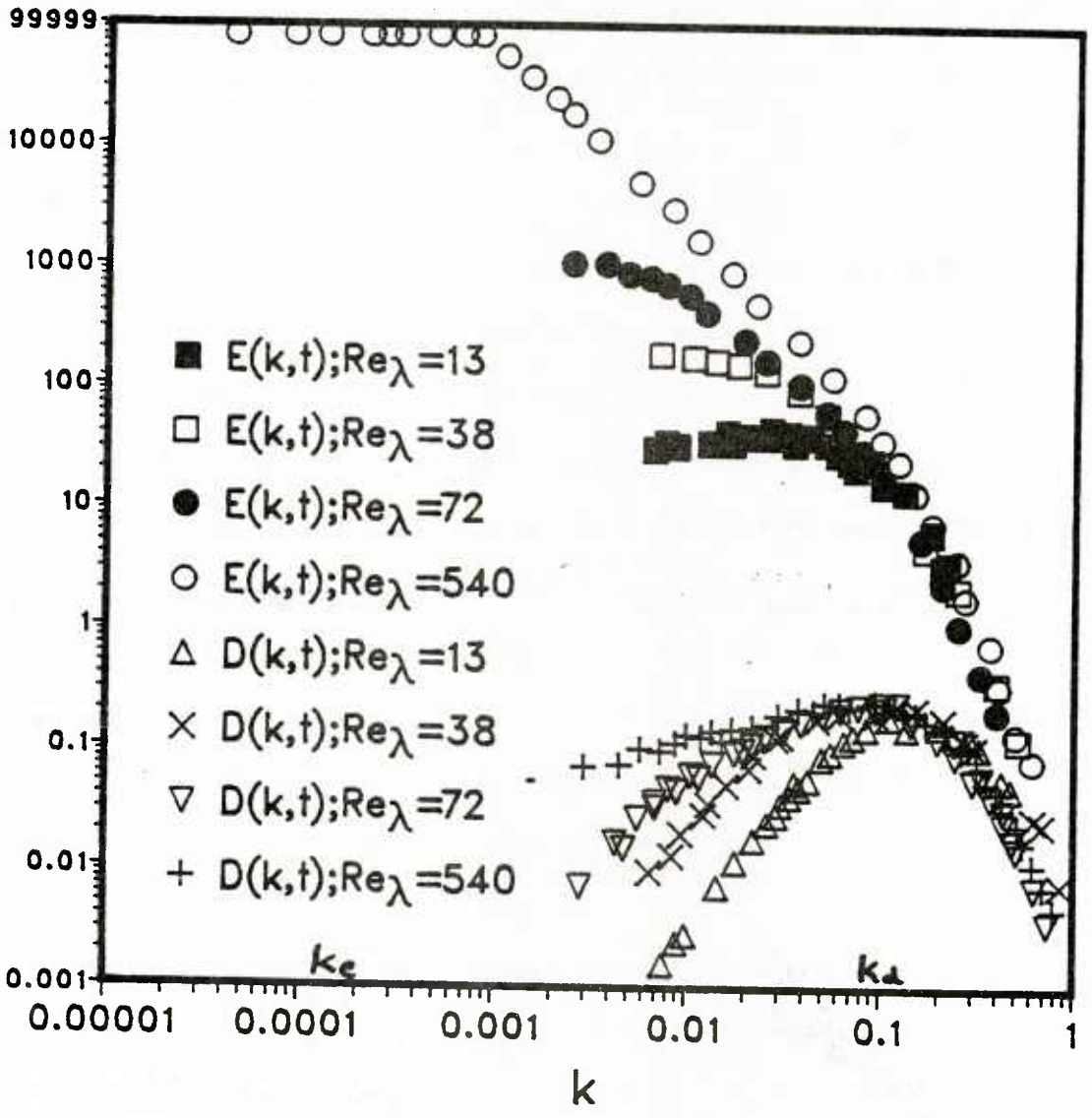

Figure 2.2. Energy and dissipation spectra for various Re_λ

seen that the range of eddies containing most of the energy are large in size (or lower in wavenumber range) and is comparable to the width of the flow. They transfer their energy to smaller eddies. It is in this range of smaller eddies where most of the dissipation of turbulent energy occurs. The larger the Reynolds number, the smaller is the eddy size. These properties of turbulent flows are obtained by experimental measurements and not by any postulation. Hence, it seems natural to consider different scales for the modelling of the k and ε equations (2.7) and (2.8). The measurements of Frieche et al. [13] reveal that large eddies possess most of the turbulent kinetic energy in the flow and do not play any significant role in the dissipation of turbulent kinetic energy. On the other hand, Kolmogorov [12] found that small eddy characteristics are functions of (ε,ν). In the medium range of eddy size, a process described as the transfer function $T(k,t)$ derived from convection terms of the k-equation (2.7) provides a mechanism to transfer the turbulent kinetic energy possessed by large eddies to small eddies before it is consumed by the viscous dissipation and turned into thermal energy. This distinct difference in the behavior of turbulence at different wave number was known for sometime. However, it has not yet been incorporated in most of the turbulence models. The existing models characterize the velocity, length and time scales for turbulent flows based on k and ε. However, in any turbulent flow, it is the larger eddies which cascade to become smaller eddies through inertial interaction, thereby transferring energy to the smaller eddies. At the same time, viscosity effects and, with them, dissipation become more and

more important for the smaller eddies as shown in figure 2.1. For a certain range of these small eddies, it can be shown that turbulence is in statistical equilibrium. This is the range in which viscosity can be effective in smoothing out velocity fluctuations. The generation of these small scale fluctuations is made possible due to the nonlinear terms in the equations of motion. On the other hand the viscous action prevents the generation of infinitely small scales of fluctuating motion by dissipating turbulent kinetic energy into heat. One may consider that at large Reynolds numbers, the relative magnitude of viscous force compared to inertia force is so small that viscous effects in a flow tend to become vanishingly small. However, Townsend [15] reasoned that the nonlinear terms in the Navier-Stokes equations counteract this effect by generating motion at scales small enough to be affected by viscosity. In other words, as soon as the scale of the flow field becomes so large that viscosity effects could be neglected, the flow creates small scale motion thereby keeping viscosity effects and, in particular, dissipation rates at a finite level.

At these small scales, turbulent motions are statistically independent of the relatively slow large scale turbulence and of the mean flow. Hence, as Kolmogorov reasoned, the character of turbulence in this range is determined by ε, the rate of dissipation of k and the viscosity ν. These considerations led Kolmogorov to make the following hypothesis:

' At suffficiently high Reynolds numbers there is a range of high wave number where the turbulence is statistically in equilibrium and uniquely determined by the parameters ε and ν. This state of equilibrium is universal'.

Using these two parameters, ε and ν, velocity, length and time scales for small eddy motion can be characterized by

$$v = (\nu\varepsilon)^{\frac{1}{4}}; \quad \eta = (\nu^3/\varepsilon)^{\frac{1}{4}} \quad \text{and} \quad t \equiv \eta/v = (\nu/\varepsilon)^{\frac{1}{2}}$$

which can be obtained by dimensional analysis of ν and ε. On the other hand, in the large turbulent eddies, the turbulent kinetic energy, k, is important since these large eddies are responsible for carrying turbulent energy and extract energy from the flow motion to sustain turbulence. Therefore, the character of turbulence in the large eddy range is determined by ε, the rate of dissipation of k, and the turbulent kinetic energy, k, itself. Using these two parameters, ε and k, the velocity, length and time scales for large eddy motion can be characterized as

$$u = k^{\frac{1}{2}}; \quad \ell = k^{1.5}/\varepsilon \quad \text{and} \quad t \equiv \ell/u = k/\varepsilon$$

Though the above analysis was done for isotropic flow, which is not the case in many practical situations, it has been shown [12] experimentally that the fine structure of nonisotropic turbulent flows is almost isotropic (local isotropy). This is, however, not true for all experimental results. Nevertheless, many qualitative features of

isotropic turbulence, particularly the distribution of two turbulence scales, apply to phenomena in actual turbulence. Measurements of Kolmogorov fine-scale turbulence structure in various flows shows that differences between results are often sufficiently small to be negligible in the first approximation.

Several investigators [16,17] have mentioned in the past that it is the ε-equation [equation (2.8)] which needs to be carefully studied. This is because of the complexity and difficulty in modelling the ε-equation. The physical meaning of the different correlations among all sizes of eddies and fluctuating quantities is sometimes difficult to understand. As an example, the production term containing the second derivative of the mean velocity U in equation (2.8) for ε is neglected invariably by most investigators. The reason for this is that this term is assumed to be much smaller than some of the other terms in this equation. However, the physical significance of this term is still not clear. Therefore, due to lack of information about such terms the ε-equation needs to be further investigated in order to improve the accuracy and prediction capability of the model as well as making it more general.

The concept of using different time scales was first proposed by Lumley [17] in 1975. He suggested that each term in both the k and ε equations be modelled either by using the (k,ε) scales or the (k,ε,ν) scales. However, in the final form of the modelled ε-equation suggested by Lumley, the scale containing ν was neglected. Another approach

considering multiple scales was made by Hanjalic et. al [16]. They used two different time scales by dividing the whole energy spectrum into two parts -- the energy containing eddies and the dissipating eddies. For each region, a separate time scale is used to model the k and ε equations. Results were obtained for several thin shear flows which show an improvement in the level of agreement with experiments over that obtained with models employing only one time scale. The authors suggested that by dividing the spectrum into more number of parts and solving the two equations in each region, a further improvement in the result could be obtained though the computational time would considerably increase. However, the authors did not present the results.

In the present investigation of turbulence modelling, the two-scale concept is employed. The two scales are the large eddy or energy containing scale based on k and ε and the small eddy or energy dissipating scale based on ν and ε. The two-scale concept is applied to all turbulent transport equations whenever it applies.

2.3 Turbulence modelling

Before modelling the transport equations, the postulations of turbulent flow are listed below. These postulations are made by various models and summarized by Chen [18].

1. Navier-Stokes equations are valid in describing turbulent motion.

2. Turbulent diffusion of a turbulent transport quantity ($\overline{u_i u_j}$, k, ε, $\overline{u_i \theta}$) is proportional to its gradient.
3. Small eddies are isotropic.
4. All turbulent quantities are functions of $\overline{u_i u_j}$, k, ε, $\overline{u_i \theta}$, U_i, P, T, ρ, ν and α.
5. The model equations should be consistent with respect to symmetry, invariance, permutation and physical conservation laws imposed on the original equations.
6. Turbulent scales are functions of k, ε and ν. Large eddy scales based on (k,ε) are $[u] = k^{\frac{1}{2}}$, $[l] = k^{1.5}/\varepsilon$, $[t] = k/\varepsilon$ and small eddy scale based on (ν,ε) are $[u] = (\nu\varepsilon)^{\frac{1}{4}}$, $[l] = (\nu^3/\varepsilon)^{\frac{1}{4}}$, $[t] = (\nu/\varepsilon)^{\frac{1}{2}}$.
7. Turbulent constants in the model are determined from experiments.

The two-scale turbulent flow model is now derived in the following section. Both (k,ε) and (ν,ε) scales are used in the modelling of the ε-equation. As for the modelling of the $\overline{u_i u_j}$ and k equations, the large eddy scale (k,ε) is used for the reason that the large eddies which contain most of the turbulent kinetic energy are also responsible for turbulent diffusion and pressure-strain interaction. Further details are presented below.

2.3.1 Modelling of $\overline{u_i u_j}$ and k equations

The turbulent diffusion term of equation (2.6) is modelled based on postulate 2 that the diffusion of $\overline{u_i u_j}$ is proportional to its gradient or

$$-\overline{u_i u_j u_\ell + \frac{P}{\rho}(\delta_{j\ell} u_i + \delta_{i\ell} u_j)} = C_k \left[\frac{\ell^2}{t}\right] \frac{\partial \overline{u_i u_j}}{\partial x_\ell}$$

In order to keep the dimensions consistent, a quantity with a scale of $[l^2/t]$ is needed to complete the model. From dimensional analysis based on large eddy scale (k,ε), it follows that

$$[u] = k^{\frac{1}{2}};\ [\ell] = k^{1.5}/\varepsilon;\ [t] = k/\varepsilon;\quad [\ell^2/t] = k^2/\varepsilon$$

The (k,ε) scale is chosen here instead of the small eddy scale (ν,ε) based on the physical ground that diffusion of any quantity by turbulent fluctuation is largely controlled by large eddy motion. Thus

$$-\overline{u_i u_j u_\ell + \frac{P}{\rho}(\delta_{j\ell} u_i + \delta_{i\ell} u_j)} = C_k \frac{k^2}{\varepsilon} \frac{\partial \overline{u_i u_j}}{\partial x_\ell}$$

Here, C_k is a proportionality coefficient. It should be remarked here that the model observes the symmetry of the original form between i and j as stated in postulate 5. The dissipation term in equation (2.6) is modelled based on postulate 3 as

$$2\nu \overline{\frac{\partial u_i}{\partial x_\ell} \frac{\partial u_j}{\partial x_\ell}} = \frac{2}{3}\delta_{ij} \nu \overline{\frac{\partial u_m}{\partial x_\ell} \frac{\partial u_m}{\partial x_\ell}} = \frac{2}{3}\delta_{ij}\varepsilon$$

This is based on the understanding that the larger the Reynolds number the smaller the turbulent eddies are and that the smaller these eddies become the more isotropic they will be. Thus, the dissipation of turbulent stress $\overline{u_i u_j}$ by the small eddies is mainly in the isotropic

range. It should be noted here that under postulate 3 and the model presented, the dissipation of $\overline{u_i u_j}$ can occur only in the normal stress $\overline{u_i u_j}$ for i=j and not the shear stress when i≠j. However, when i=j the model term reduces to the exact expression.

The pressure-strain term is modelled based on postulates 4 and 5 as [19]

$$\overline{\frac{p}{\rho}\left(\frac{\partial u_i}{\partial x_j} + \frac{\partial u_j}{\partial x_i}\right)} = -C_1 \frac{\varepsilon}{k}\left(\overline{u_i u_j} - \frac{2}{3}\delta_{ij} k_k\right) - C_2\left(P_{ij} - \frac{2}{3}\delta_{ij} P_k\right)$$

where C_1 and C_2 are model coefficients determined from experiments and

$$P_{ij} = -\left(\overline{u_i u_l}\frac{\partial U_j}{\partial x_l} + \overline{u_j u_l}\frac{\partial U_i}{\partial x_l}\right) \quad \text{and} \quad P_k = -\overline{u_n u_m}\frac{\partial U_n}{\partial x_m}$$

Further details of the modelling of $\overline{u_i u_j}$ equation can be found in [18,19]. The modelled $\overline{u_i u_j}$ equation, thus, has the form

$$\frac{D\overline{u_i u_j}}{Dt} = \frac{\partial}{\partial x_\ell}\left[C_k \frac{k^2}{\varepsilon}\frac{\partial \overline{u_i u_j}}{\partial x_\ell} + \nu\frac{\partial \overline{u_i u_j}}{\partial x_\ell}\right] - P_{ij} \quad \frac{2}{3}\delta_{ij}\varepsilon$$

$$- C_1 \frac{\varepsilon}{k}\left[\overline{u_i u_j} - \frac{2}{3}\delta_{ij} k\right] - C_2\left[P_{ij} - \frac{2}{3}\delta_{ij} P_k\right] \qquad (2.10)$$

From this equation, the k-equation is obtained by summing i=j for i=1,2,3 and dividing the result by two. This gives

$$\frac{Dk}{Dt} = \frac{\partial}{\partial x_\ell}\left[C_k \frac{k^2}{\varepsilon}\frac{\partial k}{\partial x_\ell} + \nu\frac{\partial k}{\partial x_\ell}\right] - \overline{u_i u_\ell}\frac{\partial U_i}{\partial x_\ell} - \varepsilon \qquad (2.11)$$

It should be remembered here that in equation (2.11), where i=j, the pressure-strain term $\overline{(p/\rho)[\partial u_i/\partial x_j + \partial u_j/\partial x_i]}$ is identically equal to zero due to incompressibility requirement. Therefore, in equation (2.11), only the first term on the right hand side is modelled and the rest of the equation is exact as derived in equation (2.7). It should also be noted that equation (2.11) portrays the interaction of all turbulent eddies. The last term in equation (2.11), ε, is dominantly associated with the small eddies and is responsible for dissipation of turbulent energy that is produced, first, by $-\overline{u_i u_j}(\partial U_i/\partial x_l)$ through the stress exerted by the fluctuating motion on the mean flow motion and secondly, by turbulent and viscous diffusion shown in the first term on the right side. The diffusion term can be reasoned to be more intimately correlated with the large eddy motion. This is why the length and time scale of large eddies $[l] = k^{1.5}/\varepsilon$ and $[t] = k/\varepsilon$ is adopted in modelling the diffusion term. Although two scale concept is evident in the k-equation, there is no need to invoke the second and small scale (ε,ν) in this equation as the last term, ε, is exact. The situation, however, is different when one attempts to model the ε-equation. This is considered in the following section.

2.3.2 Modelling of ε-equation

The modelling of ε-equation is important because it governs the way in which the turbulent kinetic energy is dissipated. As mentioned earlier, the performance of the modelled ε-equation based on a single turbulent scale of large eddies is not as satisfactory as the other

modelled equations. First, the model constant, C_μ which appears in the equation for eddy viscosity and $C_{\varepsilon 1}$, which appears in the ε-equation, are found not to be constants. Secondly, the prediction of turbulent flow is quite sensitive to the values of the constants $C_{\varepsilon 1}$ and $C_{\varepsilon 2}$.

In modelling the ε-equation, equation (2.8), it should also be remarked that all eddy motions contribute in the equation. The dissipative action is dominant at the small eddy level while the convective and diffusive actions are predominant at the large eddy level.

The scale at which the small eddy is manifesting its dissipating function in a given flow, is intimately related to the large scale structure and the ratio of inertia force and viscous force or the Reynolds number as already discussed in section 2.2. The effect of large scale motion on the small eddy scale is transmitted through the transfer mechanism created by the nonlinear term of the transport equation. Each term in the ε-equation contributes differently in a different range of eddy size. Thus, it is important to model each term in ε-equation individually according to the eddy size that characterizes the physical process of the term. Proceeding in this way, the ε-equation is modelled below. The first production term in equation (2.8) is modelled as

$$\nu \frac{\partial U_i}{\partial x_j} \left(\overline{\frac{\partial u_\ell}{\partial x_i} \frac{\partial u_\ell}{\partial x_j}} + \overline{\frac{\partial u_i}{\partial x_\ell} \frac{\partial u_j}{\partial x_\ell}} \right) \approx 0$$

This is because, for i=j, the mean strain is zero from conservation of mass for incompressible flow and for i≠j, the quantity in the parenthesis is zero from the isotropic nature of small eddies at large Reynolds number which is mentioned in postulate 3.

The second production term,

$$\overline{\nu u_\ell \frac{\partial u_i}{\partial x_j}} \frac{\partial^2 U_i}{\partial x_\ell \partial x_j}$$

is also neglected, based on Lumley's [17] proposal that the correlation coefficients between two quantities, each from a different range, are of the order of the time scale ratio $Re^{-\frac{1}{2}}$. In this case, u_1 is considered to be in one range characterized by the large eddy scale and $\partial u_i/\partial x_j$ in another range by the small eddy scale and consequently the value of correlation coefficient is considered small or weak compared with the other terms in the ε-equation. For example,

$$\overline{2\nu \frac{\partial u_i}{\partial x_j} \frac{\partial u_i}{\partial x_\ell} \frac{\partial u_j}{\partial x_\ell}}$$

has a strong correlation as the terms $\partial u_i/\partial x_j$, $\partial u_i/\partial x_1$ and $\partial u_j/\partial x_1$ are in the same range. Therefore,

$$\overline{2\nu \frac{\partial u_i}{\partial x_j} \frac{\partial u_i}{\partial x_\ell} \frac{\partial u_j}{\partial x_\ell}} > \overline{2\nu u_\ell \frac{\partial u_i}{\partial x_j}} \frac{\partial^2 U_i}{\partial x_\ell \partial x_j}$$

So the second production term is dropped from the ε-equation.

The modelling of the two destruction terms is done based on postulate 4 that they are function of the quantity P_k/ε and other transport variables in accordance with Lumley's argument [17]. Here, $P_k[= -\overline{u_i u_j}(\partial U_i/\partial x_j)]$ is the production of turbulent kinetic energy. Thus

$$2\nu\overline{\frac{\partial u_i}{\partial x_j}\frac{\partial u_i}{\partial x_\ell}\frac{\partial u_j}{\partial x_\ell}} - 2\overline{[\nu\frac{\partial^2 u_i}{\partial x_\ell \partial x_\ell}]^2} = fn(\frac{P_k}{\varepsilon}, k, \varepsilon, \nu)$$

Lumley assumed that these two terms should vanish when the turbulent flow approaches equilibrium. Thus, for small deviations from turbulent equilibrium, this function may be approximately expanded to obtain

$$fn(\frac{P_k}{\varepsilon}) = [\frac{\varepsilon}{t}][1 - \frac{P_k}{\varepsilon}] = [\frac{1}{t}][\varepsilon - P_k]$$

Here $[\varepsilon/t]$ is the dimension needed so that the overall dimension of the ε-equation and that of the two destructive terms are consistent. t is the time scale that characterizes the physical action for destruction of ε. Since the dissipation or destruction of ε physically is dominated in the small eddy range, the time scale, $t=(\nu/\varepsilon)^{\frac{1}{2}}$, based on Kolmogorov hypothesis, is used in the present work. Hence, the modelled destruction term is

$$2\nu\overline{\frac{\partial u_i}{\partial x_j}\frac{\partial u_i}{\partial x_\ell}\frac{\partial u_j}{\partial x_\ell}} - 2\overline{[\nu\frac{\partial^2 u_i}{\partial x_\ell \partial x_j}]^2} = -C_{\varepsilon 1}(\varepsilon/\nu)^{\frac{1}{2}}\overline{u_i u_j}\frac{\partial U_i}{\partial x_j} - C_{\varepsilon 2}(\varepsilon/\nu)^{\frac{1}{2}}\varepsilon$$

This model differs from the existing turbulence model [19] in that the Kolmogorov scale (ε,ν) is used for the scaling of time [t] instead of

the conventional scale based on (k,ε) which leads to the conventional ε-equation given in equation (1.10).

The diffusion term in ε-equation is modelled according to postulate 2 that it is proportional to the gradient of ε, or

$$-\overline{\varepsilon' u_i} - \overline{\frac{2\nu}{\rho}\frac{\partial u_i}{\partial x_j}\frac{\partial P}{\partial x_j}} = C_\varepsilon\left[\frac{\ell^2}{t}\right]\frac{\partial \varepsilon}{\partial x_j} = C_\varepsilon \frac{k^2}{\varepsilon}\frac{\partial \varepsilon}{\partial x_j}$$

Here the length and time scales are modelled based on the large eddy or

$$\ell = k^{1.5}/\varepsilon \quad \text{and} \quad t = k/\varepsilon$$

as shown before. Thus the modelled ε-equation based on the two-scale concept and Lumley's suggestion for destruction term is

$$\frac{D\varepsilon}{Dt} = \frac{\partial}{\partial x_\ell}\left[C_\varepsilon \frac{k^2}{\varepsilon}\frac{\partial \varepsilon}{\partial x_\ell} + \nu\frac{\partial \varepsilon}{\partial x_\ell}\right] - C_{\varepsilon 1}(\varepsilon/\nu)^{\frac{1}{2}}\overline{u_i u_j}\frac{\partial U_i}{\partial x_\ell} - C_{\varepsilon 2}(\varepsilon/\nu)^{\frac{1}{2}}\varepsilon \qquad (2.12)$$

Here C_ε, $C_{\varepsilon 1}$ and $C_{\varepsilon 2}$ are model proportionality coefficients. In general, they can be a function of fluid or flow properties such as Prandtl number or Reynolds number.

2.3.3 Modelling of $\overline{u_i\theta}$-equation

Finally the modelling of the $\overline{u_i\theta}$-equation [equation (2.9)] is done to complete the turbulence closure problem. Using the same postulates as those for modelling the $\overline{u_i u_j}$ equation, the diffusion term of this equation is modelled as

$$- \overline{u_i u_\ell \theta} - \delta_{i\ell} \overline{\frac{p\theta}{\rho}} = C_T \frac{k^2}{\varepsilon} \frac{\partial \overline{u_i \theta}}{\partial x_\ell}$$

and for $\alpha = \nu$,

$$\alpha \overline{u_i \frac{\partial \theta}{\partial x_\ell}} + \nu \overline{\theta \frac{\partial u_i}{\partial x_\ell}} = \alpha \frac{\partial \overline{u_i \theta}}{\partial x_\ell}$$

The dissipation term vanishes due to the assumption of isotropic nature of small eddies or postulate 3, i.e.,

$$- (\alpha + \nu) \overline{\frac{\partial u_i}{\partial x_\ell} \frac{\partial \theta}{\partial x_\ell}} = 0$$

The pressure strain term (P-θ) is modelled according to Launder [20] as

$$\overline{\frac{P}{\rho} \frac{\partial \theta}{\partial x_i}} = - C_{T1} \frac{\varepsilon}{k} \overline{u_i \theta} + C_{T2} u_m \theta \frac{\partial U_i}{\partial x_m}$$

The frictional term in $\overline{u_i \theta}$-equation is neglected as it is an order of magnitude smaller than the other terms. Hence the modelled $\overline{u_i \theta}$-equation takes the form

$$\frac{D\overline{u_i \theta}}{Dt} = \frac{\partial}{\partial x_\ell} [C_T \frac{k^2}{\varepsilon} \frac{\partial \overline{u_i \theta}}{\partial x_\ell} + \alpha \frac{\partial \overline{u_i \theta}}{\partial x_\ell}] - [\overline{u_i u_\ell} \frac{\partial T}{\partial x_\ell} + u_\ell \theta \frac{\partial U_i}{\partial x_\ell}]$$

$$- C_{T1} \frac{\varepsilon}{k} \overline{u_i \theta} + C_{T2} \frac{\partial U_i}{\partial x_m} \overline{u_m \theta} \qquad (2.13)$$

Again, C_T, C_{T1} and C_{T2} are model coefficients.

Summarizing the two-scale second order turbulence model, we have the following equations

$$\frac{\partial U_i}{\partial x_i} = 0 \tag{2.1}$$

$$\rho\frac{DU_i}{Dt} = -\rho G_i - \frac{\partial P}{\partial x_i} + \frac{\partial \tau_{ij}}{\partial x_j} + \frac{\partial \tau_{ij}^t}{\partial x_j} \tag{2.2}$$

$$\rho c\frac{DT}{Dt} = \tau_{ij}\frac{\partial U_i}{\partial x_j} - \frac{\partial q_i}{\partial x_i} - \frac{\partial q_i^t}{\partial x_i} + \phi \tag{2.3}$$

$$\frac{D\overline{u_iu_j}}{Dt} = \frac{\partial}{\partial x_\ell}\left[C_k \frac{k^2}{\varepsilon}\frac{\partial \overline{u_iu_j}}{\partial x_\ell} + \nu\frac{\partial \overline{u_iu_j}}{\partial x_\ell}\right] - P_{ij} \quad \frac{2}{3}\delta_{ij}\varepsilon$$

$$- C_1\frac{\varepsilon}{k}\left[\overline{u_iu_j} - \frac{2}{3}\delta_{ij}k\right] - C_2\left[P_{ij} - \frac{2}{3}\delta_{ij}P_k\right] \tag{2.10}$$

$$\frac{Dk}{Dt} = \frac{\partial}{\partial x_\ell}\left[C_k \frac{k^2}{\varepsilon}\frac{\partial k}{\partial x_\ell} + \nu\frac{\partial k}{\partial x_\ell}\right] - \overline{u_iu_\ell}\frac{\partial U_i}{\partial x_\ell} - \varepsilon \tag{2.11}$$

$$\frac{D\varepsilon}{Dt} = \frac{\partial}{\partial x_\ell}\left[C_\varepsilon \frac{k^2}{\varepsilon}\frac{\partial \varepsilon}{\partial x_\ell} + \nu\frac{\partial \varepsilon}{\partial x_\ell}\right] - C_{\varepsilon 1}(\varepsilon/\nu)^{\frac{1}{2}}\overline{u_iu_j}\frac{\partial U_i}{\partial x_\ell} - C_{\varepsilon 2}(\varepsilon/\nu)^{\frac{1}{2}}\varepsilon \tag{2.12}$$

$$\frac{D\overline{u_i\theta}}{Dt} = \frac{\partial}{\partial x_\ell}\left[C_T \frac{k^2}{\varepsilon}\frac{\partial \overline{u_i\theta}}{\partial x_\ell} + \alpha\frac{\partial \overline{u_i\theta}}{\partial x_\ell}\right] - \left[\overline{u_iu_\ell}\frac{\partial T}{\partial x_\ell} + \overline{u_\ell\theta}\frac{\partial U_i}{\partial x_\ell}\right]$$

$$- C_{T1}\frac{\varepsilon}{k}\overline{u_i\theta} + C_{T2}\frac{\partial U_i}{\partial x_m}\overline{u_m\theta} \tag{2.13}$$

2.4 Determination of Turbulent Coefficients

The above 11 equations for turbulent quantities have 9 dimensionless coefficients or constants, namely, C_k, C_1, C_2, C_ε, $C_{\varepsilon 1}$, $C_{\varepsilon 2}$, C_T, C_{T1} and C_{T2} to be determined from experiments. The determination of the value of turbulent coefficients in principle is similar to the one for laminar flow where an experiment has to be performed to obtain the values of viscosity and thermal diffusivity of the fluid. The laminar coefficients which are dimensional such as kinematic viscosity ν and thermal diffusivity α turned out to be dependent on fluid and thermodynamic variables, temperature T and pressure P. The turbulent coefficients are dimensionless and can, in general, be functions of fluid and flow properties such as Prandlt number or Reynolds number. If the turbulent flow equations are properly modelled, the model coefficients should remain universal and can be evaluated once for all from the chosen experiments. Thus, the process of determining the constants is not a case of experimental data fitting. It should be remarked that although these coefficients may depend on fluid properties like laminar flow coefficients ν and α, they are determined mainly from experiments performed in air and water. Many investigators consider that these coefficients remain the same for both fluids. Whether these coefficients are valid for turbulent flows in other fluids such as oil or liquid metal is not known. The following subsections highlight the method of obtaining these constants.

2.4.1 $C_{\varepsilon 1}$ and $C_{\varepsilon 2}$

The coefficients $C_{\varepsilon 1}$ and $C_{\varepsilon 2}$ are obtained from experimental data of homogeneous shear flow and turbulence behind a grid [21]. Consider a uniform flow of velocity U_o passing a square grid with spacing M. The flow behind the grid can be made isotropic by contracting the area of cross section by a factor of 1.27. The k and ε equations for isotropic turbulent flow behind a grid (figure 2.3) are

$$U_o \frac{dk}{dx} = -\varepsilon$$

and

$$U_o \frac{d\varepsilon}{dx} = -C_{\varepsilon 2}(\varepsilon/\nu)^{\frac{1}{2}}\varepsilon$$

Here x is the coordinate along the flow direction. It should be remarked here that the diffusion terms of k and ε equations in their exact form are zero for isotropic flow. Nondimensionalizing these equations using the variables

$$x' = \frac{x}{M}; \quad k' = \frac{k}{U_o^2}; \quad \varepsilon' = \frac{\varepsilon}{U_o^3/M}; \quad Re = \frac{U_o M}{\nu}$$

the following equations are obtained, i.e.,

$$\frac{dk'}{dx'} = -\varepsilon'$$

and

$$\frac{d\varepsilon'}{dx'} = -C_{\varepsilon 2}Re^{-\frac{1}{2}}\varepsilon'^{1.5}$$

From figure 2.4, the relation between k and x is found to be approximately for air [18]

$$k' = \frac{450}{40000}\, x'^{-1}$$

between $10 < x/M < 200$ for the approximately isotropic range and for Re_M ranging from 10^3 to 10^4. Substituting this in the k-equation gives a relation between ε and x, which is

$$\varepsilon' = -\frac{dk'}{dx'} = \frac{450}{40000}x'^{-2}$$

This is now substituted in the ε-equation to give

$$-\frac{450}{40000}\, x'^{-3} * 2 = -C_{\varepsilon 2}Re^{\frac{1}{2}}\left(\frac{450}{40000}\right)^{1.5}x'^{-3}$$

Hence, $C_{\varepsilon 2}$ is calculated to be

$$C_{\varepsilon 2} = 2\left(\frac{40000}{450}\right)^{\frac{1}{2}}Re^{-\frac{1}{2}} = \frac{18.9}{\sqrt{Re}}$$

It should be mentioned that the flow behind uniform grid is not truly an isotropic flow since u^2/v^2 is always greater than one. u^2/v^2 starts with about 1 immediately behind the screen for $Re_\lambda > 10^3$ and increases to 1.55 downstream [18]. Therefore, decay data for turbulent kinetic energy k' versus x' beyond $x/M > 200$ should not be considered as an isotropic data and used in determination of turbulent coefficients. The value of

$C_{\varepsilon 1}$ is next obtained from homogeneous shear flow as shown in figure 2.5. For such a flow, the k and ε equations are

$$0 = -uv\frac{\partial U}{\partial y} - \varepsilon$$

and

$$0 = -C_{\varepsilon 1}(\varepsilon/\nu)^{\frac{1}{2}}\ uv\frac{\partial U}{\partial y} - C_{\varepsilon 2}(\varepsilon/\nu)^{\frac{1}{2}}\varepsilon$$

Substituting the k-equation into the ε-equation gives

$$C_{\varepsilon 1}(\varepsilon/\nu)^{\frac{1}{2}}\varepsilon - C_{\varepsilon 2}(\varepsilon/\nu)^{\frac{1}{2}}\varepsilon = 0$$

Therefore,

$$C_{\varepsilon 1} = C_{\varepsilon 2} = 18.9\ Re^{-\frac{1}{2}}$$

The diffusion terms in k and ε equations are assumed to be approximately zero here. Strictly speaking they are nonzero. Consequently the determination of $C_{\varepsilon 1}$ should be considered only an approximate one. The coefficients $C_{\varepsilon 1}$ and $C_{\varepsilon 2}$ for the destruction term in the ε-equation were found to be function of Reynolds number based on a characteristic mean flow velocity U_o and a characteristic length M. The appearance of Reynolds number in $C_{\varepsilon 1}$ and $C_{\varepsilon 2}$ reflects that the small eddies responsible for destruction for ε are indeed a function of mean Reynolds number. In other words, the size of small eddy and the time scale that characterizes the destruction of ε changes when Reynolds number changes.

It should be remarked here that in the one-scale turbulence model the coefficients $C_{\varepsilon 1}$ and $C_{\varepsilon 2}$ in equation (1.10) are found to be independent of Reynolds number. Their values are not universal and require modification in some flow configurations such as between plane jet and round jet. To compensate the contribution of diffusion $C_{\varepsilon 1}$ in the present study is taken to be approximately $17.5\ Re^{-\frac{1}{2}}$. The fact that $C_{\varepsilon 1}$ and $C_{\varepsilon 2}$ required modification weakens the predictability of the one scale turbulence model and motivates the present investigation of the two scale turbulence model to improve the predictability of the model.

2.4.2 C_1 and C_2

The constants C_1 and C_2 in equation (2.10) are obtained in a way similar to $C_{\varepsilon 1}$ and $C_{\varepsilon 2}$ [18]. Experimental result of anisotropic turbulence behind a grid by Uberoi [21] are used. For such a flow, $U=U_o$=constant and $V=W=0$. By passing this flow through a 4:1 contraction of flow cross-section area, the turbulence becomes strongly anisotropic. With U_o= constant, the exact equation for $\overline{u_i u_j}$ [equation (2.6)] where $\overline{u^2} > \overline{v^2} = \overline{w^2}$ becomes

$$U_o \frac{\partial \overline{u^2}}{\partial x_\ell} = - 2\nu \overline{\frac{\partial u}{\partial x_\ell} \frac{\partial u}{\partial x_\ell}} + \overline{\frac{2p}{\rho} \frac{\partial u}{\partial x}}$$

when i=j and the modelled equation is

$$U_o \frac{\partial \overline{u^2}}{\partial x_\ell} = - \frac{2}{3}\varepsilon - C_1 \frac{\varepsilon}{k}(\overline{u^2} - \frac{2}{3}k)$$

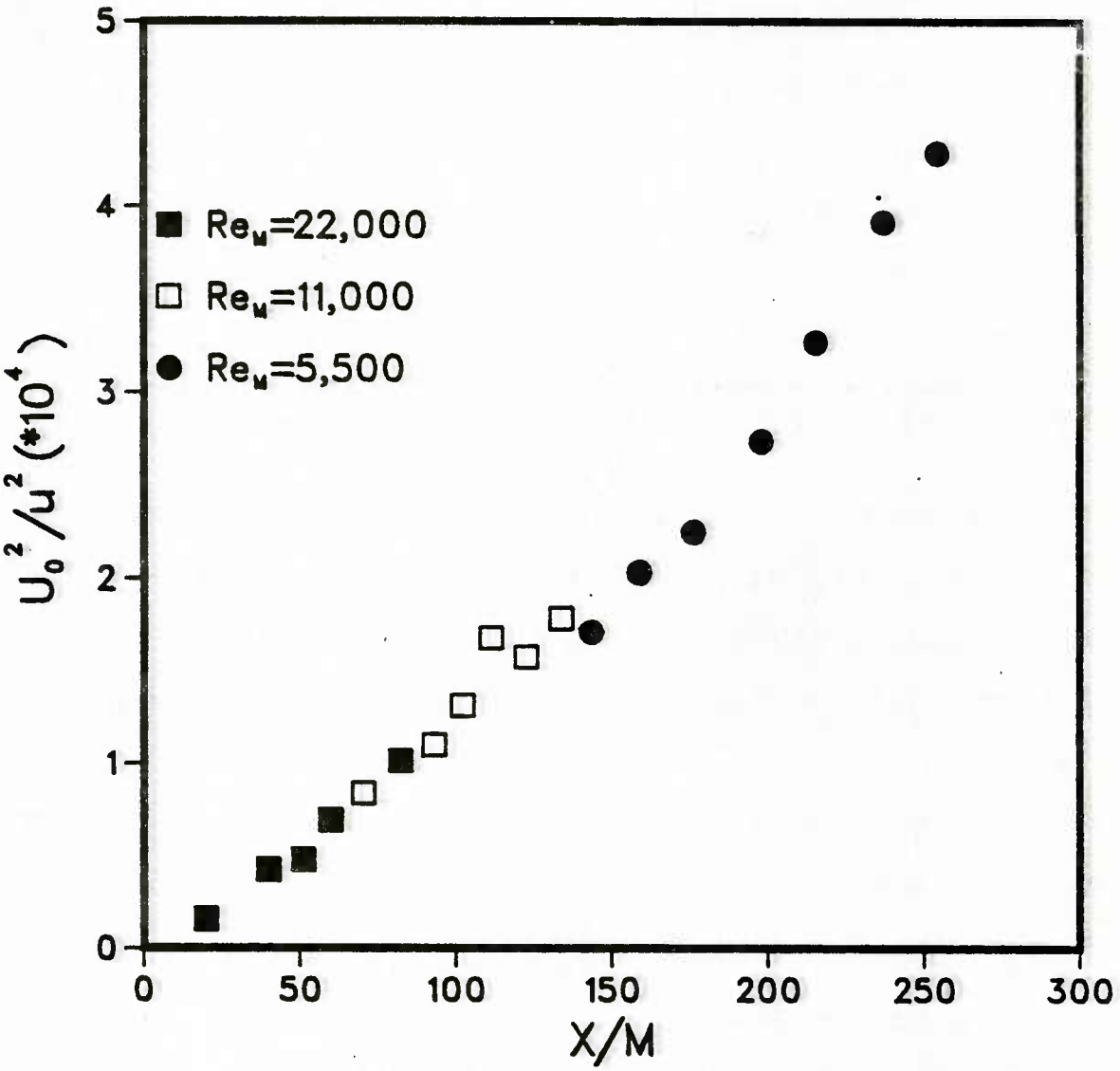

Figure 2.3. Isotropic flow behind a grid

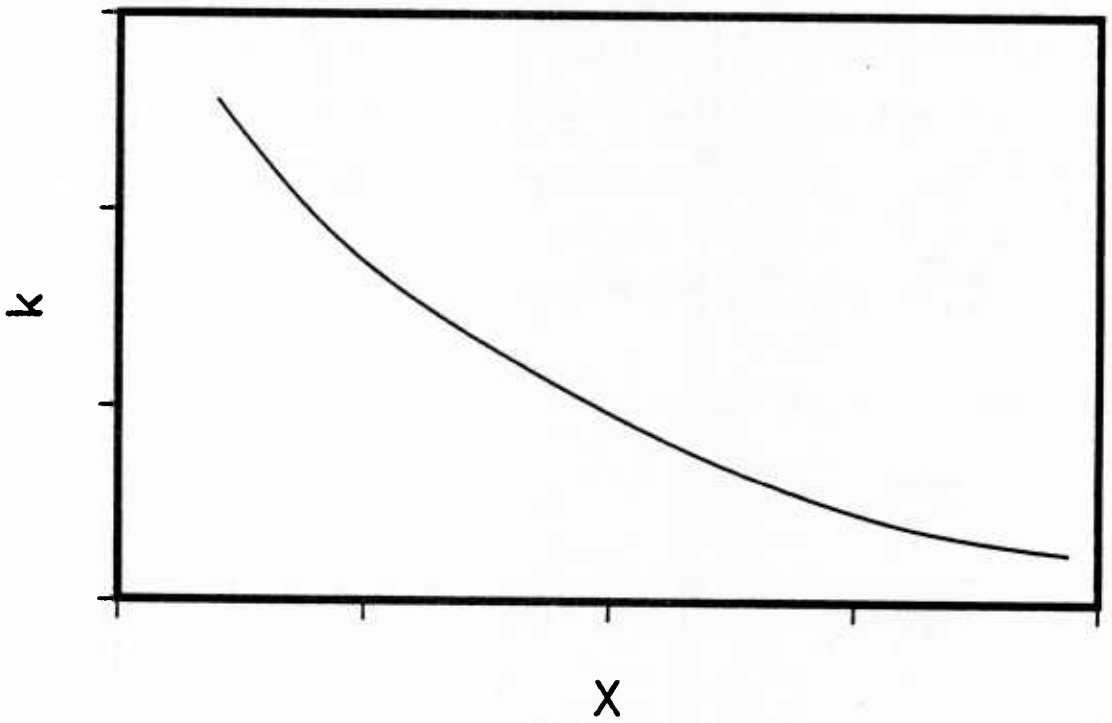

Figure 2.4. k-distribution in an isotropic flow

Dividing the second term on RHS of each equation by the first term on the RHS gives

$$\frac{\overline{\frac{2\rho}{\rho}\frac{\partial u}{\partial x}} \qquad - C_1 \frac{\varepsilon}{k}(\overline{u^2} - \frac{2}{3}k)}{\overline{2\nu\frac{\partial u}{\partial x_\ell}\frac{\partial u}{\partial x_\ell}}} = \frac{}{\frac{2}{3}\varepsilon} = - C_1(\frac{3\overline{u^2}}{2k} - 1)$$

In order to accurately determine C_1 one needs to avoid data of $1.5(\overline{u^2}/k)$ which is close to one since it will make the right hand side of the above expression zero. In other words, one should consider the data in the strongly anisotropic range, $\overline{u^2}/\overline{v^2} > 1$, or between x/M equal to 0 and 40. From figure 2.6, $(\overline{v^2}/\overline{u^2})=1.83$ for x/M=25 where $\overline{w^2}=\overline{v^2}$. Thus

$$\frac{3}{2}\frac{\overline{u^2}}{k} = \frac{3\overline{v^2}/1.83}{\overline{v^2}(1/1.83 + 2)} = 0.644$$

From figure 2.7, at x/M = 25,

$$\frac{\overline{\frac{2P}{\rho}\frac{\partial u}{\partial x}}}{\overline{2\nu\frac{\partial u}{\partial x_\ell}\frac{\partial u}{\partial x_\ell}}} = 1.0$$

Hence

$$- C_1(\frac{3\overline{u^2}}{2k} - 1) = 1.0$$

and

$$C_1 = 2.8$$

If data at x/M = 12.5 is used, C_1 = 2.88.

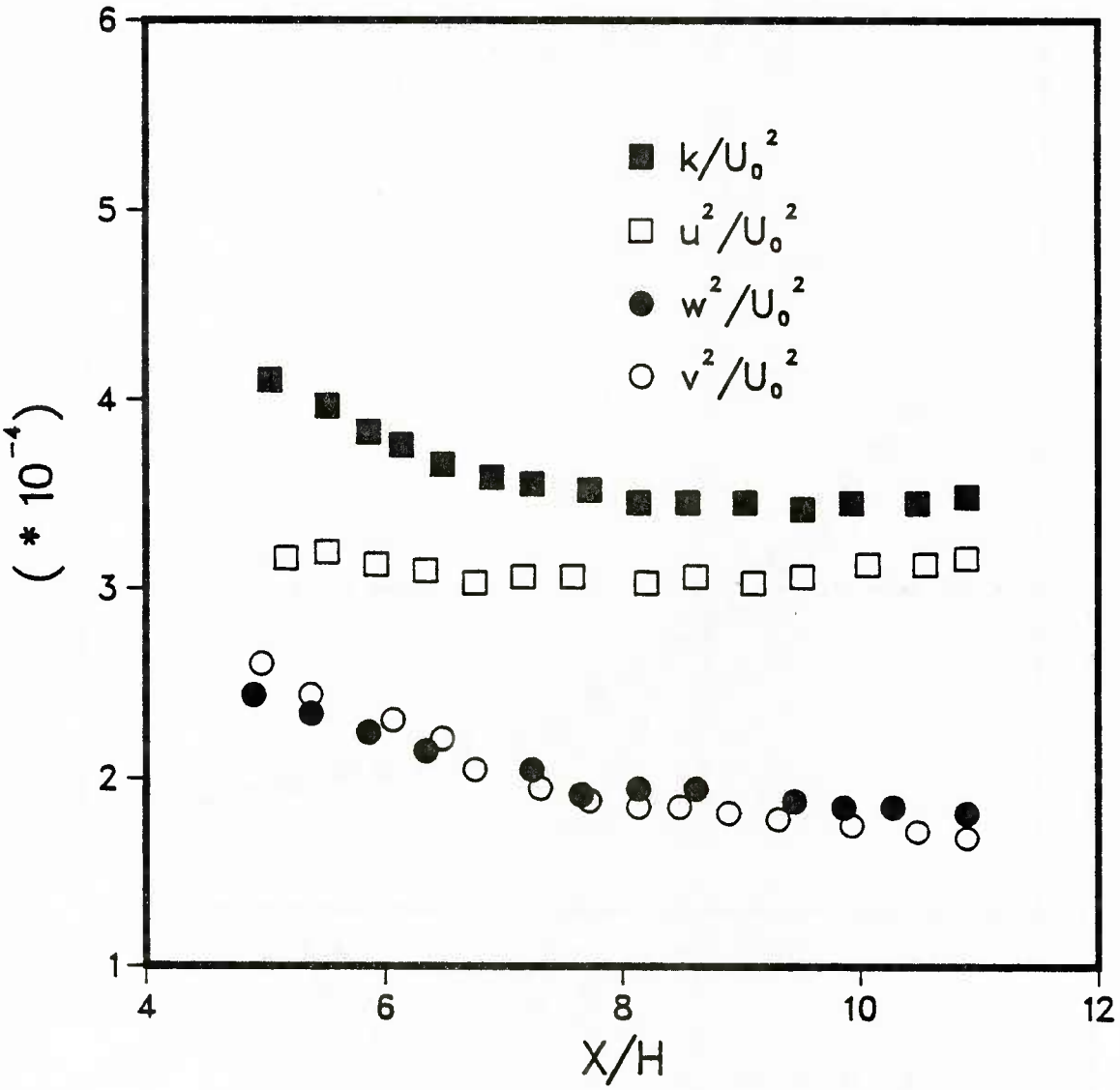

Figure 2.5. Homogeneous shear flow

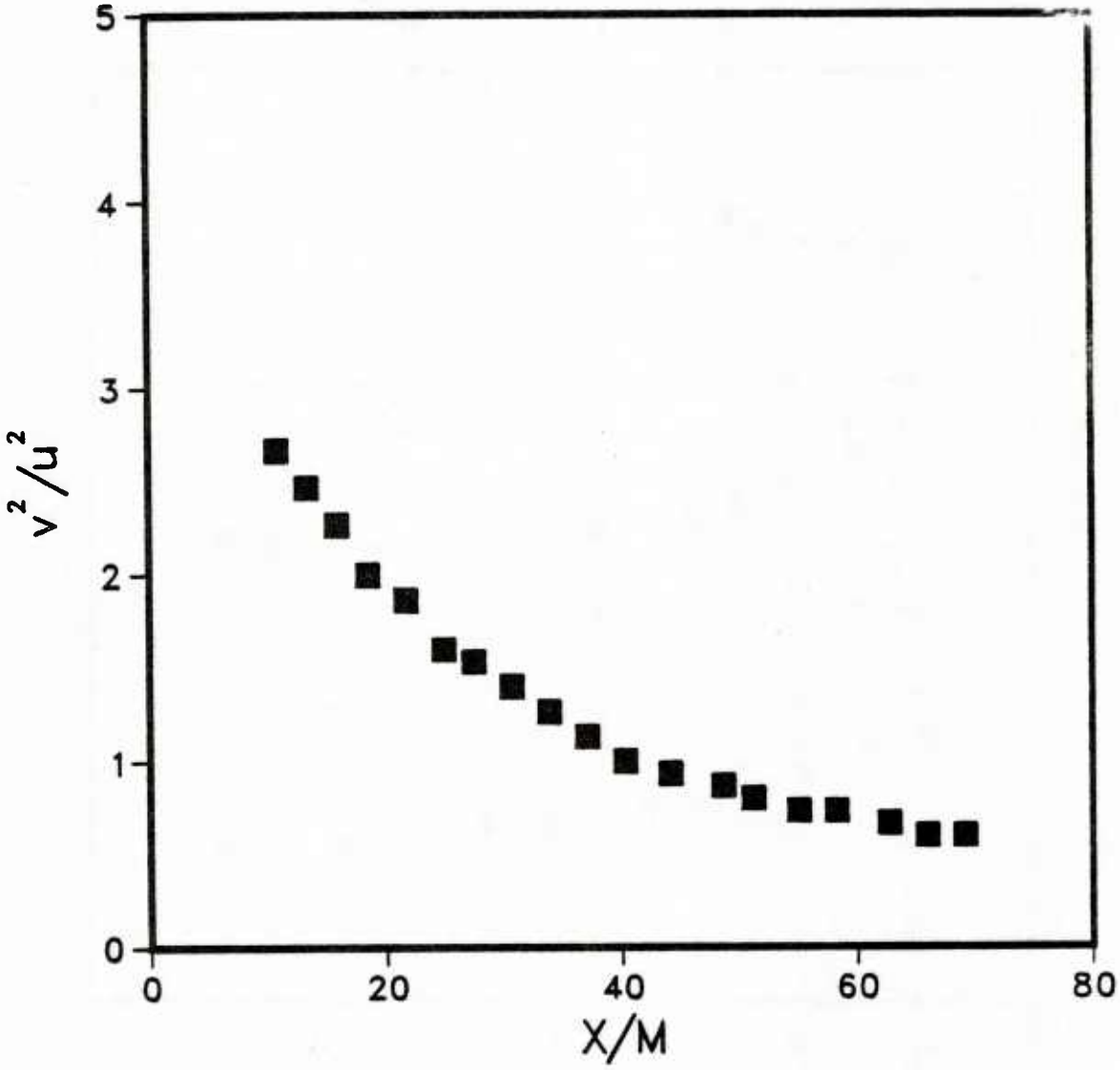

Figure 2.6. Experimental data of Uberoi.

Next, C_2 is obtained from experimental data of homogeneous shear flow. Figure 2.5 shows the values of k, $\overline{u^2}$, $\overline{v^2}$ and $\overline{w^2}$ for such a flow. The modelled Reynolds stress equation (2.10) for $\overline{u^2}$ becomes

$$0 = 0 - 2\overline{uv}\frac{\partial U}{\partial y} - \frac{2}{3}\varepsilon - C_1\frac{\varepsilon}{k}(\overline{u^2} - \frac{2}{3}k) - C_2(2 - \frac{2}{3})\overline{uv}\frac{\partial U}{\partial y}$$

The k-equation (2.11) becomes

$$0 = 0 - \overline{uv}\frac{\partial U}{\partial y} - \varepsilon$$

From figure 2.5, at x/H=10,

$$(\overline{u^2} - \frac{2}{3}k)/k = 0.22$$

Substituting the above value and ε in the $\overline{u^2}$ equation gives

$$4(1 - C_2)/3C_1 = 0.22$$

For C_1=2.8, C_2 is found to be approximately 0.54. The commonly used values of C_1 and C_2 are 2.3 and 0.4.

2.4.3 C_{T1} and C_{T2}

For these coefficients, the experimental data of homogeneous shear flow with a temperature gradient obtained by Webster [22] is used. The modelled equation for $\overline{u_i\theta}$ is

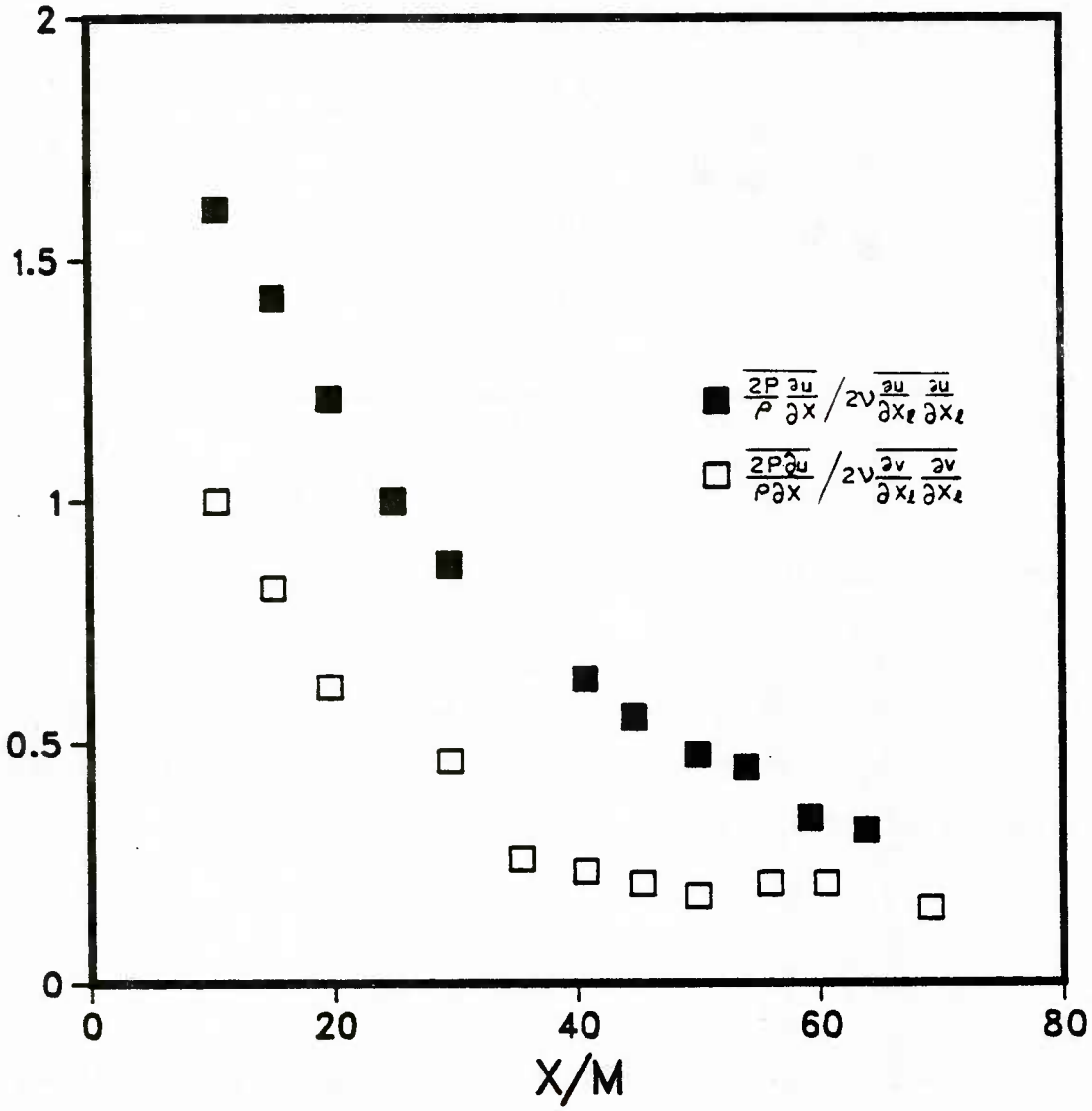

Figure 2.7. Experimental data of Uberoi.

$$\frac{D\overline{u_i\theta}}{Dt} = \frac{\partial}{\partial x_\ell}\left[C_T \frac{k^2}{\varepsilon}\frac{\partial \overline{u_i\theta}}{\partial x_\ell} + \alpha\frac{\partial \overline{u_i\theta}}{\partial x_\ell}\right] - \left[\overline{u_i u_\ell}\frac{\partial T}{\partial x_\ell} + u_\ell\theta\frac{\partial U_i}{\partial x_\ell}\right]$$

$$- C_{T1}\frac{\varepsilon}{k}\overline{u_i\theta} + C_{T2}\frac{\partial U_i}{\partial x_m}\overline{u_m\theta} \qquad (2.13)$$

To determine C_{T1}, i is set to 2. For the homogeneous shear flow, this gives

$$0 = 0 - \left(\overline{v^2}\frac{\partial T}{\partial y} - 0\right) - C_{T1}\frac{\varepsilon}{k}\overline{v\theta}$$

and the k-equation gives

$$0 = 0 - \overline{uv}\frac{\partial U}{\partial y} - \varepsilon$$

Therefore,

$$C_{T1} = -\frac{\overline{v^2}}{\varepsilon}\frac{k}{\overline{v\theta}}\frac{(\partial T/\partial y)}{} = \frac{\overline{v^2}}{\overline{uv}}\frac{k}{\overline{v\theta}}\frac{(\partial T/\partial y)}{(\partial U/\partial y)}$$

From experimental data of Webster as shown in figure 2.8 the magnitude of $\overline{uv}$, $\overline{v^2}$, k and $\overline{v\theta}$ are found to be about 0.5, 1.9, 3.23 and 0.38, respectively. These values are for Richardson number, Ri, of 0 as indicated by the dashed lines, which represent the averaged value of the experimental data. Further, the ratio of the temperature gradient to the velocity gradient is obtained from experimental date to be 0.1. Substituting these values in the above relation, C_{T1} is calculated to be 3.2. Similarly, C_{T2} is found by letting i=1 in the modelled $\overline{u_i\theta}$ equation. This gives

$$0 = 0 - [\overline{uv}\frac{\partial T}{\partial y} + \overline{v\theta}\frac{\partial U}{\partial y}] - C_{T1}\frac{\varepsilon}{k}\overline{u\theta} + C_{T2}\,\overline{v\theta}\frac{\partial U}{\partial y}$$

Again, from experimental data of figure 2.8, $\overline{u\theta}$ is 0.47 at Ri = 0. Hence, C_{T2} is calculated to be 0.5.

2.4.4 C_k, C_ε and C_T

The coefficients C_k, C_ε and C_T are obtained by computer optimization to be 0.9, 2.00 and 0.13 respectively. Several investigators [18] have obtained these constants from experimental data of near wall turbulence. Their values are not used in the present model. Instead, the modified values that give best results are used. However, once the values are determined they are kept constants for all calculations in the present study.

2.5 Concluding remarks

From the above discussion, the 9 turbulent coefficients or constants are determined to be as follows:

C_k=0.9; C_ε=2.00; C_T=0.13

C_1=2.8; $C_{\varepsilon 1}$=17.5/(Re)$^{\frac{1}{2}}$; C_{T1}=3.2

C_2=0.4; $C_{\varepsilon 2}$=18.9/(Re)$^{\frac{1}{2}}$; C_{T2}=0.5

where Re is the Reynolds number based on the problem characteristic velocity and length. These coefficients are determined from different experiments. However, if the turbulence model is to have predictability,

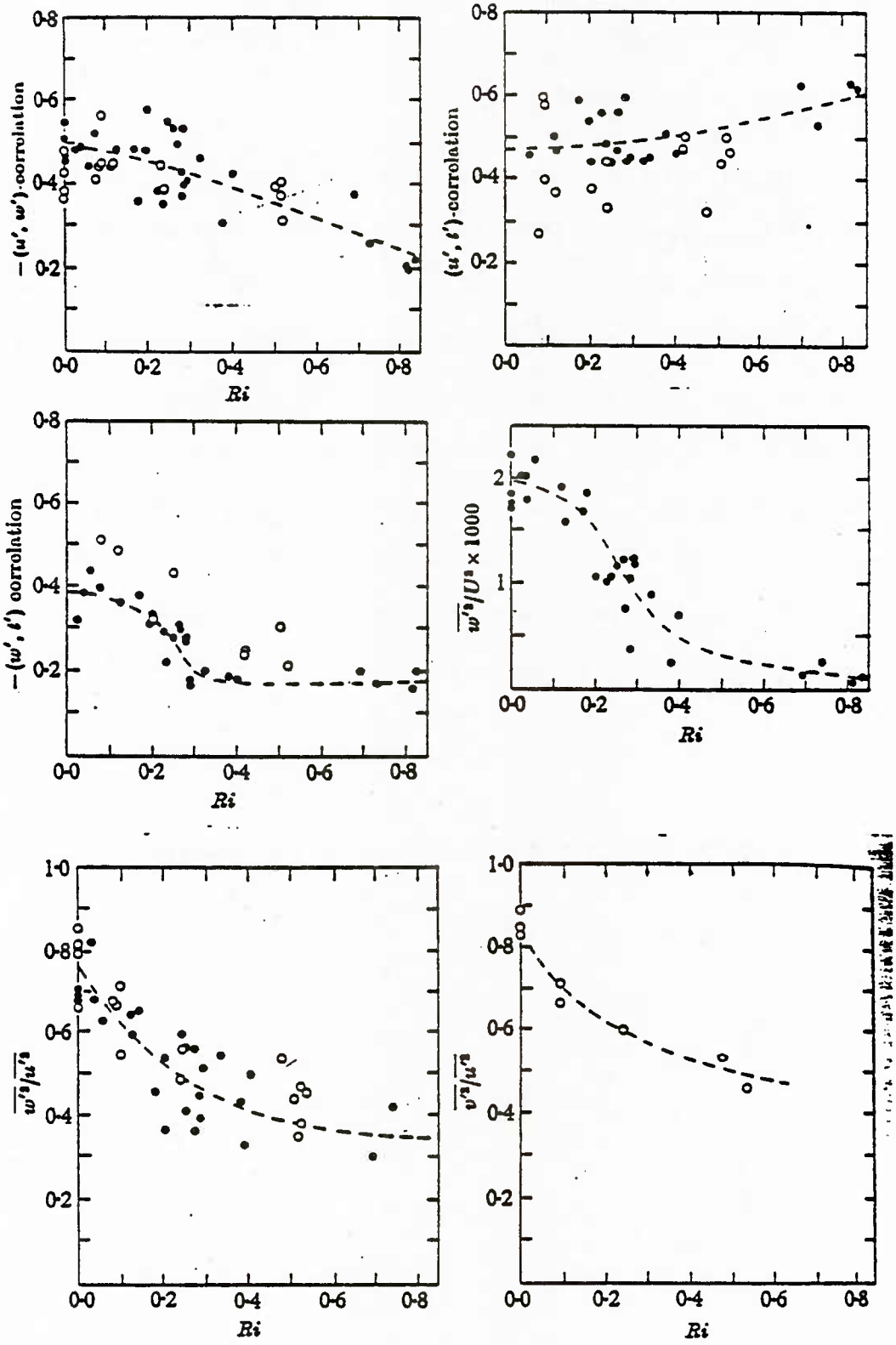

Figure 2.8. Experimental data for homogeneous shear flow (Webster)

the coefficients should remain the same in other turbulent flows. This will be examined in Chapter V.

It should be remarked that Reynolds number appears in the turbulent coefficients for the two-scale turbulence model. This was not the case for the one-scale turbulence model. The appearance of Reynolds number is expected since, as discussed in section 2.2, turbulent flows are still Reynolds number dependent and also because small scale (ν,ε) proposed by Kolmogorov for dissipation of turbulent kinetic energy contains kinematic viscosity. Physically, this implies that Reynolds number changes the magnitude of the destruction of ε and hence affect the magnitude of ε and range of eddy size that is responsible for the dissipating the kinetic energy.

CHAPTER III

TWO SCALE K-Σ-$\overline{\theta^2}$ TURBULENCE MODEL FOR BUOYANT FREE SHEAR FLOWS

Flow patterns in nature are complicated due to change in density caused either by a temperature or concentration difference. The force produced by this variation is called buoyancy force. In this chapter, the two-scale turbulence model derived in the previous chapter for incompressible flow is extended to include turbulent buoyant flows.

3.1 Boussinesq's approximation and governing equations

For flows where the density gradient is not large, the buoyant force can be incorporated into the governing equations by making the Boussinesq approximation. In this approximation [18], the density variation is considered significant only in the gravitational term. In other words, the effect of density difference in the conservation of mass, in the time rate change of momentum and in the work done due to density changes are considered negligible.

The governing equations for such flows are

$$\frac{\partial U_i^*}{\partial x_i} = 0 \tag{3.1}$$

$$\rho_s \frac{DU_i^*}{Dt} = - \frac{\partial P_t^*}{\partial x_i} + \rho^* g_i + \mu \frac{\partial^2 U_i^*}{\partial x_j \partial x_j} \tag{3.2}$$

and

$$\rho_s c \frac{DT^*}{Dt} = K \frac{\partial^2 T^*}{\partial x_j \partial x_j} + \phi^* \tag{3.3}$$

ϕ^* is the heat source due to dissipation by viscous force. c or c_p and K are the specific heat and thermal conductivity. The superscript, *, represents an instantaneous quantity. If P_t^* and ρ^* at the static state ($U_i^*=0$) are P_s and ρ_s, then the momentum equation becomes

$$0 = - \frac{\partial P_s}{\partial x_i} + \rho_s g_i + 0 \tag{3.4}$$

Subtracting the two momentum equations (3.2 and 3.4), we have

$$\rho_s \frac{DU_i^*}{Dt} = - \frac{\partial}{\partial x_i}(P_t^* - P_s) - (\rho^* - \rho_s) g_i + \mu \frac{\partial^2 U_i^*}{\partial x_j \partial x_j} \tag{3.5}$$

With the Boussinesq approximation, the pressure and density relations are given by

$$P^* = P_t^* - P_s; \quad (\rho^* - \rho_s)/\rho_s \simeq - \beta(T^* - T_s) = - \beta \Delta T^*$$

where P^* is the pressure above the static state and T_s is the absolute temperature at the static state. β is the volumetric expansion coefficient or $-1/\beta(\partial\rho/\partial T)_p$ evaluated at T_s, P_s. The governing equations, therefore, become

$$\frac{\partial U_i^*}{\partial x_i} = 0 \tag{3.6}$$

$$\frac{DU_i^*}{Dt} = -\frac{\partial P^*}{\rho_s \partial x_i} - \beta \Delta T^* g_i + \nu \frac{\partial^2 U_i^*}{\partial x_j \partial x_j} \tag{3.7}$$

and

$$\frac{DT^*}{Dt} = \alpha \frac{\partial^2 T^*}{\partial x_j \partial x_j} + \frac{\tau_{ij}^*}{\rho c} \frac{\partial U_i^*}{\partial x_j} \tag{3.8}$$

τ_{ij}^* is the instantaneous viscous stress and α is the thermal diffusivity or $K/\rho_s c$. These equations are exactly the same as the equations for non-buoyant flows except that the momentum equation has an additional buoyancy term $\beta \Delta T^* g_i$. Letting

$$U_i^* = U_i + u_i;\ P^* = P + p;\ \tau_{ij}^* = \tau_{ij} + \tau_{ij}';\ T^* = T + \theta$$

and taking an ensemble average of these equations, the resulting equations obtained are

$$\frac{\partial U_i}{\partial x_i} = 0 \tag{3.9}$$

$$\frac{DU_i}{Dt} = -\frac{\partial P}{\rho \partial_s x_i} - \beta \Delta T g_i + \nu \frac{\partial^2 U_i}{\partial x_j \partial x_j} - \frac{\partial \overline{u_i u_j}}{\partial x_j} \tag{3.10}$$

and

$$\frac{DT}{Dt} = \alpha\frac{\partial^2 T}{\partial x_j \partial x_j} - \frac{\partial \overline{u_i\theta}}{\partial x_i} + \frac{\overline{\tau_{ij}'\frac{\partial u_i}{\partial x_j}}}{\rho_s c} + \frac{\phi}{\rho_s c} \tag{3.11}$$

where

$$\phi = \mu\left(\frac{\partial U_i}{\partial x_j} + \frac{\partial U_j}{\partial x_i}\right)\frac{\partial U_i}{\partial x_j}$$

The term

$$\overline{\left(\tau_{ij}'\frac{\partial u_i}{\partial x_j} + \phi\right)}$$

may be considered as frictional heating due to the fluctuating and mean flow motion. This is normally small in turbulent buoyant flows and can be omitted in most of buoyant flow studies. The above equations have terms $\overline{u_i u_j}$ and $\overline{u_i\theta}$ which need to be modelled. The equations for $\overline{u_i u_j}$, k, ε and $\overline{u_i\theta}$ are obtained in the same way as those in chapter II. The final form of these equations is

$$\frac{D\overline{u_i u_j}}{Dt} = \frac{\partial}{\partial x_\ell}\left[-\overline{u_i u_j u_\ell} - \overline{\frac{p}{\rho_s}(\delta_{ij}u_i + \delta_{i\ell}u_j)} + \nu\frac{\partial \overline{u_i u_j}}{\partial x_\ell}\right] - \beta\left[g_i\overline{u_j\theta} + g_j\overline{u_i\theta}\right]$$

$$-\left[\overline{u_i u_\ell}\frac{\partial U_j}{\partial x_\ell} + \overline{u_j u_\ell}\frac{\partial U_i}{\partial x_\ell}\right] - 2\nu\overline{\frac{\partial u_i}{\partial x_\ell}\frac{\partial u_i}{\partial x_\ell}} + \overline{\frac{p}{\rho_s}\left(\frac{\partial u_i}{\partial x_j} + \frac{\partial u_j}{\partial x_i}\right)} \tag{3.12}$$

$$\frac{D\overline{u_i\theta}}{Dt} = \frac{\partial}{\partial x_\ell}\left[\overline{-u_\ell u_i\theta} - \delta_{i\ell}\frac{\overline{p\theta}}{\rho_s} + \alpha\overline{u_\ell\frac{\partial\theta}{\partial x_\ell}} + \nu\overline{\theta\frac{\partial u_i}{\partial x_\ell}}\right] - \beta g_i\theta^2$$

$$-\left(\overline{u_i u_\ell}\frac{\partial T}{\partial x_\ell} + \overline{u_\ell\theta}\frac{\partial U_i}{\partial x_\ell}\right) - (\alpha+\nu)\overline{\frac{\partial u_i}{\partial x_\ell}\frac{\partial\theta}{\partial x_\ell}} + \overline{\frac{p}{\rho}\frac{\partial\theta}{\partial s x_i}} + \frac{1}{\rho_s c}\overline{\phi' u_i} \tag{3.13}$$

$$\frac{Dk}{Dt} = \frac{\partial}{\partial x_\ell}[-\overline{u_\ell\left(\frac{u_i u_i}{2} + \frac{p}{\rho_s}\right)} + \nu\frac{\partial k}{\partial x_\ell}] - \overline{u_i u_\ell}\frac{\partial U_i}{\partial x_\ell} - \beta g_i \overline{u_i\theta} - \varepsilon \qquad (3.14)$$

$$\frac{D\varepsilon}{Dt} = \frac{\partial}{\partial x_\ell}[-\nu\overline{u_\ell\frac{\partial u_i}{\partial x_j}\frac{\partial u_i}{\partial x_j}} - \overline{\frac{2\nu}{\rho_s}\frac{\partial u_\ell}{\partial x_j}\frac{\partial p}{\partial x_j}} + \nu\frac{\partial \varepsilon}{\partial x_\ell}] - 2\nu\frac{\partial U_i}{\partial x_j}[\overline{\frac{\partial u_\ell}{\partial x_i}\frac{\partial u_\ell}{\partial x_j}} + \overline{\frac{\partial u_i}{\partial x_\ell}\frac{\partial u_j}{\partial x_\ell}}]$$

$$-2\nu\overline{u_\ell\frac{\partial u_i}{\partial x_\ell}\frac{\partial^2 U_i}{\partial x_\ell \partial x_j}} - 2\nu\overline{\frac{\partial u_i}{\partial x_j}\frac{\partial u_i}{\partial x_\ell}\frac{\partial u_j}{\partial x_\ell}} - 2[\nu\overline{\frac{\partial^2 u_i}{\partial x_\ell \partial x_\ell}}]^2 - 2\beta g_i \nu\overline{\frac{\partial u_i}{\partial x_j}\frac{\partial \theta}{\partial x_j}} \qquad (3.15)$$

where

$$P_k = -\overline{u_i u_1}\frac{\partial U_i}{\partial x_1}$$

and

$$\phi' = \mu[(\frac{\partial u_i}{\partial x_j} + \frac{\partial u_j}{\partial x_i})\frac{\partial U_i}{\partial x_j} + (\frac{\partial U_i}{\partial x_j} + \frac{\partial U_j}{\partial x_i})\frac{\partial u_i}{\partial x_j} + (\frac{\partial u_i}{\partial x_j} + \frac{\partial u_j}{\partial x_i})\frac{\partial u_i}{\partial x_j}]$$

In equations (3.12) and (3.14), each of the terms $-\beta(g_i\overline{u_j\theta} + g_j\overline{u_i\theta})$ and $-\beta g_i\overline{u_i\theta}$ is called the buoyancy production and is a new source term in the budget of Reynolds stress and turbulent kinetic energy. The turbulent heat flux $\rho c\overline{u_i\theta}$ now assumes an additional role, because it participates in the production terms for both k and $\overline{\theta^2}$. In the $\overline{u_i\theta}$ equation above, the new term due to buoyancy is $\beta g_i\overline{\theta^2}$ which needs to be modelled as it is an additional unknown. To model it, a transport equation for $\overline{\theta^2}$ is next derived. This equation is obtained by multiplying the equation for θ by 2θ and taking the ensemble average. This results in

$$\frac{D\overline{\theta^2}}{Dt} = \frac{\partial}{\partial x_\ell}\left[- \overline{u_i\theta^2} + \alpha\frac{\partial\overline{\theta^2}}{\partial x_\ell}\right] - 2\overline{u_\ell\theta}\frac{\partial T}{\partial x_\ell} - 2\alpha\overline{\frac{\partial\theta}{\partial x_\ell}\frac{\partial\theta}{\partial x_\ell}} + \frac{1}{\rho c}\overline{\theta\phi'} \qquad (3.16)$$

The quantity $\overline{\theta^2}$ can be considered as the intensity of temperature fluctuation. Thus, $\rho c_p\sqrt{\overline{\theta^2}}$ represents the fluctuating thermal energy. In other words, $\overline{\theta^2}$ is to the turbulent heat flux as k or $\overline{u_iu_i}/2$ is to the turbulent stress. In equation (3.16), the rate of change of $\overline{\theta^2}$ is controlled by turbulent and molecular transport of $\overline{\theta^2}$ (the first two terms on the right hand side of the equation), the gradient production (which is like the production term of turbulent kinetic energy), by molecular dissipation (α is the thermal diffusivity) and the frictional heating (the last term).

The molecular dissipation of temperature fluctuation (the fourth term on RHS of equation (3.16)) is similar to the dissipation of turbulent kinetic energy, ε. This term, $\overline{\alpha(\partial\theta/\partial x_1)(\partial\theta/\partial x_1)}$, is denoted by ε_θ, in analogy with ε, and represents the dissipation of the temperature fluctuation $\overline{\theta^2}$ or the fluctuating thermal energy. ε_θ is an unknown and, therefore, an empirical relation or a transport equation similar to ε-equation is needed to solve it. Here, the transport equation for ε_θ is derived by differentiating equation (2.5) with respect to x_i, then multiplying it by $2\alpha(\partial\theta/\partial x_1)$ and taking the average. This gives

$$\frac{D\varepsilon_\theta}{Dt} = \frac{\partial}{\partial x_\ell}\left[- \overline{\varepsilon_\theta' u_\ell} + \alpha\frac{\partial\varepsilon_\theta}{\partial x_\ell}\right] - 2\alpha\frac{\partial U_1}{\partial x_i}\overline{\frac{\partial\theta}{\partial x_\ell}\frac{\partial\theta}{\partial x_\ell}} - 2\alpha\frac{\partial T}{\partial x_i}\overline{\frac{\partial\theta}{\partial x_i}\frac{\partial u_\ell}{\partial x_i}}$$

$$- 2\alpha\overline{\frac{\partial u_\ell}{\partial x_i}\frac{\partial\theta}{\partial x_i}\frac{\partial\theta}{\partial x_\ell}} - 2\overline{\left[\alpha\frac{\partial^2\theta}{\partial x_\ell\partial x_i}\right]^2} + 2\alpha\overline{\frac{\partial\phi'}{\partial x_i}\frac{\partial\theta}{\partial x_i}} \qquad (3.17)$$

It should be noted that ε_θ appears only in the $\overline{\theta^2}$-equation and hence plays a less important role than ε-equation in the determination of the mean flow quantities such as U_i, P and T. For this reason some researchers [23] employed a simpler, empirical relation to model the behaviour of ε_θ to minimize the complexity in turbulence modelling. This will be discussed in more detail later. For buoyant flows, the terms $\overline{u_i\theta}$ appear in both $\overline{u_iu_j}$ and k equations and so the turbulent momentum transfer and thermal energy transfer are now coupled.

All nonbouyant terms are modelled the same as before in chapter II and so only the modelling of the buoyant terms is given in the next section.

3.2 Turbulence model

In equation (3.12) for $\overline{u_iu_j}$, the only term that requires additional modelling is the pressure strain term. To model this term, the divergence of equation for fluctuating velocity, which is equation (3.7) subtracted from equation (3.10), is taken to give

$$\frac{\nabla^2 p}{\rho_s} = -\left[\frac{\partial^2(\overline{u_\ell u_m} - u_\ell u_m)}{\partial x_\ell \partial x_m} + 2\frac{\partial U_\ell}{\partial x_m}\frac{\partial u_m}{\partial x_\ell} + \beta g_\ell \frac{\partial \theta}{\partial x_\ell}\right] \tag{3.18}$$

Using Green's theorem, pressure is obtained to be

$$\frac{p}{\rho_s} = \frac{1}{4\pi}\int_{vol}\left[\frac{\partial^2(\overline{u_\ell u_m} - u_\ell u_m)}{\partial x_1 \partial x_m} + 2\frac{\partial U_\ell}{\partial x_m}\frac{\partial u_m}{\partial x_\ell} + \beta g_\ell \frac{\partial \theta}{\partial x_\ell}\right]\frac{dvol}{r}$$

$$+ \frac{1}{\pi}\int_s\left[\frac{P}{\rho_s}\frac{\partial}{\partial x}\left(\frac{1}{r}\right) + \frac{1}{r}\frac{\partial}{\partial x}\left(\frac{P}{\rho_s}\right)\right]ds \qquad (3.19)$$

where the surface integral, the second term on the right side, is negligible for flows far away from the solid wall. Thus, when the volume of integration is sufficiently large, the pressure strain term in equation (3.12) becomes

$$\overline{\frac{p}{\rho_s}\left(\frac{\partial u_i}{\partial x_j} + \frac{\partial u_j}{\partial x_i}\right)} = \frac{1}{4\pi}\int_{vol}\overline{\left[\frac{\partial^2(\overline{u_\ell u_m} - u_\ell u_m)}{\partial x_\ell \partial x_m} + 2\frac{\partial U_\ell}{\partial x_m}\frac{\partial u_m}{\partial x_\ell} + \beta g_\ell \frac{\partial \theta}{\partial x_\ell}\right]^*}$$

$$\overline{\left(\frac{\partial u_i}{\partial x_j} + \frac{\partial u_j}{\partial x_i}\right)}\frac{dvol}{r}$$

$$= \phi_{ij,1} + \phi_{ij,2} + \phi_{ij,3} \qquad (3.20)$$

The superscript * denotes the term involving the integration variable. Here $\phi_{ij,1}$, $\phi_{ij,2}$ and $\phi_{ij,3}$ correspond respectively to the first, second and third terms in the volume integral. The reason for dividing it into 3 parts is that the pressure strain is caused by the fluctuating strain rate, $\phi_{ij,1}$, the mean strain rate, $\phi_{ij,2}$, and buoyancy, $\phi_{ij,3}$. The modelling of terms $\phi_{ij,1}$ and $\phi_{ij,2}$ is the same as before and is

$$\phi_{ij,1} + \phi_{ij,2} = -C_1\frac{\varepsilon}{k}\left(\overline{u_i u_j} - \frac{2}{3}\delta_{ij}k\right) - C_2\left(P_{ij} - \frac{2}{3}\delta_{ij}P_k\right)$$

where

$$P_{ij} = -\overline{u_i u_l}\frac{\partial U_j}{\partial x_l} \quad \text{and} \quad P_k = -\overline{u_i u_l}\frac{\partial U_i}{\partial x_l}$$

The third term, which is a new term related to the the buoyancy, is modelled as [20]

$$\phi_{ij,3} = \frac{1}{4\pi} \int \beta g_\ell \overline{\frac{\partial \theta^*}{\partial x_\ell}\left(\frac{\partial u_i}{\partial x_j} + \frac{\partial u_j}{\partial x_i}\right)} \frac{dvol}{r}$$

$$= C_3[\beta g_j \overline{u_i\theta} + \beta g_i \overline{u_j\theta} - \frac{2}{3}\beta g_i \overline{u_i\theta}]$$

$$= - C_3[P_{ij,b} - \frac{2}{3}\delta_{ij} P_b]$$

where

$$P_{ij,b} = - \beta g_j \overline{u_i\theta} - \beta g_i \overline{u_j\theta}$$

and

$$P_b = - \beta g_i \overline{u_i\theta}$$

The RHS of this equation is the return-to-isotropy part due to buoyancy and is similar to $\phi_{ij,1}$, which is the return-to-isotropy due to velocity fluctuation. These models are obtained by contracting the volume to a small value and ensuring that when the flow is approximately incompressible or i=j the pressure strain is zero. Hence the modelled $\overline{u_i u_j}$-equation is

$$\frac{D\overline{u_i u_j}}{Dt} = \frac{\partial}{\partial x_\ell}[C_k \frac{k^2}{\varepsilon} \frac{\partial \overline{u_i u_j}}{\partial x_\ell} + \nu \frac{\partial \overline{u_i u_j}}{\partial x_\ell}] - P_{ij} - P_{ij,b} - \frac{2}{3}\delta_{ij}\varepsilon \qquad (3.21)$$

$$- C_1 \frac{\varepsilon}{k}[\overline{u_i u_j} - \frac{2}{3}\delta_{ij} k] - C_2[P_{ij} - \frac{2}{3}\delta_{ij} P_k] - C_3[P_{ij,b} - \frac{2}{3}\delta_{ij} P_b]$$

The modelled k-equation can be directly obtained from the above equation by substituting i=j and summing to give

$$\frac{Dk}{Dt} = \frac{\partial}{\partial x_\ell}\left[C_k \frac{k^2}{\varepsilon}\frac{\partial k}{\partial x_\ell} + \nu\frac{\partial k}{\partial x_\ell}\right] - \overline{u_i u_\ell}\frac{\partial U_i}{\partial x_\ell} - \beta g_i \overline{u_i \theta} - \varepsilon \qquad (3.22)$$

It should be remarked here that except the first term on the right side of equation (3.22), which is modelled, every other term in the equation is exact. In modelling the ε-equation (3.15), the new gravitational term $2\beta g_i \overline{\nu(\partial u_i/\partial x_j)\ (\partial\theta/\partial x_j)}$ is set approximately equal to zero due to the postulation of isotropic dissipation for small eddies. However, the destruction terms, the last two terms in equation (3.15), are modelled based on the two-scale concept to include the influence of buoyancy. This is based on Lumley's assumption that the destruction term is

$$-2\nu\overline{\frac{\partial u_i}{\partial x_j}\frac{\partial u_i}{\partial x_\ell}\frac{\partial u_j}{\partial x_\ell}} - 2\overline{\left[\nu\frac{\partial^2 u_i}{\partial x_\ell \partial x_\ell}\right]^2} = \text{Constant} * \left[\frac{\varepsilon}{t}\right]\left[\frac{\text{Prod of k}}{\varepsilon} - 1\right]$$

Here the production of k comprises of both production due to shear force, P_k, and buoyant force, P_b, in equation (3.22) and t is the time scale of destruction. Thus, based on the two scale turbulence model concept

$$-2\nu\overline{\frac{\partial u_i}{\partial x_j}\frac{\partial u_i}{\partial x_\ell}\frac{\partial u_j}{\partial x_\ell}} - 2\overline{\left[\nu\frac{\partial^2 u_i}{\partial x_\ell \partial x_\ell}\right]^2} = \text{Constant} * \left[\frac{1}{t}\right][P_k + P_b - \varepsilon]$$

$$= \text{Constant} * (\varepsilon/\nu)^{\frac{1}{2}}[P_k + P_b - \varepsilon]$$

where

$$P_k = -\overline{u_i u_i}\,\frac{\partial U_i}{\partial x_\ell} \quad \text{and} \quad P_b = -\beta g_i \overline{u_i \theta}$$

Here, again the time scale, t, is based on Kolmogorov scale and not the convective scale (k,ε) for large eddies. Therefore, the final modelled ε-equation is

$$\frac{D\varepsilon}{Dt} = \frac{\partial}{\partial x_\ell}\left[C_\varepsilon \frac{k^2}{\varepsilon}\frac{\partial \varepsilon}{\partial x_\ell} + \nu\frac{\partial \varepsilon}{\partial x_\ell}\right] - C_{\varepsilon 1}(\varepsilon/\nu)^{\frac{1}{2}}\overline{u_i u_j}\,\frac{\partial U_i}{\partial x_\ell}$$

$$- C_{\varepsilon 2}(\varepsilon/\nu)^{\frac{1}{2}}\varepsilon + C_{\varepsilon 3}(\varepsilon/\nu)^{\frac{1}{2}}P_b \qquad (3.23)$$

The exact $\overline{u_i\theta}$-equation is

$$\frac{D\overline{u_i\theta}}{Dt} = \frac{\partial}{\partial x_\ell}\left[-\overline{u_\ell u_i \theta} - \delta_{i\ell}\overline{\frac{P\theta}{\rho}} + \alpha u_\ell \overline{\frac{\partial \theta}{\partial x_\ell}} + \nu\,\overline{\theta\frac{\partial u_i}{\partial x_\ell}}\right] - \beta g_i \overline{\theta^2}$$

$$-\left(\overline{u_i u_\ell}\frac{\partial T}{\partial x_\ell} + \overline{u_\ell \theta}\frac{\partial U_i}{\partial x_\ell}\right) - (\alpha+\nu)\overline{\frac{\partial u_i}{\partial x_\ell}\frac{\partial \theta}{\partial x_\ell}} + \overline{\frac{P}{\rho}\frac{\partial \theta}{\partial x_i}} + \frac{1}{\rho c}\overline{\phi' u_i} \qquad (3.24)$$

The last term in equation (3.24) is the frictional contribution to $\overline{u_i\theta}$ which is normally small and will be omitted in the study. The only term that requires additional modelling when buoyancy prevails in equation (3.24) is the pressure strain term which is obtained by multiplying equation (3.19) by $\partial\theta/\partial x_j$ and taking an average, or

$$\overline{\frac{p}{\rho}\frac{\partial \theta}{\partial x_i}} = \frac{1}{4\pi}\int_{vol}\left[\overline{\frac{\partial^2 u_\ell^* u_m^*}{\partial x_\ell \partial x_m}\frac{\partial \theta}{\partial x_i}} + 2\frac{\partial U_m^*}{\partial x_m}\overline{\frac{\partial u_m^*}{\partial x_\ell}\frac{\partial \theta}{\partial x_i}} - \beta g_\ell \overline{\frac{\partial \theta^*}{\partial x_\ell}\frac{\partial \theta}{\partial x_i}}\right]\frac{dvol}{r} \qquad (3.25)$$

Shrinking the integral to a small volume, this term may be approximately set equal to

$$\overline{\frac{p}{\rho}\frac{\partial\theta}{\partial x_i}} = \text{Const} * \left[\overline{\frac{\partial^2 u_\ell u_m}{\partial x_\ell \partial x_m}\frac{\partial\theta}{\partial x_i}} + 2\frac{\partial U_m}{\partial x_m}\overline{\frac{\partial u_m}{\partial x_\ell}\frac{\partial\theta}{\partial x_i}} - \beta g_\ell \overline{\frac{\partial\theta}{\partial x_\ell}\frac{\partial\theta}{\partial x_i}}\right]\ell^2$$

$$= - C_{T1}\frac{\varepsilon}{k}\overline{u_i\theta} + C_{T2}\frac{\partial U_i}{\partial x_m}\overline{u_m\theta} - C_{T3}\beta g_i\overline{\theta^2}$$

Hence, the modelled $\overline{u_i\theta}$-equation is

$$\frac{D\overline{u_i\theta}}{Dt} = \frac{\partial}{\partial x_\ell}\left[C_T\frac{k^2}{\varepsilon}\frac{\partial\overline{u_i\theta}}{\partial x_\ell} + \alpha\frac{\partial\overline{u_i\theta}}{\partial x_\ell}\right] - \left[\overline{u_i u_\ell}\frac{\partial T}{\partial x_\ell} + \overline{u_\ell\theta}\frac{\partial U_i}{\partial x_\ell}\right]$$

$$- C_{T1}\frac{\varepsilon}{k}\overline{u_i\theta} + C_{T2}\frac{\partial U_i}{\partial x_m}\overline{u_m\theta} - (1 + C_{T3})\beta g_i\overline{\theta^2} \qquad (3.26)$$

The $\overline{\theta^2}$-equation in exact form is

$$\frac{D\overline{\theta^2}}{Dt} = \frac{\partial}{\partial x_\ell}\left[-\overline{u_i\theta^2} + \alpha\frac{\partial\overline{\theta^2}}{\partial x_\ell}\right] - 2\overline{u_\ell\theta}\frac{\partial T}{\partial x_\ell} - 2\alpha\overline{\frac{\partial\theta}{\partial x_\ell}\frac{\partial\theta}{\partial x_\ell}} + \frac{1}{\rho c}\overline{\theta\phi'} \qquad (3.27)$$

The diffusion term is modelled according to postulate 2 in the principle of modelling outlined in chapter II to be

$$-\overline{u_\ell\theta^2} = C_\theta\frac{k^2}{\varepsilon}\frac{\partial\overline{\theta^2}}{\partial x_\ell}.$$

Letting the friction term, $\overline{\phi'\theta}$, to be negligible, the modelled $\overline{\theta^2}$-equation is

$$\frac{D\overline{\theta^2}}{Dt} = \frac{\partial}{\partial x_\ell}\left[\left(C_\theta\frac{k^2}{\varepsilon} + \nu\right)\frac{\partial\overline{\theta^2}}{\partial x_\ell}\right] - 2\overline{u_\ell\theta}\frac{\partial T}{\partial x_\ell} - 2\varepsilon_\theta \qquad (3.28)$$

It should be remarked that the ε_θ term in the above equation is an unknown and can be modelled by an empirical relation such as equation (3.28a) based on Launder's suggestion [20] or by solving a transport equation. For most practical cases, it is sufficient to use such a simple empirical relation by assuming that ε_θ is a function of ε or

$$\varepsilon_\theta = C_{\theta 1} \frac{\overline{\theta^2}}{k} \varepsilon \tag{3.28a}$$

where $C_{\theta 1}$ is a dimensionless constant and $\overline{\theta^2}/k$ is required to make the dimension consistent. For more rigorous modelling, the exact equation for ε_θ can be derived as

$$\frac{D\varepsilon_\theta}{Dt} = \frac{\partial}{\partial x_\ell}\left[- \overline{\varepsilon_\theta' u_\ell} + \alpha \frac{\partial \varepsilon_\theta}{\partial x_\ell}\right] - 2\alpha \frac{\partial U_\ell}{\partial x_i} \overline{\frac{\partial \theta}{\partial x_i} \frac{\partial \theta}{\partial x_\ell}} - 2\alpha \frac{\partial T}{\partial x_i} \overline{\frac{\partial \theta}{\partial x_i} \frac{\partial u_\ell}{\partial x_i}}$$

$$- 2\alpha \overline{\frac{\partial u_\ell}{\partial x_i} \frac{\partial \theta}{\partial x_i} \frac{\partial \theta}{\partial x_\ell}} - \overline{2\left[\alpha \frac{\partial^2 \theta}{\partial x_\ell \partial x_i}\right]^2} + 2\alpha \overline{\frac{\partial \phi'}{\partial x_i} \frac{\partial \theta}{\partial x_i}} \tag{3.29}$$

The diffusion term is modelled as

$$- \overline{\varepsilon_\theta' u_\ell} = C_e \frac{k^2}{\varepsilon} \frac{\partial \varepsilon_\theta}{\partial x_\ell}$$

The production term is small due to isotropic dissipation and incompressibility. Hence,

$$\alpha \frac{\partial U_\ell}{\partial x_i} \overline{\frac{\partial \theta}{\partial x_i} \frac{\partial \theta}{\partial x_\ell}} = 0$$

The terms

$$\overline{\alpha\frac{\partial\theta}{\partial x_i}\frac{\partial u_\ell}{\partial x_i}} \quad \text{and} \quad \overline{\alpha\frac{\partial\phi'}{\partial x_i}\frac{\partial\theta}{\partial x_i}}$$

are also small due to isotropic dissipation. The destruction term is modelled based on Lumley's assumption. Thus

$$-2\alpha\overline{\frac{\partial u_\ell}{\partial x_i}\frac{\partial\theta}{\partial x_i}\frac{\partial\theta}{\partial x_\ell}} - 2\overline{[\alpha\frac{\partial^2\theta}{\partial x_\ell\partial x_i}]^2} = \text{Constant} * [\frac{\varepsilon_\theta}{t}][\frac{\text{Prod of } \overline{\theta^2}}{\varepsilon_\theta} - 1]$$

In the present investigation of the two-scale turbulence model, the time scale in the above equation is taken to be that of the destruction term in the ε-equation namely that of Kolmogorov scale $[t] = (\nu/\varepsilon)^{\frac{1}{2}}$. Destruction of ε_θ is modelled as

$$-2\alpha\overline{\frac{\partial u_\ell}{\partial x_i}\frac{\partial\theta}{\partial x_i}\frac{\partial\theta}{\partial x_\ell}} - 2\overline{[\alpha\frac{\partial^2\theta}{\partial x_\ell\partial x_i}]^2} = -C_{e1}(\varepsilon/\nu)^{\frac{1}{2}}\overline{u_\ell\theta}\frac{\partial T}{\partial x_\ell} - C_{e2}(\varepsilon/\nu)^{\frac{1}{2}}\varepsilon_\theta$$

Therefore, the modelled ε_θ equation is

$$\frac{D\varepsilon_\theta}{Dt} = \frac{\partial}{\partial x_\ell}[(C_e\frac{k^2}{\varepsilon} + \nu)\frac{\partial\varepsilon_\theta}{\partial x_\ell}] - C_{e1}(\varepsilon/\nu)^{\frac{1}{2}}\overline{u_\ell\theta}\frac{\partial T}{\partial x_\ell} - C_{e2}(\varepsilon/\nu)^{\frac{1}{2}}\varepsilon_\theta \qquad (3.30)$$

Summarizing the complete two-scale turbulence model for buoyant flows, the equations for the turbulent quantities are

$$\frac{D\overline{u_iu_j}}{Dt} = \frac{\partial}{\partial x_\ell}[C_k\frac{k^2}{\varepsilon}\frac{\partial\overline{u_iu_j}}{\partial x_\ell} + \nu\frac{\partial\overline{u_iu_j}}{\partial x_\ell}] - P_{ij} - P_{ij,b} - \frac{2}{3}\delta_{ij}\varepsilon \qquad (3.21)$$

$$- C_1\frac{\varepsilon}{k}[\overline{u_iu_j} - \frac{2}{3}\delta_{ij}k] - C_2[P_{ij} - \frac{2}{3}\delta_{ij}P_k] - C_3[P_{ij,b} - \frac{2}{3}\delta_{ij}P_b]$$

$$\frac{Dk}{Dt} = \frac{\partial}{\partial x_\ell}\left[C_k \frac{k^2}{\varepsilon}\frac{\partial k}{\partial x_\ell} + \nu\frac{\partial k}{\partial x_\ell}\right] - \overline{u_i u_\ell}\frac{\partial U_i}{\partial x_\ell} - \beta g_i \overline{u_i \theta} - \varepsilon \tag{3.22}$$

$$\frac{D\varepsilon}{Dt} = \frac{\partial}{\partial x_\ell}\left[C_\varepsilon \frac{k^2}{\varepsilon}\frac{\partial \varepsilon}{\partial x_\ell} + \nu\frac{\partial \varepsilon}{\partial x_\ell}\right] - C_{\varepsilon 1}(\varepsilon/\nu)^{\frac{1}{2}}\overline{u_i u_j}\frac{\partial U_i}{\partial x_\ell}$$

$$- C_{\varepsilon 2}(\varepsilon/\nu)^{\frac{1}{2}}\varepsilon + C_{\varepsilon 3}(\varepsilon/\nu)^{\frac{1}{2}}P_b \tag{3.23}$$

$$\frac{D\overline{u_i\theta}}{Dt} = \frac{\partial}{\partial x_\ell}\left[C_T \frac{k^2}{\varepsilon}\frac{\partial \overline{u_i\theta}}{\partial x_\ell} + \alpha\frac{\partial \overline{u_i\theta}}{\partial x_\ell}\right] - \left[\overline{u_i u_\ell}\frac{\partial T}{\partial x_\ell} + \overline{u_\ell \theta}\frac{\partial U_i}{\partial x_\ell}\right]$$

$$- C_{T1}\frac{\varepsilon}{k}\overline{u_i\theta} + C_{T2}\frac{\partial U_i}{\partial x_m}\overline{u_m\theta} - (1 + C_{T3})\beta g_i \overline{\theta^2} \tag{3.26}$$

$$\frac{D\overline{\theta^2}}{Dt} = \frac{\partial}{\partial x_\ell}\left[\left(C_\theta \frac{k^2}{\varepsilon} + \nu\right)\frac{\partial \overline{\theta^2}}{\partial x_\ell}\right] - 2\overline{u_\ell\theta}\frac{\partial T}{\partial x_\ell} - 2\varepsilon_\theta \tag{3.28}$$

$$\frac{D\varepsilon_\theta}{Dt} = \frac{\partial}{\partial x_\ell}\left[\left(C_e \frac{k^2}{\varepsilon} + \nu\right)\frac{\partial \varepsilon_\theta}{\partial x_\ell}\right] - C_{e1}(\varepsilon/\nu)^{\frac{1}{2}}\overline{u_\ell\theta}\frac{\partial T}{\partial x_\ell} - C_{e2}(\varepsilon/\nu)^{\frac{1}{2}}\varepsilon_\theta \tag{3.30}$$

In addition to incompressible turbulent flow equation for $\overline{u_i u_j}$, k, ε and $\overline{u_i\theta}$, two additional equations for $\overline{\theta^2}$ and ε_θ are needed in the buoyant flows. Also, in addition to 9 turbulent coeffecients C_k, C_1, C_2, C_ε, $C_{\varepsilon 1}$, $C_{\varepsilon 2}$, C_T, C_{T1} and C_{T2} needed for nonbuoyant flows, 6 more coefficients are needed in the turbulent buoyant flow prediction, namely, C_3, $C_{\varepsilon 3}$, C_{T3}, C_e, C_{e1} and C_{e2}.

3.3 Governing Equations for turbulent free shear flows with buoyancy

For two-dimensional turbulent free shear flows, the above governing equations can be simplified considerably. The assumptions made in obtaining turbulent free shear flow equations are

1. Diffusion in the direction normal (y coordinate) the flow is much larger than the diffusion in the direction parallel (x coordinate) to the flow.
2. Pressure gradient is small in the flow.
3. Laminar shear stress is much smaller than the turbulent shear stress.
4. Boussinesq approximation applies.
5. Frictional heating is negligible.

With these assumptions, the mean equations (3.9), (3.10) and (3.11) for turbulent Shear flows under Boussinesq approximation are

$$\frac{\partial U}{\partial x} + \frac{\partial V}{\partial y} = 0 \tag{3.31}$$

$$U\frac{\partial U}{\partial x} + V\frac{\partial U}{\partial y} = -\frac{1}{y^j}\frac{\partial}{\partial y}[y^j\overline{uv}] + g\frac{T - T_a}{T_a} \tag{3.32}$$

and

$$U\frac{\partial T}{\partial x} + V\frac{\partial T}{\partial y} = -\frac{1}{y^j}\frac{\partial}{\partial y}[y^j\overline{v\theta}] \tag{3.33}$$

where T_a is the ambient temperature. j=0 for plane flows and j=1 for axisymmetric flows. Equations for the turbulent quantities reduced from equations (3.21), (3.22), (3.23) and (3.26) with the x-direction aligned to the gravitational vector.

$$U\frac{\partial\overline{uv}}{\partial x} + V\frac{\partial\overline{uv}}{\partial y} = \frac{1}{y^j}\frac{\partial}{\partial y}[y^j C_k \frac{k\overline{v^2}}{\varepsilon}\frac{\partial\overline{uv}}{\partial y}] - \overline{uv}\frac{\partial U}{\partial y} - \beta g\overline{v\theta}$$
$$- C_1\frac{\varepsilon}{k}\overline{uv} + C_2\overline{uv}\frac{\partial U}{\partial y} + C_3 g\overline{u\theta}\beta \qquad (3.34)$$

$$U\frac{\partial k}{\partial x} + V\frac{\partial k}{\partial y} = \frac{1}{y^j}\frac{\partial}{\partial y}[y^j C_k \frac{k\overline{v^2}}{\varepsilon}\frac{\partial k}{\partial y}] - \overline{uv}\frac{\partial U}{\partial y} + g\frac{\overline{u\theta}}{T_a} - \varepsilon \qquad (3.35)$$

$$U\frac{\partial\varepsilon}{\partial x} + V\frac{\partial\varepsilon}{\partial y} = \frac{1}{y^j}\frac{\partial}{\partial y}[y^j C_\varepsilon \frac{k\overline{v^2}}{\varepsilon}\frac{\partial k}{\partial y}] + C_{\varepsilon 1}(\varepsilon/\nu)^{\frac{1}{2}}(-\overline{uv}\frac{\partial U}{\partial y})$$
$$+ C_{\varepsilon 3}(\varepsilon/\nu)^{\frac{1}{2}} g\frac{\overline{u\theta}}{T_a} - C_{\varepsilon 2}(\varepsilon/\nu)^{\frac{1}{2}}\varepsilon \qquad (3.36)$$

$$U\frac{\partial\overline{u\theta}}{\partial x} + V\frac{\partial\overline{u\theta}}{\partial y} = \frac{1}{y^j}\frac{\partial}{\partial y}[y^j C_T \frac{k\overline{v^2}}{\varepsilon}\frac{\partial\overline{u\theta}}{\partial y}] - \overline{uv}\frac{\partial T}{\partial y} - \overline{v\theta}\frac{\partial U}{\partial y}$$
$$- C_{T1}\frac{\varepsilon}{k}\overline{u\theta} + C_{T2}\overline{v\theta}\frac{\partial U}{\partial y} + g\frac{(1 - C_{T3})}{T_a}\overline{\theta^2} \qquad (3.37)$$

$$U\frac{\partial\overline{\theta^2}}{\partial x} + V\frac{\partial\overline{\theta^2}}{\partial y} = \frac{1}{y^j}\frac{\partial}{\partial y}[y^j C_\theta \frac{k\overline{v^2}}{\varepsilon}\frac{\partial\overline{\theta^2}}{\partial y}] - 2\overline{v\theta}\frac{\partial T}{\partial y} - C_{\theta 1}\frac{\varepsilon\overline{\theta^2}}{k} \qquad (3.38)$$

It should be remarked that since the term $\overline{\theta^2}$ appears in equation (3.37), a transport equation for $\overline{\theta^2}$ is used. In equation (3.38) an approximation for ε_θ, as suggested by Launder in equation (3.28a), is made so that an equation for ε_θ is not required.

It is necessary to solve all the above equations to complete the prediction of turbulent buoyant shear flows. However, a considerable amount of computational effort would be required to solve the whole set of equations. Therefore, some simplifying assumptions are further made to reduce the number of differential equations to be solved. One such assumption is to neglect the convective and diffusive transport terms of $\overline{u_i u_j}$ and $\overline{u_i \theta}$ equations. This leads to the following approximated algebraic relations for the $\overline{uv}$, $\overline{v^2}$, $\overline{v\theta}$, $\overline{u\theta}$ and $\overline{\theta^2}$ terms.

$$-\overline{uv} = \frac{1 - C_2}{C_1} \frac{\overline{v^2}}{k} \left[1 + \frac{kg(\partial T/\partial y)}{C_{T1}\varepsilon T_a(\partial U/\partial y)}\right]\frac{k^2}{\varepsilon}\frac{\partial U}{\partial y} \tag{3.39}$$

$$\overline{v^2} = C_2 k \tag{3.40}$$

$$-\overline{v\theta} = \frac{1}{C_{T1}} \frac{\overline{v^2}}{k}\frac{k^2}{\varepsilon}\frac{\partial T}{\partial y} \tag{3.41}$$

$$\overline{u\theta} = \frac{k}{C_{T1}\varepsilon}\left[-\overline{uv}\frac{\partial T}{\partial y} - \overline{v\theta}(1 - C_{T2})\frac{\partial U}{\partial y} - g\frac{(1 - C_{T3})}{T_a}\overline{\theta^2}\right] \tag{3.42}$$

$$\overline{\theta^2} = -\frac{k}{C_{\theta 1}\varepsilon}\overline{v\theta}\frac{\partial T}{\partial y} \tag{3.43}$$

In the present investigation, these algebraic equations are solved with two-scale k and ε equations in differential equation form. This simplified turbulence model is known as the two-scale k-ε model and is perhaps most practical model for predicting details of mean motion and turbulent transport properties.

3.4 Determination of coefficients

Most of the coefficients in the above equations have been derived in chapter II and so only the two additional coefficients C_{T3} and $C_{\theta 1}$ required in solving buoyant free shear flows are discussed here.

3.4.1 Coefficient $C_{\theta 1}$

This coefficient is obtained from experimental data of temperature fluctuations behind a grid. Figure 3.1 shows the decay of $\overline{\theta^2}$ measured by Gibson and Schwarz [24]. From this figure, $\overline{\theta^2}$ is found to vary inversely as the three-halves power of distance behind the grid.

For such a flow, the $\overline{\theta^2}$-equation [equation (3.38)] becomes

$$U_o \frac{d\overline{\theta^2}}{dx} = - 2C_{\theta 1}\varepsilon\frac{\overline{\theta^2}}{k} \tag{3.44}$$

Non-dimensionalizing this equation with the variables

$$x' = \frac{x}{M}; \quad k' = \frac{k}{U_o^2}; \quad \varepsilon' = \frac{\varepsilon}{U_o^2/M}; \quad \overline{\theta^{2'}} = \frac{\overline{\theta^2}}{T^2}$$

the following equation is obtained.

$$\frac{d\overline{\theta^{2'}}}{dx'} = - 2C_{\theta 1} \frac{\varepsilon'}{k'}\overline{\theta^{2'}} \tag{3.45}$$

In section 2.4.1, k and ε were found to be

$$k' = \frac{450}{40000}x'^{-1} \quad \text{and} \quad \varepsilon' = \frac{450}{40000}x'^{-2}$$

Further, from figure 3.1, the relation between $\overline{\theta^{2'}}$ and x' is found to be

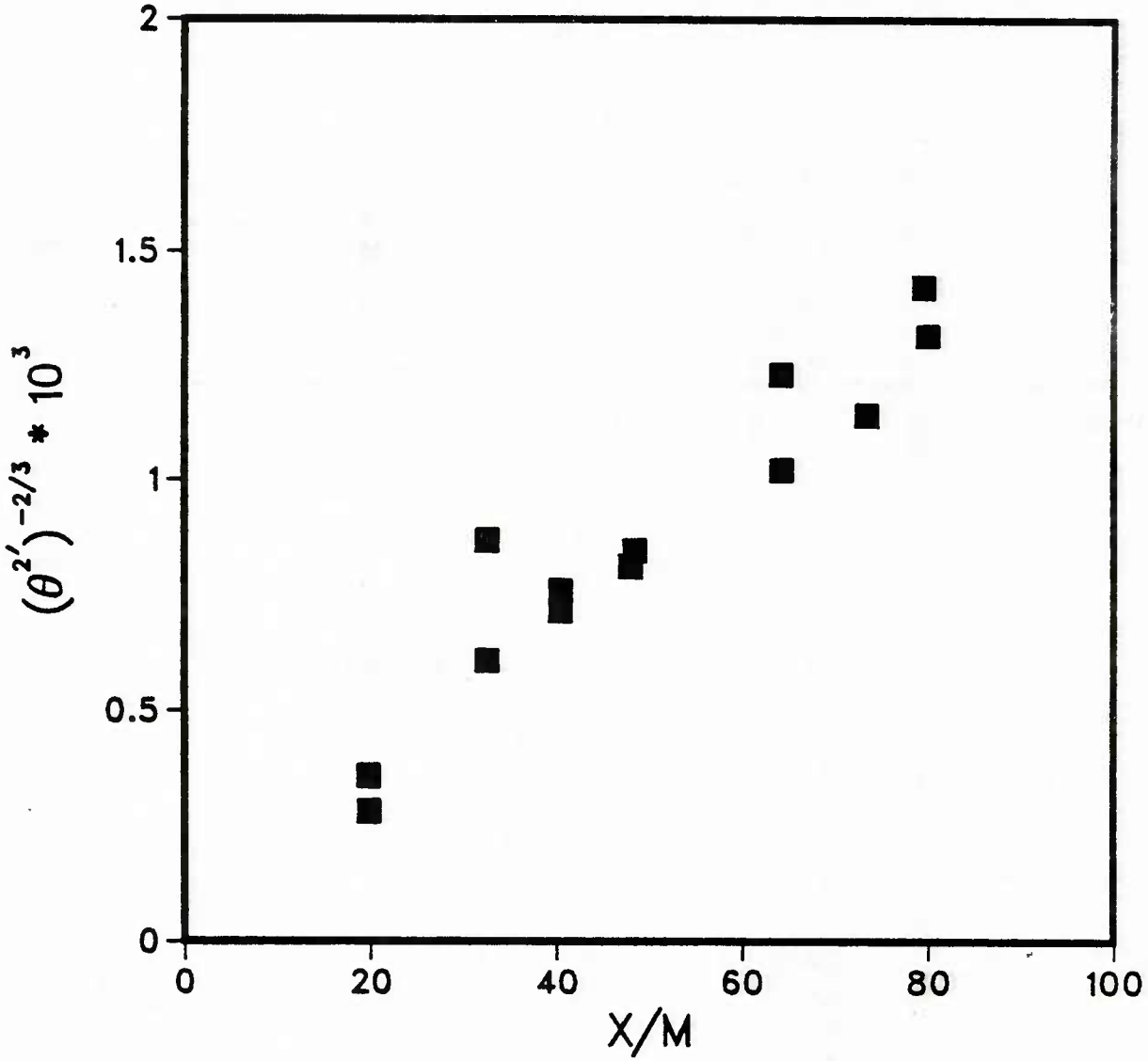

Figure 3.1. Decay of $\overline{\theta^2}$ measured by Gibson et al.

$$\overline{\theta^{2}}' = 3.1x'^{-1.5}$$

Substituting these in equation (3.45) gives

$$-\frac{3}{2}*3.1*x'^{-2.5} = -2C_{\theta 1}\left(\frac{450}{40000}\right)x'^{-2}\left(\frac{40000}{450}\right)x'(3.1*x'^{-1.5})$$

This results in

$$C_{\theta 1} = \frac{3}{4} = 0.75$$

the commonly used value of $C_{\theta 1}$ is 0.62. This is, however, obtained from Launder's assumption in equation (3.28a). In the present investigation, a value of 0.75 will be used.

3.4.2 Coefficient C_{T3}

This coefficient is generally set equal to C_{T2} [20] which has been obtained earlier in chapter II to be 0.5. Hence, a value of 0.5 is used for C_{T3}.

3.5 Concluding remarks

In section 3.3, it was mentioned that due to Launder's argument, the equation for ε_{θ} was replaced by an algebraic relation. Hence, the structure of the turbulent heat flux $\overline{\theta^2}$ is represented by only the (k,ε) scale only. In flow situations, where ε_{θ} might be an important parameter, the need for solving the complete ε_{θ}-equation [equation (3.30)] would be important. This would bring in the influence of the

two-scale concept or the effect of viscous dissipation in the thermal dissipation or destruction ε_θ in the turbulence model.

CHAPTER IV

REVIEW OF EXPERIMENTAL WORK

4.1 General remark

This chapter briefly reviews various experimental data for free shear flows. The types of flows considered are jets, wakes, mixing layers, coaxial jets and buoyant jets. Reliable experimental data are selected for comparison with the predicted solution obtained from the proposed two-scale turbulence model. Table 4.1 shows the definition of the spreading rate, S, for different flows which will be used for comparison later. This rate of spread is a gross parameter independent of the distance x. The symbols used in the definition of S are shown in figure 4.1. In addition to the rate of spread, detail of velocity and other profiles are given in the following section.

4.2 Jets flowing into stagnant surrounding

The gross parameter of importance to the jet flows is the spreading rate, S, which is defined as

$$S = \frac{dy_{\frac{1}{2}}}{dx}$$

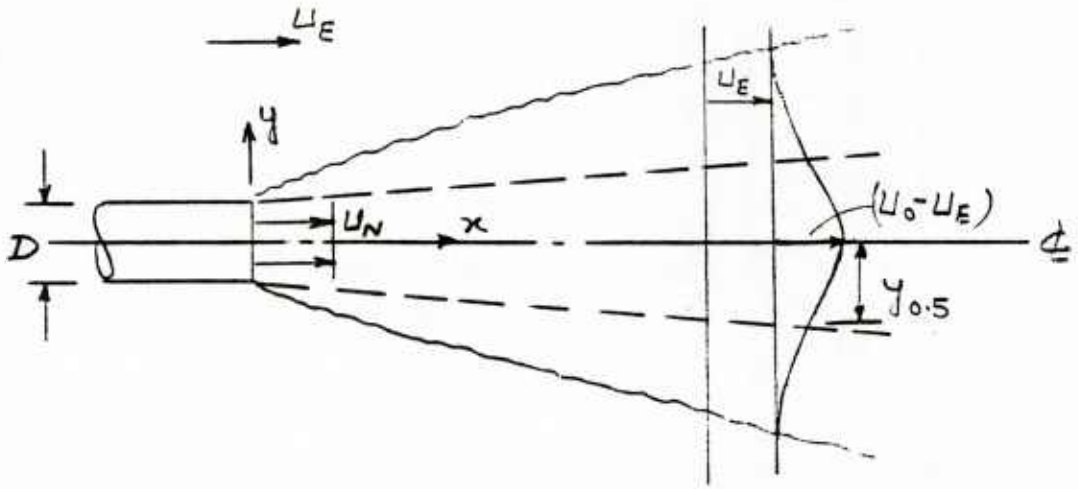

Plane or Round Jet

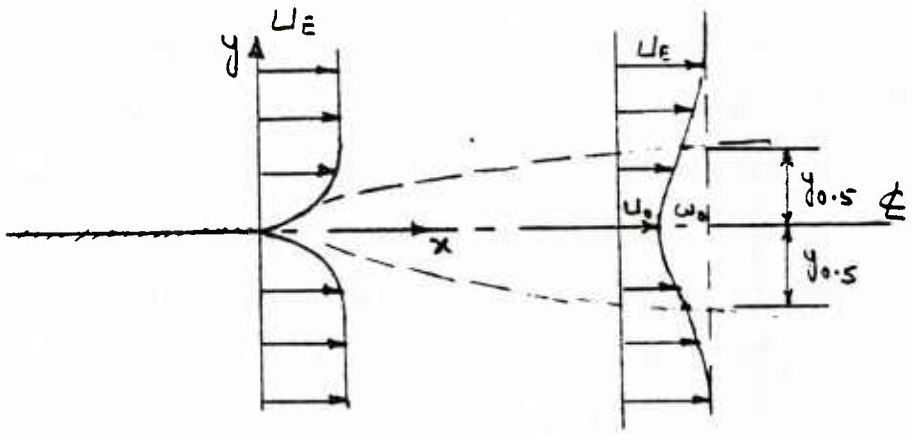

Plane Wake

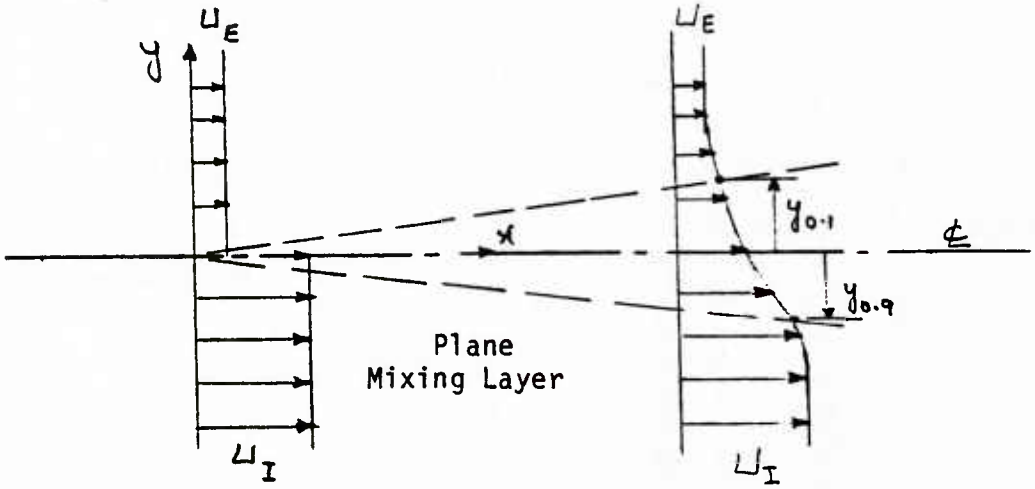

Figure 4.1. Definition of symbols.

Table 4.1

Definition of spreading rate S

Flow	S
Jets	$dy_{\frac{1}{2}}/dx$
Wakes	$(U_E/w_o)[dy_{\frac{1}{2}}/dx]$
Mixing Layers	$d(y_{0.5} - y_{0.9})/dx$

Here, $y_{\frac{1}{2}}$ is the normal distance from the jet axis where the axial component of the velocity is one-half the centerline velocity U_c. The spreading rate S is found to be a constant when the flow becomes self-similar in the far region. The definition of self-similarity or self-preserving is that the profile or distribution of dependent variables are similar from one station to another and become identical when they are made dimensionless by the local reference quantities. It should be remarked that experimentally it is found that although both profiles of the mean flow variables and turbulent transport quantities become similar the former usually occurs first. It is also found that the initial condition at the nozzle exit affects only the near jet region. Therefore, the rate of spread and various profiles far downstream are the same regardless of the inlet conditions.

4.2.1 Plane jet

Table 4.2 summarizes the important flow parameters measured for plane

jet by several investigators [25-29]. The range of experimental data was between 5 and 150 times the nozzle width. In each of the cases, self preservation started at a different location downstream of the nozzle. This could possibly be due to the different initial conditions such as velocity profiles or turbulent intensity level. Nevertheless, the rate of spread, center-line turbulent kinetic energy and the maximum shear stress in the self preserving region obtained by various investigators are about the same. The results of Bradbury [25], however, showed that self-similarity was not reached and the rate of spread continued to increase beyond a distance of 70 nozzle widths. One reason for this was that in Bradbury's experiment the surrounding air was not stagnant. Rodi [4] also found that jets flowing into moving surroundings are only approximately self-similar. However, Bradbury [25] indicated that by reducing the velocity of the surrounding air the velocity and the turbulent kinetic energy do not change appreciably.

Figure 4.2 shows the velocity profile in the self-similar region of a plane jet obtained by Bradbury [25], Heskestad [26], Patel [27], Gutmark [28] and Robins [29]. Except for a small region near the edge of the jet boundary, there is close agreement between all measurements. Hence, it provides a good test for a turbulence model. Figure 4.3 gives the profile of turbulent kinetic energy k in the far region as obtained by various investigators. There is a large amount of scatter in these results. Gutmark's results seem to be inaccurate since some

Table 4.2

Parameters for plane jets

Investigator	Bradbury	Heskestad	Patel	Gutmark	Robins
Nozzle size(cm)	46 * .95	150 * 1.25	80 * .7	50 * .13	--
Range x/D	14-70	47-155	12-152	10-150	5-100
Reynolds number	30,000	4700-37,000	35,000	30,000	10,000-60,000
Self-pres. x/D	30	65+	30	120	60
S	---	0.11	0.103	0.102	0.103
Maximum Reynolds stress	0.026	0.021	0.021	0.024	0.02
Max turb kinetic energy k	0.067	0.07	0.064	0.077	0.064

abnormalities were reported by him in his experiment that the velocity decay had an abrupt change at x/D=65 and the dissipation rate was only 20 % of the production of turbulent kinetic energy. Heskestad's results indicated an increase in the value of $\overline{u_c^2}/U_o^2$ even beyond 160 nozzle widths. Also, Bradbury indicated that his measurements of $\overline{v^2} > \overline{u^2}$ seem physically unlikely. Experimental results of Patel and Robins are also shown for comparison purpose. In general, their measurements are smaller than that of Gutmark, Heskstad and Bradbury. In figure 4.4, Bradbury's measurements of the Reynolds stress are shown at two

different locations. The maximum value of Reynolds stress is 0.026 which is slightly higher than that of other investigators quoted in table 4.2. A plot of the centerline velocity decay along the jet axis is given in figure 4.5 as obtained by Bradbury et al. [30] and Van der Hegge [31]. From this figure, the potential core length or zone of development is estimated to be about 6 times the exit jet width. Bradbury's data shows a lower decay rate than that of Van der Hegge. This slight difference in the two results could be due to different inlet and free stream conditions as it is known that by changing the inlet turbulent kinetic energy, the length of the core will vary.

4.2.2 Round jet

Table 4.3 shows some of the gross parameters obtained by Hetsroni [32], Wygnanski and Fiedler [33], Rodi [4] and Shearer and Faeth [34] for a round jet. The measurements for mean quantities by Hetsroni and by Wygnanski were done up to a distance of x/D=35 and 40 respectively. Shearer measured the flow quantities up to a distance x/D=510 and the measurements were slightly different from the other two investigators. It is, therefore, assumed that the initial condition still has a significant influence on the measurements at x/D=40 and the flow profile may not reach the self-similar condition. Hence, Shearer's results are assumed to be more reasonable. For comparison purposes, the latter result will be used.

The velocity profile is shown in figure 4.6 where there is a small variation between the measurements of Wygnanski and Shearer. The

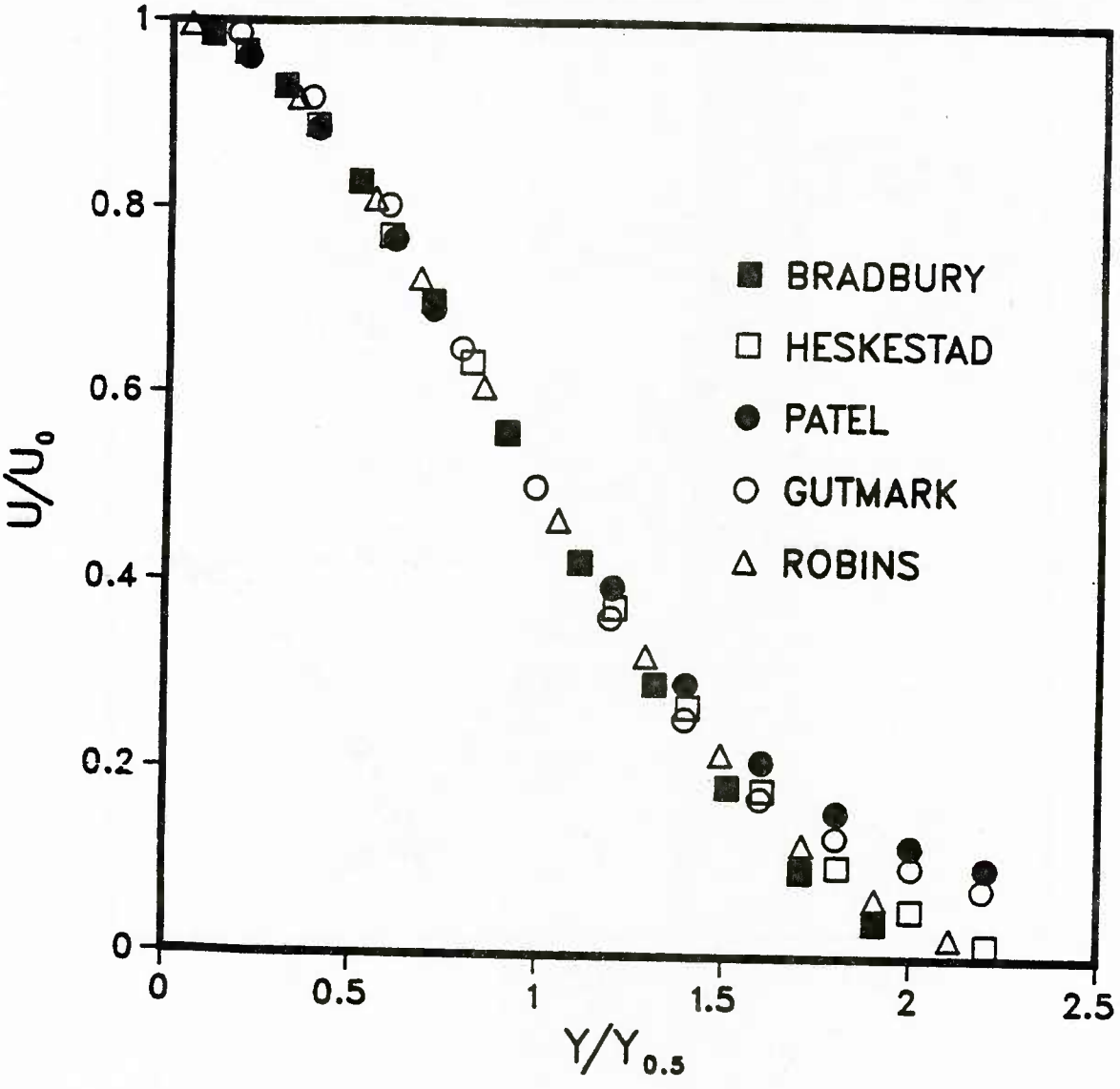

Figure 4.2. Measured velocity profiles in a stagnant plane jet

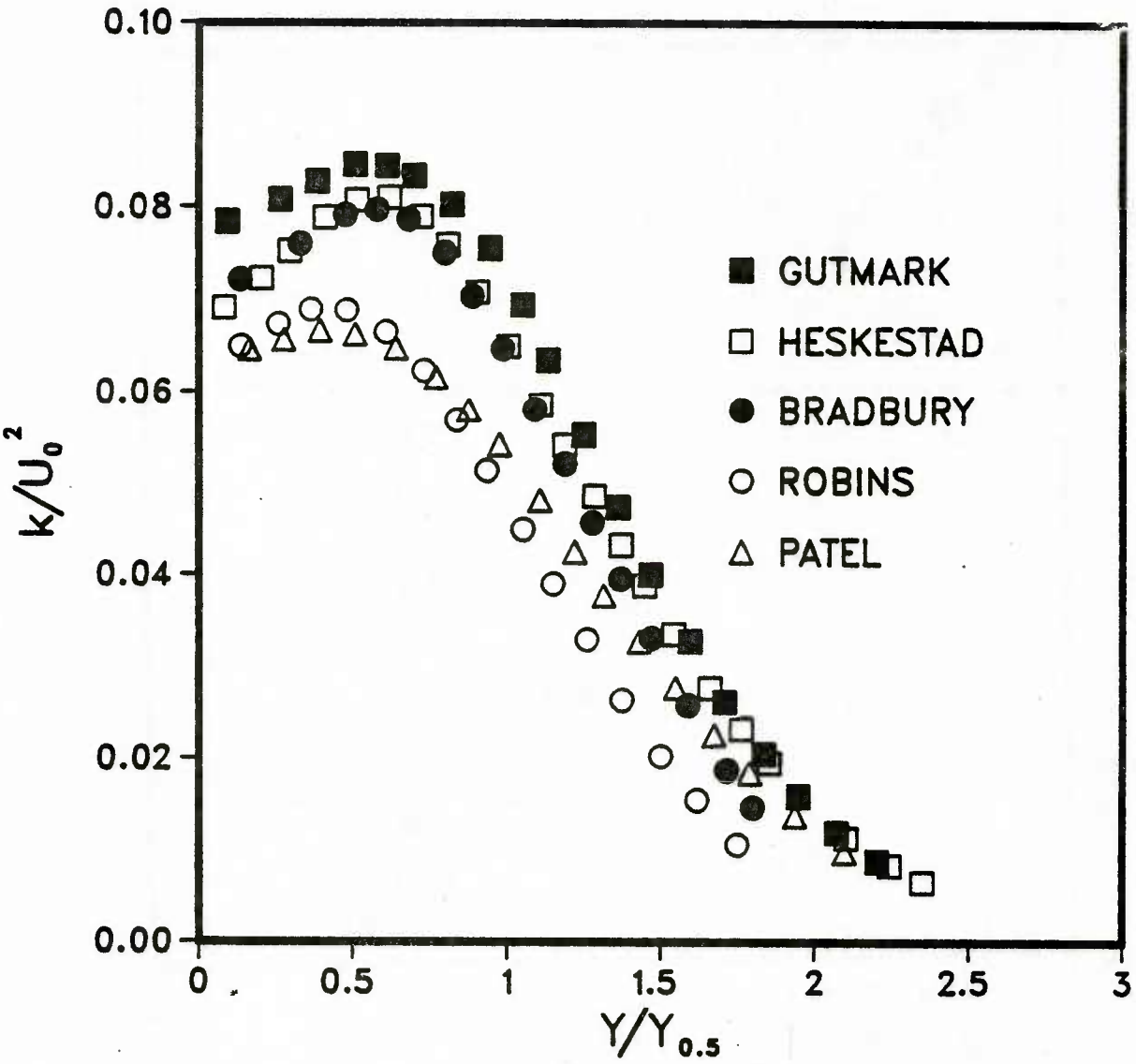

Figure 4.3. Measured k-profiles
in a stagnant plane jet

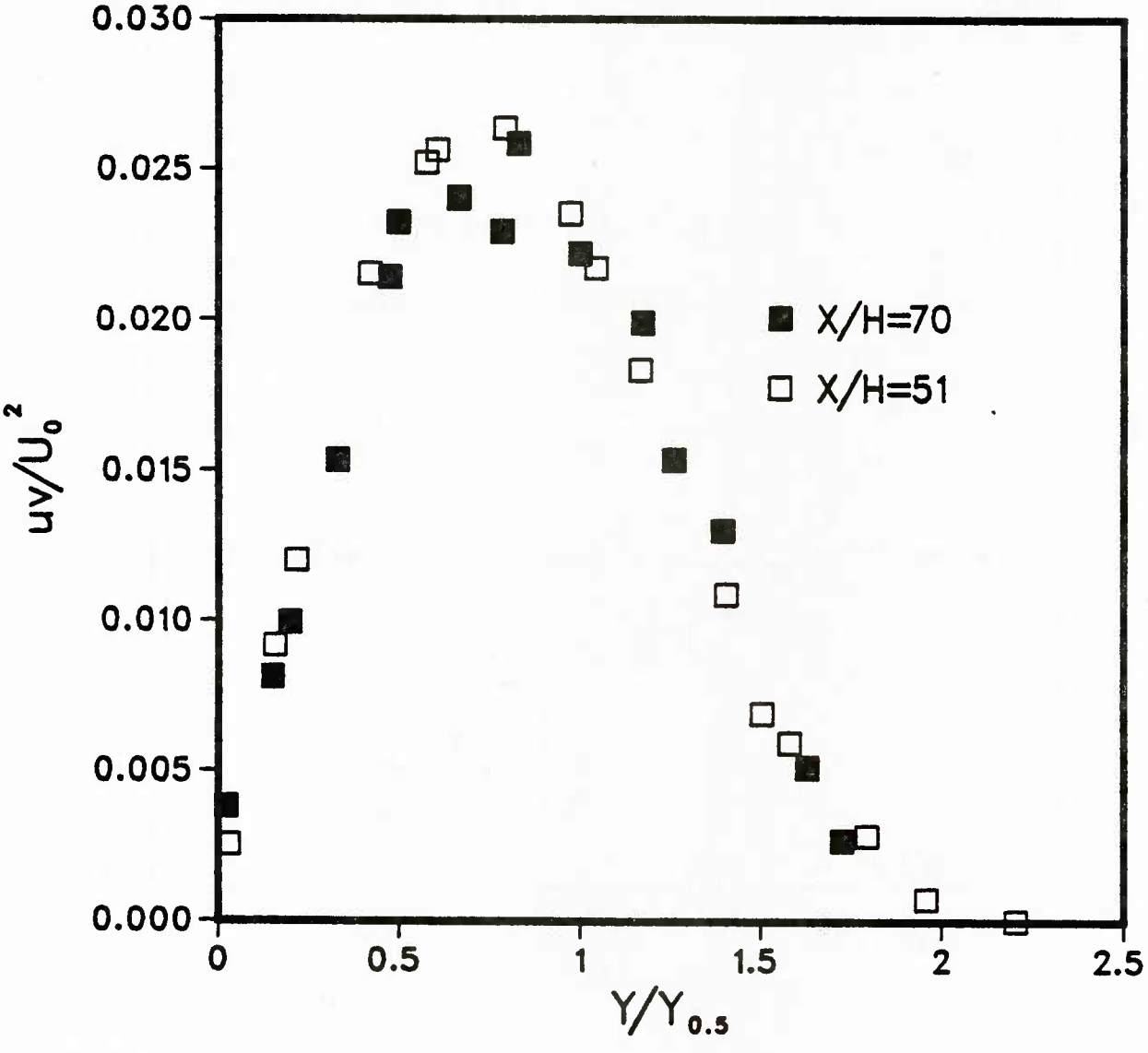

Figure 4.4. Measured Reynolds stress in a stagnant plane jet (Bradbury)

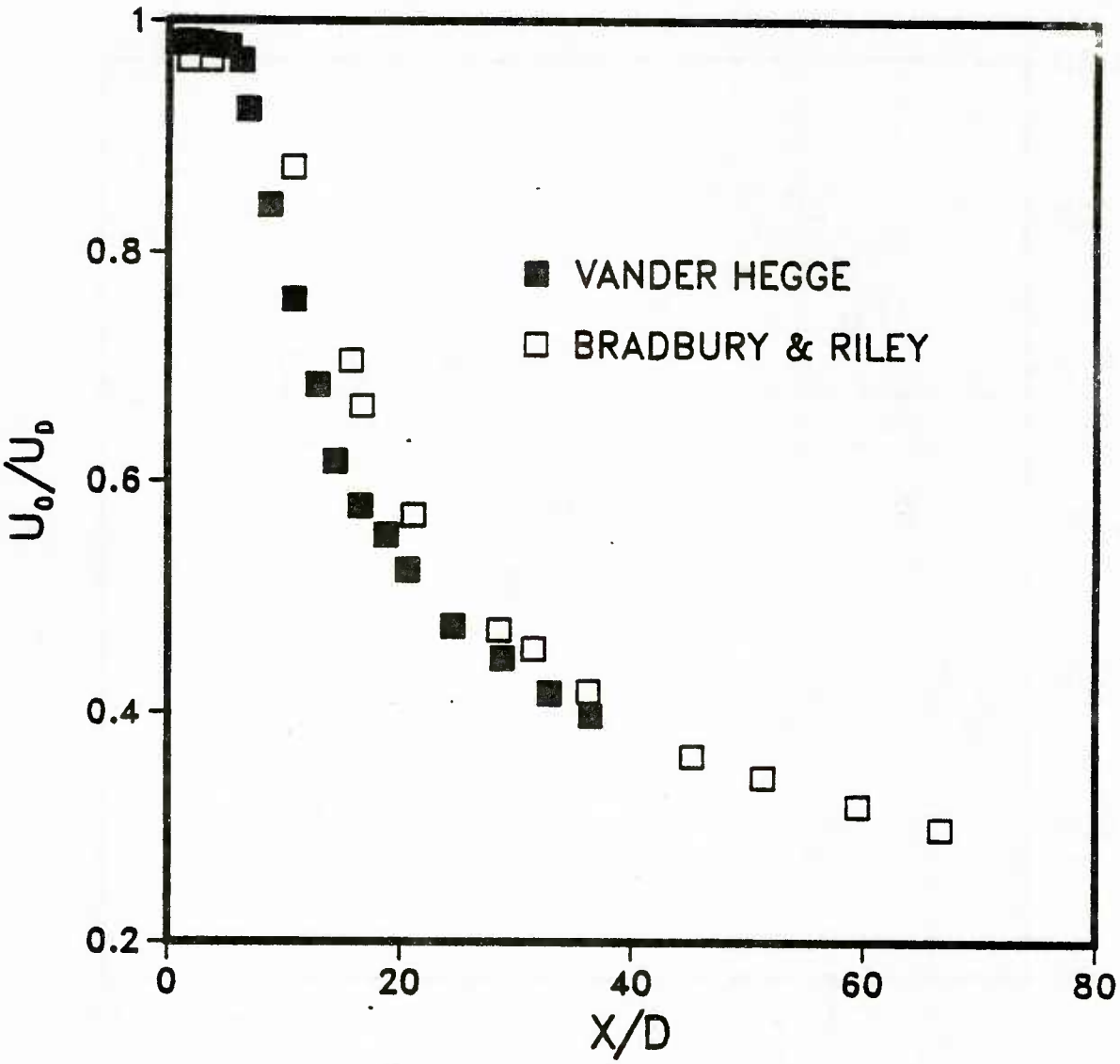

Figure 4.5. Center-line velocity decay in a stagnant plane jet

difference could be explained by the lack of similarity at x/D=40. This discrepency in the result is further amplified in the measurement of the kinetic energy as shown in figure 4.7. Wygnanski and Fiedler obtained a value of 0.1 for the centerline kinetic energy at a distance x/D=40. However, Shearer's measurements indicate a value of 0.08 at x/D=510. This value seems to be more reliable and realistic because the measurements were taken sufficiently far away where the jet is most likely self similar and there is no influence of the inlet conditions. The variation of Reynolds stress is shown in figure 4.8. Here, too, the measurements of Shearer are slightly different from those of Wygnanski whose data is for x/D=60 and 70. Some scatter of data is obvious from the figure. The decay of centerline velocity for a round jet is presented in figure 4.9. Along with the data of Shearer and Wygnanski, the measurements of Corssin [35] are also provided. These data are more agreeable, though the measurements of Shearer start from x/D=50.

4.3 Plane wake

One of the important global parameters for the wake flow is the spreading rate of the wake. The spreading rate for the plane wake, S, is defined as

$$S = \frac{U_E}{w_o} \frac{dy_{\frac{1}{2}}}{dx}$$

Here, $y_{\frac{1}{2}}$ is the normal distance from the symmetry line to the location where the x-component velocity U is $(U_c + U_E)/2$. U_c and U_E are

Table 4.3

Parameters for round jets

Investigator	Hetsroni	Wygnanski	Rodi	Shearer
Nozzle size(cm)	2.5	2.6	1.29	0.1194
Range x/D	15-40	40-98	62-75	170-510
Reynolds number	---	100,000	87,000	---
Self-pres x/D	15	70	62	----
S	0.0713	0.086	0.086	---
Maximum Reynolds stress	---	0.0165	0.0186	0.0195
Max turb kinetic energy k	---	0.101	----	0.078

respectively the velocity at the symmetry line and the free stream line. w_o is the defect velocity or $(U_E - U_c)$.

Extensive measurements have been made, over several decades, in the wakes of two-dimensional bodies. Data is available both in the near wake and far wake regions. The earliest one was by Chevray and Kovasznay [36], who measured the mean velocity and turbulence quantities in the near region of symmetric wake of a flat plate. They measured the spreading rate and obtained a value of 0.062 but this value was still increasing with x. Their spreading rate measurement did not agree well

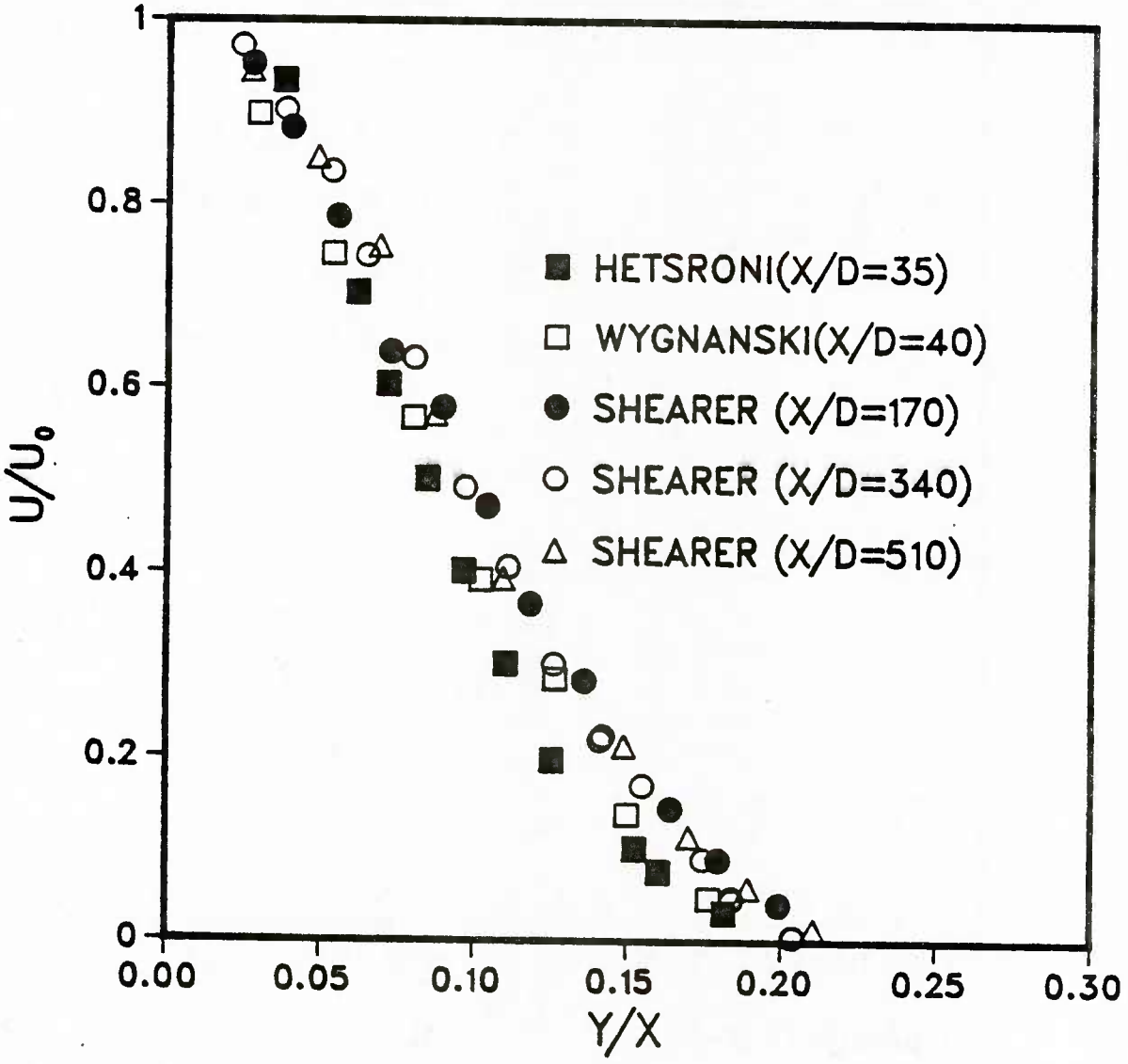

Figure 4.6. Measured velocity profiles in a stagnant round jet

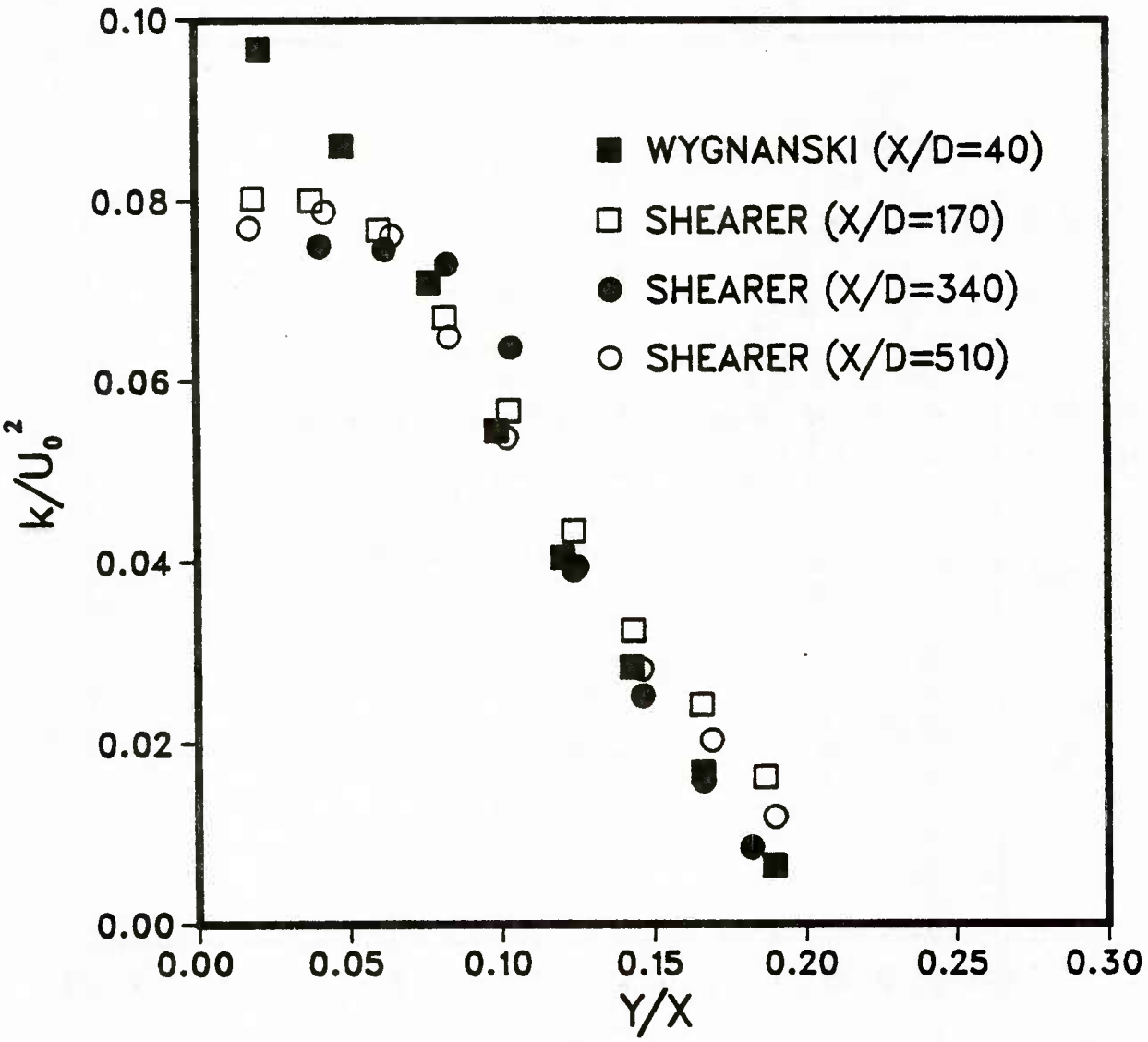

Figure 4.7. Measured k-profiles
in a stagnant round jet

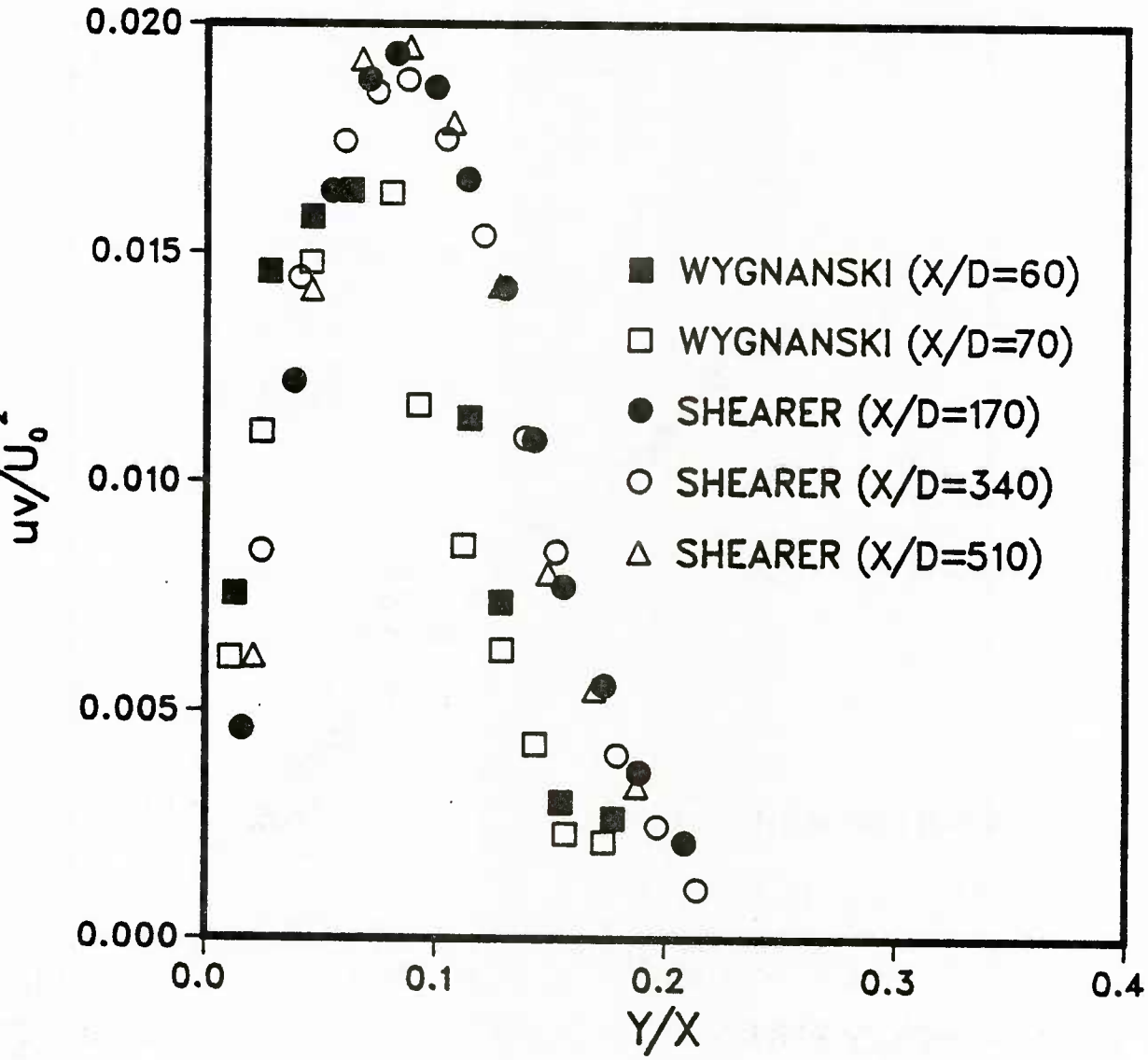

Figure 4.8. Measured Reynolds stress in a stagnant round jet

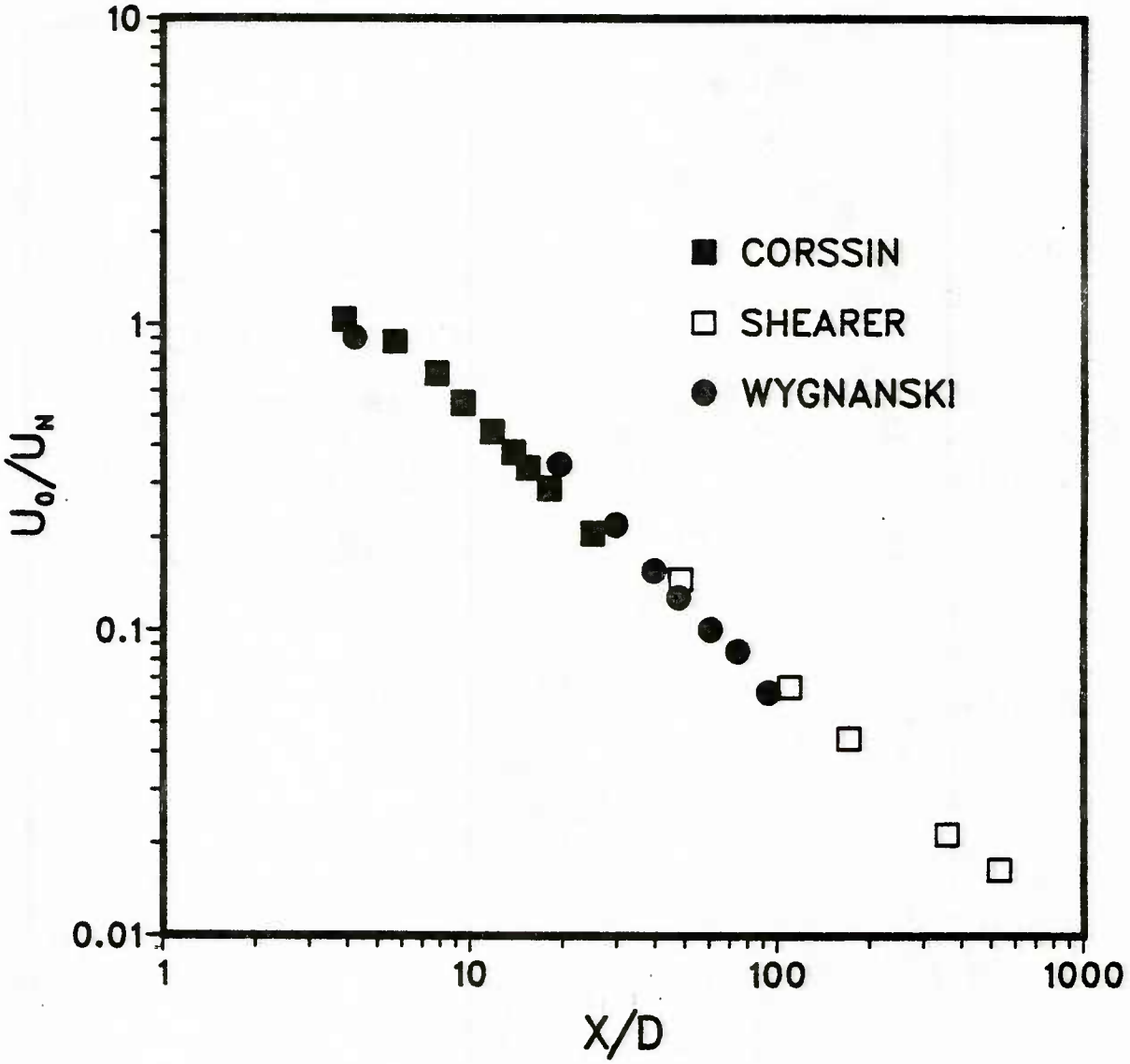

Figure 4.9. Center-line velocity decay in a stagnant round jet

with that of others who obtained values ranging from 0.09 to 0.11. The disagreement is due to the fact that the wake was formed behind a streamlined body which may influence the wake structure. Patel [37] observed that it takes a distance of 300θ for a wake to become self-similar. Therefore, a change in the initial condition at the trailing edge before wake formation could influence the mean and turbulence quantities in the wake region for a considerable distance downstream. A physical explanation for this behaviour is that unlike jet flows the production of turbulent kinetic energy is low in the wake flow and dissipation is high. Therefore, the initial or the upstream conditions for the wake must be accurately prescribed if one hopes for a meaningful comparison between the prediction and measurement. In particular, the turbulent kinetic energy level and the shear stress may be influenced by the initial conditions far downstream.

Comparisons between prediction and measurements were limited to the decay of center-line velocity deficit. However, recent measurements by Andreopoulos [38], Pot [39] and Ramaprian et al. [40] provided abundant experimental data for comparison with the prediction based on turbulence models. The measurements of Andreopoulos and Ramaprian were done in the near wake region while those of Pot were in the asymptotic region for flow past a flat plate. Hence, their data provides a good test for the performance of the two-scale k-ε turbulence model in both the near wake and far wake. Table 4.4 summarizes some of the work done in recent years. Figure 4.10 shows the asymptotic velocity deficit profile

obtained from the asymptotic theory along with the result of Pot. There is a slight difference at the edge of the wake which is probably due to the fact that the flow is not fully turbulent in that region. In figure 4.11, the Reynolds stress profile is shown and compared with the asymptotic solution. Except for a small region near the edge of the boundary layer and around $y/y_{\frac{1}{2}}$ of 0.90 , the solution lies on the data points. The measurement of the centerline velocity deficit variation with x/θ is shown in figure 4.12. θ is the momentum thickness based on the velocity profile at the trailing edge of the flat plate.

Table 4.4

Parameters for plane wake

Investigator	Chevray Kovaszny	Ramaprian et al.	Andreo polous	Pot
Body	flat plate	flat plate	flat plate	flat plate
Range x/θ	0-207	10-79	0-43	3-948
Re_θ	1580	5220	13600	2940
S	0.062		0.12	
Max Rey stress		0.05		0.05
Max Turb kinetic energy		0.07		0.18

4.4 Plane mixing layer

Table 4.5 summarizes the experimental data measured by various investigators [41-46]. The spreading rate, S, is defined as

$$S = \frac{d(y_{0.1} - y_{0.9})}{dx}$$

where $y_{0.1}$ and $y_{0.9}$ are respectively the normal distance from the dividing plane to the location where the x-component velocity is 0.1 and 0.9 of $(U_I - U_E)$. Both Reynolds stress and turbulent kinetic energy are normalized with $(U_I - U_E)$. It can be seen from the table that there is a large variation in the spreading rate. This is a major source of concern in recent years [46]. However, recent data by Husain and Hussain [47] indicates that an isolated mixing layer does reach a unique asymptotic spreading rate.

Nevertheless, the developing region of a mixing layer is not very well understood. This is due to complex interaction of the two wall boundary layers and the two shear layers. For calculation purposes, it is important that well defined initial conditions and sufficient turbulence measurements be available to characterize the main features of the flow. Also, the data should cover the complete mixing region. At present, no totally satisfactory set of data is available. Howevér, some of the measurements of the velocity are shown in figure 4.13. Most of the data falls on one curve indicating that the results are in good agreement. These results were obtained under different conditions at

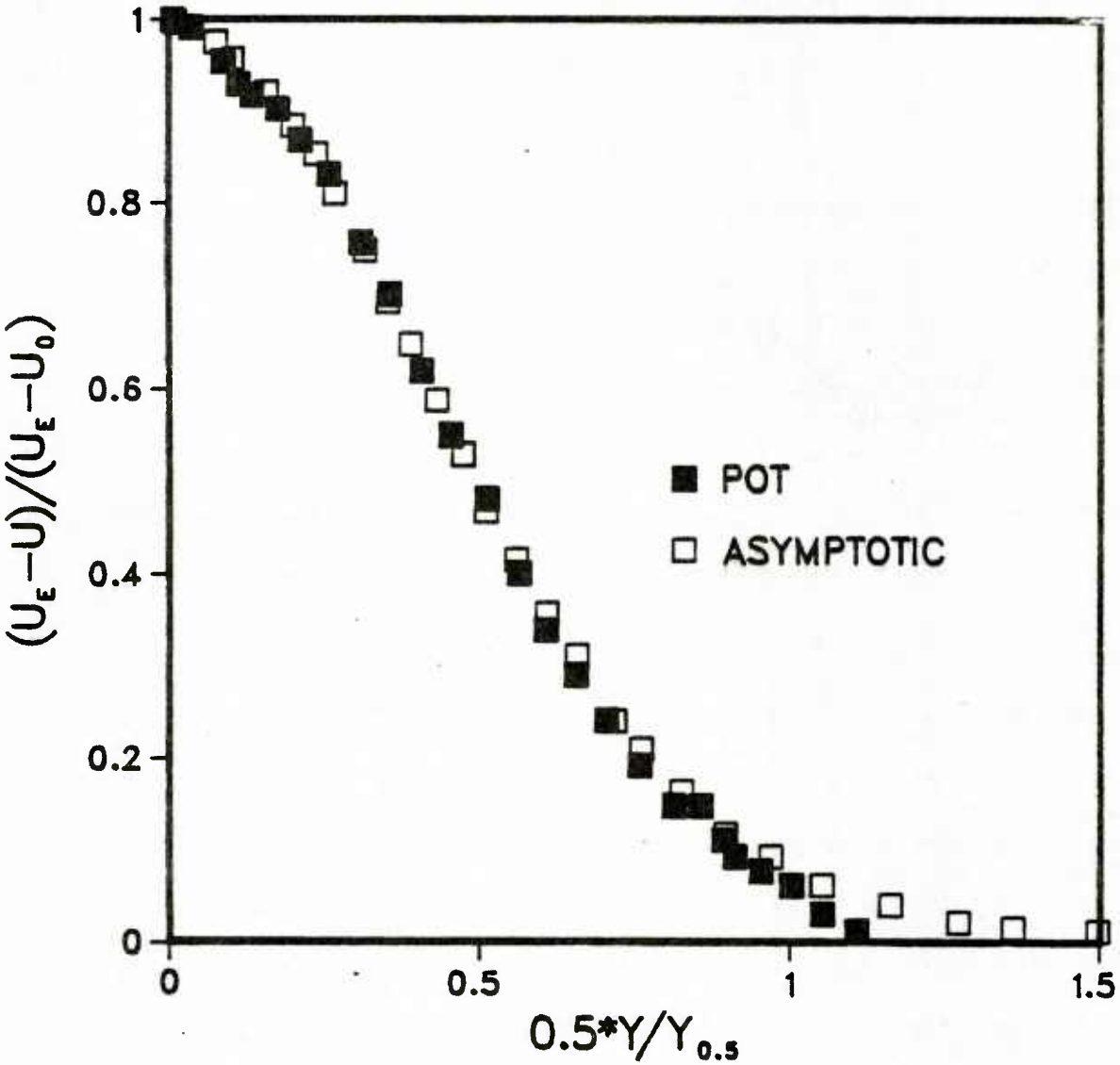

Figure 4.10. Asymptotic velocity-defect profile in a plane wake

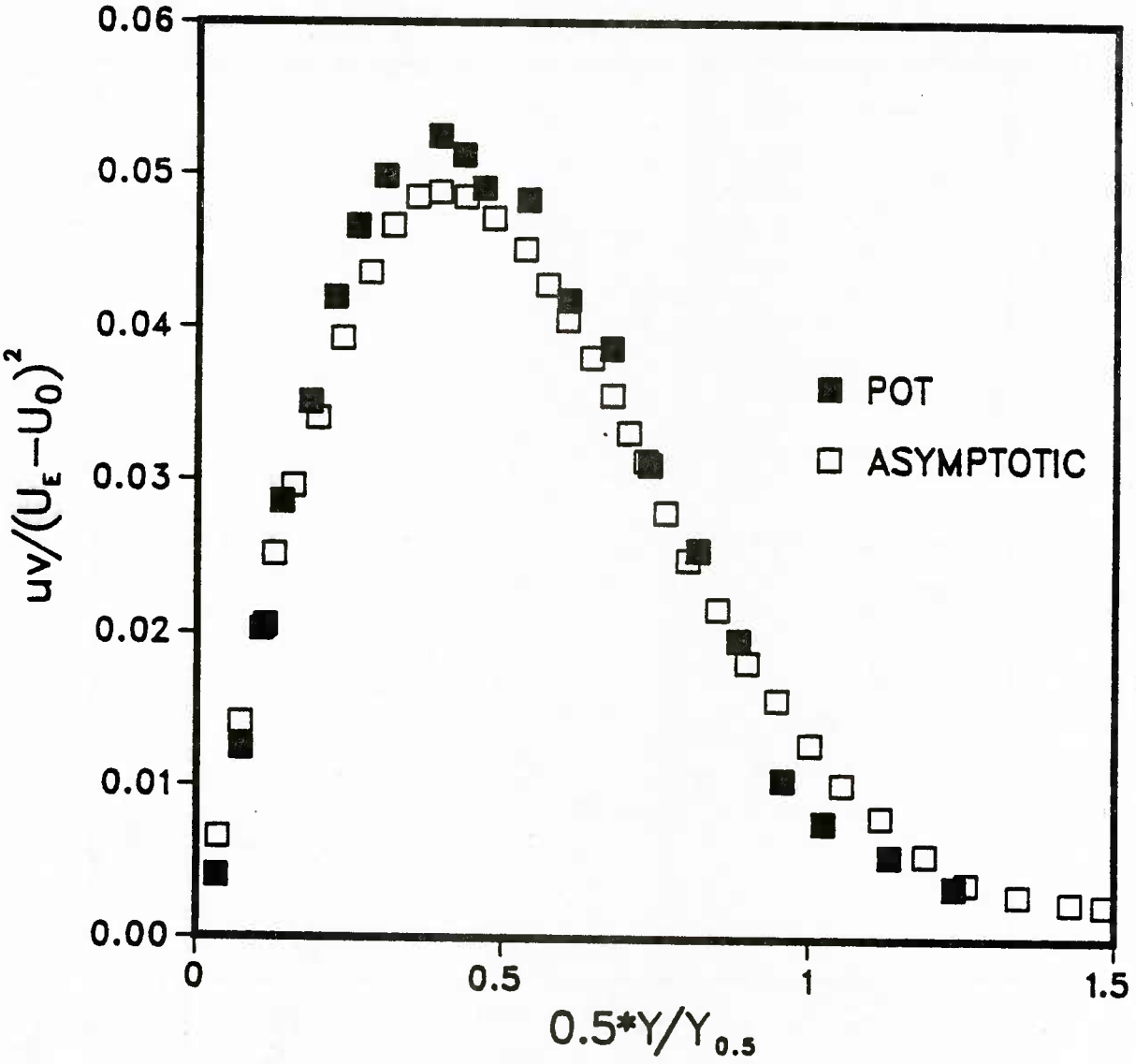

Figure 4.11. Asymptotic Reynolds stress in a plane wake

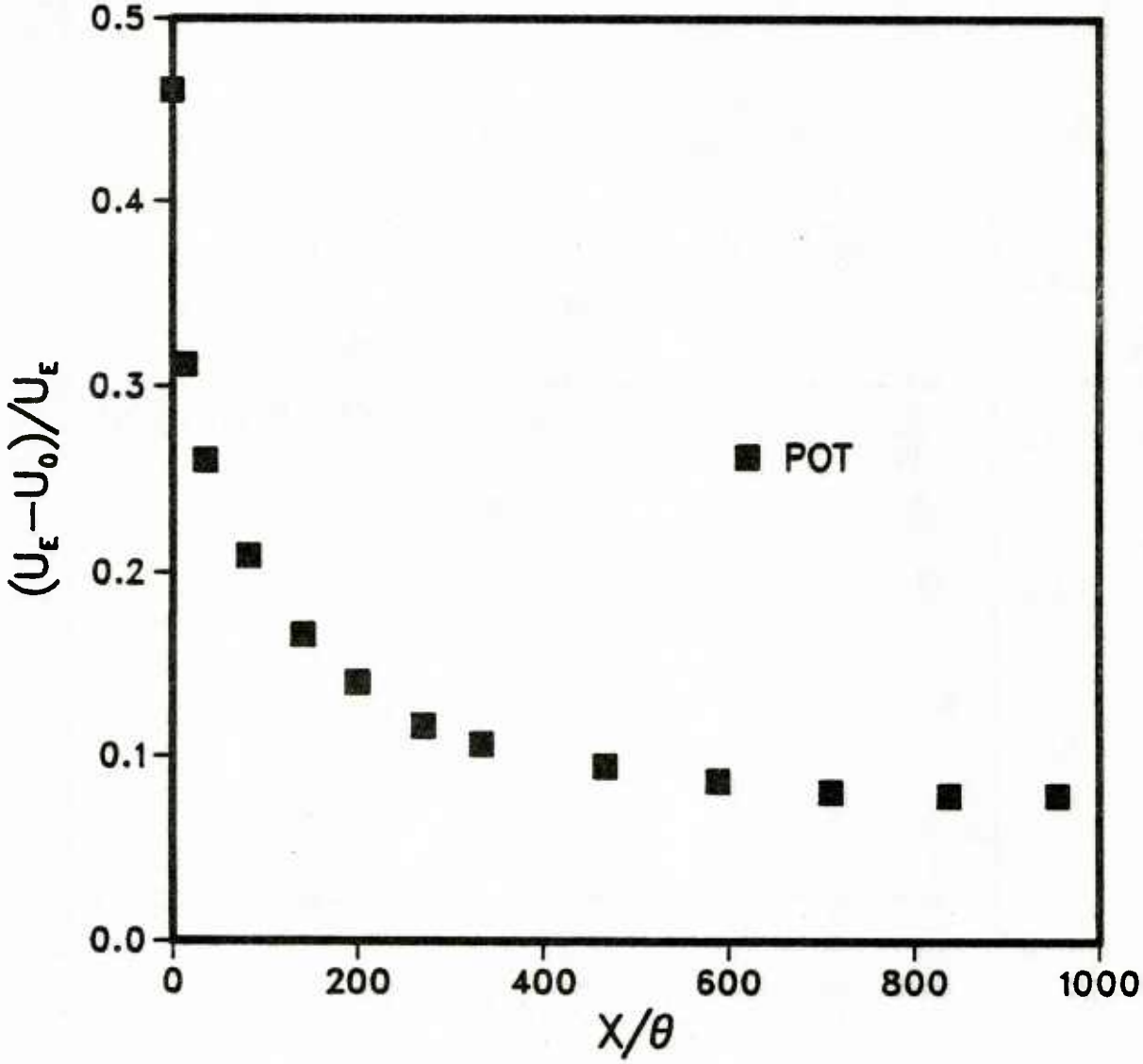

Figure 4.12. Center-line velocity defect in a plane wake

Table 4.5

Parameters for plane mixing layers

Investigator	Wygnanski	Liepmann	Patel	Sami
Dimension (cm)	51 * 18	152 * 19	76 * 43	30 dia.
Range x/D	58	90	100	450
Max Re	465,000	1,100,000	1,800,000	660,000
S	0.2	0.16	0.165	0.163
Maximum Reynolds Stress	0.0091	0.008	0.01	0.0109.
Max turb kinetic energy k	0.035	0.02	0.0275	--

the start of the mixing layer. Measurements of Albertson et al. [43] and Sunyach et al. [44] were in the initial region of a plane jet while Sami [45] and Bradshaw [46] obtained data in the initial region of a large round jet which is approximately considered to be two dimensional. In figure 4.14, the kinetic energy profiles of self similar mixing layers are shown. Unlike the velocity profile, there is a large amount of scatter and, thus, it is difficult to say which data is more accurate. Part of this discrepency is due to the variation in the initial condition.

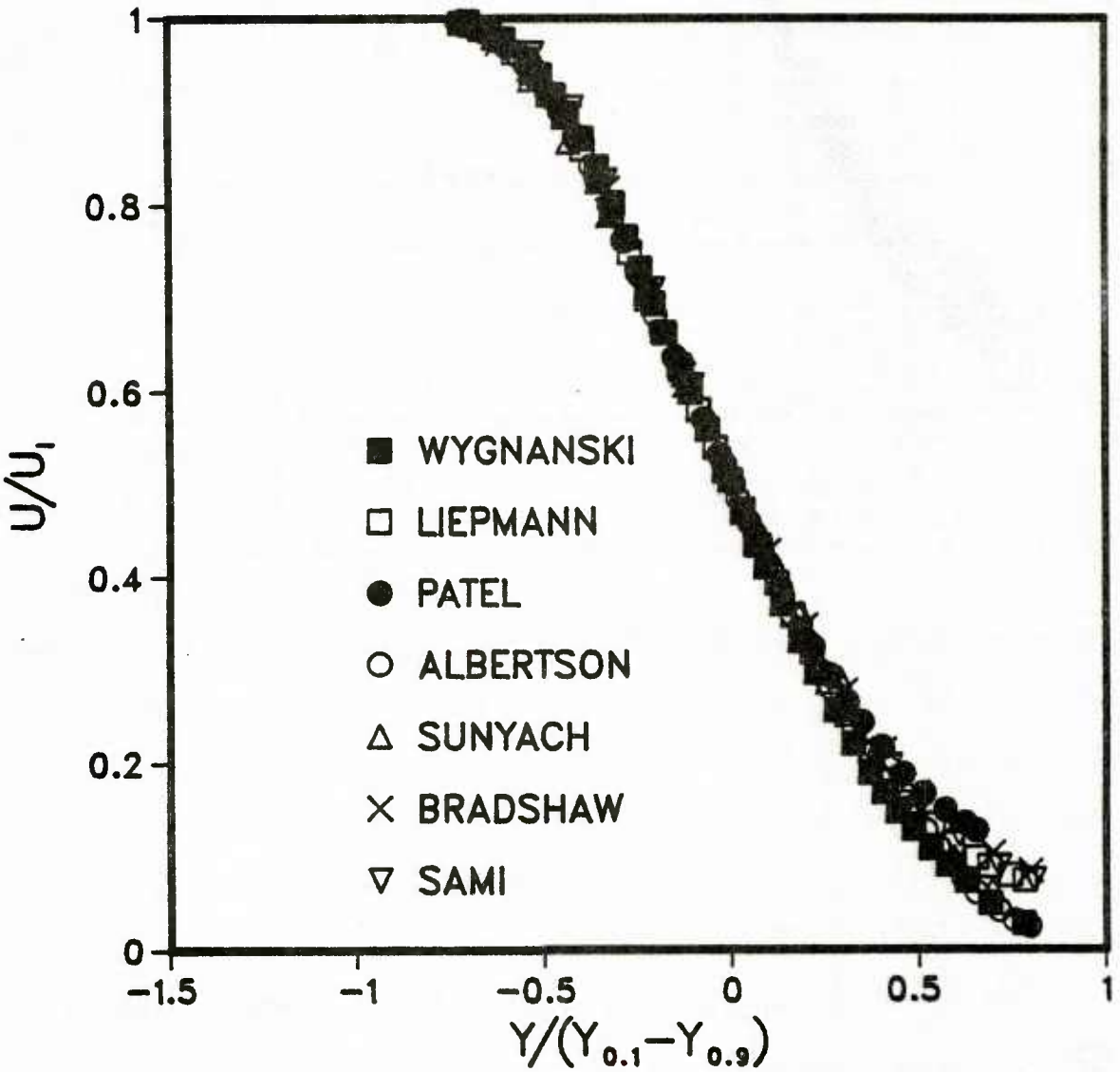

Figure 4.13. Measured velocity profile in a plane mixing layer

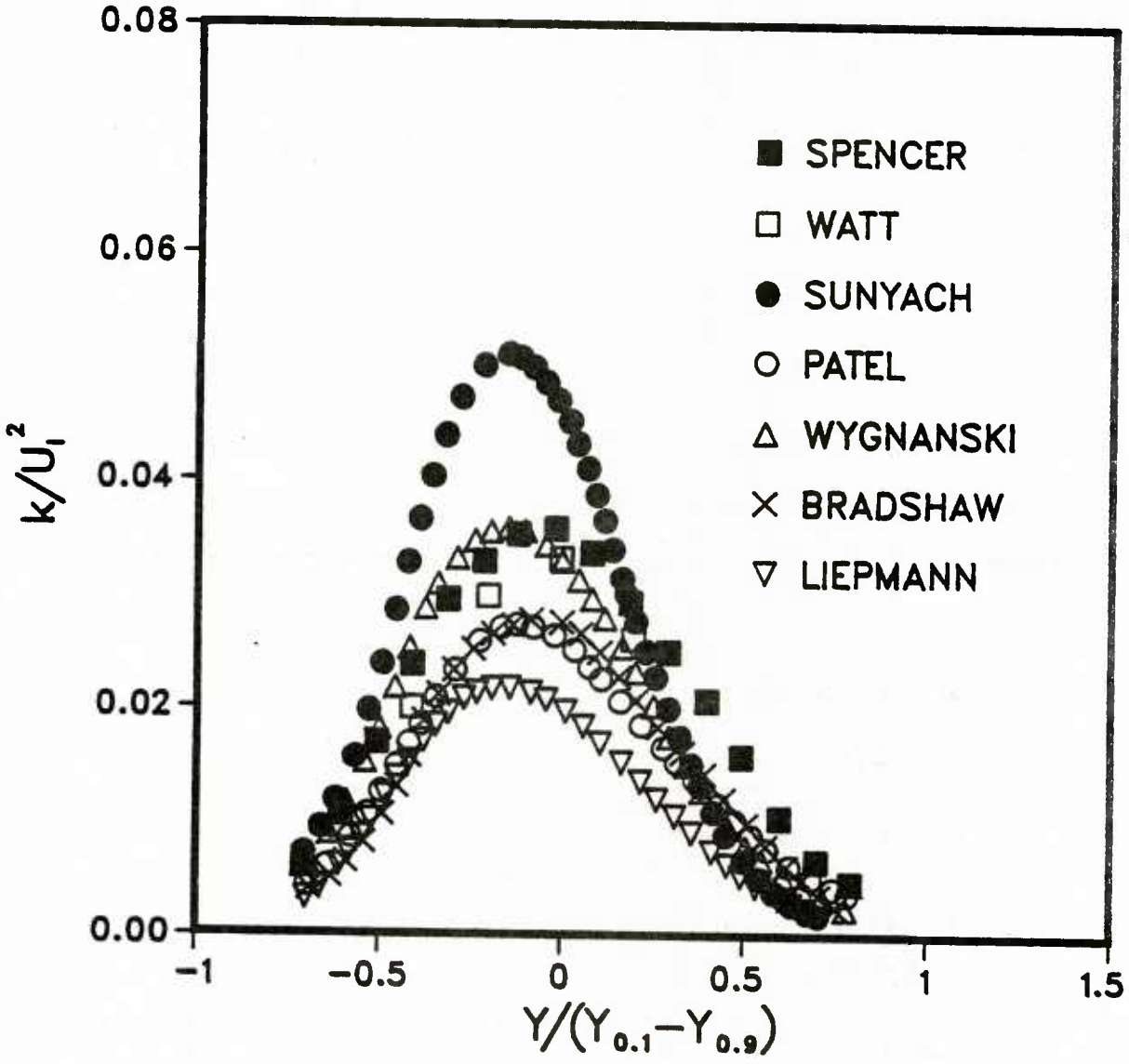

Figure 4.14. Measured k-profile in a plane mixing layer

4.5 Jets flowing into a parallel moving stream

Unlike the flow of jets into stagnant surrounding, this type of flow is known to be approximately self-similar. Due to the presence of the moving fluid in the surrounding, the flow has two distinct characteristic regions. Close to the jet or the near region, the centerline velocity U_o is much larger than the free stream velocity U_E, i.e.

$$\frac{U_o}{U_E} >> 1$$

Therefore, the mean strain rate is high. In this region, the flow properties are similar to that of a stagnant jet. Far downstream, the jet centerline velocity is only slightly larger than the free stream velocity, i.e.

$$\frac{U_o}{U_E} = 1 + \delta$$

where δ is small. Hence, the strain rate is weak and the velocity profile resembles an inverted wake velocity profile. This region is sometimes termed the 'wake like ' region.

Due to the change in the flow characteristic from large strain rate to small strain rate, jets flowing into moving stream provide a good case for testing a turbulence model.

4.5.1 Plane jet

Although the spread of turbulent jets issuing into parallel moving streams has been the subject of a number of theoretical treatments [48], reliable experimental data on these flows are still comparatively sparce.

Figure 4.15 shows the velocity profile measurements made by Bradbury et al. [30] for several ratios of $U_E/(U_o - U_E)$. Since the centerline velocity decreases with x, these ratios effectively correspond to different x locations in the flow field. All the profiles coincide into a single curve indicating that the flow is approximately self-similar. In figure 4.16, the centerline velocity decay is shown. In both the figures, the ratio of the free stream velocity U_E to the nozzle velocity U_N was 0.3.

4.5.2 Round jet

Figure 4.17 shows the plot of mean velocity profiles at three different stations as obtained by Antonia et al. [49]. All velocity profiles fall into a single curve, indicating that the mean flow is almost self-similar. The ratio U_E/U_N for this data is 0.3.

In figure 4.18, the Reynolds shear stress is shown for various locations of x/D ranging from 38 to 248. There is a considerable amount of scatter at $y/y_{\frac{1}{2}} < 0.8$. However, the shape of the data curve is similar and has a peak at about $y/y_{\frac{1}{2}}=0.8$.

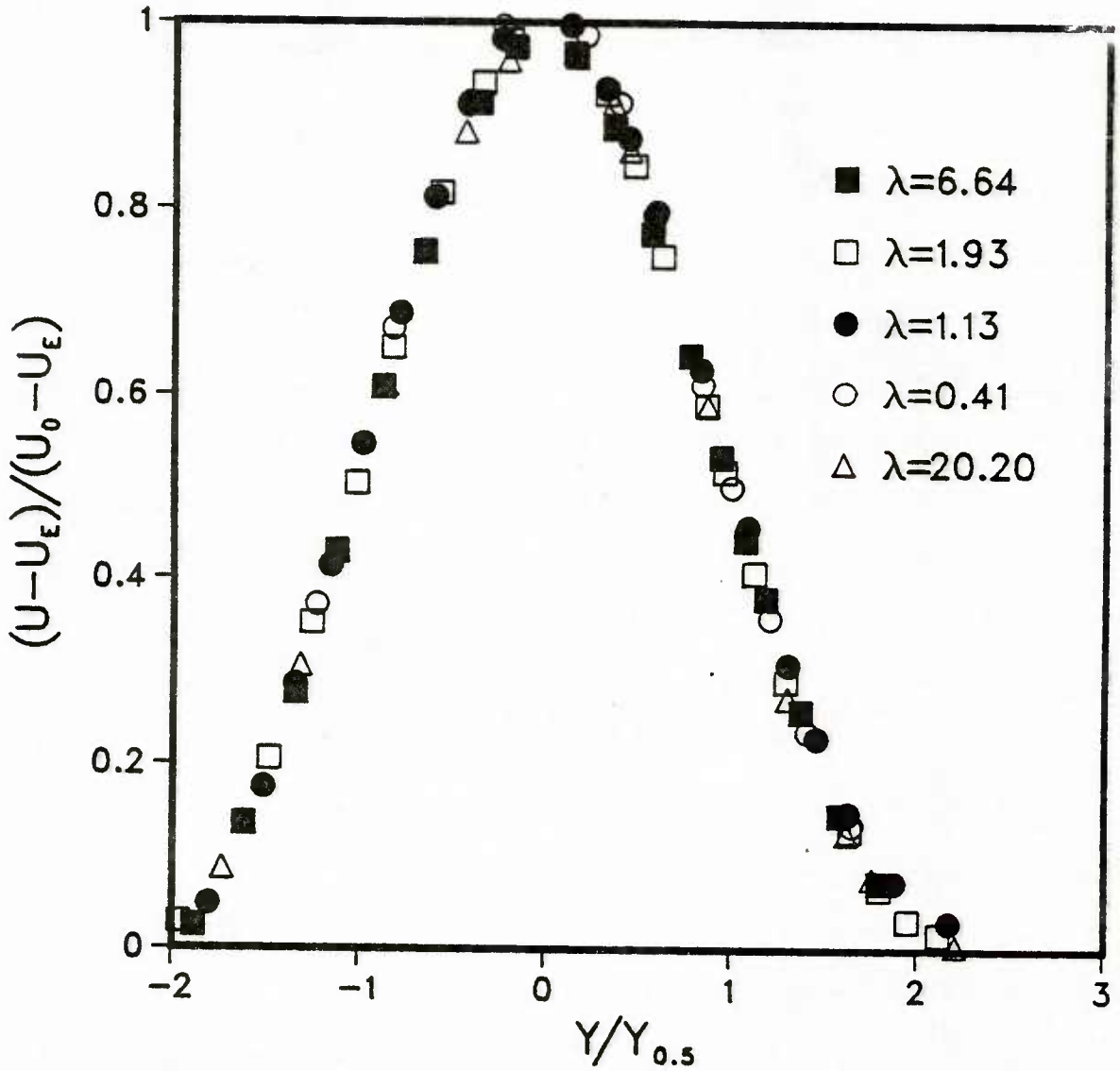

Figure 4.15. Measured velocity profile of a plane jet in moving surrounding

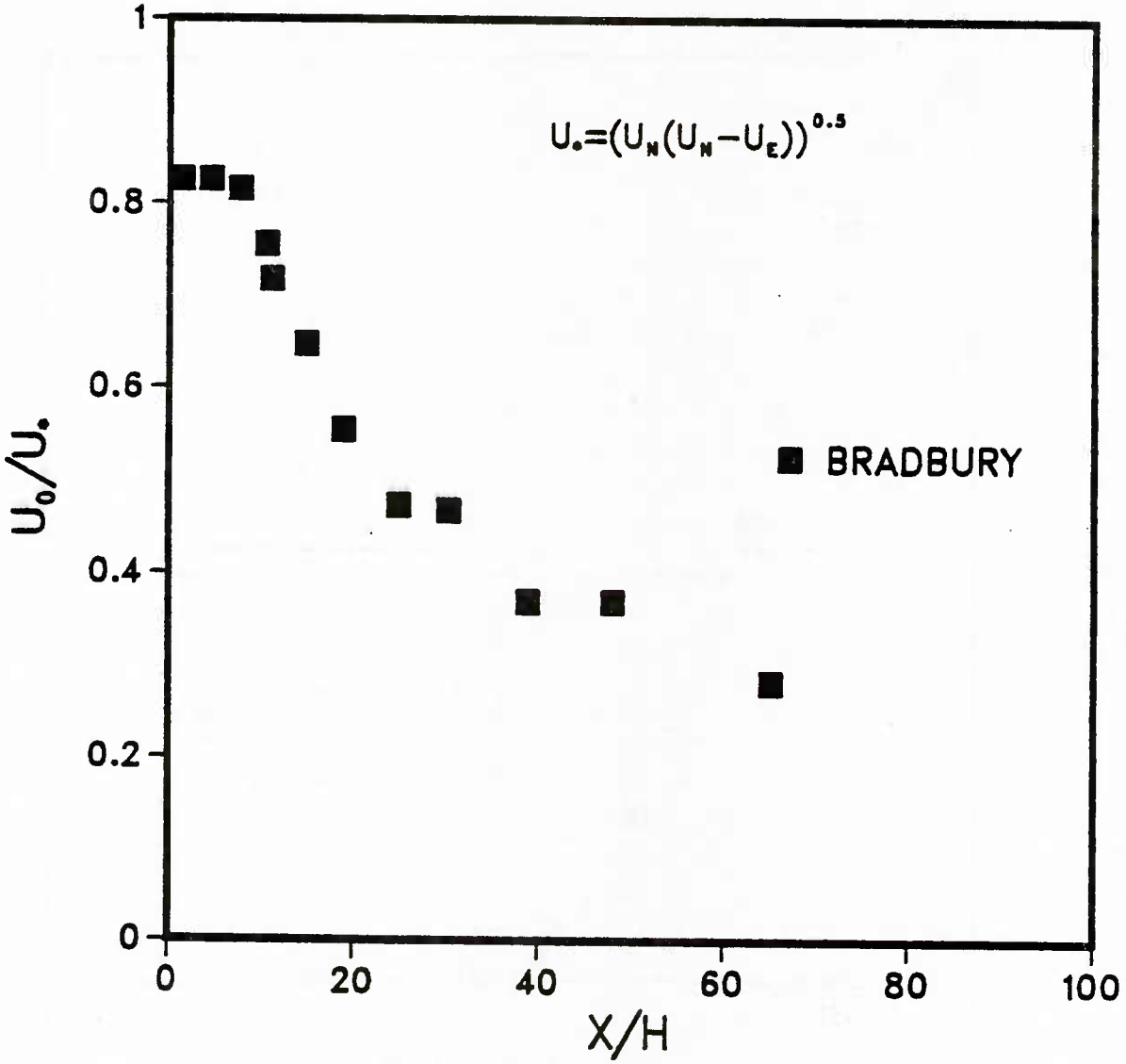

Figure 4.16. Centerline velocity decay of a plane jet in moving surrounding

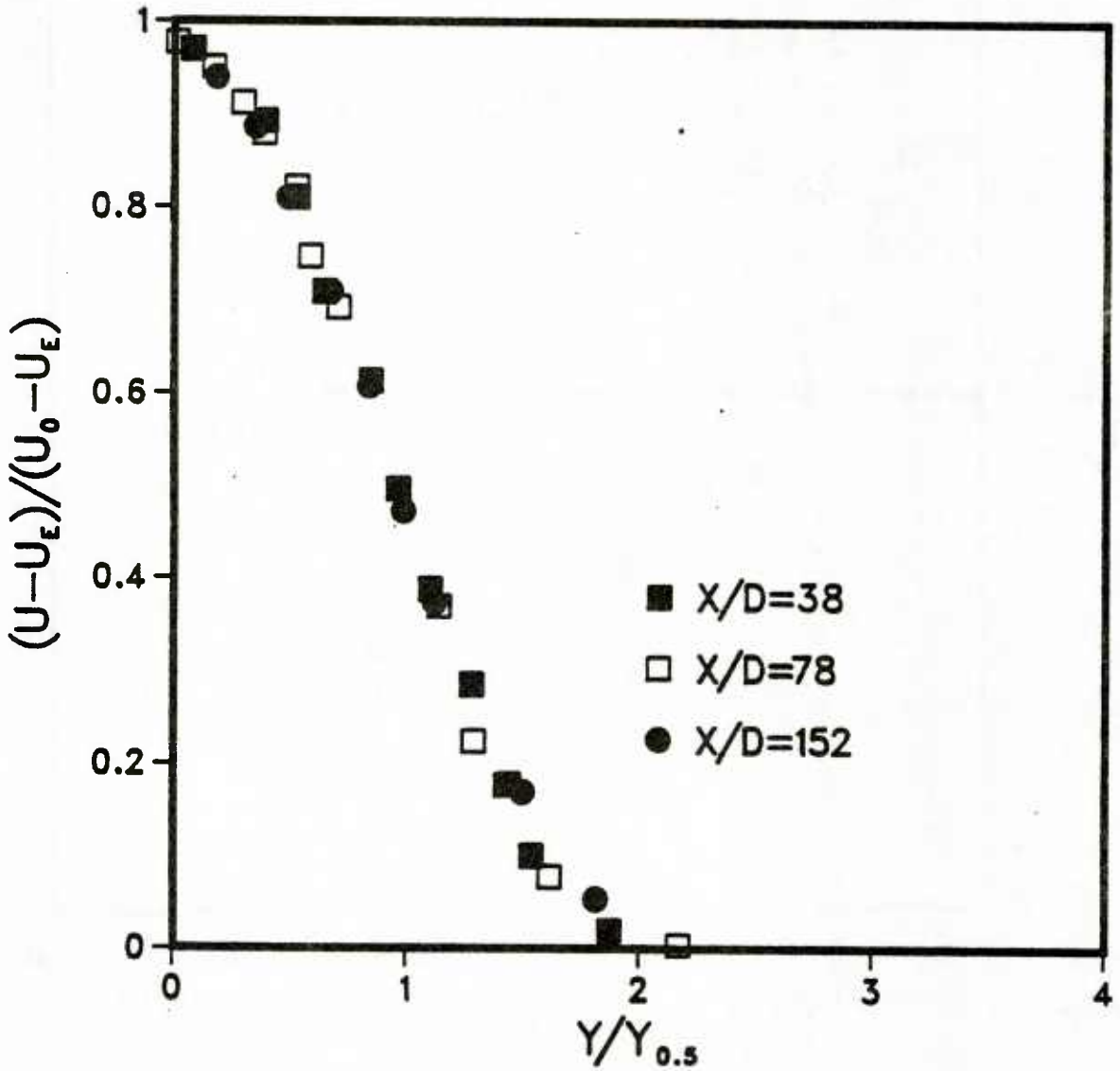

Figure 4.17. Measured velocity for a round jet in a moving surrounding

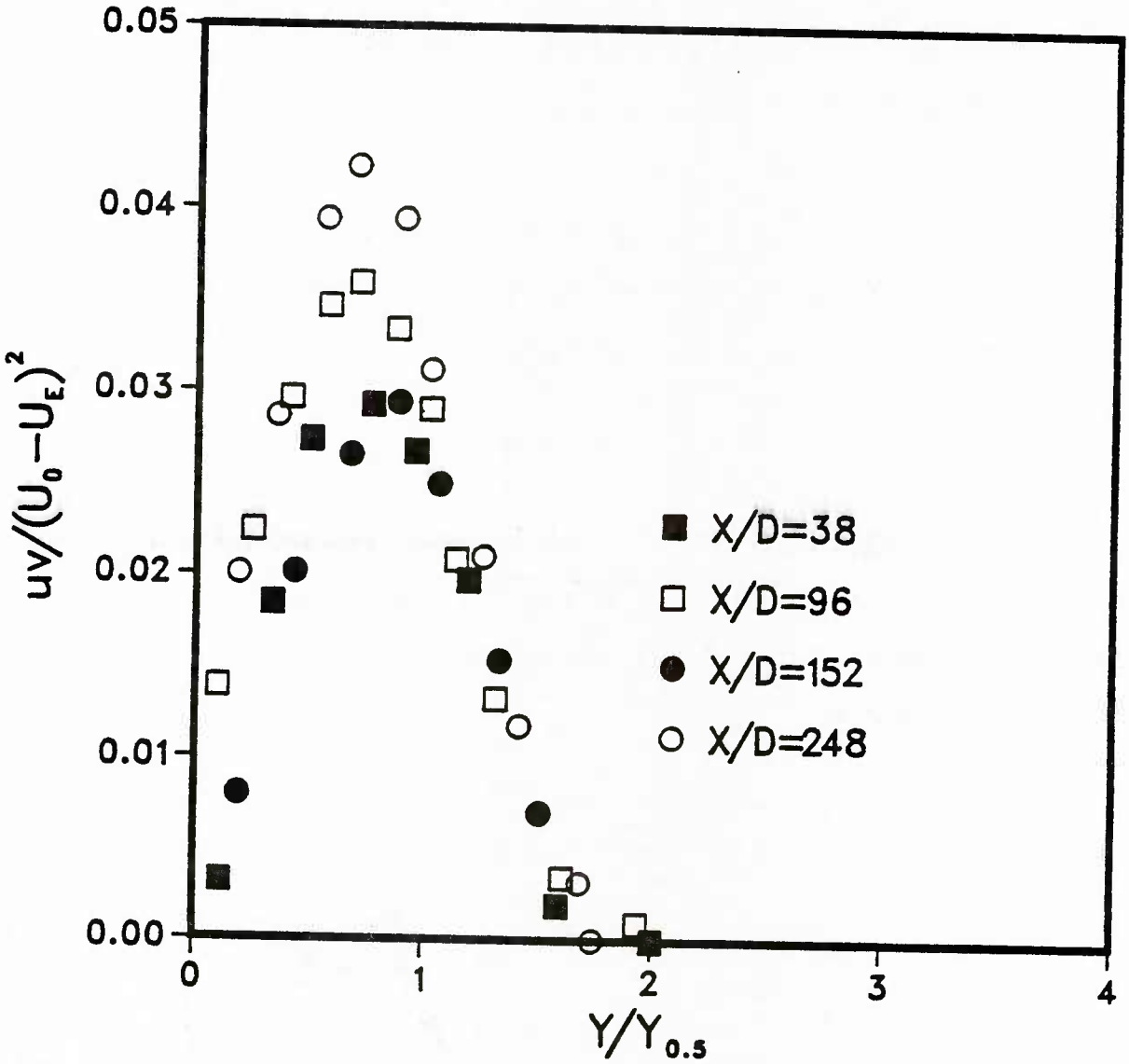

Figure 4.18. Measured Reynolds stress for a round jet

4.6 Buoyant jets

The turbulence model for the prediction of the turbulent buoyant flow is given in chapter III. In order to verify the model, some reliable experimental data is necessary. The existing turbulence models do not predict the mean and turbulent quantities close to experimental data unless the model constants are altered. Chen and Rodi [50] have collected available data on buoyant jets which can be used to verify the performance of the two-scale model. Unfortunately, experimental data, especially the turbulence quantities, for buoyant flows are not sufficient for an accurate test of the model.

4.6.1 Plane buoyant jet

Table 4.6 shows the plume region of buoyant plane jets. The modified Grashoff number, which is the product of the Grashoff number and the heat flux, ranges from 3,900,000 to about 966,000,000. The Grashoff number is defined as

$$Gr = \frac{g(\rho_a - \rho_o)D^3}{\rho_o \nu^2}$$

where

ρ_a=ambient fluid density,

ρ_o=fluid density at nozzle exit

ν =kinematic viscosity

D =jet width or diameter

The rate of velocity spread which is defined as

$$S = \frac{dy_{\frac{1}{2}}}{dx}$$

is measured by the various investigators to vary from 0.095 to 0.147. The recommended value is 0.12. The thermal rate of spread is defined as

$$S_T = \frac{dy_{\frac{1}{2}T}}{dx}$$

where $y_{\frac{1}{2}T}$ is the location where the temperature is one-half that of the centerline temperature. From the temperature measurements, the thermal rate of spread has been obtained by most investigators to be around 0.13.

Table 4.6

Gross parameters for buoyant plane jets

Investigator	Rouse	Kotsovinos	Harris	Anwar
Modified Gr No. $*10^5$	39	470	9660	-
Froude No.	-	1.4-5.9	4-193	16-100
(x/D)	650	43	70	50
S	.15/.14	.095	-	-
Thermal Spread rate	.13/.14	.12	.135	.131

The velocity and temperature profiles for a plane jet are shown in figures 4.19 and 4.20. The first figure is for a pure jet measured by Bradbury and Van der Hegge while the second is for a pure plume obtained by Rouse et al. [51]. These are two extreme cases of a buoyant jet. The centerline velocity according to Chen and Rodi [50] can be divided into three distinct regions in a buoyant jet, namely, the near or the non-buoyant region, the intermediate region and the plume region. In all the three regions, the experimental data lies closely to the theoretical lines which are obtained from similarity analysis. Hence the profiles at all Froude numbers should lie between those of pure jet and pure plume. Figure 4.21 shows the Reynolds shear stress for plane buoyant jets obtained by Ramaprian et al. [52]. Their measurements around $y/y_{\frac{1}{2}}=1$ shows some scatter. In figure 4.22, the turbulent normal stress distributions measured by Kotsovinos [53] and Bradbury [30] are shown. Bradbury's data is for a pure jet while Kotsovinos's measurements are for a pure plume. It can be seen that the turbulent intensity in a pure plume is much larger than that in a pure jet.

4.6.2 Round buoyant jet

For a round buoyant jet, Table 4.7 summarizes the gross parameters obtained by different investigators. The modified Grashoff number varies from 10^9 to 10^{10}. The rate of velocity spread varies from 0.084 to 0.12. The recommended value is 0.112. The value suggested for the thermal rate of spread is 0.1.

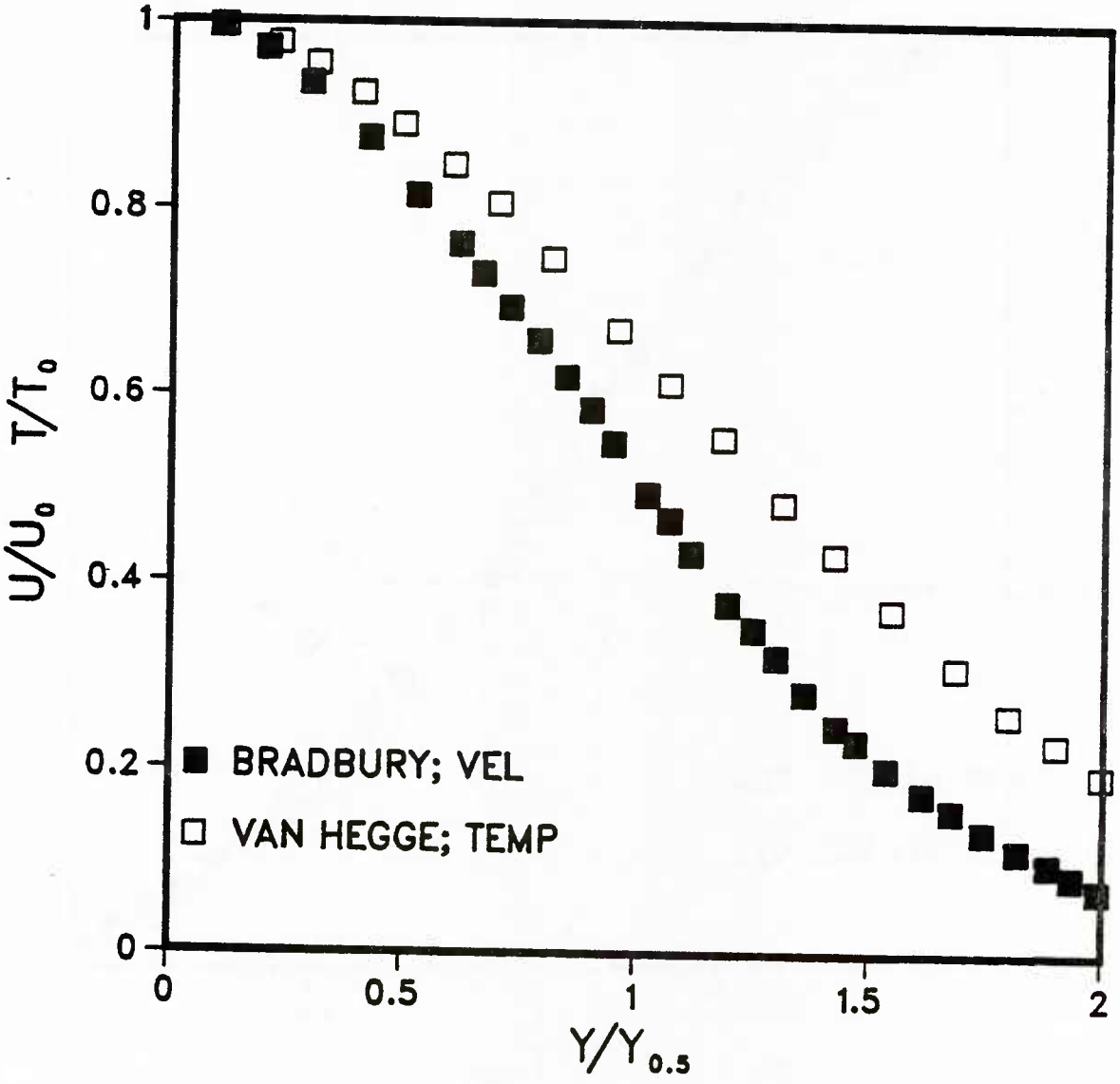

Figure 4.19. Velocity and
Temperature for a pure plane jet

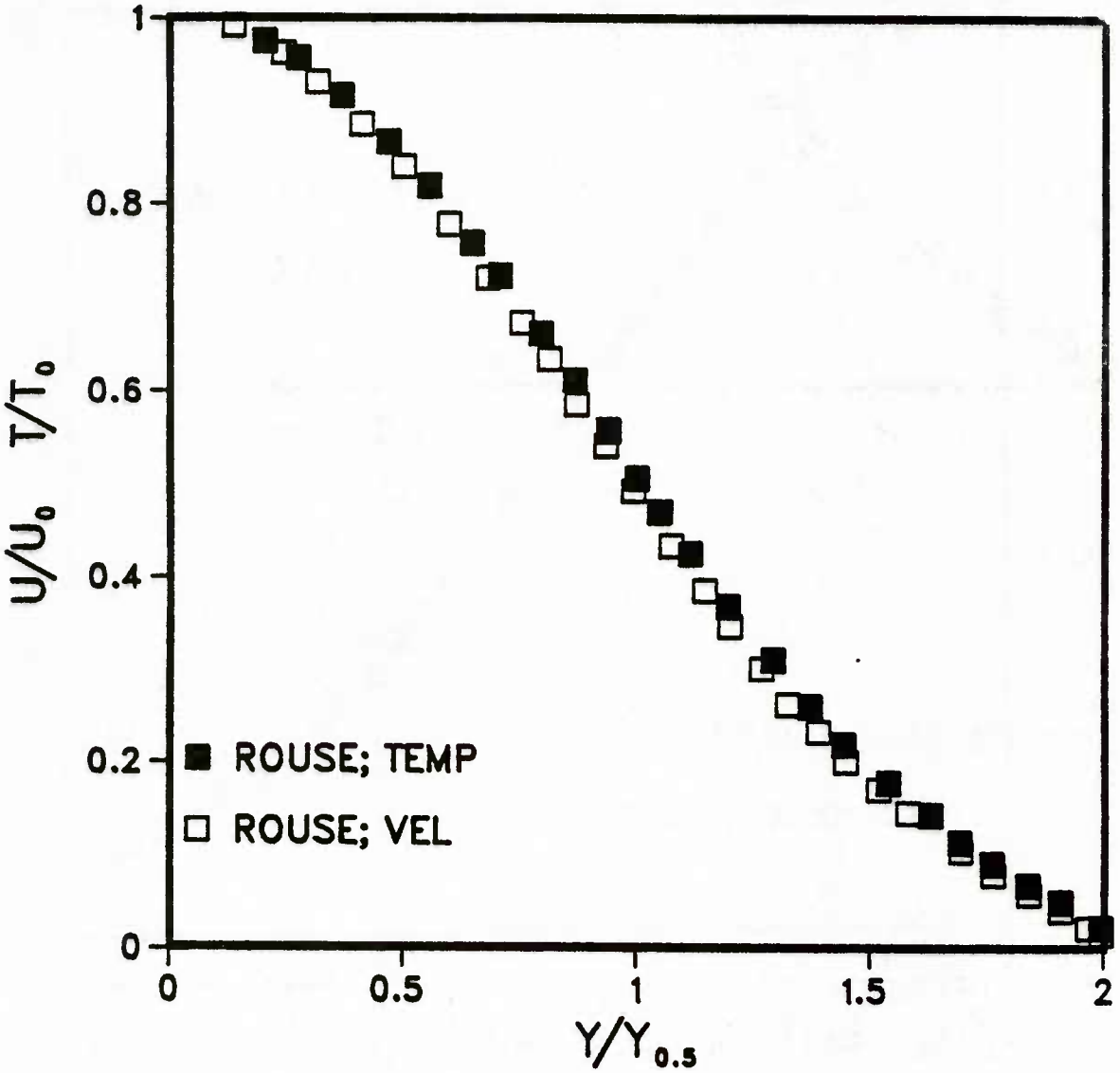

Figure 4.20. Velocity and Temperature for a pure plume

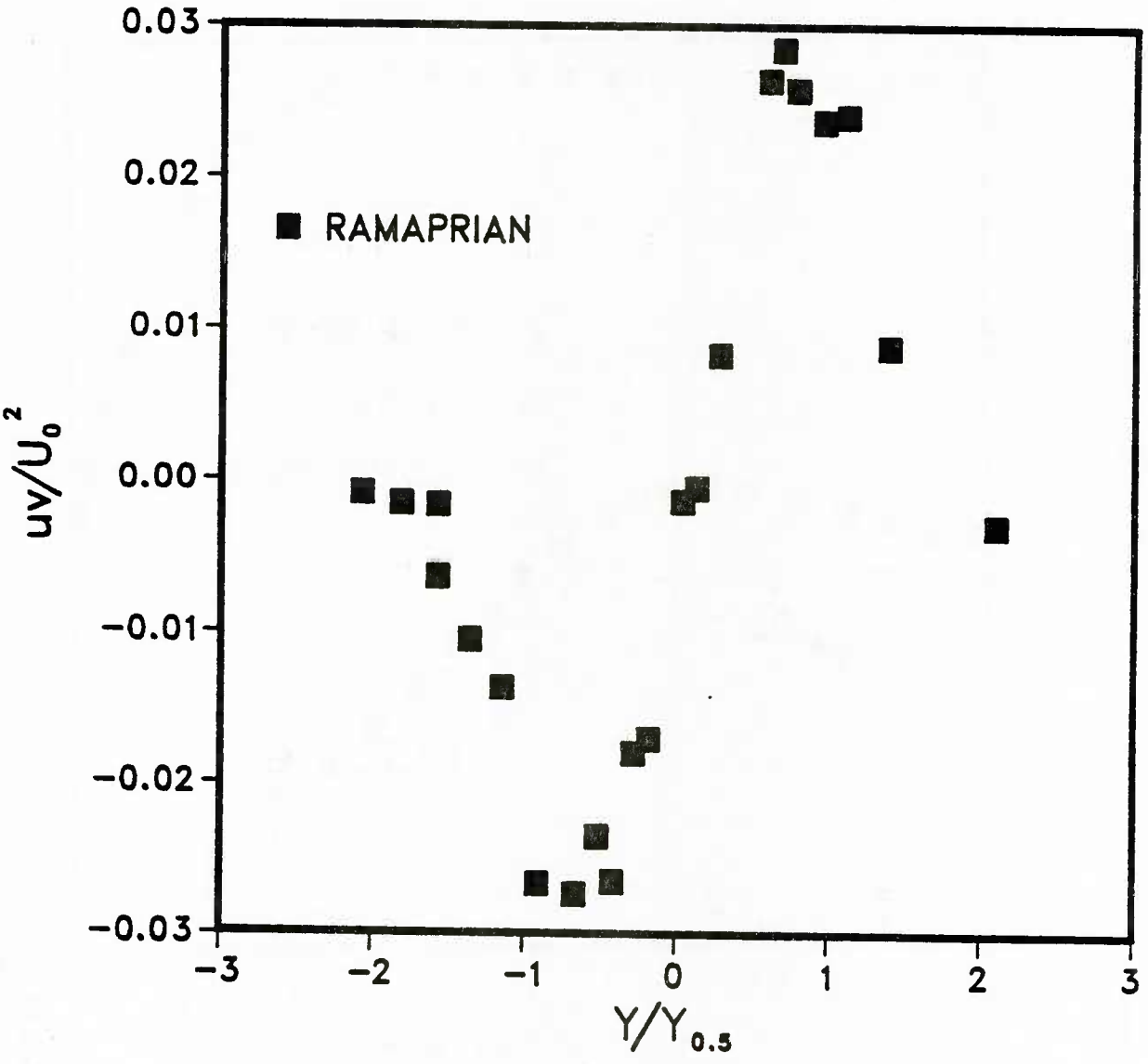

Figure 4.21. Measured Reynolds stress for a plume

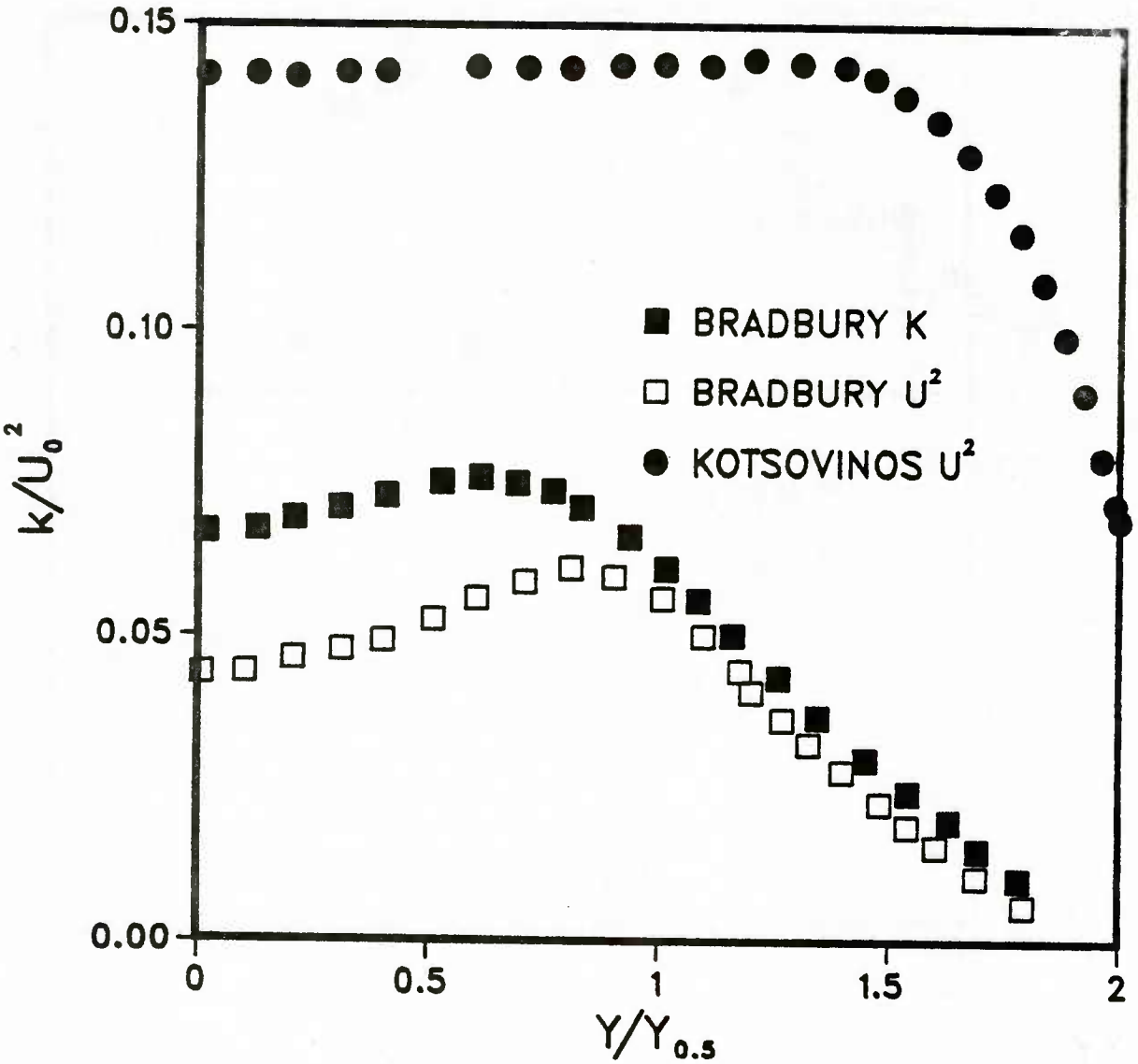

Figure 4.22. Measured normal stress and k for a plume

Table 4.7

Gross parameters for a buoyant round jet

Investigator	Rouse	George	Abraham
Modified Gr No. $*10^9$	1.38	13.3	4.53
Froude No.	-	.714	1.82
(x/D)	75	16	26
S	.084	.112	-
Thermal Spread rate	.098	.104	-

In figure 4.23 the velocity and temperature profiles are shown for a pure jet where the Froude number is infinite. The data is obtained by Rodi for velocity and Ruden for temperature. On the other hand, figure 4.24 shows the velocity and temperature distributions obtained by George et al. [54] for a pure plume where the Froude number is 0. The turbulent kinetic energy in buoyant jets is shown in figure 4.25. Rodi's measurements are for a pure jet while George's measurements are for a pure plume. Unlike the plane buoyant jet, there is a decrease in the turbulence intensity for a round jet due to the presence of buoyancy. Hence, more experimental data is needed before a meaningfull conclusion of the accuracy of the turbulence model can be made.

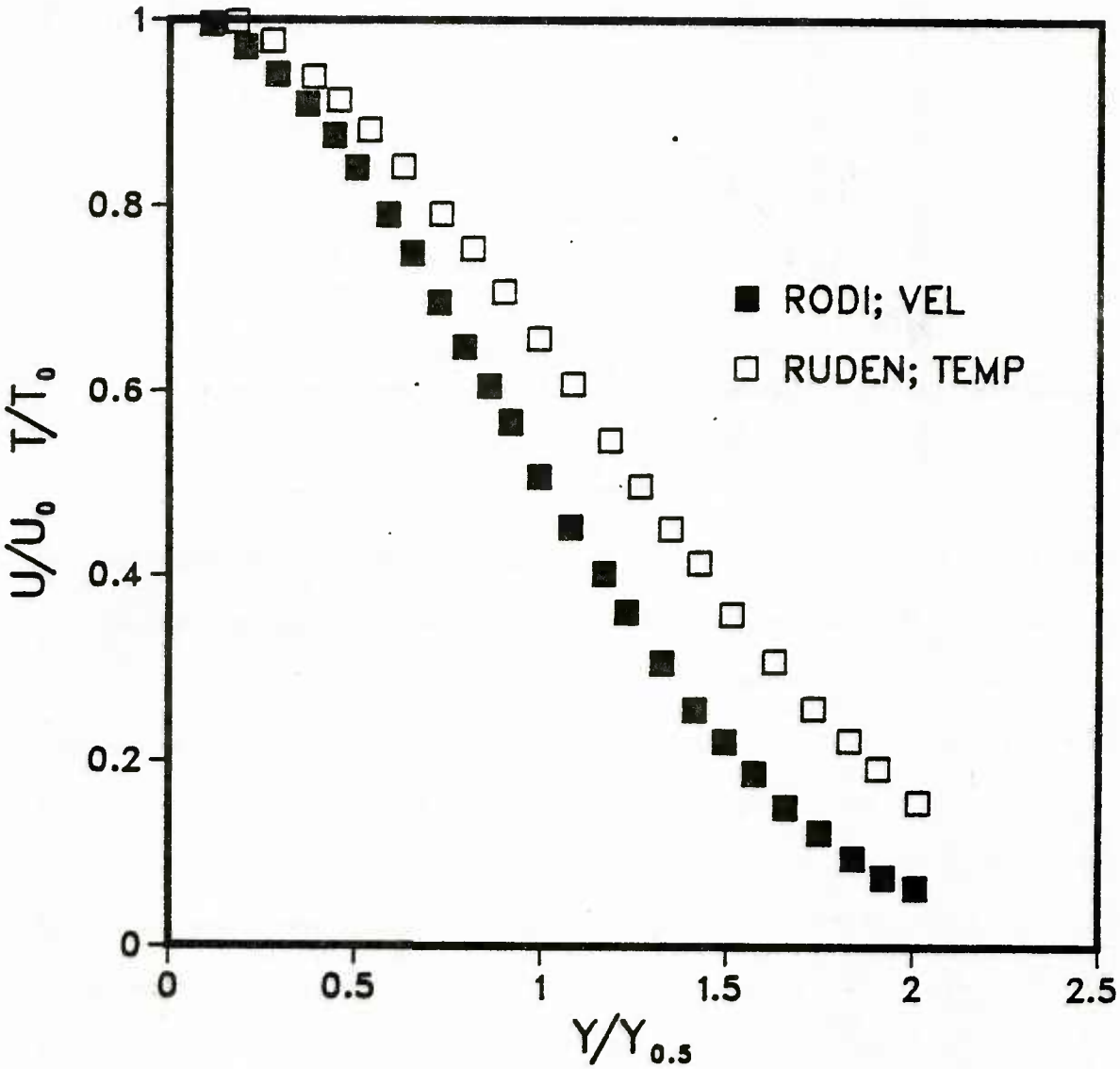

Figure 4.23. Velocity and
Temperature in a pure round jet

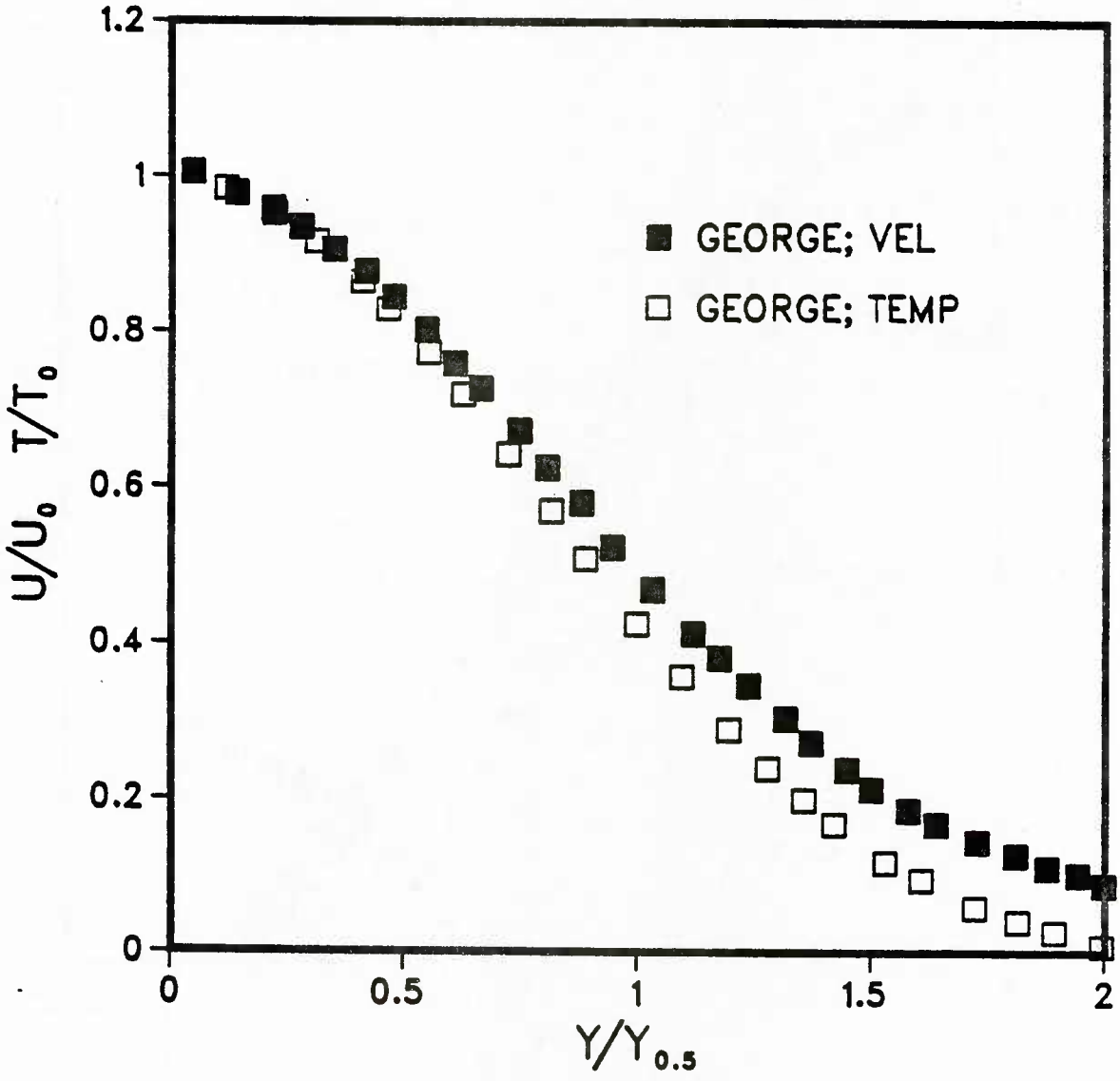

Figure 4.24. Velocity and
Temperature in a pure round plume

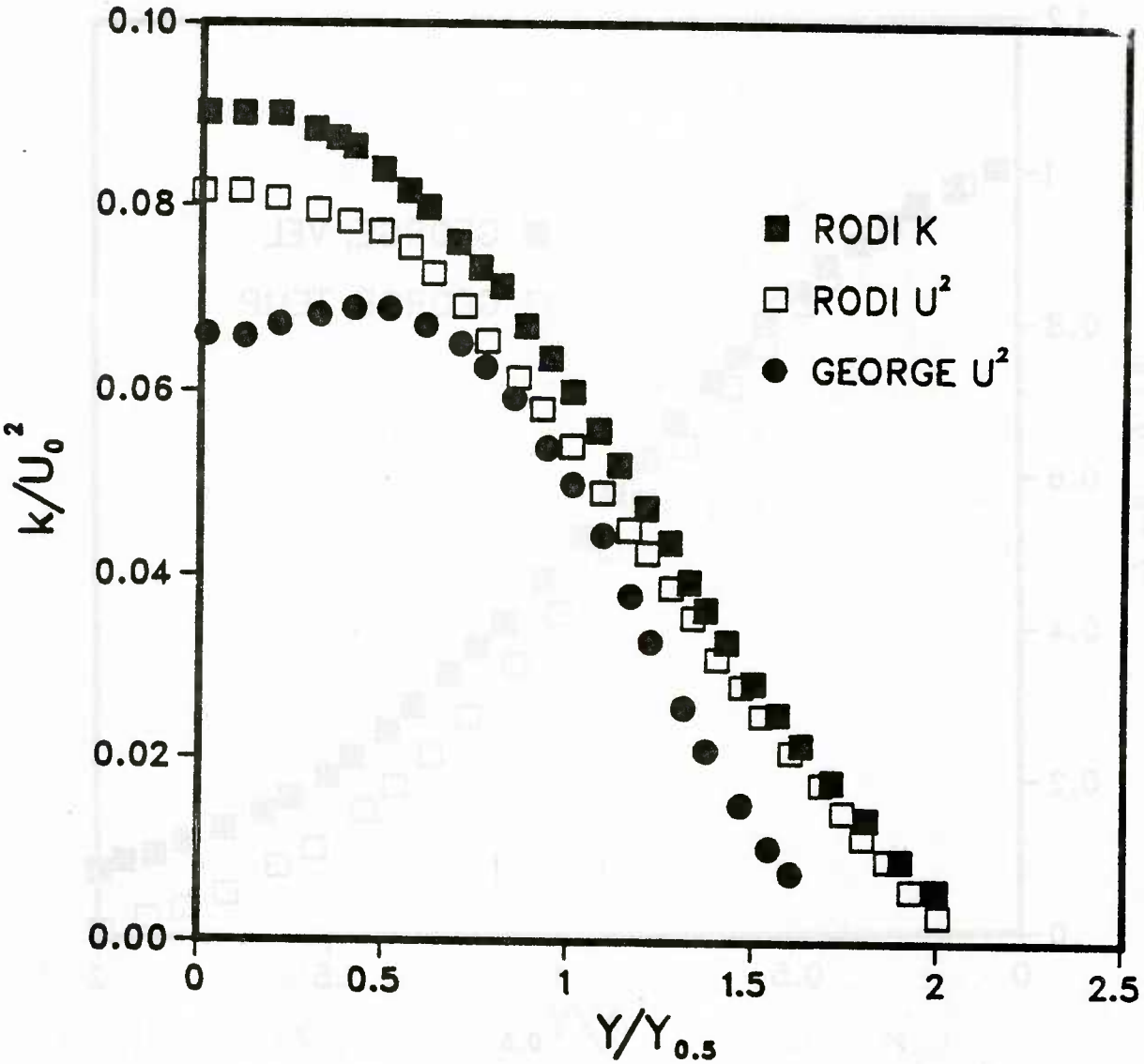

Figure 4.25. Measured k and normal stress in round jets and plumes

4.7 Summary

From the experimental data reviewed above, it can be summarized that though the amount of data is enough to adequately test a model, it is still not complete. In most cases, there is no experimental data of turbulence quantities at the inlet, thereby making it difficult to compare the prediction of flow near the initial region particularly in the near region of the wake flow. Also, in wake and jet flows, the turbulence at the inlet influences the velocity and kinetic energy in the near region. Therefore, small discrepencies between experimental data and numerical calculation using the turbulence model may not indicate that the model is unsuitable. Due to lack of initial condition some trial and error or guess of initial turbulent condition during computation is necessary in order to examine or compare the experimental data with numerical results in some region of the flow.

In chapter V, the prediction based on of the two-scale turbulence model for nonbuoyant flows is compared with the experimental data. Chapter VI contains a comparison of the results of the two scale model for buoyant flows and experimental data for such flows.

CHAPTER V

PREDICTION OF TURBULENT NON-BUOYANT FLOWS

This chapter presents the results obtained by the two-scale turbulence model for non-buoyant flows based on equations (2.2), (2.3), (2.11), (2.12) and (2.13) with the turbulent constants of C_k=0.9, C_1=2.8, C_2=0.47, C_ε=2.00, $C_{\varepsilon 1}=17.5/(Re)^{\frac{1}{2}}$, $C_{\varepsilon 2}=18.9/(Re)^{\frac{1}{2}}$, C_T=0.13, C_{T1}=3.2 and C_{T2}=0.5. The predicted results are compared with the experimental data discussed in chapter IV. Furthermore, prediction of the one-scale turbulence model is shown and compared. For the one-scale turbulence model, instead of equation (2.12) for ε, equation (1.10) is used and instead of C_k=0.9, C_ε=2.00, $C_{\varepsilon 1}=17.5/(Re)^{\frac{1}{2}}$, $C_{\varepsilon 2}=18.9/(Re)^{\frac{1}{2}}$, the values used are 0.225, 0.15, 1.435 and 1.92, respectively.

As mentioned earlier, the selection of turbulent free shear flows as the first type of flow to verify the predictability of the turbulence model is based on the following considerations. First, there is sufficient data available for comparison for both mean velocity and turbulent transport properties. Second, the pressure gradient in free shear flows is negligible so that the pressure gradient will not play a major role in determining the flow field. Therefore, the prediction of the free shear flow field is most sensitive to the modelling of the Reynolds stress, turbulent kinetic energy and its dissipation. Third,

the complexity of the near-wall turbulence is absent in free shear flows. Therefore, the error in the approximate treatment of near wall turbulence can be excluded from the problem and the accuracy of the turbulence model can be carefully examined. Fourth, although it is secondary, the numerical procedure in calculating turbulent free shear flows is simpler than that in wall shear flows or separated flows.

5.1 Numerical procedure

The equations derived in chapter II for free shear flows are parabolic in nature and so the GENMIX program developed by Patankar and Spalding [55] is used. The program has been modified by Chen and Nikitopolous [23] and Chen and Chen [56] to include the governing equations for k, ε and $\overline{\theta^2}$.

Briefly, in the computation, the two coordinates chosen are the x and Ψ coordinates instead of x and y coordinates. The governing equations are transformed from the x-y coordinate system to the x-Ψ system. Thus the governing equations for U, T, k, ε and $\overline{\theta^2}$ are cast in the same form. The initial conditions are specified for U, T, k, ε and $\overline{\theta^2}$ at x=0. These conditions for each flow are given later in the individual section describing the flow. The inner boundary conditions are the symmetry conditions for jets and wake. For the mixing layer, the free stream conditions apply at the inner side. The outer boundary conditions are zero or constant velocity and no turbulence.

The solution at each section normal to the mean flow direction is obtained by using an implicit method. The marching step Δx at each station is calculated from various flow parameters. The grid size Δy is 0.01 times Δx. A total of 40 points are chosen in the cross-stream direction which is verified by Chen and Nikitopolous [23] to provide grid independent solution.

The calculations were performed upto a maximum distance of x/D=75 for jet flows and x/θ of 600 for wake behind a flat plate.

5.2 Prediction of gross parameters

The first thing to be concerned with is the prediction of gross characters of the flow field. For this the spread parameter is chosen. When a model is not capable of predicting an accurate spread rate for free shear flows, it is not very meaningful to examine further the details of flow and turbulent structure in the flow.

Table 5.1 shows the spreading rate for various non-buoyant flows. For jets, the spread rate S is defined as the slope of $y_{\frac{1}{2}}$ in the flow direction, where $y_{\frac{1}{2}}$ is the location in the normal direction of a point where the U velocity is one-half the centerline velocity, i.e. $U_{\frac{1}{2}}=0.5U_c$. For wake, S is the spread rate times the free stream velocity, U_E, and divided by the velocity defect, w_o, or $(U_E - U_c)$ as defined in figure 4.1. In the case of the mixing layer, the spread rate is obtained in terms of the width of the mixing layer. The width is defined as the distance between the edges of mixing layer where the velocity is 10% and

90% of the free stream velocity. From Table 5.1, it is seen that the values of S predicted by the one-scale model for round jet and plane wake without altering the turbulent constants are significantly different from the experimental data while the two-scale turbulence model predicts satisfactory results for all cases calculated. This demonstrates that the two-scale turbulence model indeed provides better prediction than the one-scale turbulence model.

Table 5.1

Spreading rate S

Flow Type	Spread Parameter	One scale	Exp. data	Two scale
Round jet	$\frac{dy_{\frac{1}{2}}}{dx}$	0.1189	0.08	0.081
Plane jet	"	0.1125	0.11	0.109
Plane wake	"	0.068	0.098	0.0975
Mixing layer	"	0.159	0.16	0.15

5.3 Jets flowing into stagnant surrounding

As mentioned earlier, jets flowing into stagnant surrounding become self-similar far downstream. For mean quantities, it should take a minimum of 40 diameters to establish self-similarity and about 60 to 70 diameters for turbulent quantities depending on the initial conditions at the jet exit. In the near region, the flow parameters are dependent

on the initial conditions like the velocity and turbulent kinetic energy at the jet nozzle. It is necessary to compare experimental data and prediction for both near and far regions in order to verify the accuracy of the one-scale and two-scale models. Unfortunately, most of the available data do not provide complete information about the initial conditions prevailing at the nozzle such as, velocity profile, turbulent kinetic energy or dissipation. This could lead to differences in the decay of centerline velocity and turbulent Reynolds stress or dissipation function. The results for both plane and round jets are discussed below.

5.3.1 Plane jet

In the present calculations, the initial condition for the velocity is

$$U=U_N\exp(-y^2)$$

The k and ε initial conditions are

$$k=0.06U_N^2\exp(-y^2)$$

$$\varepsilon=0.09k^{1.5}/H$$

Here U_N is the jet nozzle velocity. The 6% and 9% levels of intensity are taken here so that the predicted result in the near field resembles closely that of the measured data. Similar values were used by Chen and Nikitopolous [23].

Figure 5.1 shows the comparison of velocity profile for a plane jet in the region of self-preservation at x/D=75. The experimental data shown in the previous chapter is represented once again in figure 5.1 and most of the points fall in one line. The dashed line is the predicted result of the one-scale model while the chain-dashed line gives the results of the two-scale model. The agreement is excellent between calculations and experiment, except near the outer edge of the jet.

In figure 5.2, the turbulent kinetic energy is shown. As mentioned in chapter IV, there is a large amount of scatter between various experimental data, where the maximum k may vary from 0.065 to about 0.084. All the experimental data are shown once again along with the predictions of the one-scale and two-scale models. The two-scale model predicts turbulent kinetic energy within experimental scatter near the centerline. In the outer edge of the jet, the two-scale model predicts a larger k. This larger 'tail' is, perhaps, due to the numerical diffusion problem.

The Reynolds stress profile of a self-preserving plane jet at x/D=75 is shown in figure 5.3. There is a slight difference in value between experimental data, one-scale and two-scale models away from $y/y_{\frac{1}{2}}=1.5$. The maximum Reynolds stress obtained by various investigators, as shown in table 4.2, varies from about 0.02 to about 0.026. The prediction of the two-scale model shows good agreement with the data by giving a larger peak than the one-scale model. These predictions can be considered accurate within experimental uncertainty.

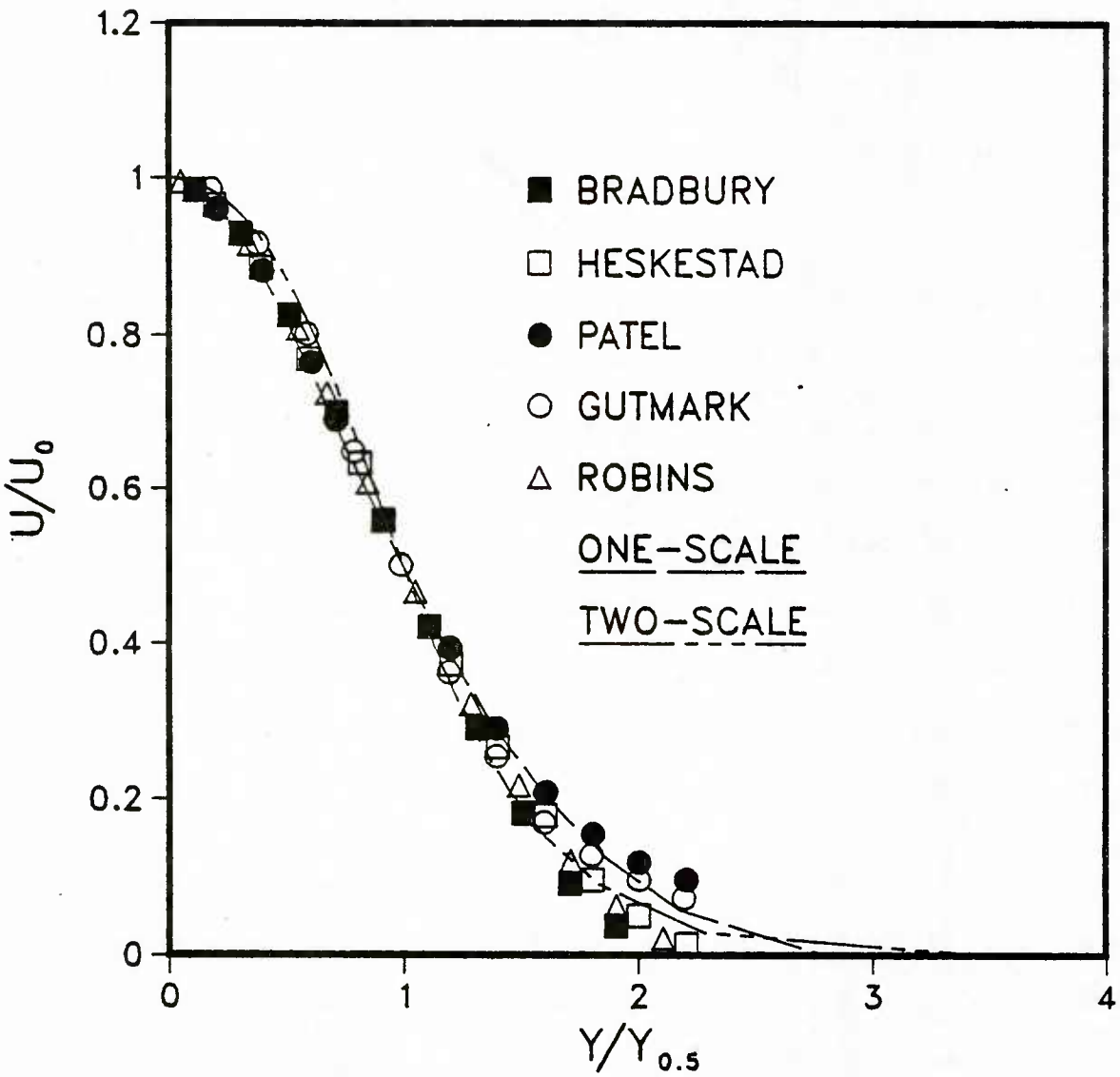

Figure 5.1. Velocity profile for a plane jet

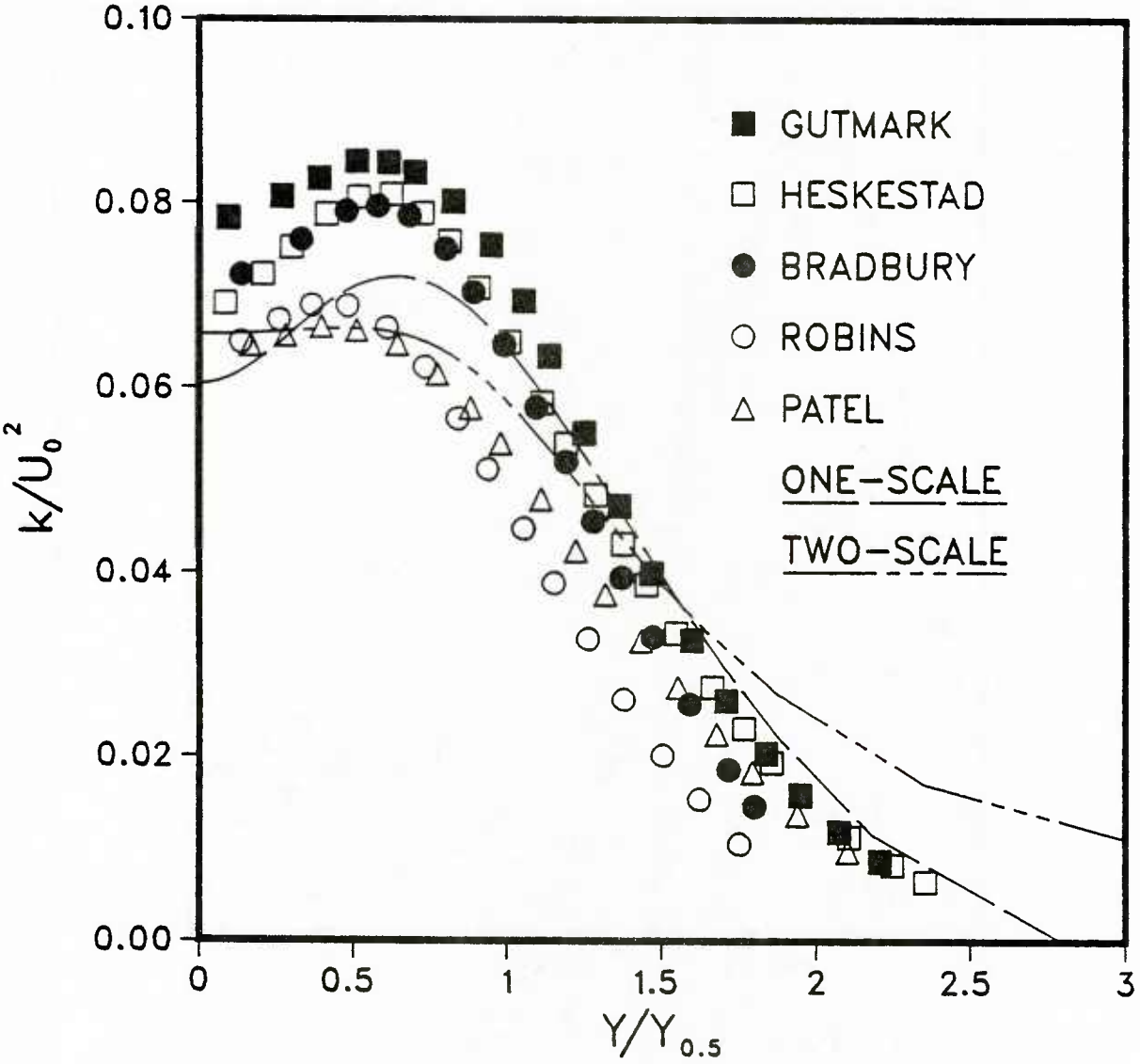

Figure 5.2. k-profile for a plane jet

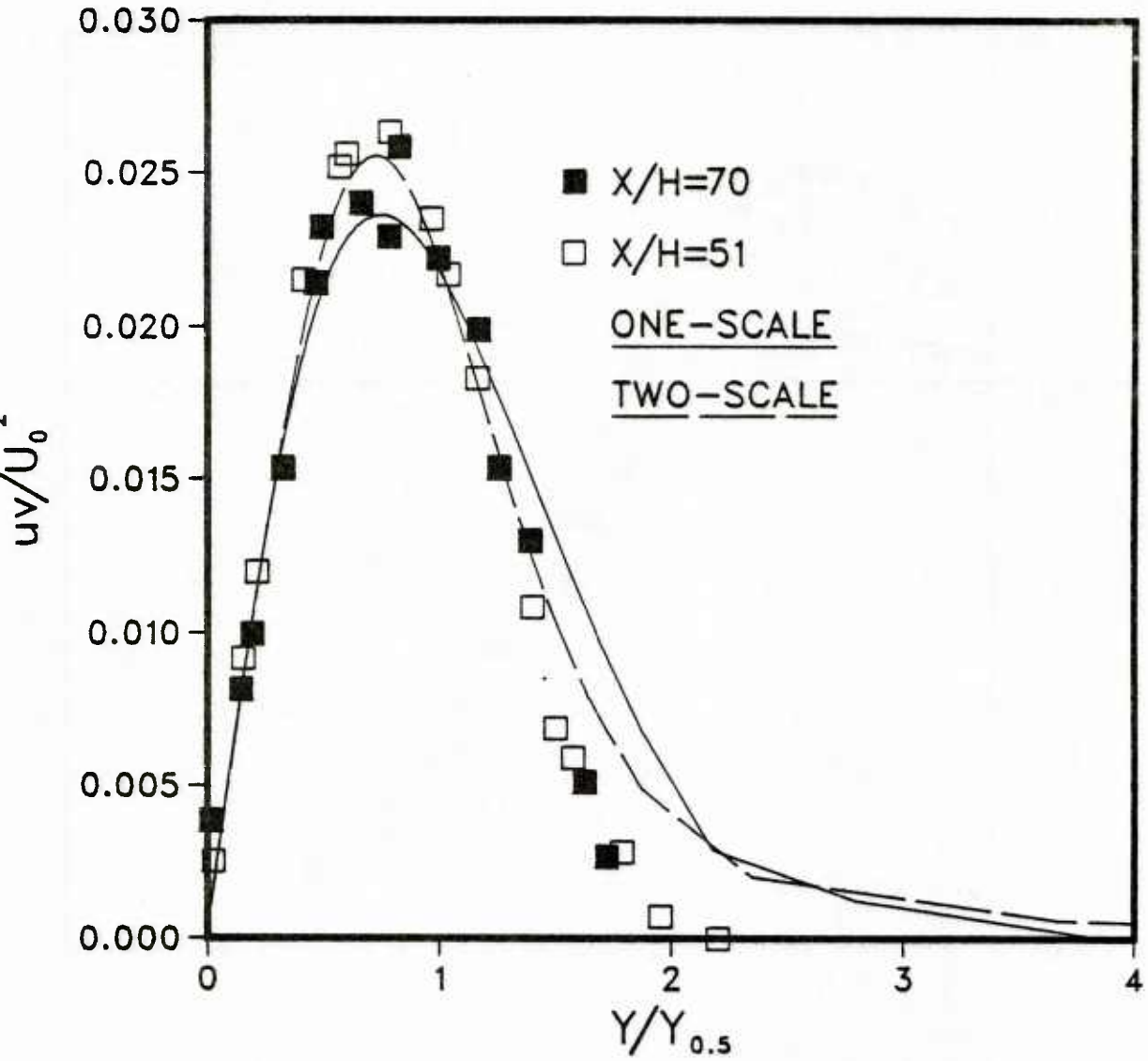

Figure 5.3. Reynolds stress in a plane jet

The results discussed so far are in the self-preserving region of a plane jet where x/D >40. Figure 5.4 shows the velocity decay in the near region of a jet. The slight difference in the results can be attributed to the difference in initial conditions at the nozzle. Chen and Nikitopolous [23] found that the larger the turbulence intensity at the jet exit, the shorter is the potential core length. They found that when the initial turbulent intensity is taken to be 6% of the mean flow kinetic energy, the predicted potential core agrees with that measured by experiment [57]. Therefore, 6% value is used in the present calculations. The experimental data of Van der Hegge [31] and Bradbury [30] are shown along with the prediction of the two models. With 6% turbulence intensity, the two-scale model predicts the core length less than that of the one-scale model. Hence, it is assumed that a smaller turbulent intensity might be necessary for the two-scale model to have better agreement with experiment.

The spreading rate obtained by the one-scale and the two-scale models are 0.112 and 0.109 respectively, both of which are close to the recommended value of 0.11 obtained experimentally.

5.3.2 Round jet

One of the major improvements of the two-scale turbulence model is the prediction of round jet flow field. As shown in table 5.1, the two-scale model predicts correctly a spreading rate of 0.081 for the round jet while the one-scale model, without varying the turbulent constants

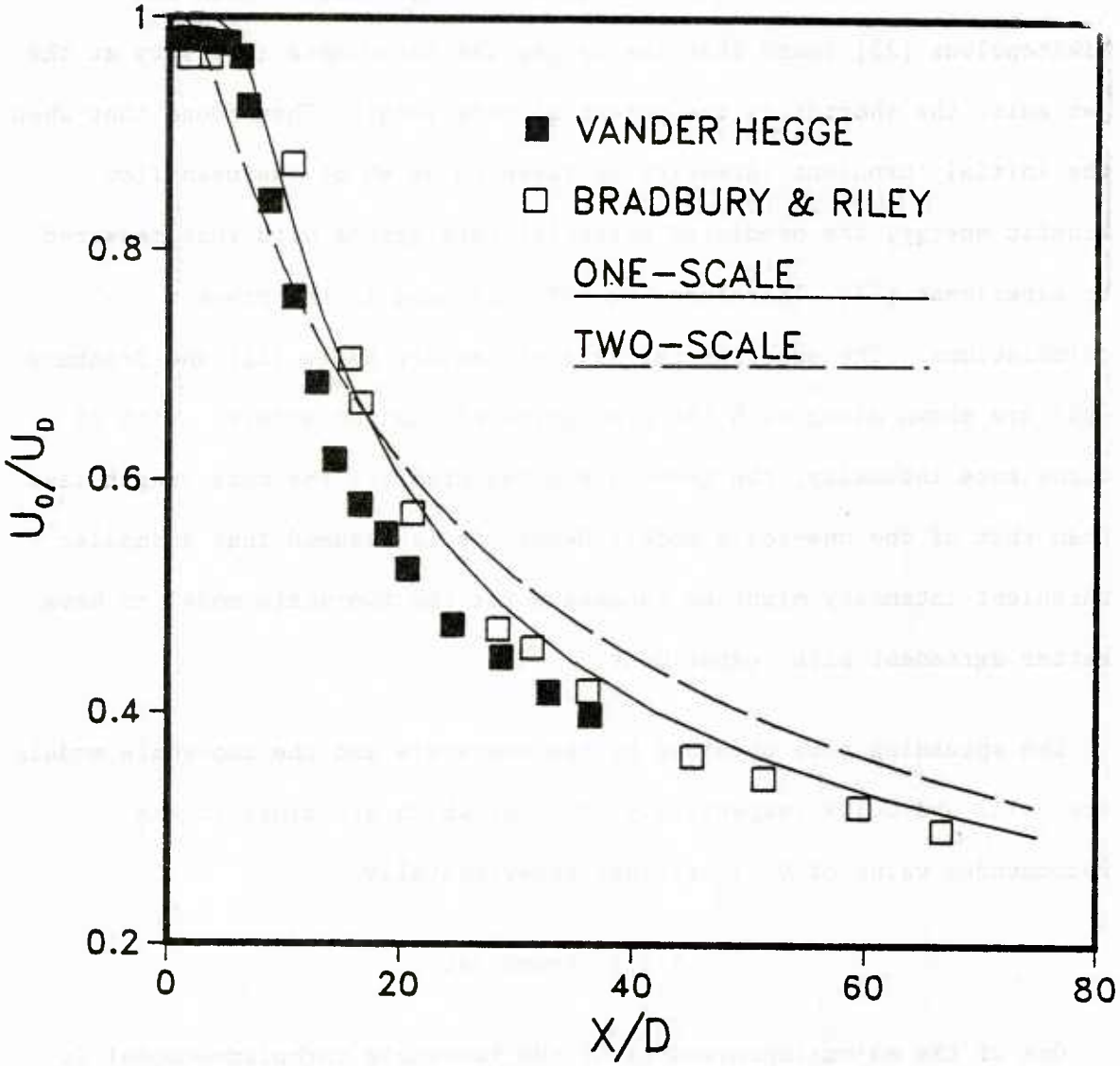

Figure 5.4. Centerline velocity decay for a plane jet

from that used in the plane jet prediction, gives 0.119, a 45% larger spread rate than the experimental value. It should be remarked that in order to remedy the deficiency of the one-scale model in predicting the round jet flow field, many ad hoc proposals [58-60] were put forth. Pope [58] proposed that the constant $C_{\varepsilon 2}$ be modified as

$$C_{\varepsilon 2}=1.9 - 0.79\chi$$

where

$$\chi = \frac{1}{4}\left(\frac{k}{\varepsilon}\right)^3 \left(\frac{\partial U}{\partial r} - \frac{\partial V}{\partial r}\right)^2 \frac{V}{r}$$

Rodi [4] proposed a modification of the constant $C_{\varepsilon 2}$ used in the ε-equation. The correction is

$$C_{\varepsilon 2} = 1.92 - 0.0667\left[\frac{y_{\frac{1}{2}}}{2U_c}\left(\left|\frac{dU_c}{dx}\right| - \frac{dU_c}{dx}\right)\right]^{0.2}$$

Several other modifications have also been suggested, namely, by Morse [59] and McGuirk and Rodi [60].

The velocity profile for a round jet is shown in figure 5.5. The initial conditions for U, k and ε at the jet exit are the same as those of a plane jet. It should be remarked that the abscissa is now y/x. The prediction of the one-scale model with the same constants as for plane jet gives incorrect spread rate as shown in figure 5.5.

The experimental data plotted in figure 5.5 are obtained for a wide range of x/D. Hetsroni's [32] measurements were upto a distance of x/D=35 while Wygnanski [33] measured up to x/D=40. These measurements are somewhat different from those of Shearer [34] et al. who collected data as far as 510 diameters downstream. Overall, these data points fall in one curve within a certain amount of scatter indicating that the mean flow reaches similarity some distance downstream of x/D=40. This is further confirmed by the result predicted by the two-scale model where the result of the calculations are taken at x/D=75. The predicted results agree very well with the experiment throughout the whole region, except near the edge of the outer region where the measurement may be affected by the intermittency between laminar and turbulent flow. The fact that the centerline velocity predicted at x/D=75 agrees well with the data shows that the velocity decay along the axial line is satisfactory.

Figure 5.6 gives the distribution of turbulent kinetic energy in a round jet. The calculations are taken at x/D=75. From this figure, it is clear that there is a large variation near the center of the jet. Wygnanski's data, taken at x/D=40 only, indicates a value of k_c/U_o^2 of 0.1 which is higher than 0.08 measured by Shearer. The latter made measurements up to x/D of 510. This difference in the centerline kinetic energy could be due to the fact that turbulence quantities become self-preserving much after the mean quantities become self-similar. The one-scale model due to its inability to predict correctly the spreading rate

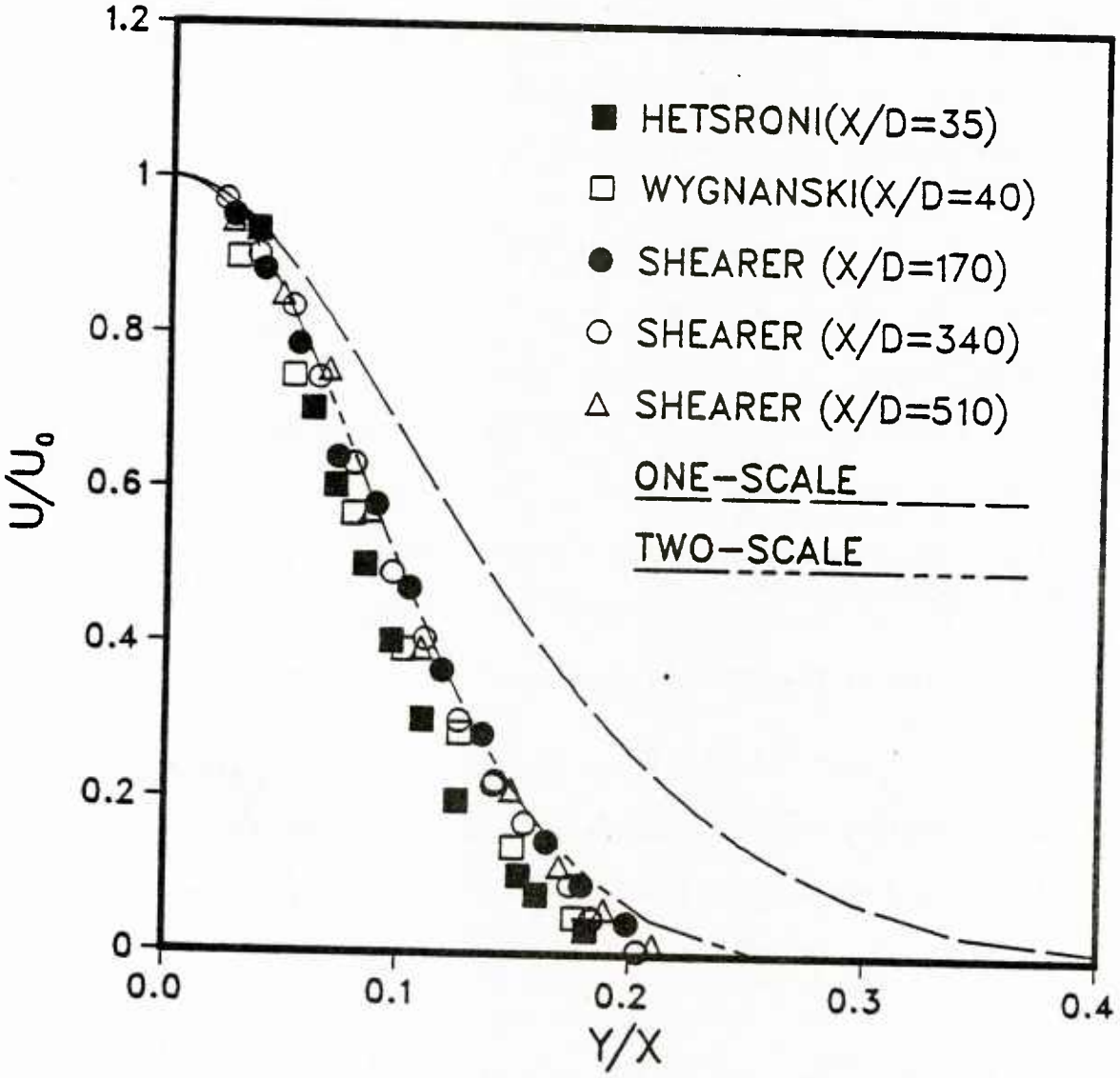

Figure 3.5. Velocity profile for a round jet

predicts turbulent kinetic energy distribution further away from the experimental data. Using the one-scale turbulence model without the modified constants, a maximum value of 0.095 is obtained at the centerline while the two-scale model predicts a value of 0.067. Although more experimental data are necessary to decide the level of turbulence intensity at the jet centerline, it seems that the two-scale model may predict a smaller turbulent intensity than the available data.

Figure 5.7 shows the Reynolds stress distribution in a round jet. There is, once again, a difference of about 20% in the maximum value of the Reynolds stress as obtained by Wygnanski and by Shearer. The former measured a peak value of 0.0168 while Shearer got a value of 0.020. The prediction of the one-scale model indicates a maximum Reynolds stress of 0.025 whereas the value of 0.019 obtained by the two-scale model is closer to the experimental data of Shearer. In general, the two-scale model predicts satisfactory results.

Figure 5.8 gives the centerline velocity decay for a round jet using the one-scale and two-scale models along with the experimental data of Corssin [35], Wygnanski [33] and Shearer [34]. The difference in the result is due to the initial condition of the turbulent kinetic energy and the mean velocity profile. Chen and Nikitopolous [23] showed that the initial potential core length is a strong function of the initial mean velocity profile and turbulent kinetic energy. For fixed turbulent intensity at 1.25% of the mean kinetic energy, the core length is about 7.3 jet diameters with a flat exit velocity profile and 3.25 with a

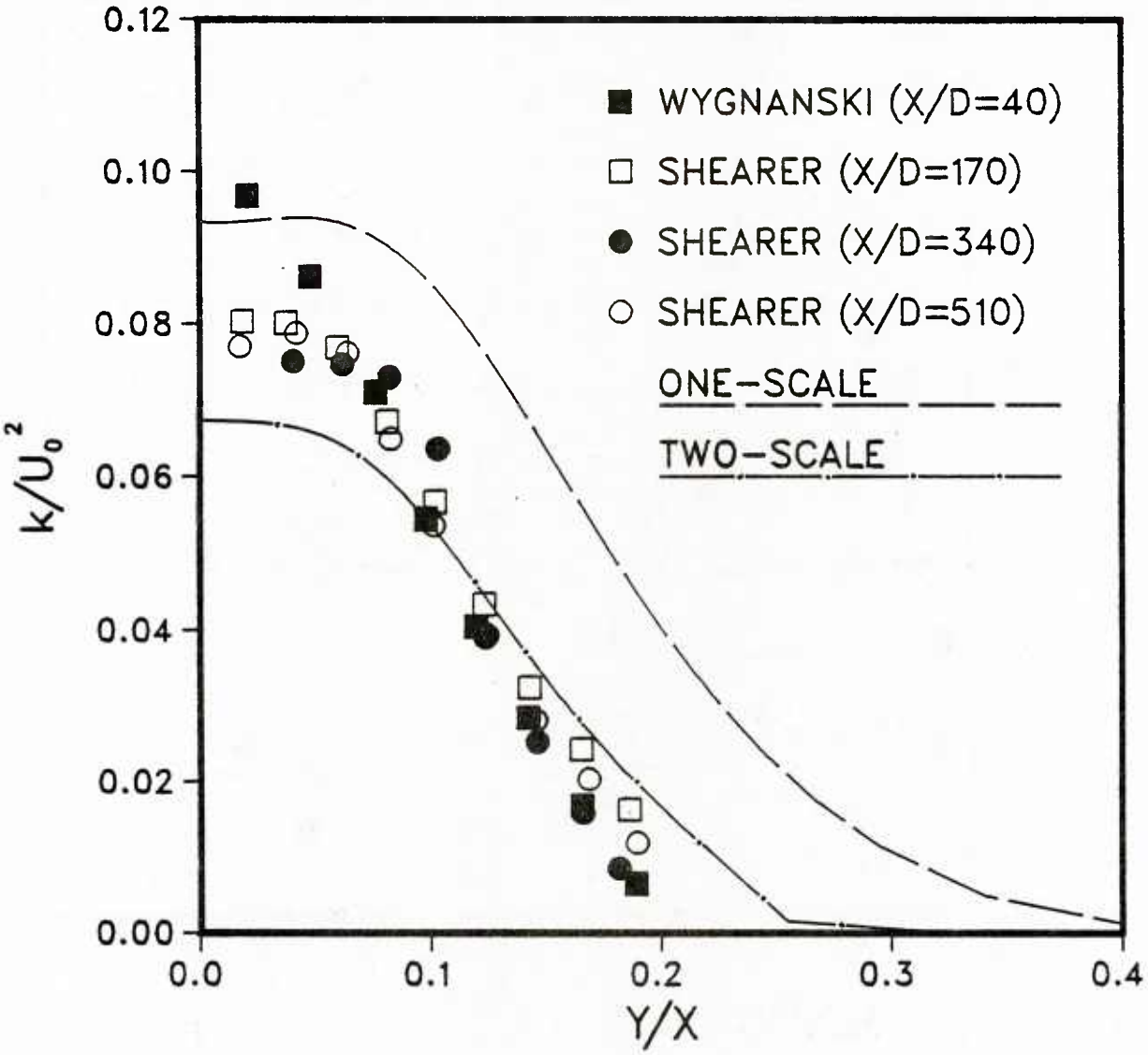

Figure 5.6. k-profile for a round jet

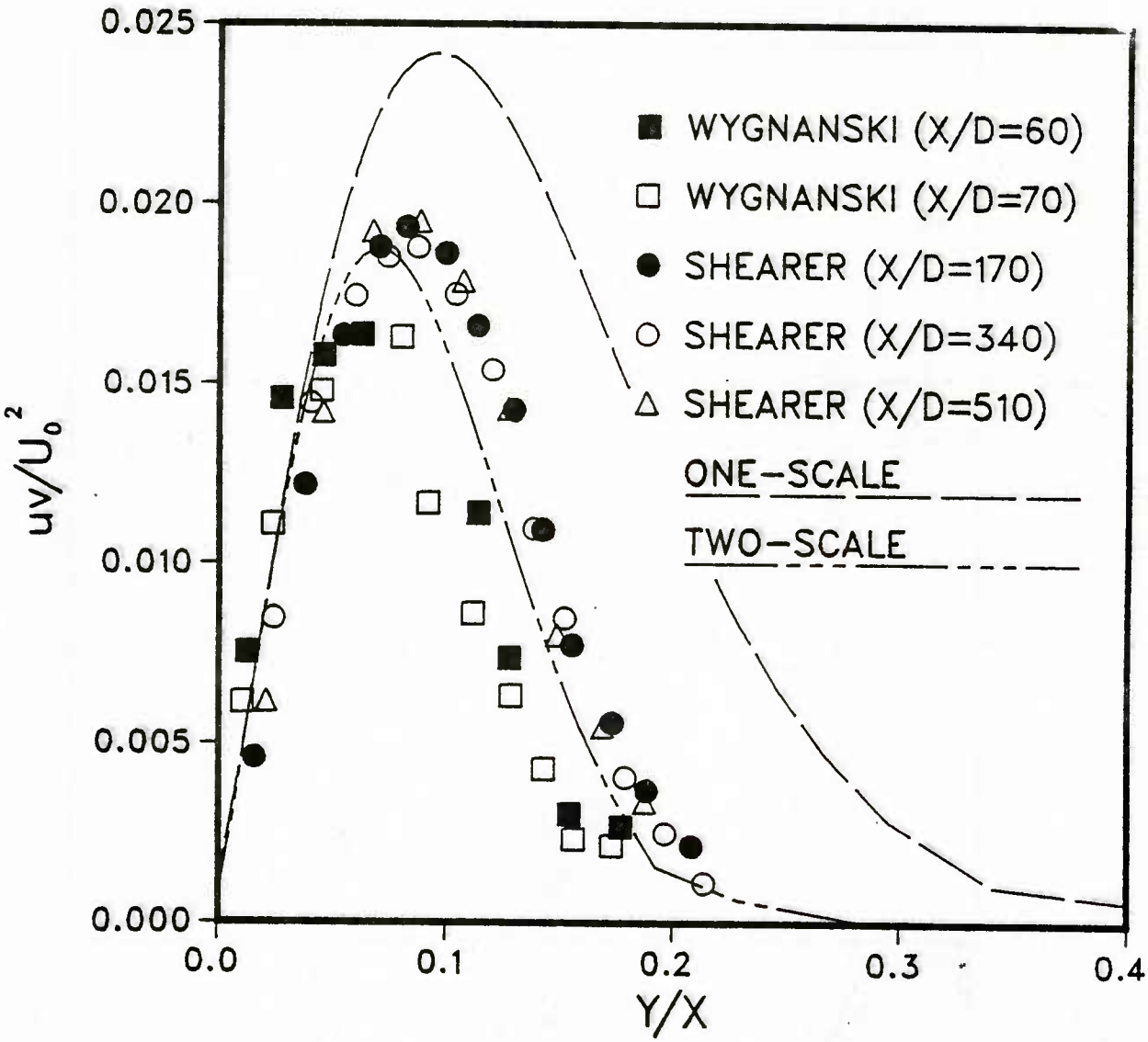

Figure 5.7. Reynolds stress for a round jet

triangular exit velocity profile. In the present calculation, a turbulent intensity of 6% and the exit mean velocity profile given by

$$U=U_N\exp(-y^2)$$

was used. The prediction of the two-scale turbulence model indicates a core length of about 5 diameters which agrees with the measured core length.

5.4 Plane wake

The initial conditions used in the calculations of the plane wake are

$$U=U_E(y/\delta)^{1/7}$$

$$k=0.008U_E^2\mathrm{Sin}[1.57(1 - y/\delta)]$$

$$\varepsilon=0.09k^{1.5}/\delta$$

where U_E is the free stream velocity and δ is the boundary layer thickness at the beginning of the wake flow. Most of the existing turbulence models used in the calculation of turbulent flows do not accurately predict some of the flow parameters of turbulent wakes, in particular, the spread rate of the wake. This is, perhaps, due to the fact that the turbulent process in a wake involves complex interaction among turbulent diffusion, production and dissipation and also due to the fact that the flow in the far wake region is not fully turbulent. As shown in table 5.1 , the one-scale model underpredicts the spreading rate by about 30%. The measured spreading rate, defined as

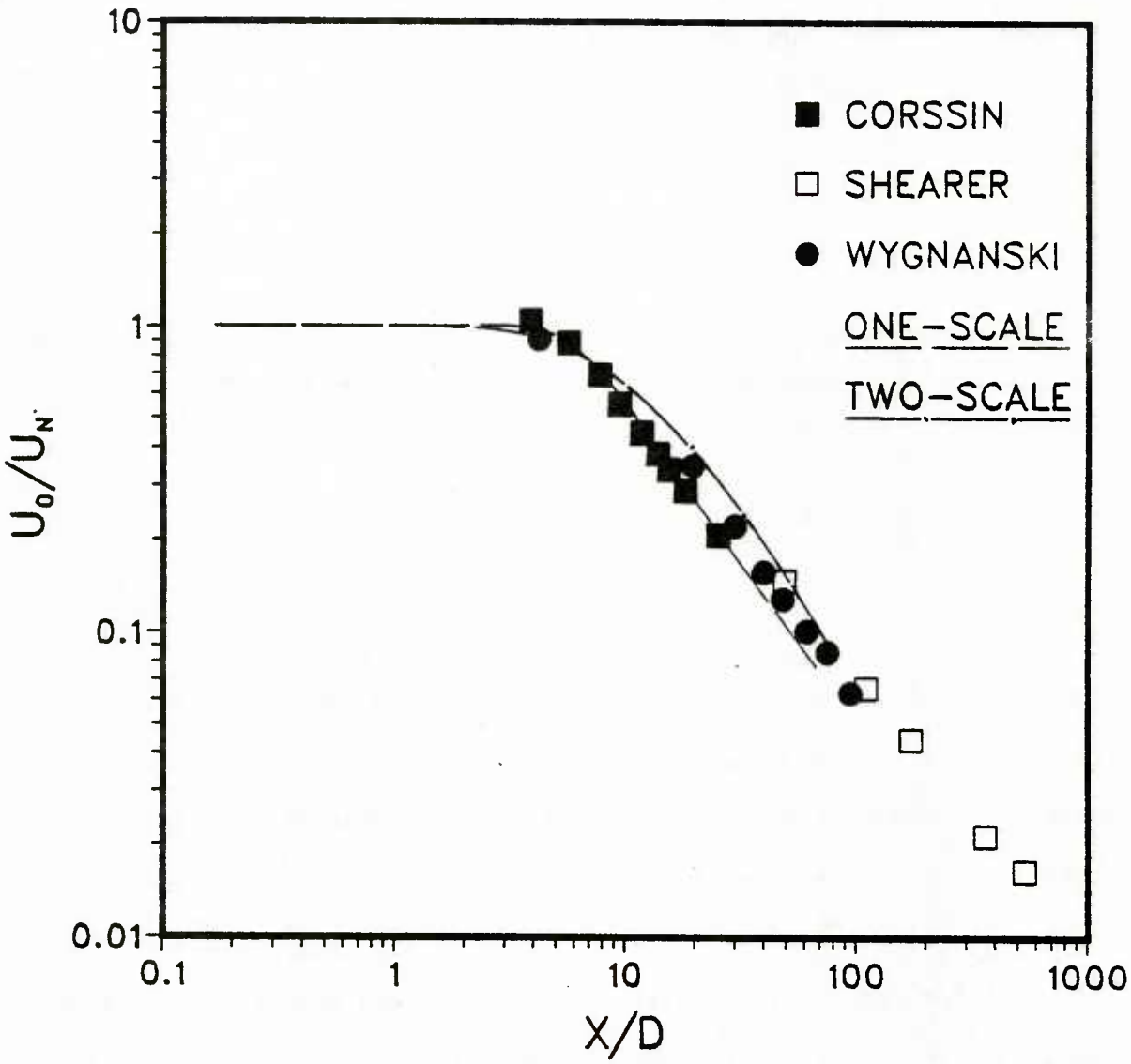

Figure 5.8. Centerline velocity decay for a round jet

$$S = \frac{U_E}{w_o} \frac{dy_{\frac{1}{2}}}{dx}$$

is 0.098 while the one-scale model gives 0.068. On the other hand, the two-scale model predicts quite satisfactorily a spread rate of 0.0975.

Figure 5.9 shows the asymptotic velocity profile in the far wake region where $x/\theta=600$. The momentum thickness, θ, is obtained from the velocity profile at the trailing edge. The experimental result is that of Pot [39], taken at $x/\theta=1000$, which compares very well with the predicted profile of the two-scale model except at the edge of the wake. When the predicted velocity profile is plotted against $y/y_{\frac{1}{2}}$, the one-scale and two-scale turbulence models differ somewhat near the edge of the wake. However, it should be noted that the $y_{\frac{1}{2}}$ predicted by the one-scale model is 30% lower than experimental value.

In figure 5.10, the Reynolds stress versus $y/y_{\frac{1}{2}}$ is shown for the far wake. The values calculated from the one-scale model differ considerably from that by the two-scale model and experiment. Patel et al. [37] improved the one-scale turbulence model with the turbulent constants altered and by introducing the intermittency near the edge of the flow. Their result showed some improvement in the prediction. However, it is emphasized that no modification of turbulent constants were needed for the two-scale turbulence model in predicting the wake flow.

Figure 5.11 gives the center-line velocity defect in the near and far wake region. U_E and U_o are the free stream and centerline velocity

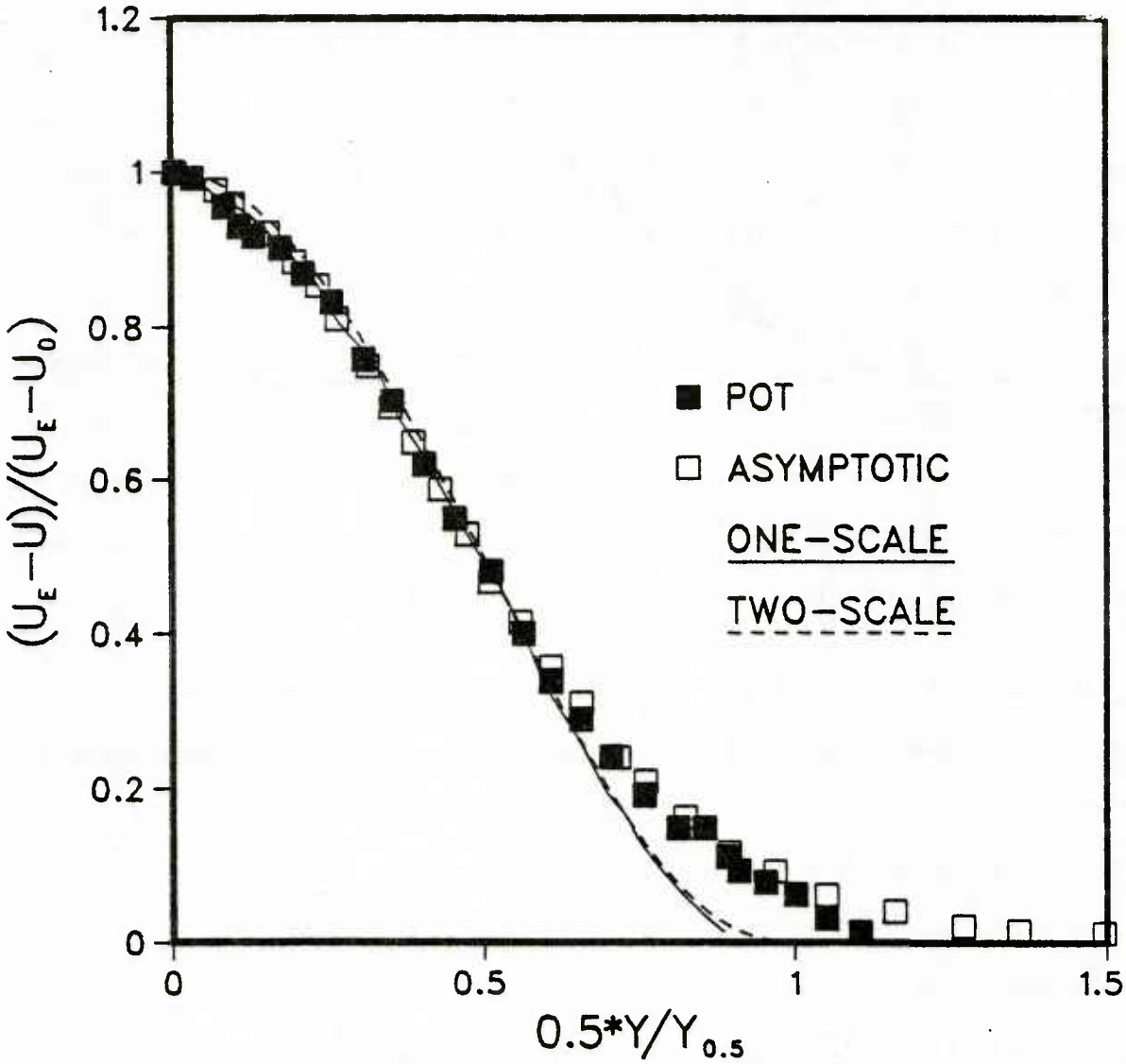

Figure 5.9. Asymptotic velocity profile in a far wake

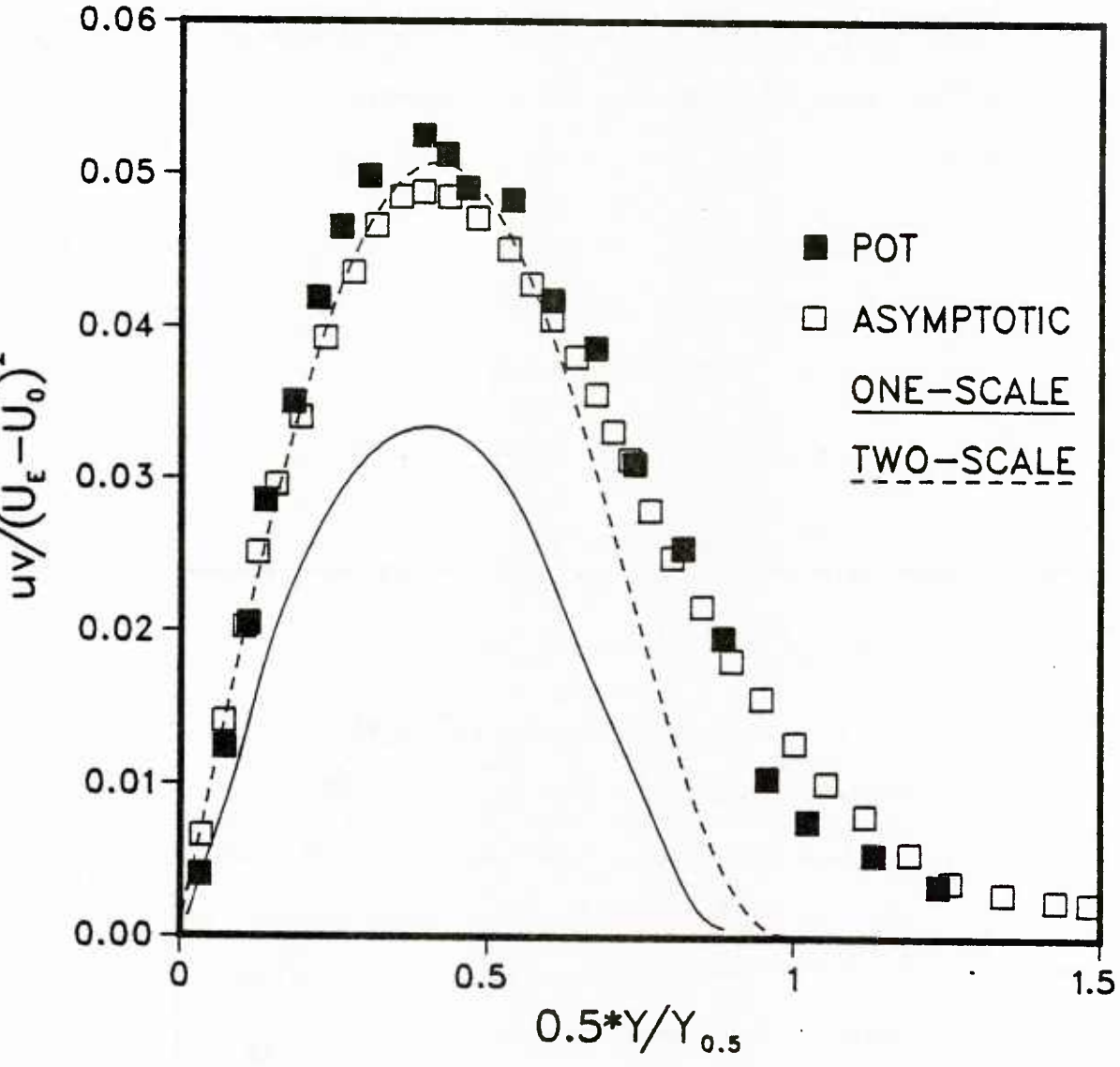

Figure 5.10. Reynolds stress in a far wake

respectively. The results of both the one-scale and two-scale models are in good agreement with experimental results.

5.5 Plane mixing layer

The accurate prediction of mixing layer flow depends heavily on the initial conditions since the mixing flow resembles the initial development of a jet.

Figure 5.12 shows the velocity profile in a mixing layer obtained at x/D=5. Here D is the width of the jet exit. The calculations were done from x/D=0 to x/D=5 with the initial conditions for U and k as

$$U=0 \text{ for } y>0$$

$$U=U_I \text{ for } y<0$$

$$k=0.01U_I^2\exp(-y^2) \text{ for } y<0$$

where U_I is the initial velocity of the mixing flow. The calculations are presented only for the two-scale model since one-scale model predicts satisfactorily the gross properties. The two-scale model also predicts velocity distribution which is in good agreement with experimental results. The kinetic energy profile obtained by various experiments [41-46] varies considerably as shown in figure 5.13. However, the model generally predicts satisfactory results.

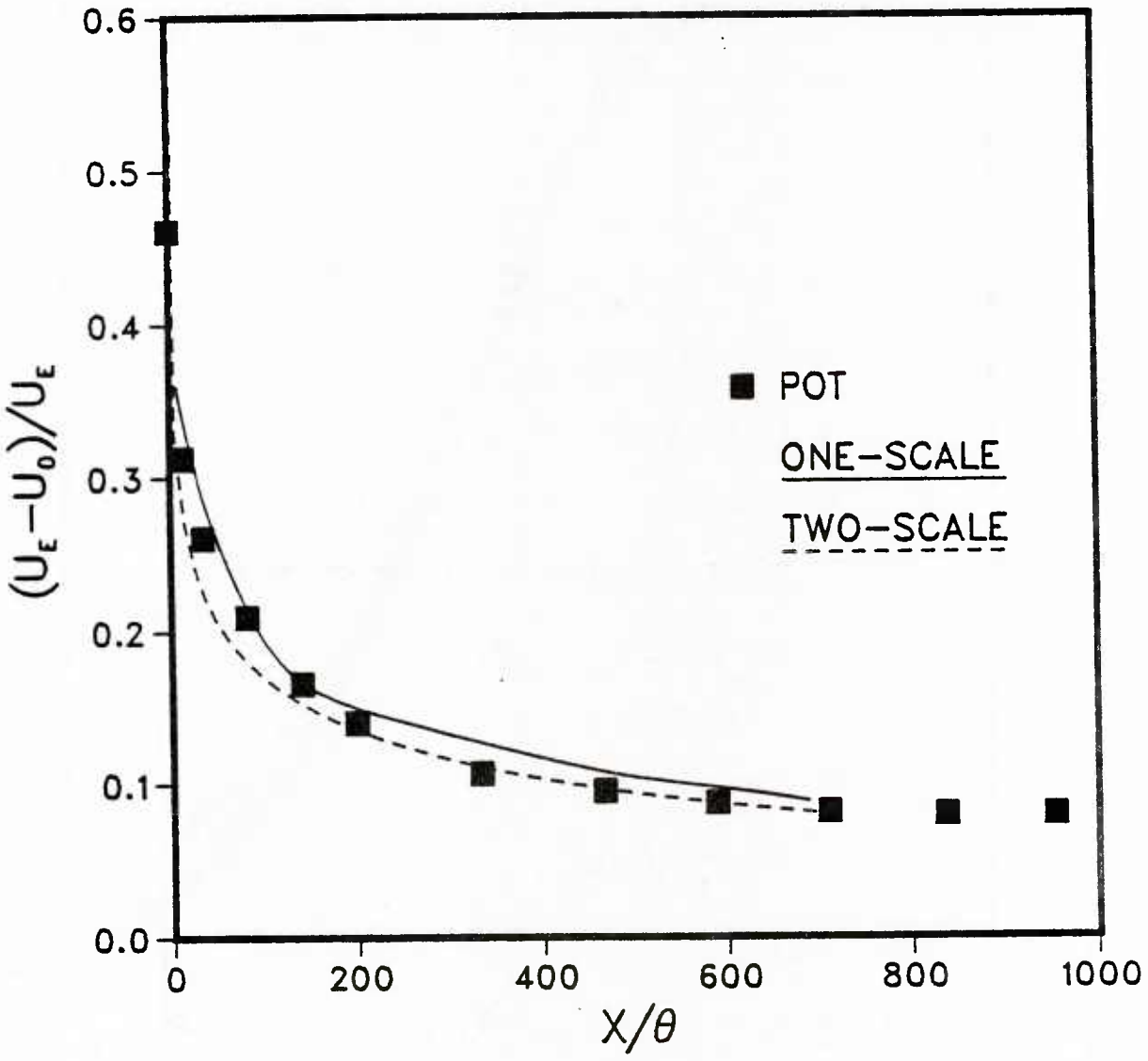

Figure 5.11. Centerline velocity decay in a wake

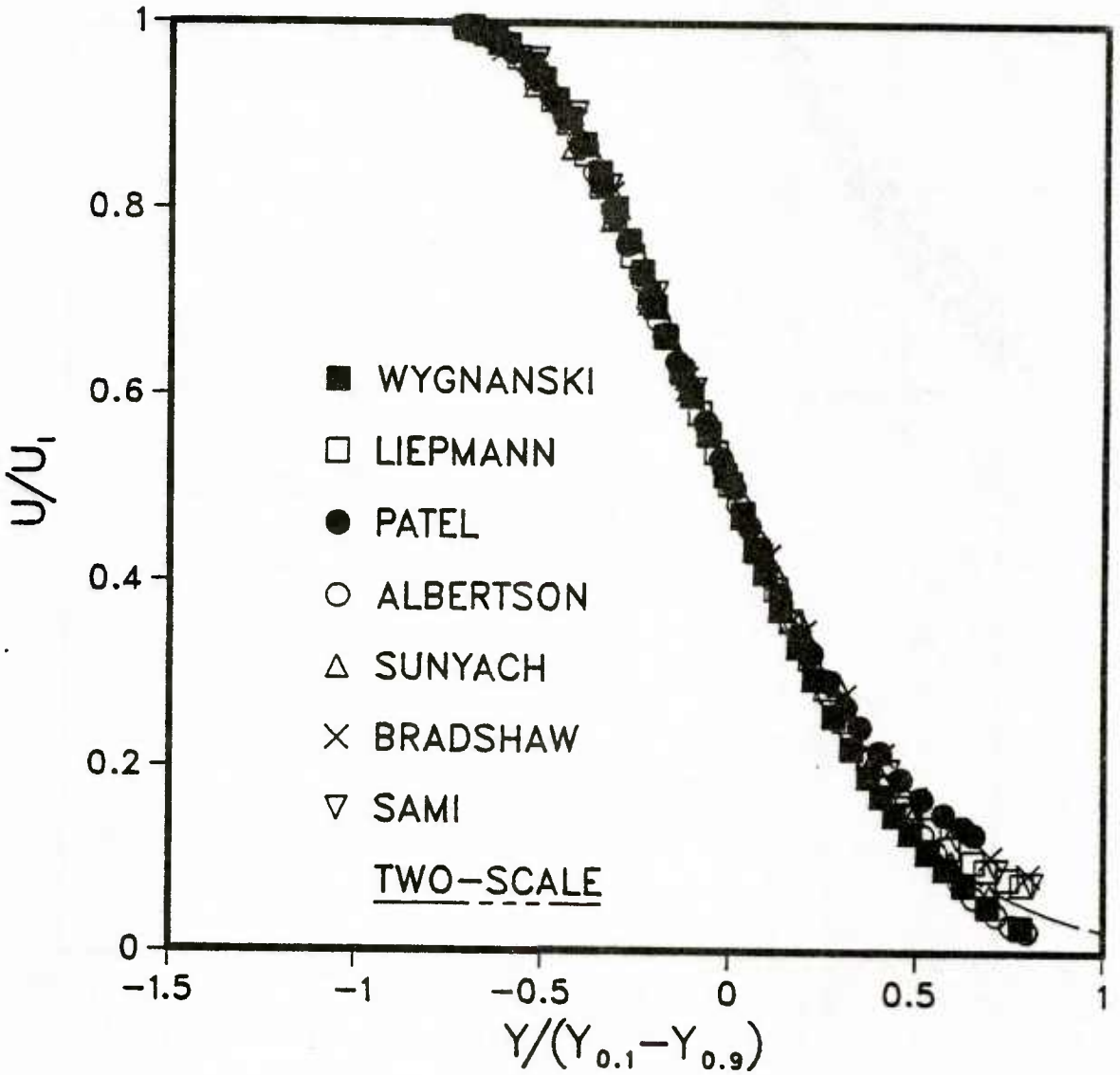

Figure 5.12. Velocity profile in a mixing layer

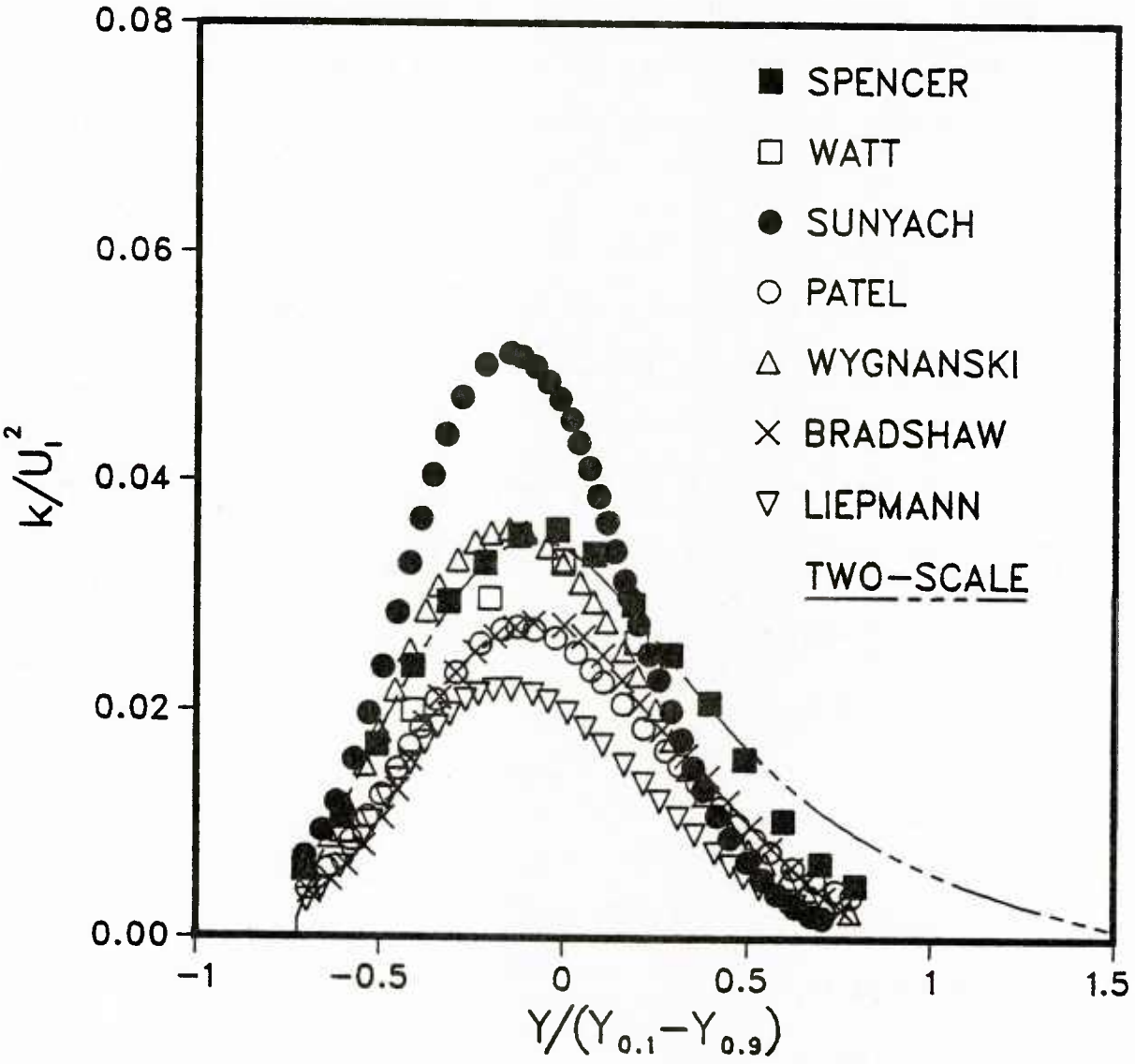

Figure 5.13. Kinetic energy in a mixing layer

5.6 Jets flowing into moving surrounding

In this section, jet flows into moving surroundings are considered where the jet exit velocity is larger than the free-stream velocity. As mentioned in chapter IV, jets flowing into moving surrounding are only approximately self-similar. The flow field can be approximately divided into two regions, namely, strong jet region where the strain rate is large and a weak region where the strain rate falls from relatively large to small values. This weak jet region is an important test case for turbulence models, since turbulence process in this region of weak strain rate involves not only turbulent production and dissipation but also significant amount of turbulent diffusion. Therefore, unless the turbulent transport equations are properly modelled, the predictability may not be accurate. The initial conditions for the jet are

$$U=U_N\exp(-y^2)$$

$$k=0.06U_N^2\exp(-y^2)$$

and for the free stream are

$$U=U_E=\text{Constant}$$

$$K=0$$

5.6.1 Plane jet

Experimental data of Bradbury and Riley [30] shows that except near the nozzle exit, the velocity profiles collapse into a single curve independent of the ratio

$$\lambda = \frac{U_E}{U_E - U_o}$$

where U_E is the free stream velocity and U_o is the centerline velocity. With U_o varying in the axial coordinate, the ratio, λ, may be used to denote various distances downstream and to indicate when self-similarity is achieved. Figure 5.14 shows the velocity profiles for a plane jet. The calculations of the one-scale and two-scale models are shown along with the experimental data. Since the flow far downstream becomes approximately self-similar, calculations are shown for only one location x/D=75. The ratio, U_N/U_E, of jet exit velocity to free stream velocity used in the calculation was 3.3. The results of the two models show good agreement with the experimental data of Bradbury and Riley [30].

In figure 5.15, the decay of centerline velocity of the plane jet is shown. The predicted centerline velocity by the two-scale model gives slightly slower decay rate. Nevertheless, the calculations tend to reach experimental value far downstream.

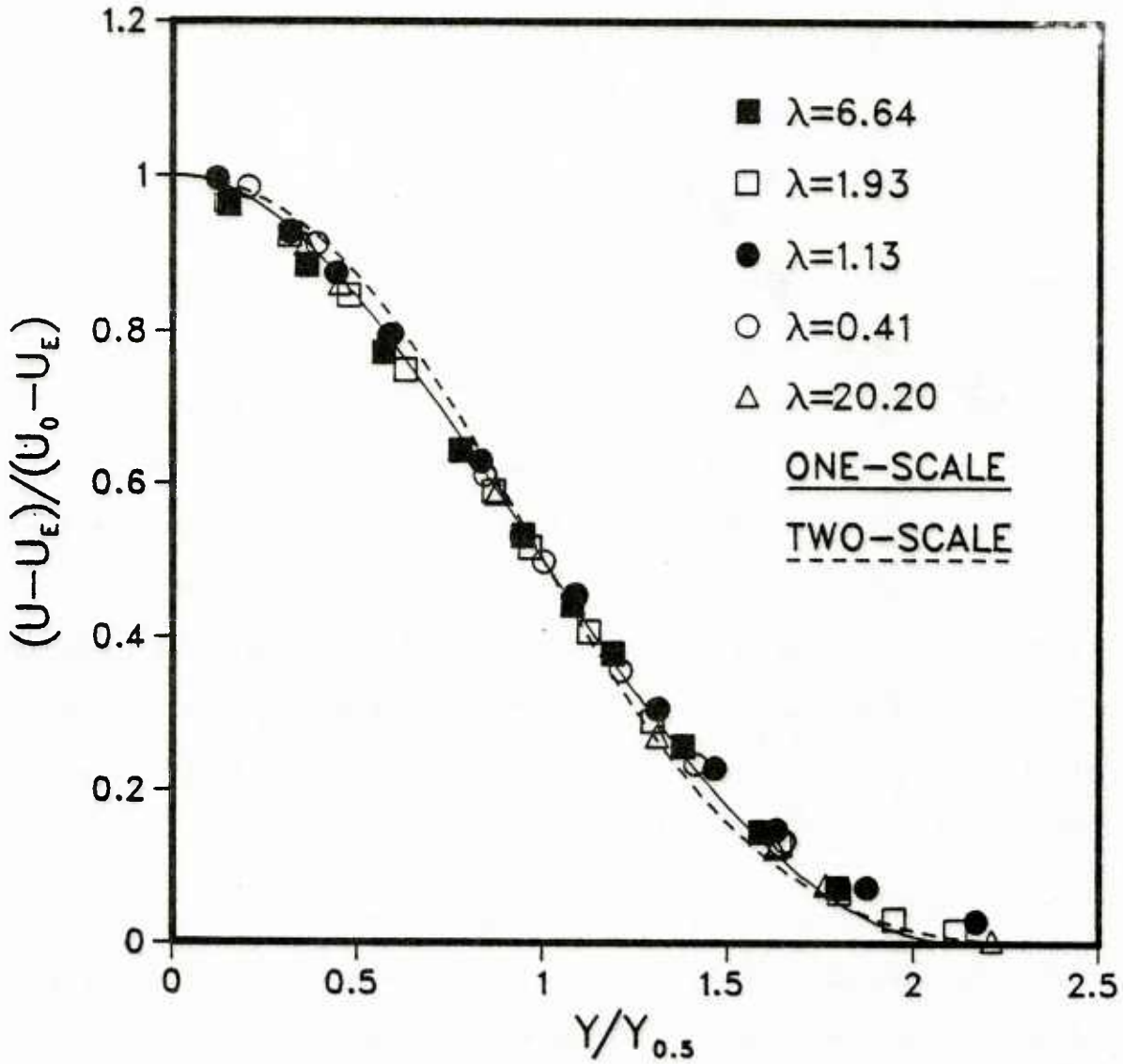

Figure 5.14. Velocity profile for a plane jet in moving surrounding

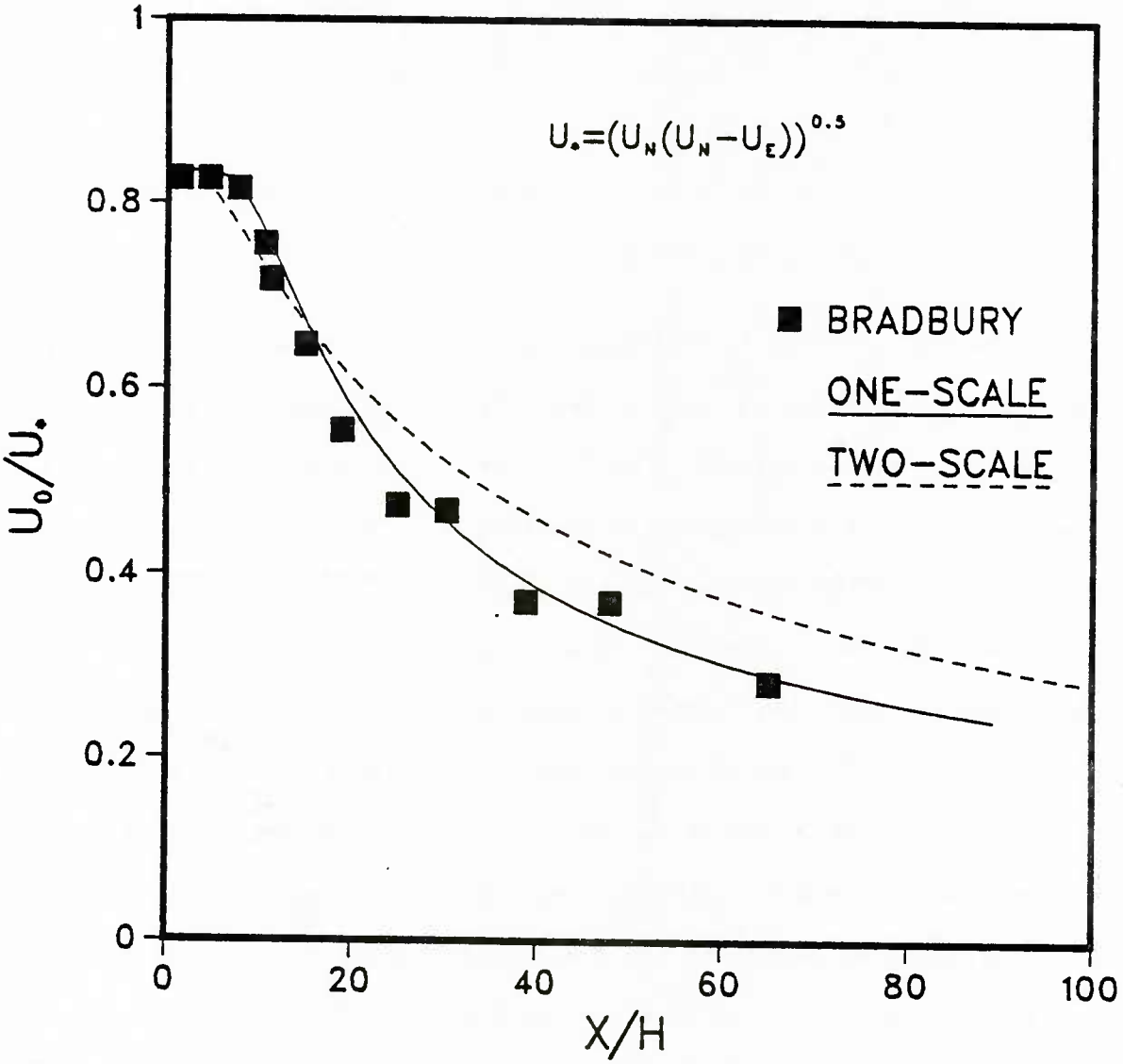

Figure 5.15. Centerline velocity decay of a plane jet in moving surrounding

5.6.2 Round jet

For a round jet, the predictions of the one-scale and two-scale models are compared with the experimental result of Antonia and Bilger [49] as shown in figure 5.16. The experimental data collapse into a single curve for all distances beyond x/D=38. Hence, the velocity profile at x/D=75 is shown where the flow is approximately self-similar. The ratio of the nozzle velocity U_N to the free stream velocity U_E chosen is 3.3. There is a good agreement between the experimental result and the two turbulence models.

The Reynolds stress is shown in figure 5.17 for x/D=75. According to the experimental data of Antonio and Bilger, the stress at x/D=248 is larger than that at x/D=152. This indicates that the turbulence quantities have not reached self-similarity. The calculations of the one-scale and two-scale models are shown for x/D of 75. Around $y/y_{\frac{1}{2}}$ of 0.8, there is some difference between the two models and the experimental data. The predicted Reynolds stress in general follows the trend of the experiment but gives smaller magnitude particularly near the peak or $y/y_{\frac{1}{2}}$=0.8. The cause of large value of measured Reynolds stress probably is due to the initial conditions where in the experiment the nozzle of the round jet has a finite thickness while it is assumed infinitely thin in the computation. Furthermore, an increase in the initial turbulent kinetic energy for the calculation can not only cause steeper decay of centerline velocity than that shown in figure 5.15 but also increase the predicted Reynolds stress in figure 5.17.

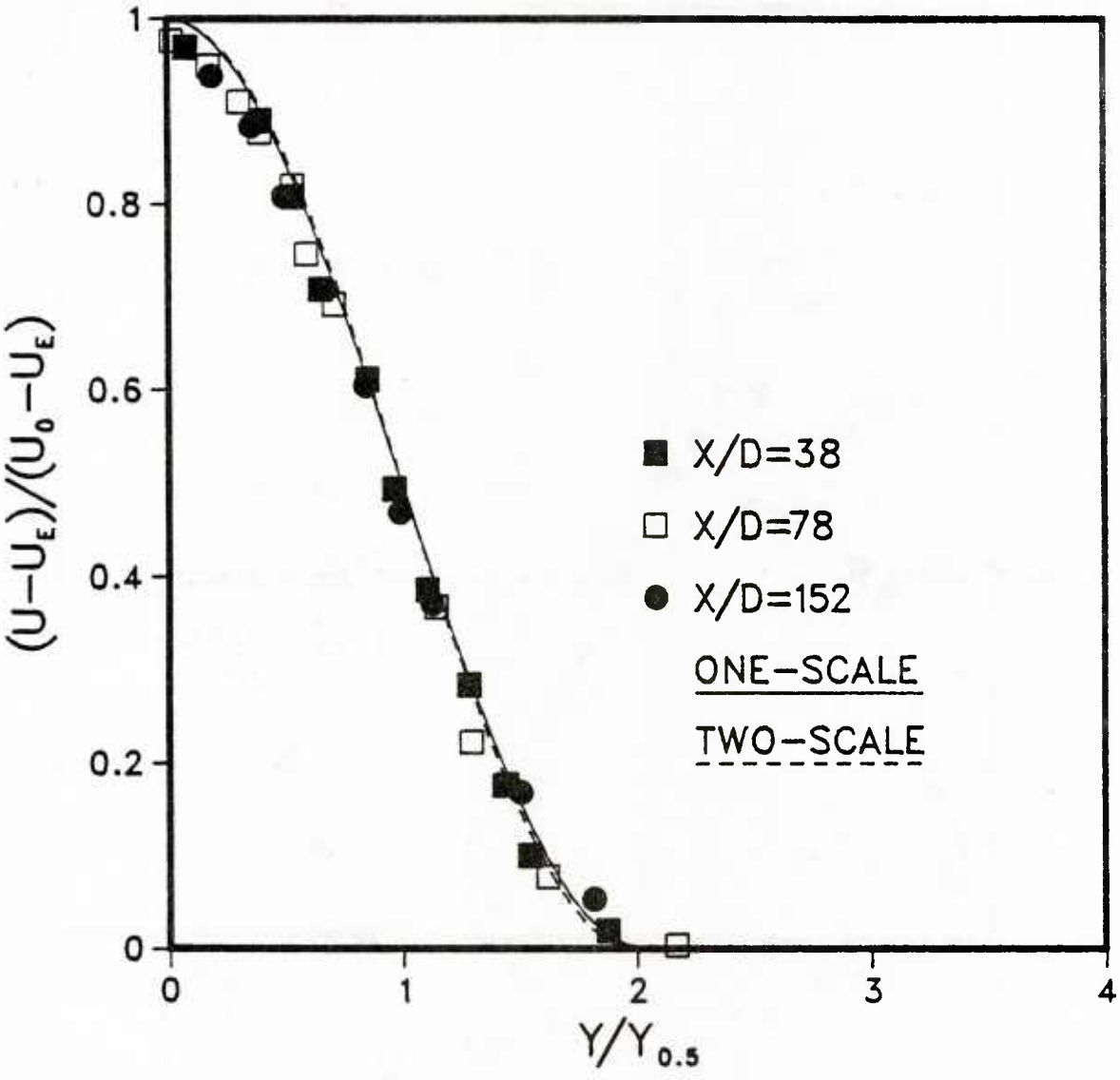

Figure 5.16. Velocity profile for a round jet in a moving surrounding

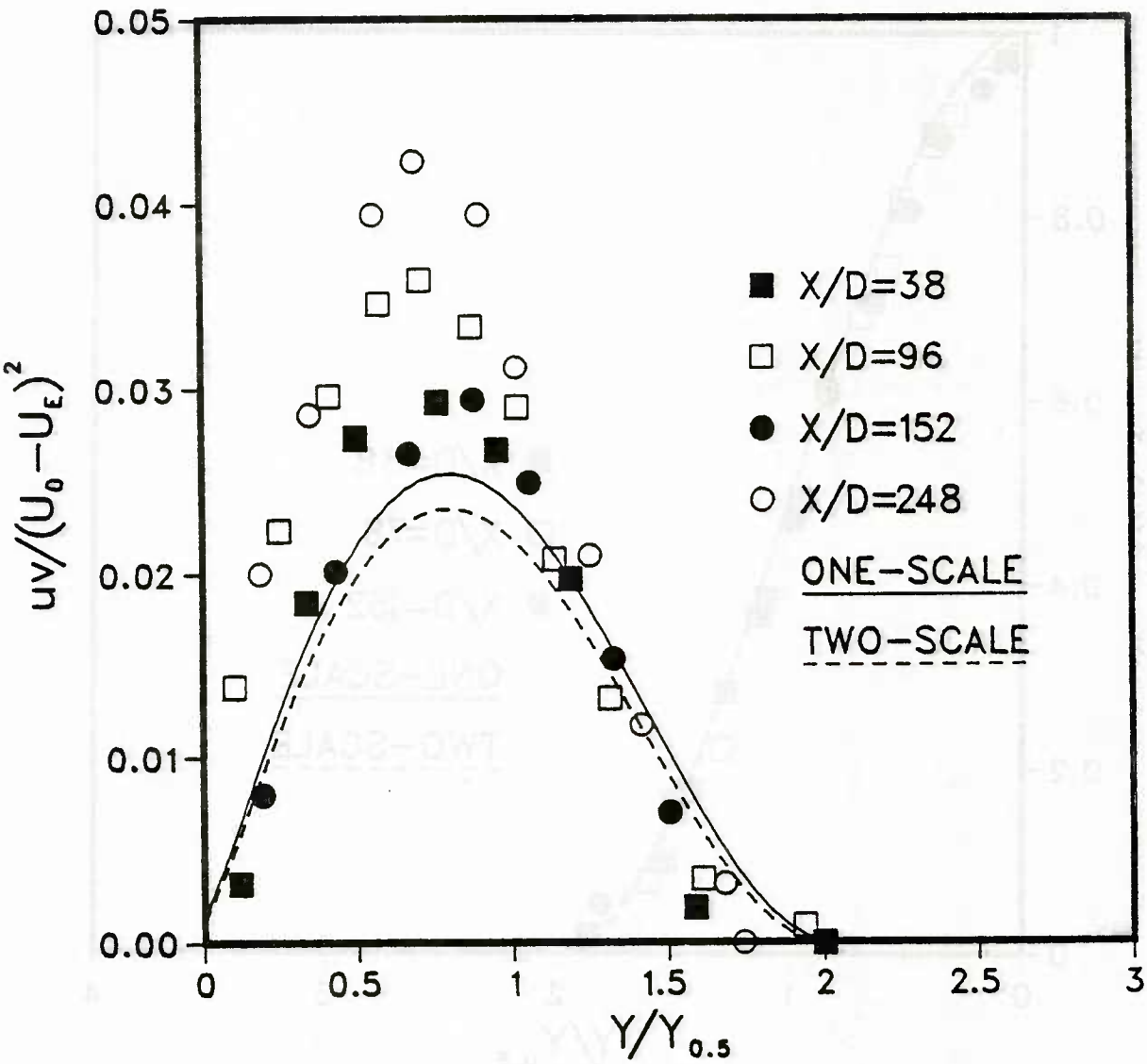

Figure 5.17. Reynolds stress for a round jet

5.7 Sensitivity of the Coefficients

This section gives a brief discussion of the sensitivity of the coefficients $C_{\varepsilon 1}$ and $C_{\varepsilon 2}$ in the ε-equation. From homogeneous shear flow and flow behind a grid turbulence, these coefficients were found to be $18.90/(Re)^{\frac{1}{2}}$ for the two-scale second order closure model of $\overline{u_i u_j}$, k and ε. However, the coefficient $C_{\varepsilon 1}$ was modified to be $17.50/(Re)^{\frac{1}{2}}$ for the two-scale k-ε model. This modification was made because, in the calibration of $C_{\varepsilon 1}$ and $C_{\varepsilon 2}$, the diffusion terms in k and ε equations for both homogeneous and grid turbulence flows were neglected which is not the case. The values $C_{\varepsilon 1}=17.5/(Re)^{\frac{1}{2}}$ and $C_{\varepsilon 2}=18.9/(Re)^{\frac{1}{2}}$ were obtained by solving the plane jet flow where the turbulent diffusion term is increased in the calculation.

It is known that flow prediction based on the one-scale turbulence model is very sensitive to the $C_{\varepsilon 2}$ coefficient which has a value between 1.90 and 1.92. Any value outside this range may cause the prediction to change significantly. On the other hand, for computation based on the two-scale turbulence model, $C_{\varepsilon 2}$ may be changed from $11.90/(Re)^{\frac{1}{2}}$ to $18.90/(Re)^{\frac{1}{2}}$ and $C_{\varepsilon 1}$ from $10.50/(Re)^{\frac{1}{2}}$ to $17.50/(Re)^{\frac{1}{2}}$, the prediction is quite stable and satisfactory as long as the same difference of $1.4/(Re)^{\frac{1}{2}}$ between $C_{\varepsilon 1}$ and $C_{\varepsilon 2}$ is kept.

Table 5.2 shows the spreading rate for a plane jet for various values of $C_{\varepsilon 1}$ and $C_{\varepsilon 2}$. These calculations were done for Reynolds number ranging from 12,000 to 120,000.

Table 5.2

Sensitivity of spreading rate on the coefficients

Re	$C_{\varepsilon 1}/(Re)^{\frac{1}{2}}$	$C_{\varepsilon 2}/(Re)^{\frac{1}{2}}$	S
12,000	17.50	18.90	0.1017
"	15.50	16.90	0.1146
"	10.50	11.90	0.1200
24,000	17.50	18.90	0.1000
120,000	17.50	18.90	0.1009

The spreading rate varies from 0.1 to 0.12 for a change in $C_{\varepsilon 2}$ from $10.50/(Re)^{\frac{1}{2}}$ to $18.90/(Re)^{\frac{1}{2}}$ at a Reynolds number of 12,000. Hence it can be concluded that there is a slight change in S even with an appreciable change in the coefficients. This difference can be attributed more to the GENMIX program than to the physical phenomenon.

The effect of the Reynolds number is also shown in table 5.2 for a plane jet flow. The values of $C_{\varepsilon 1}$ and $C_{\varepsilon 2}$ used are 17.50 and 18.90 respectively. The Reynolds number is changed from 10^4 to 10^6. The change in the spreading rate is again very small. Thus, it can be said that a change in Reynolds number does not affect the overall structure of the jet. It should be remarked, however, that by changing the coefficients and keeping Reynolds number fixed is effectively the same as keeping the coefficients fixed and changing Reynolds number. Since there is no set pattern in the value of S, the difference is due to the numerical problem.

To further study the effect of Reynolds number, the kinetic energy is calculated for various Reynolds numbers. Figure 5.18 showsthat there is very little difference in the kinetic energy profile at different Reynolds numbers. The difference shown in this figure may be due to the numerical diffusion in the program which calculates the flow using dimensional quantities.

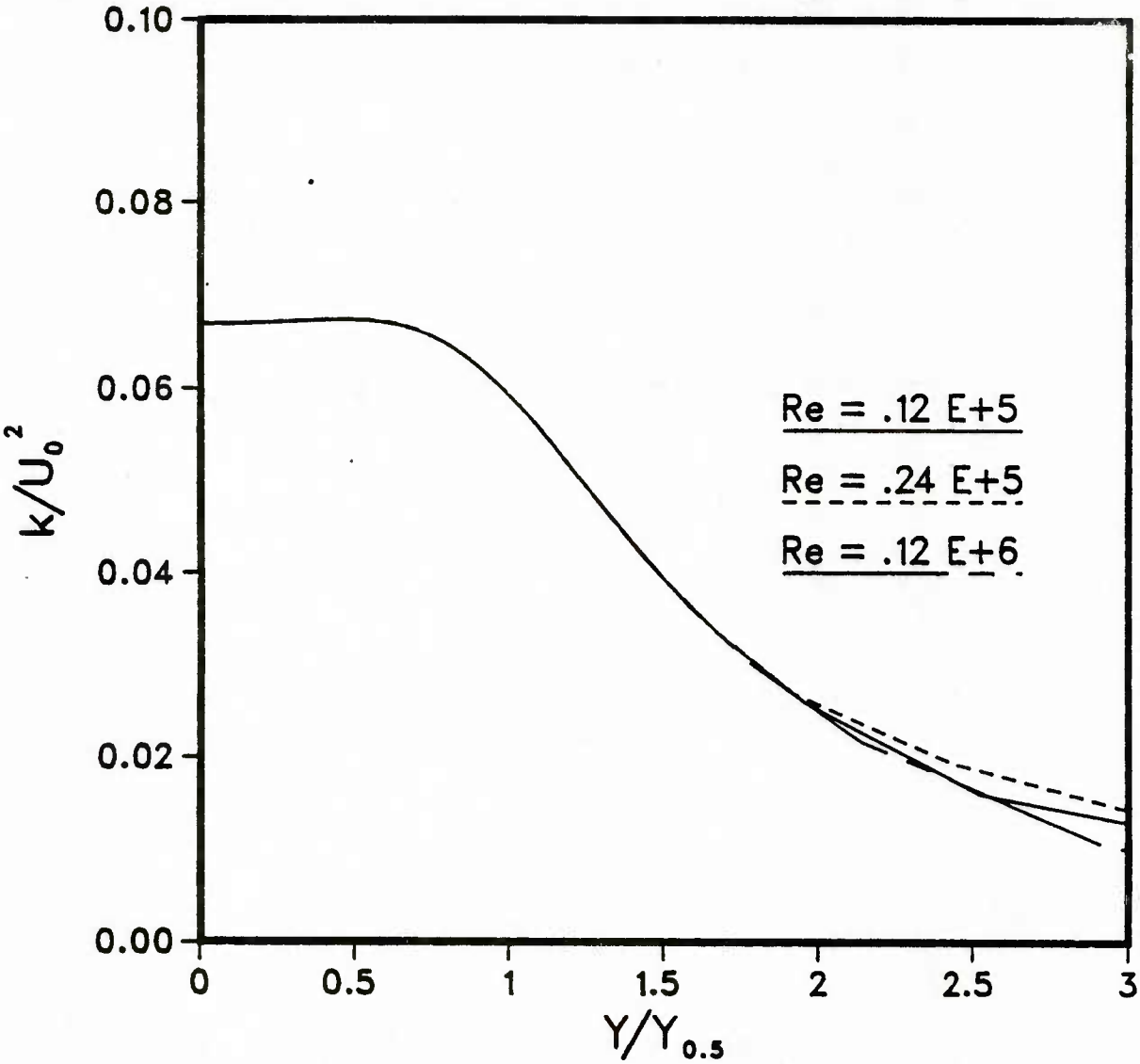

Figure 5.18. Reynolds number effect on plane jet

CHAPTER VI

PREDICTION OF TURBULENT BUOYANT JETS

This chapter shows the predictions of the two-scale turbulence model for buoyant jets based on equations (3.31), (3.32), (3.33), (3.35) and (3.36) and that of the one-scale model based on equations (3.31), (3.32), (3.33), (3.35) and (1.10). As mentioned in chapter IV, the amount of experimental data available for turbulent transport quantities in buoyant jets is scarce and insufficient to test the accuracy of the turbulence model. Hence, most of the comparison between one-scale model, two-scale model and experimental data is confined to mean flow quantities. The velocity and temperature decay along the jet axis are shown for various Froude numbers. In the present study, Froude number is defined as

$$F = \frac{\rho_o U_o^2}{g(\rho_o - \rho_a)D}$$

where

ρ_o=fluid density at jet exit

ρ_a=ambient fluid density

U_o=jet exit velocity

D =diameter or width of jet

Some of the measurements of normal stress u^2 and the kinetic energy are also presented, whenever available.

6.1 Bouyant plane jet

The exit and initial conditions for plane buoyant jets are the same as that of nonbuoyant jets, namely

$$U=U_N\exp(-y^2)$$

$$k=0.06U_N^2\exp(-y^2)$$

$$\varepsilon=0.09k^{1.5}/H$$

For the temperature, T and fluctuating temperature, $\overline{\theta^2}$, the jet exit conditions were set as

$$T - T_a=(T_o - T_a)\exp(-y^2)$$

$$\overline{\theta^2}=0.06(T_o - T_a)^2\exp(-y^2)$$

The calculation procedure is carried out similar to that for the nonbuoyant jet except that additional equations for T and $\overline{\theta^2}$ are included.

The most significant characteristic to be predicted by the turbulence model is the temperature or velocity rate of spread for buoyant jets. These parameters are defined as

$$S_U = \frac{dy_{\frac{1}{2}U}}{dx}$$

and

$$S_T = \frac{dy_{\frac{1}{2}T}}{dx}$$

The recommended experimental value of the spread rate of velocity is 0.12 while that for temperature is 0.13. In the present study, the spread rates predicted by the two-scale turbulence model are 0.11 for velocity and 0.135 for temperature. The one-scale turbulence model predicted values of 0.11 and 0.116 for velocity and temperature spreading rates. In comparison, the two-scale turbulence model seems to give better prediction.

The centerline velocity has been found to be a function of the distance x. The dimensionless grouping for velocity

$$\frac{U_c}{U_N} F^{1/3} \left(\frac{\rho_o}{\rho_a}\right)^{-1/3}$$

versus distance

$$\left(\frac{X}{D}\right) F^{-2/3} \left(\frac{\rho_o}{\rho_a}\right)^{-1/3}$$

was first derived by Chen and Rodi [50]. In these dimensionless plots, Chen and Rodi showed that all centerline velocity decay of turbulent buoyant jets can be collapsed into a single curve. The buoyant jet flow can be divided into three different regions, namely, nonbuoyant,

intermediate and plume region. From experimental data the following correlations were obtained. For the nonbuoyant region,

$$\frac{U_c}{U_N} = 2.4\left(\frac{\rho_o}{\rho_a}\right)^{1/2}\left(\frac{X}{D}\right)^{-1/2}$$

for

$$0 \leq \frac{X}{D}F^{-2/3}\left(\frac{\rho_o}{\rho_a}\right)^{-1/3} \leq 0.5$$

In the intermediate region, the relation is

$$\frac{U_c}{U_N} = 2.85F^{-1/3}\left(\frac{\rho_o}{\rho_a}\right)^{5/12}\left(\frac{X}{D}\right)^{-1/4}$$

for

$$0.5 \leq \frac{X}{D}F^{-2/3}\left(\frac{\rho_o}{\rho_a}\right)^{-1/3} \leq 5$$

and in the plume region,

$$\frac{U_c}{U_N} = 1.9F^{-1/3}\left(\frac{\rho_o}{\rho_a}\right)^{1/3}$$

for

$$5 < \frac{X}{D}F^{-2/3}\left(\frac{\rho_o}{\rho_a}\right)^{-1/3}$$

where F is the densimetric Froude number. In this investigation, a couple of cases were selected for calculation. The Froude numbers used were 6 and 24 which lie between the extreme cases of F=0 for a pure plume and F=∞ for a pure jet.

Figure 6.1 presents the velocity profiles of the one-scale and the two-scale turbulence models in a plane buoyant jet for Froude numbers of 6.0 and 24. The experimental data of Bradbury [30] for a plane jet and of Rouse [52] for a pure plume are included for comparison. The calculated results were obtained for x/D=40. There is a good agreement between experiment and calculations.

Figure 6.2 gives the turbulent quantities, namely k and u^2 as measured by Kotsovinos [53] and Bradbury [25]. The kinetic energy at the centerline for a pure jet is 0.064 whereas the normal stress for a pure plume is 0.14. Increase in the kinetic energy or normal stress for the plume can be explained by the existence of positive buoyant force which promotes the generation of turbulence. In other words, $g(\overline{u\theta}/T_a)$ in equation (3.35) is positive. The calculations of the two-scale model and one-scale model are plotted for Froude numbers of 6.0 and 24. These profiles fall within the extreme cases of a pure jet and a pure plume. Thus the prediction can be considered to be satisfactory.

In figure 6.3, the temperature profile is shown for Froude numbers of 6.0 and 24 as obtained by the one-scale and two-scale turbulence models. These results are compared with the experimental data of Van der Hegge

[31] for a pure jet and that of Rouse et al. [51] for a pure plume. Again the predicted results for buoyant jets fall within the two envelops of pure jet and pure plume as one would expect.

The Reynolds stress for a plane buoyant jet is shown in figure 6.4. The one-scale and the two-scale model results are shown for comparison. The experimental result of Ramaprian and Chandrasekhara [52] is shown for Froude number of 2.4.

6.2 Buoyant round jet

The predicted spread rates for velocity and temperature in buoyant round jets using the two-scale turbulence model are 0.1 and 0.115 respectively. The one-scale model gives these parameters as 0.12 and 0.11. The experimental values of the velocity and thermal spreading rates are 0.112 and 0.1 indicating that the two models predict satisfactorily the gross parameters.

Figure 6.5 shows the velocity profile of a buoyant round jet. The two-scale model calculations are shown for the two cases of F=6 and F=24 while the one-scale model prediction is shown for F=6. The experimental data of Rodi [4] and George et al. [54] are also shown for pure jet and pure plume respectively. There is a good agreement between the predicted result and experimental data.

Figure 6.6 gives the temperature profile of a buoyant round jet. The pure jet profile is that of Rodi while the pure plume temperature

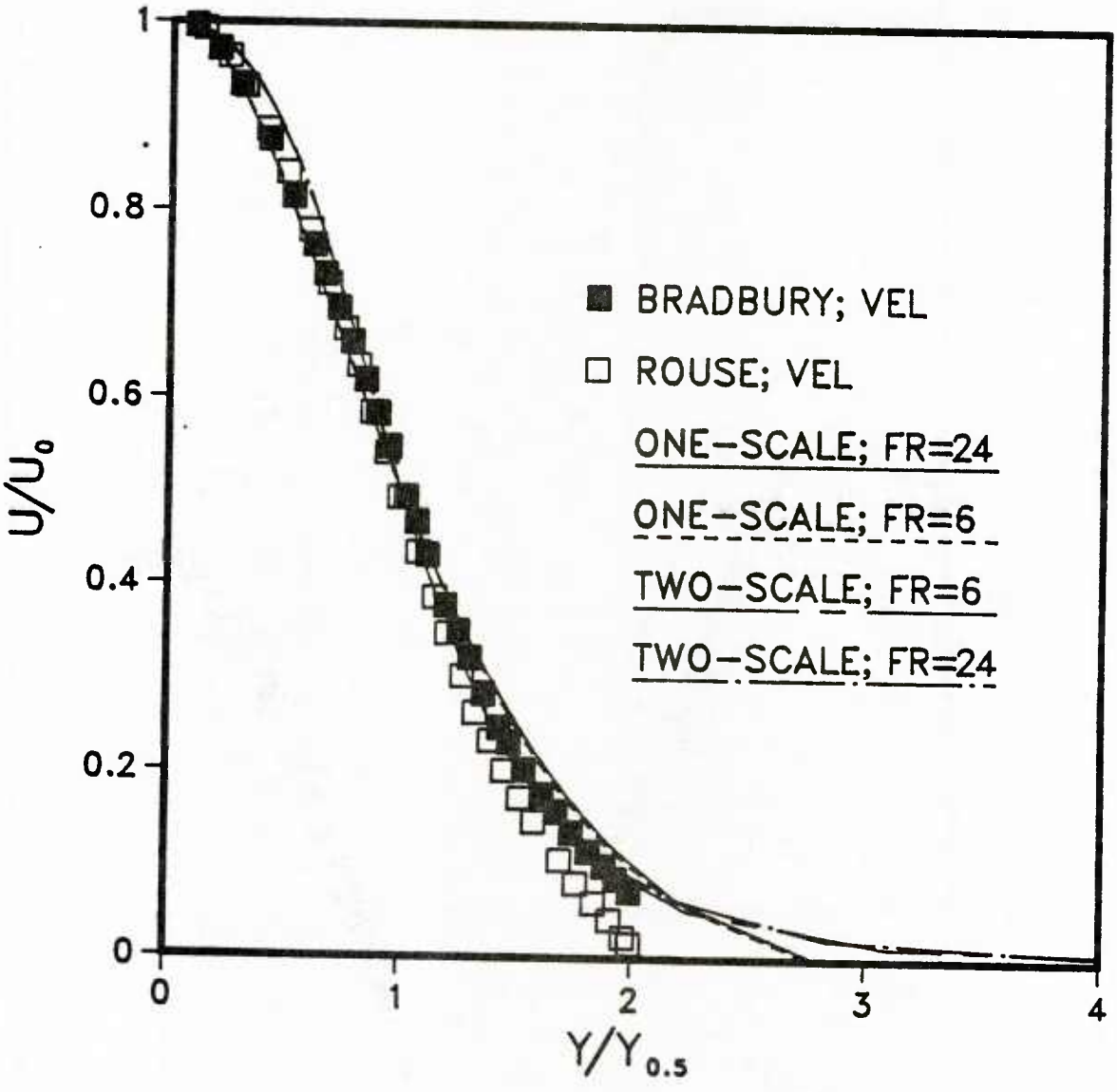

Figure 6.1. Velocity profiles for a plane buoyant jet

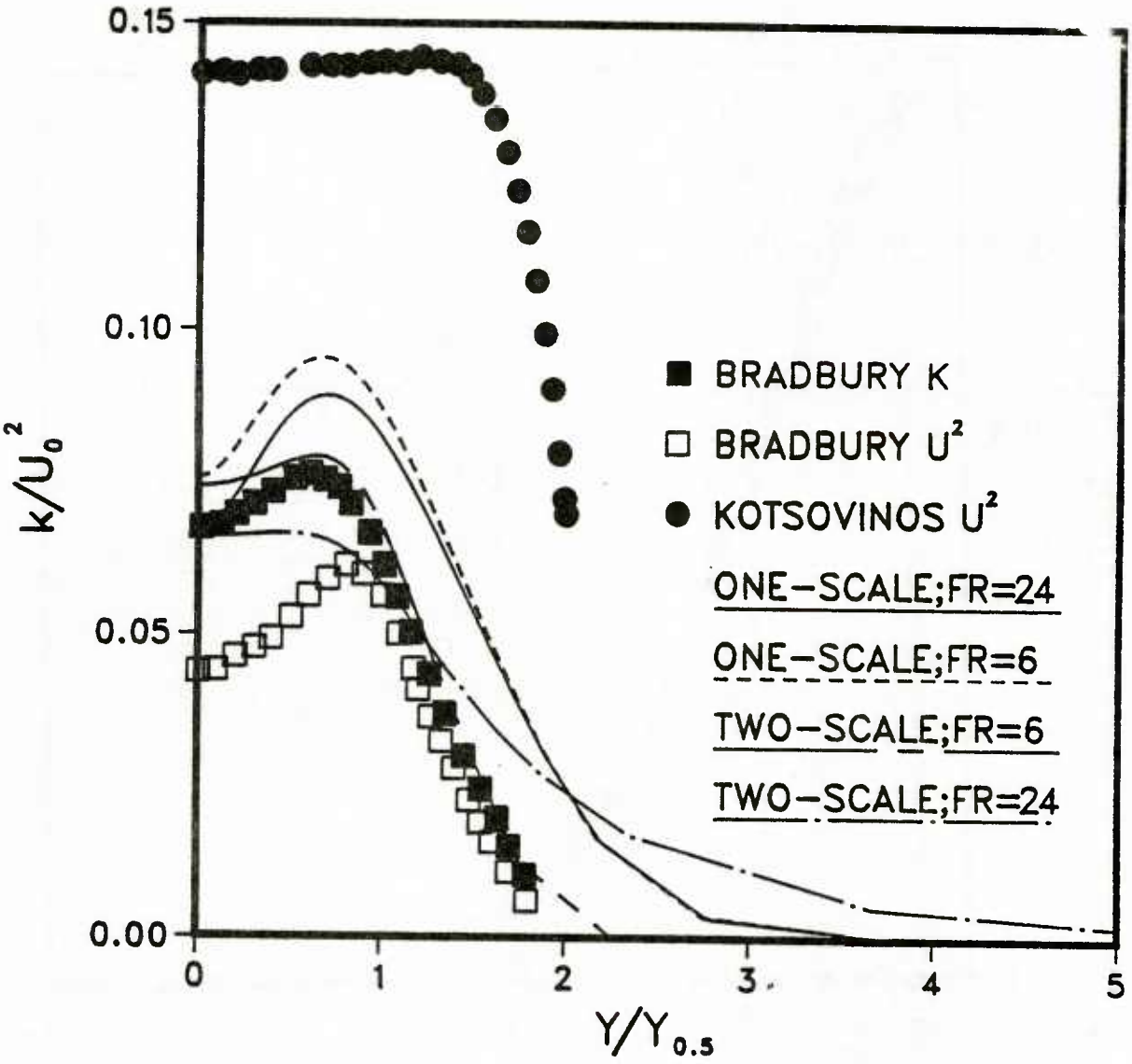

Figure 6.2. Turbulent kinetic energy and normal stress

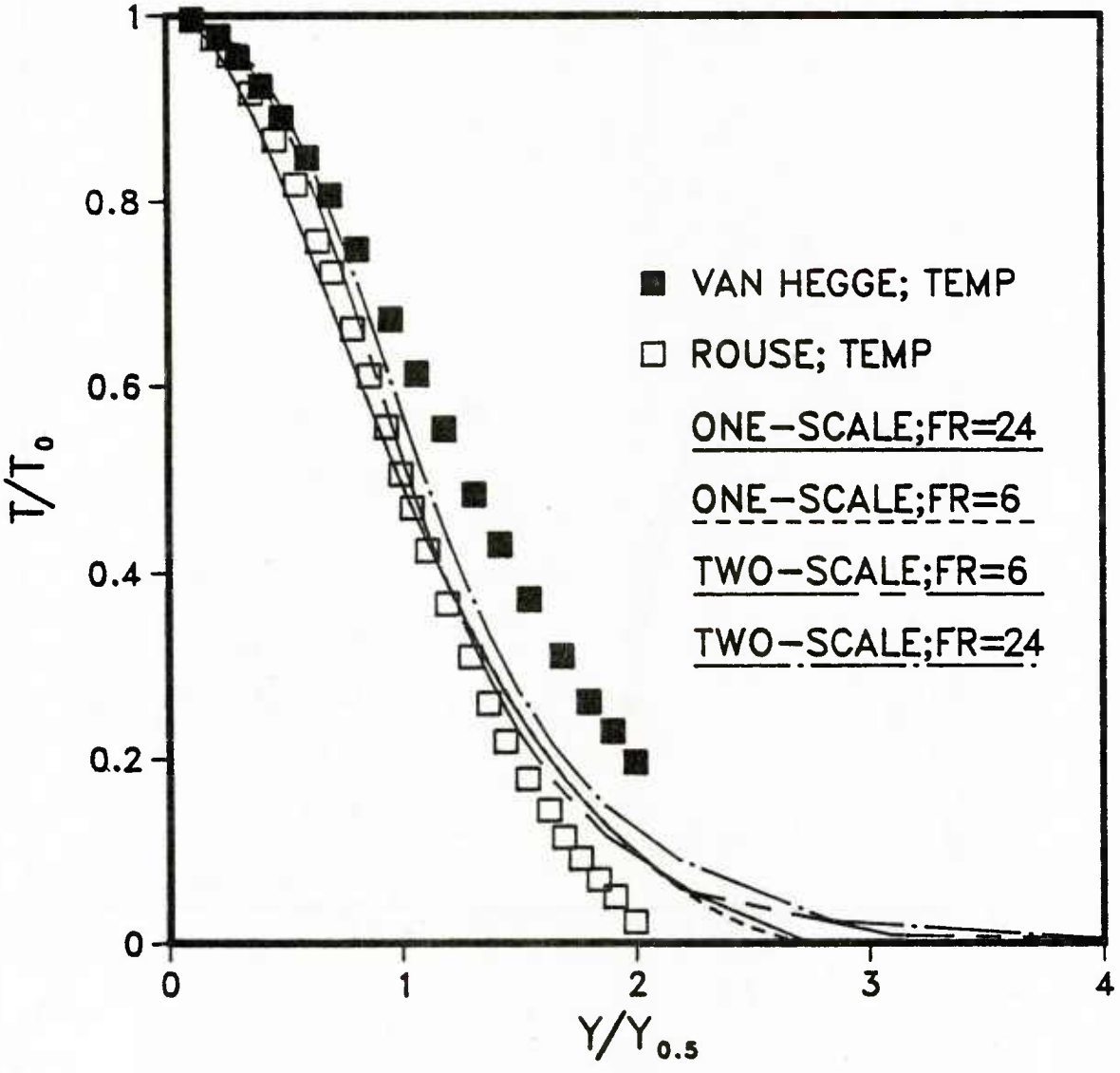

Figure 6.3. Temperature profile
for a buoyant jet

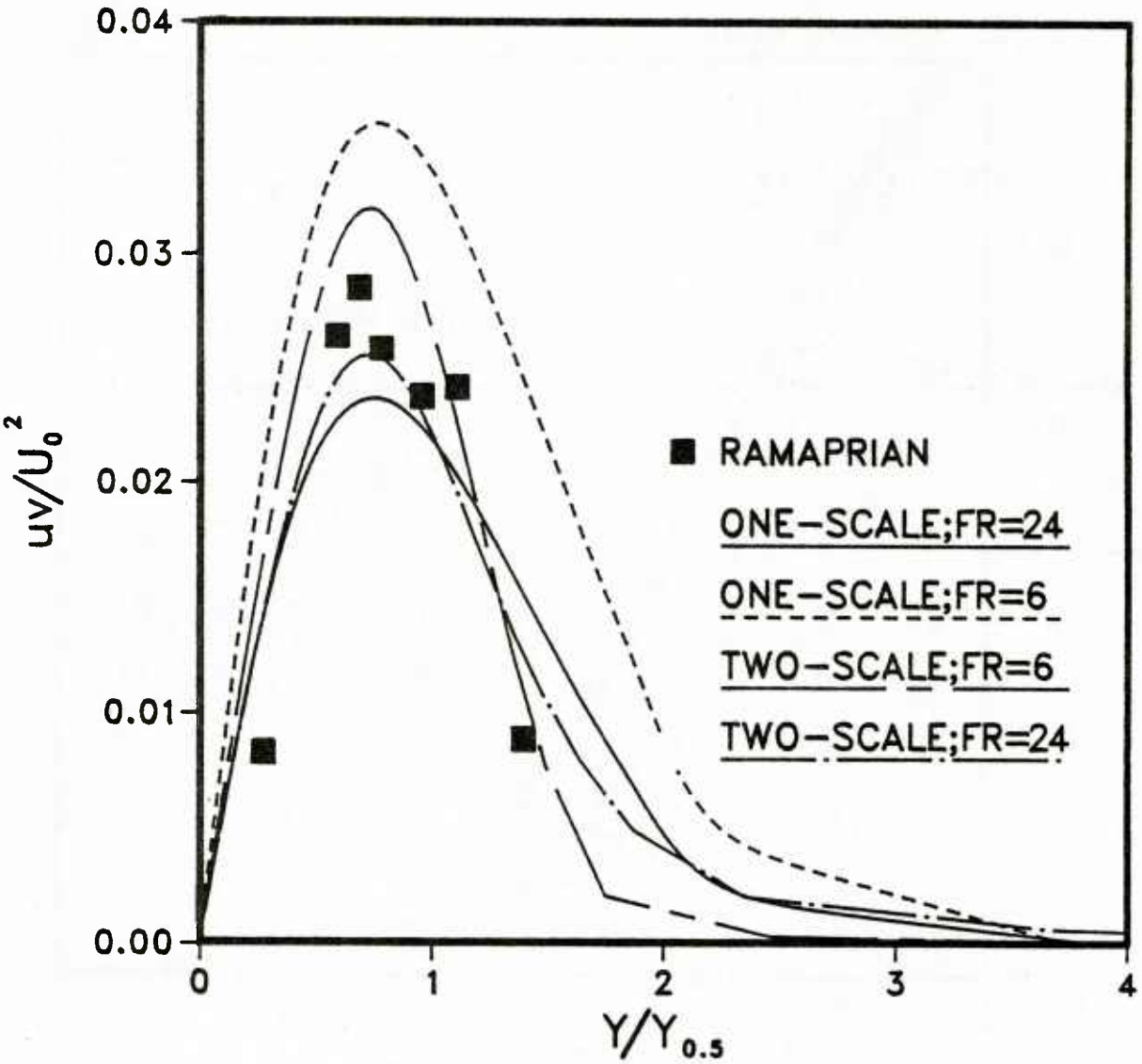

Figure 6.4. Reynolds stress for a plane jet

profile is that of George [54]. The calculations of the two-scale model and the one-scale model show temperature profiles closer to the pure plume than pure jet.

In figure 6.7, the kinetic energy and normal stress of the buoyant jet is shown. The pure plume data is that of George and the pure jet data is that of Rodi. The one-scale and two-scale results are shown for comparison. As in the case of the nonbuoyant jets the prediction of kinetic energy by the one-scale model is higher than that by the two-scale model.

6.3 Concluding remarks

Though the comparison between prediction and experiment was not extensive, it can be said that the results of the two-scale turbulence model are satisfactory. More rigorous comparisons are necessary which can be done only with better and complete set of experimental data. Further, the effect of reducing the partial differential equations for $\overline{\theta^2}$ and ε_θ into algebraic equations need to be studied. Since the equation for ε_θ was replaced by a relation suggested by Launder in equation (3.28a), the influence of the small time scales on the buoyant jets could not be studied.

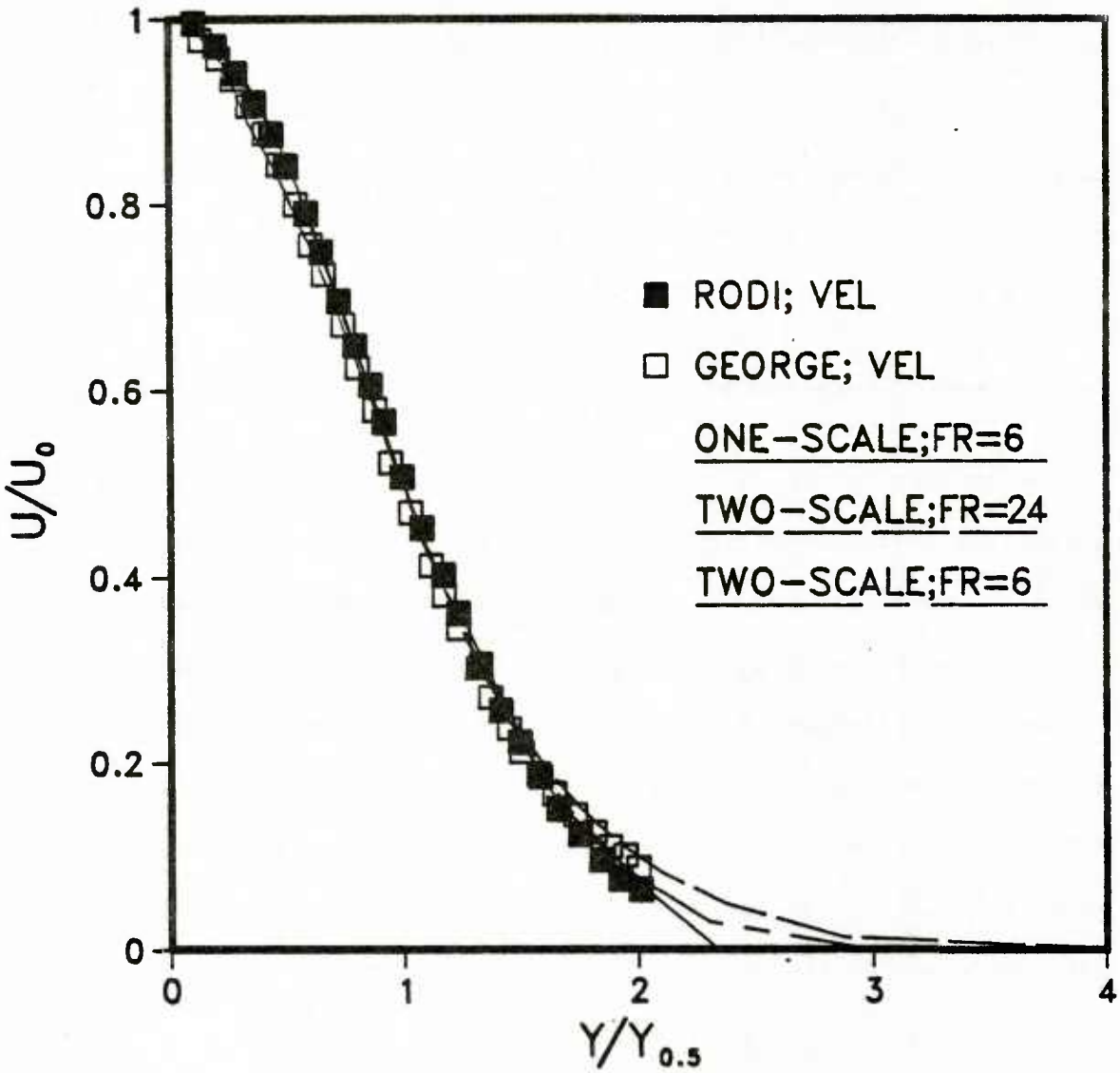

Figure 6.5. Velocity profiles in a buoyant round jet

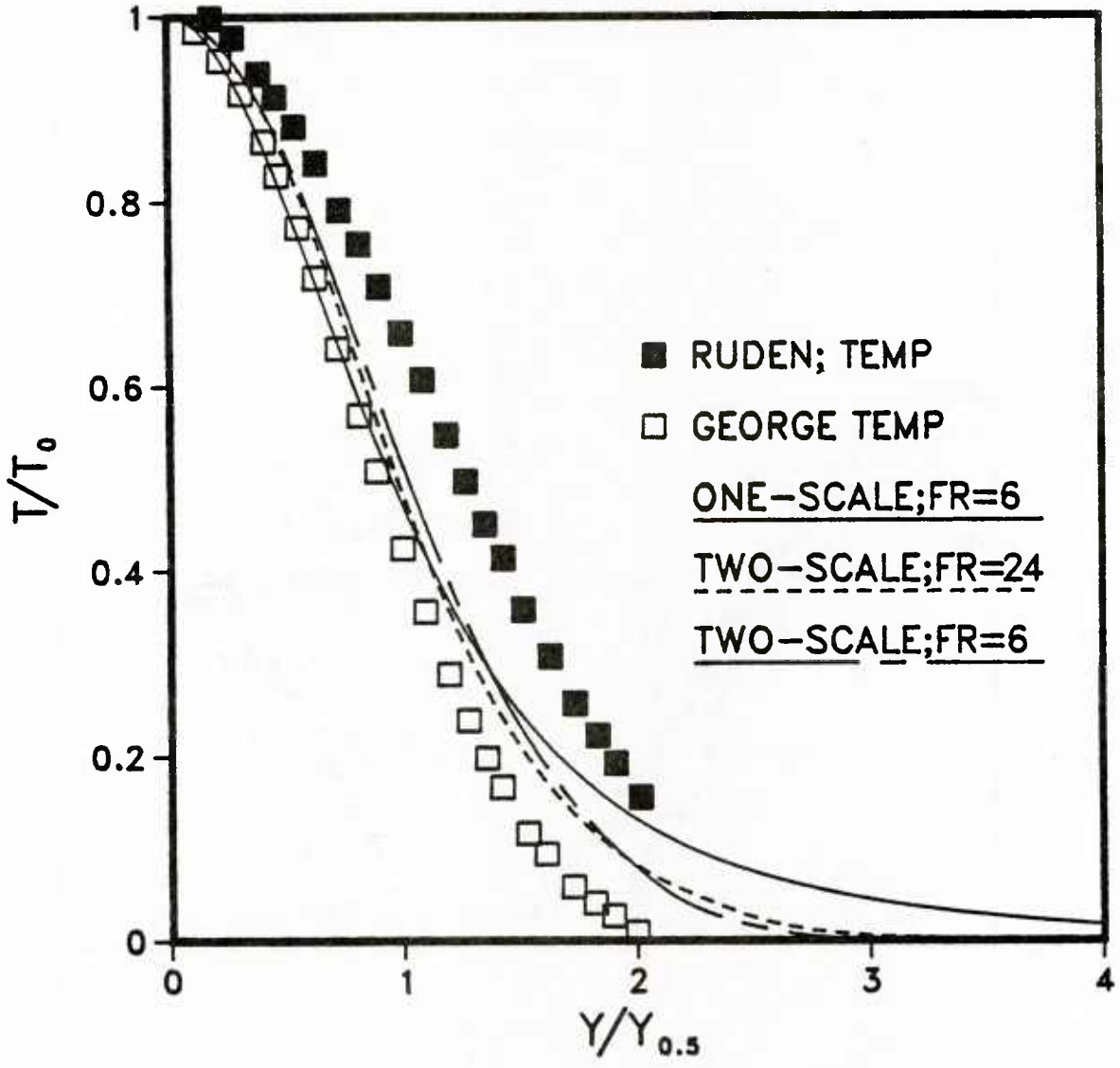

Figure 6.6. Temperature profile in a buoyant jet

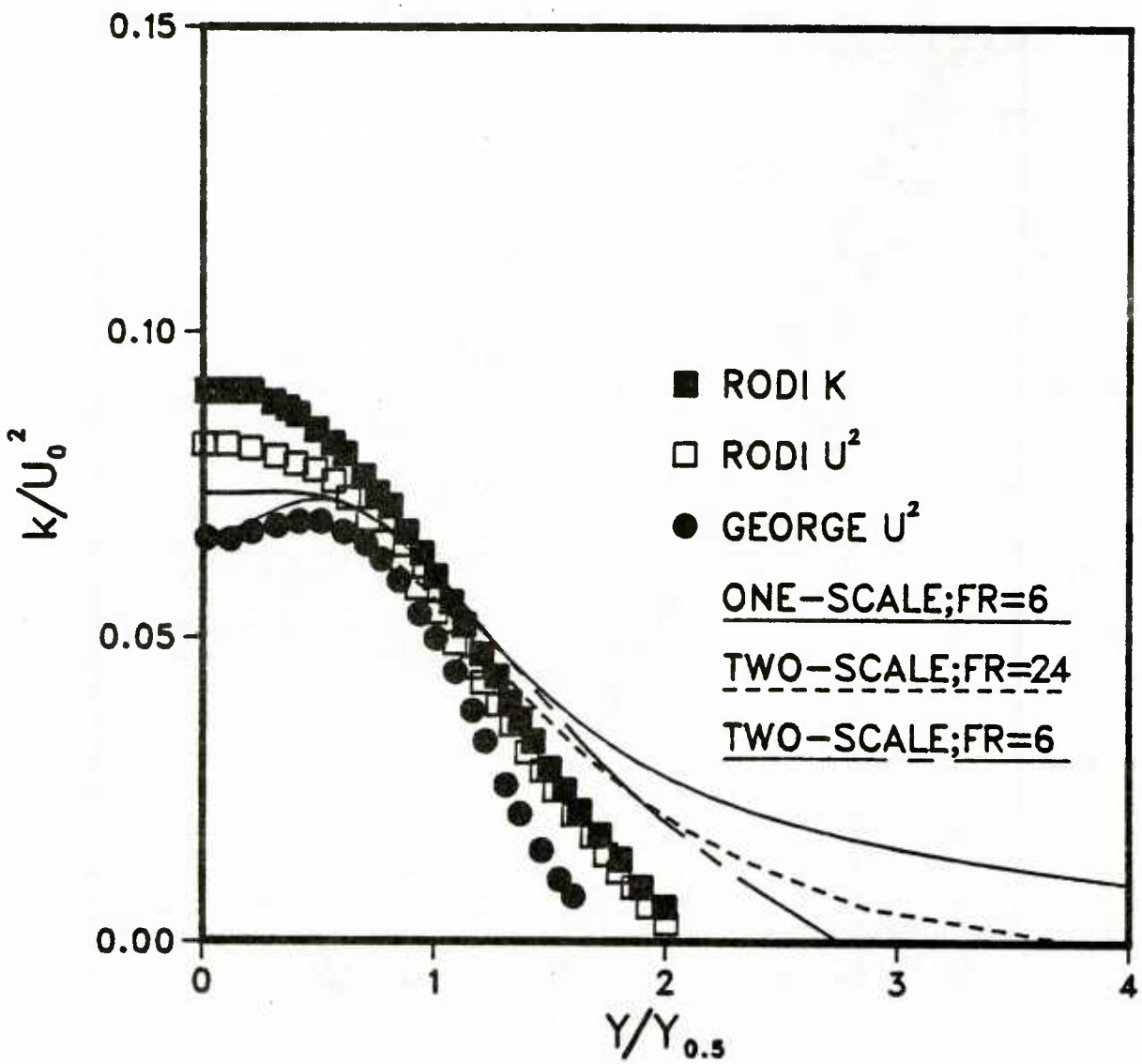

Figure 6.7. Turbulent kinetic energy and normal stress

CHAPTER VII

PREDICTION OF RECIRCULATING FLOWS

In the present investigation the emphasis is placed on prediction of turbulent free shear flows. This is because the mean velocity field of turbulent free shear flows is determined by the Reynolds stress and not by the pressure force which is likely to be a dominant force in more complex separate flows. Therefore, any turbulence model for Reynolds stress, turbulent kinetic energy or dissipation of turbulent kinetic energy can be better tested and verified by its capability of prediction without the action of the pressure force. In addition, prediction of turbulent free shear flow does not have the complexity of the near wall turbulence.

In the previous chapters, the two-scale turbulence model has been tested and verified for its prediction capability in turbulent free shear flows. In this chapter, the two-scale turbulence model is used to predict turbulent separated flows. Results are shown and compared with those obtained by the one-scale k-ε model for two different flows, namely, flow past a backward facing step and flow through an obstacle.

7.1 Flow past a backward facing step

The first case of recirculating flow chosen is the flow past a

backward facing step. This is chosen because sufficient experimental data is available including the mean velocity profiles, separation length and some turbulent quantities. Stevenson et al. [60] used laser velocimetery technique to measure mean and turbulent quantities. Eaton and Johnston [61] reviewed several other measurements of backward facing step for the 1980 Stanford Conference meeting.

The flow domain which was measured by Stevenson et al. [60] and a portion of the grid distribution near the step are shown in figure 7.1. The same domain is used in the calculation using the one-scale and two-scale turbulence models. The height of the step is H and the distance from the step to the upper wall is also H. In the calculation, the boundary or entry conditions were set at a distance of 0.02H upstream of the step where experimental data is available. The exit conditions were set at 12 step heights downstream with the boundary conditions also from experiment. Near the wall and the step, the grid distribution is nonuniform with more nodes in the vicinity of the walls where the gradient of dependent quantities is steep. The smallest grid size is about 0.02H while the largest spacing is 2.0H. The grid system for the computational domain has 30 by 17 nodes.

The governing equations for turbulent flow were derived in chapter II. These equations are written here once again. The mean flow equations are

$$\frac{\partial U_i}{\partial x_i} = 0 \tag{7.1}$$

and

$$\frac{DU_i}{Dt} = -\frac{\partial P}{\rho \partial x_i} + \nu \frac{\partial^2 U_i}{\partial x_j \partial x_j} - \frac{\partial \overline{u_i u_j}}{\partial x_j} \tag{7.2}$$

To complete the closure problem, the Reynolds stress are written using the eddy viscosity hypothesis to be

$$-\overline{u_i u_j} = C_\mu \frac{k^2}{\varepsilon} \left[\frac{\partial U_i}{\partial x_j} + \frac{\partial U_j}{\partial x_i}\right] - \frac{2}{3} k \delta_{ij} \tag{7.3}$$

The turbulent quantities k and ε are additional unknowns. The k equation is modelled as

$$\frac{Dk}{Dt} = \frac{\partial}{\partial x_\ell}\left[C_k \frac{k^2}{\varepsilon} \frac{\partial k}{\partial x_\ell} + \nu \frac{\partial k}{\partial x_\ell}\right] - \overline{u_i u_\ell} \frac{\partial U_i}{\partial x_\ell} - \varepsilon \tag{7.4}$$

The ε-equation based on one-scale model is

$$\frac{D\varepsilon}{Dt} = \frac{\partial}{\partial x_j}\left[C_\varepsilon \frac{k^2}{\varepsilon} \frac{\partial \varepsilon}{\partial x_j}\right] - C_{\varepsilon 1} \frac{\varepsilon}{k} \overline{u_i u_j} \frac{\partial U_i}{\partial x_j} - C_{\varepsilon 2} \frac{\varepsilon^2}{k} \tag{7.5}$$

with C_ε, $C_{\varepsilon 1}$ and $C_{\varepsilon 2}$ as 0.15, 1.435 and 1.92. Based on the two-scale concept the ε-equation is

$$\frac{D\varepsilon}{Dt} = \frac{\partial}{\partial x_\ell}\left[C_\varepsilon \frac{k^2}{\varepsilon} \frac{\partial \varepsilon}{\partial x_\ell} + \nu \frac{\partial \varepsilon}{\partial x_\ell}\right] - C_{\varepsilon 1} (\varepsilon/\nu)^{\frac{1}{2}} \overline{u_i u_j} \frac{\partial U_i}{\partial x_\ell} - C_{\varepsilon 2} (\varepsilon/\nu)^{\frac{1}{2}} \varepsilon \tag{7.6}$$

where C_{ε}, $C_{\varepsilon 1}$ and $C_{\varepsilon 2}$ are 2.00, $17.50/(Re)^{\frac{1}{2}}$ and $18.90/(Re)^{\frac{1}{2}}$.

The numerical method used for solving the differential equations is the Finite-analytic method developed by Chen et al. [62] [63]. The calculations were carried by the computer program (FANS-1 Finite-Analytic solution of Navier-Stokes equations) developed by Sheikholeslami [64]. This program incorporates the SIMPLER algorithm suggested by Patankar [55]. The wall function [64] is used for the near wall velocity and turbulent conditions. The velocity profile at the inlet and outlet were specified from the data of Stevenson et al. [60]. The kinetic energy profile at the inlet is about 3% of the mean velocity squared. The dissipation function ε at the inlet is calculated from the turbulent kinetic energy using the relation

$$\varepsilon = 0.09\frac{k}{H}^{1.5}$$

At the outlet, both the turbulent kinetic energy and its dissipation function are assumed to be fully developed, i.e.

$$\frac{\partial k}{\partial x} = 0 \quad \text{and} \quad \frac{\partial \varepsilon}{\partial x} = 0$$

The Reynolds number based on the mean inlet velocity and step height H is 50,000.

In figure 7.2, the contour plot of the streamlines predicted by the one-scale and the two-scale turbulence model are shown. The time step

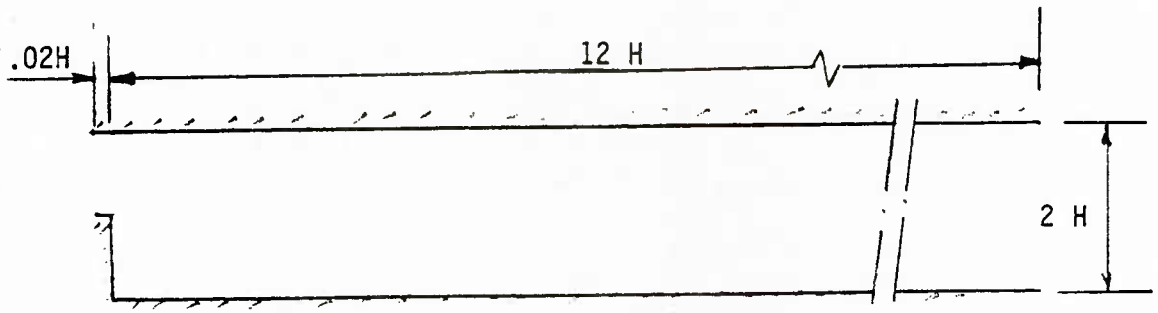

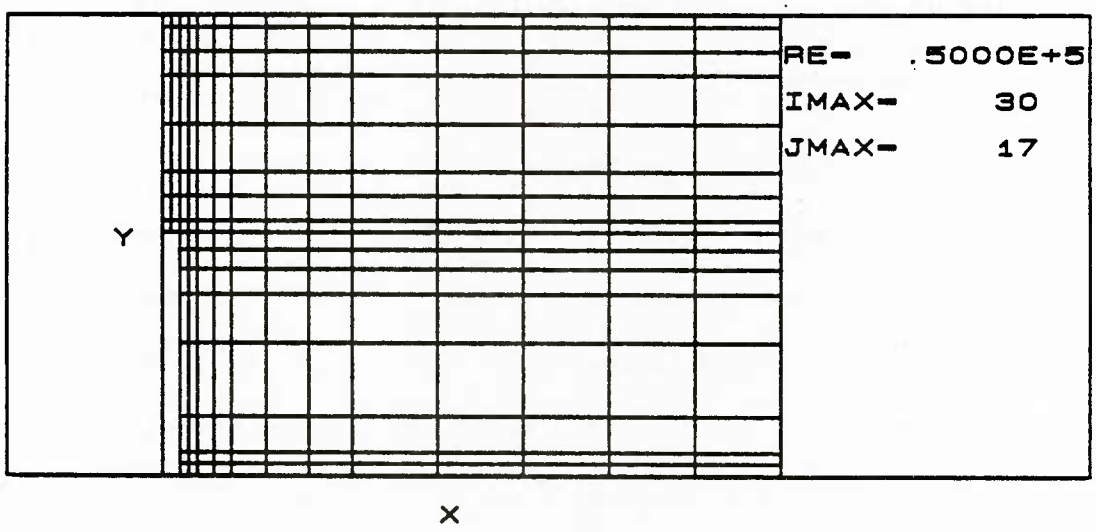

Figure 7.1. Geometry of flow
and grid distribution

used in the calculation was 0.2 and the convergence criterion between the solutions of two consecutive time steps was set at 0.0001 for velocities and 0.001 for pressure. The computational time on Prime 850 computer for both one-scale and two-scale model prediction was 60 minutes of CPU time. From figure 7.2, it can be seen that the length of separation using the two-scale model is about 7 times the step height whereas the one-scale model predicts a separation length of about 5 step heights. Since experimental data shows a separation length of about 7 step heights, the one-scale seems to underpredict the reattachment length. The reason for this is that the one-scale turbulence model in general predicts a larger turbulent kinetic energy and hence larger turbulent eddy viscosity for flow after a step. This causes greater mixing or momentum transfer resulting in a smaller separation zone.

Figure 7.3 gives horizontal velocity profiles predicted by the one-scale and the two-scale turbulence models at x/H=4.1 where the flow is separated and has a region of reverse flow. It can be seen that the two-scale model predicts a fuller velocity profile in the mid-channel and the flow is separated near the lower wall which is closer to measured values. The one-scale model predicts much smaller reverse flow than the experimental results of Stevenson et al. [60]. In figure 7.4, the velocity profiles at x/H=7.1 are given. The comparison again shows that a fuller velocity profile is predicted by the two-scale model in the mid-channel seems to have better agreement with experiment.

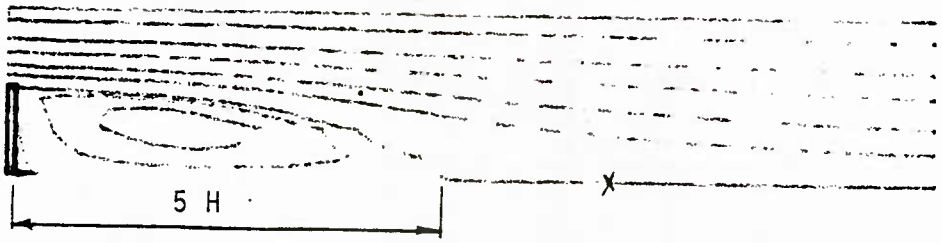

One Scale Model

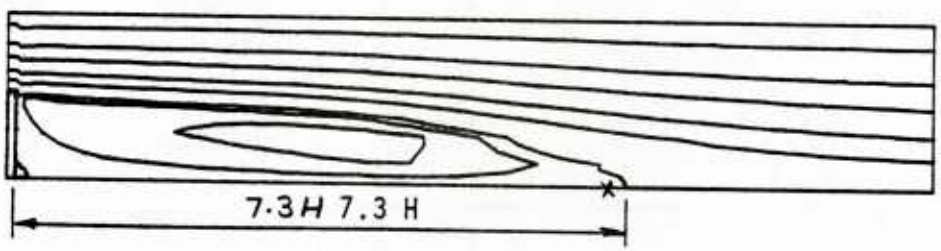

Two Scale Model

x Experimental Reattachment Point

Figure 7.2. Streamlines using one-scale and two-scale turbulence models

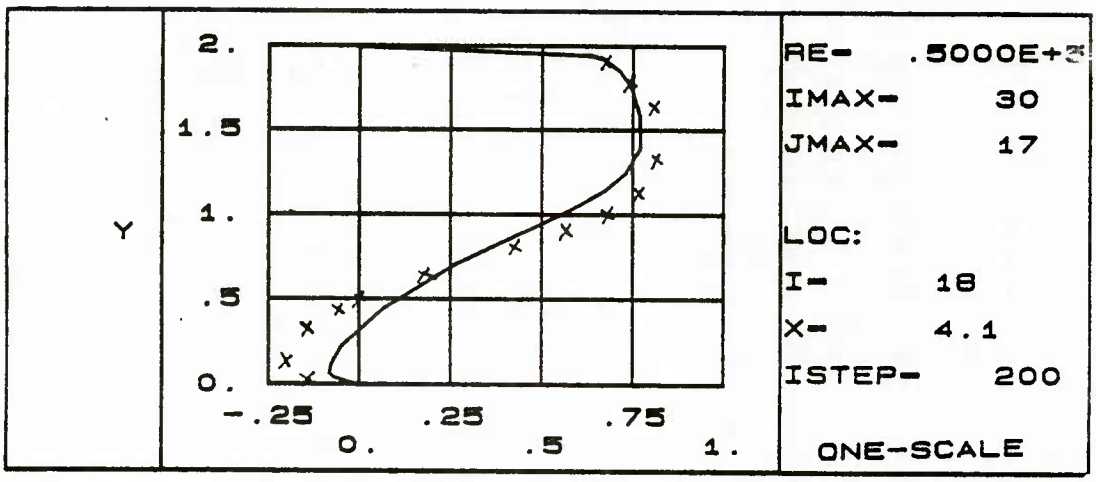

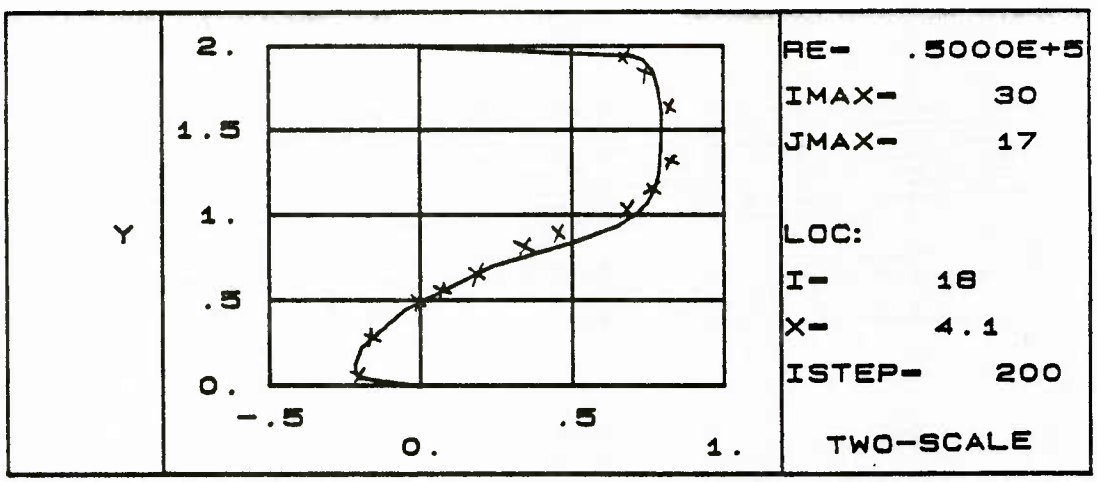

Figure 7.3. Horizontal velocity profile at x/H=4.1

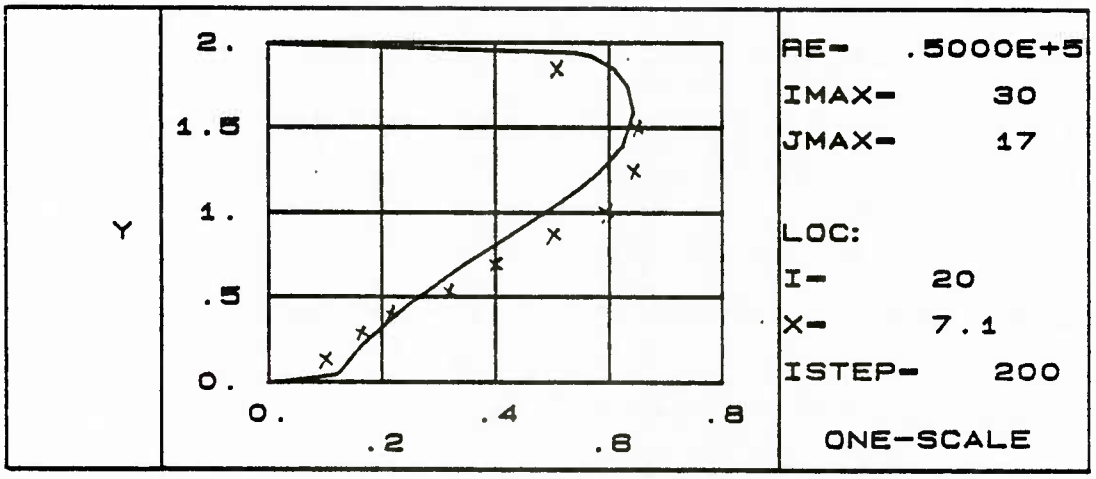

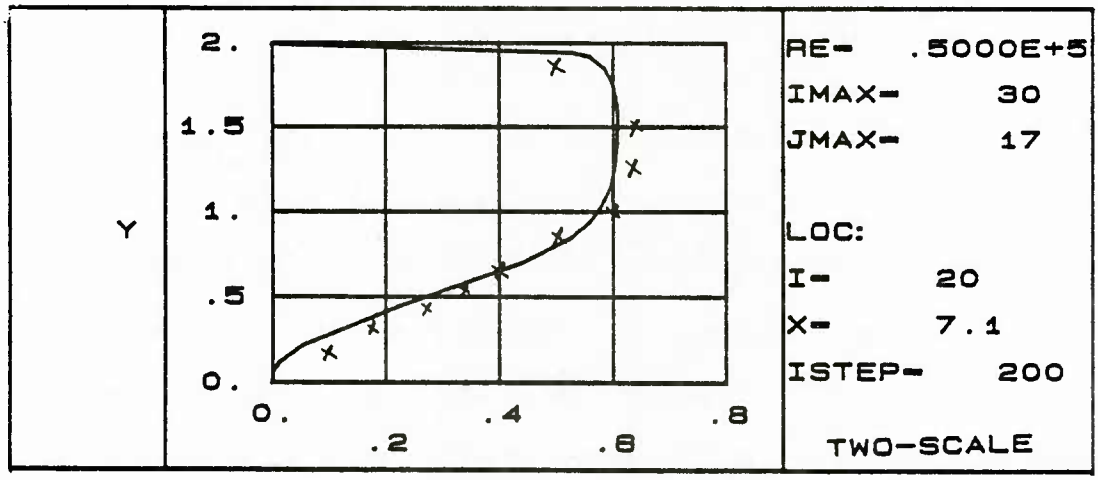

Figure 7.4. Horizontal velocity profile at x/H=7.1

The turbulent kinetic energy profiles at x/H=7.1 and 9.1 are shown in figures 7.5 and 7.6. The results of the one and two-scale models are presented along with the experimental results. Comparison with measured data reveals that both models predict correctly the general trend of distribution of turbulent kinetic energy and is only in fair agreement with experimental data. It should be remarked that the peak turbulent kinetic energy predicted by the two-scale model is slightly smaller in magnitude than that predicted by the one-scale model.

Figure 7.7 presents the shear stress at x/H=9.1 for the two models. Both models predict correctly the location of the maximum shear stress which is found from the experimental data to be at y/H=0.75 from the bottom wall. Both models predict larger negative stress $-\overline{u_i u_j}$ with the two-scale model predicting a better overall trend.

7.2 Flow past an obstacle

The second case considered in this chapter is the flow past an extended rectangular plate in a two-dimensional channel. Figure 7.8 shows the stretched geometry of the flow domain along with the grid distribution for flow past a rectangular plate with a height of H and a thickness also of H. The flow domain has 41 by 14 nodes. The same numerical procedure and the method of solution is used as that for the backward facing step. The calculation is performed from x/H=-11 to x/H=45. The velocity profiles at the inlet and outlet are the one-seventh power law. The kinetic energy at the inlet is specified using

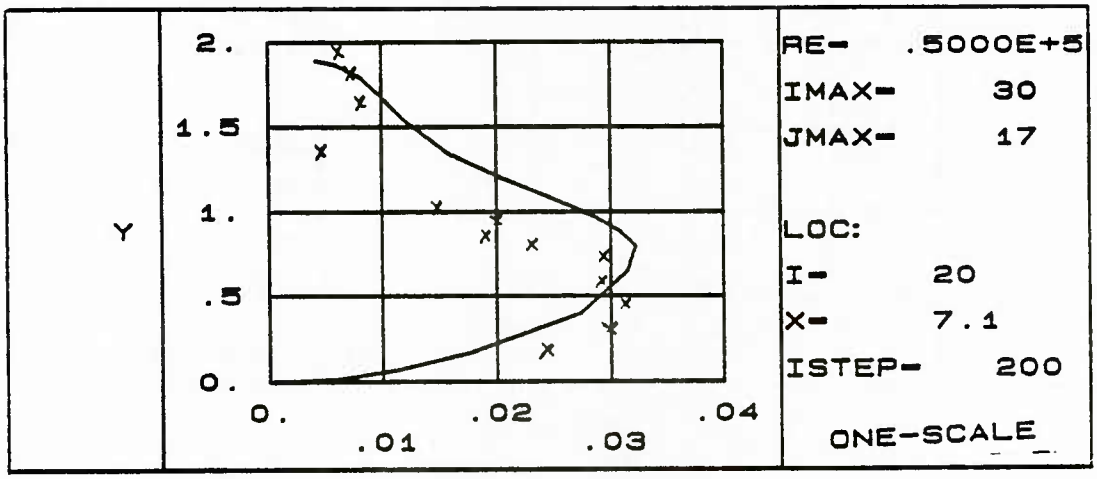

TURB.K.E

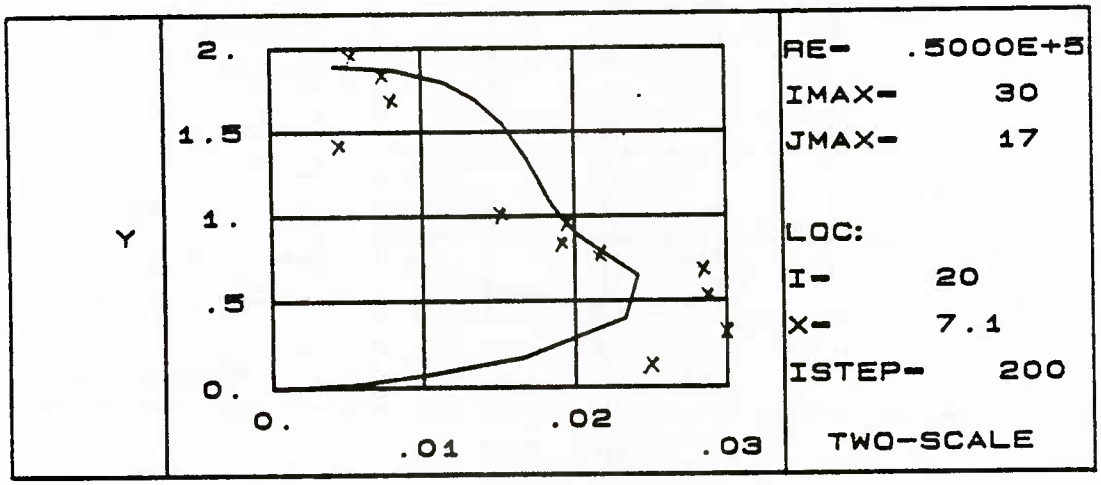

TURB.K.E

Figure 7.5. Turbulent kinetic energy at x/H=7.1

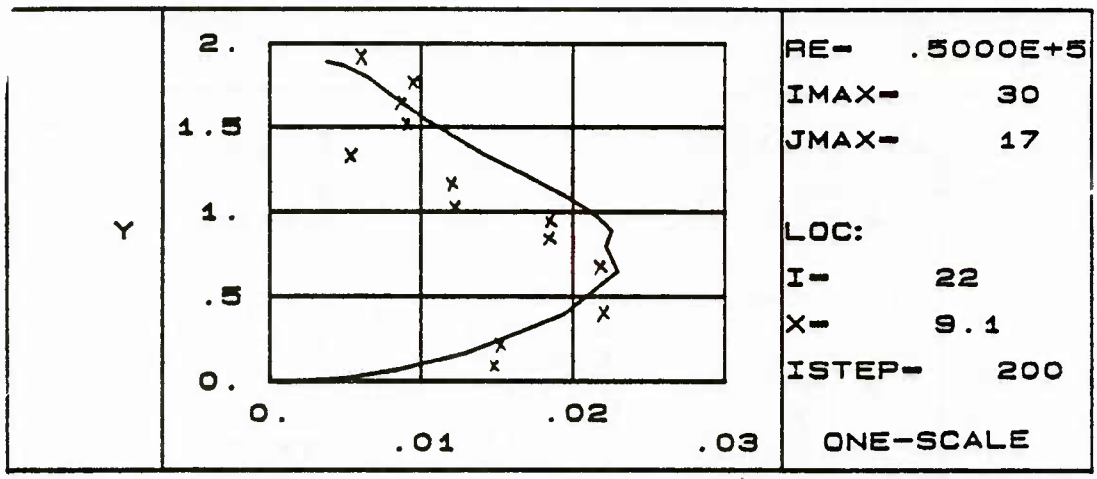

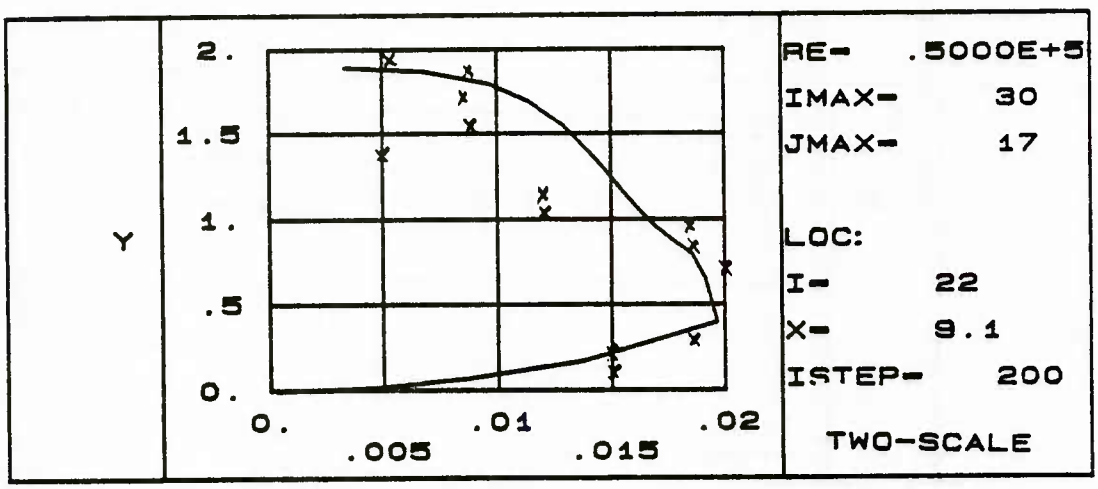

Figure 7.6. Turbulent kinetic energy at x/H=9.1

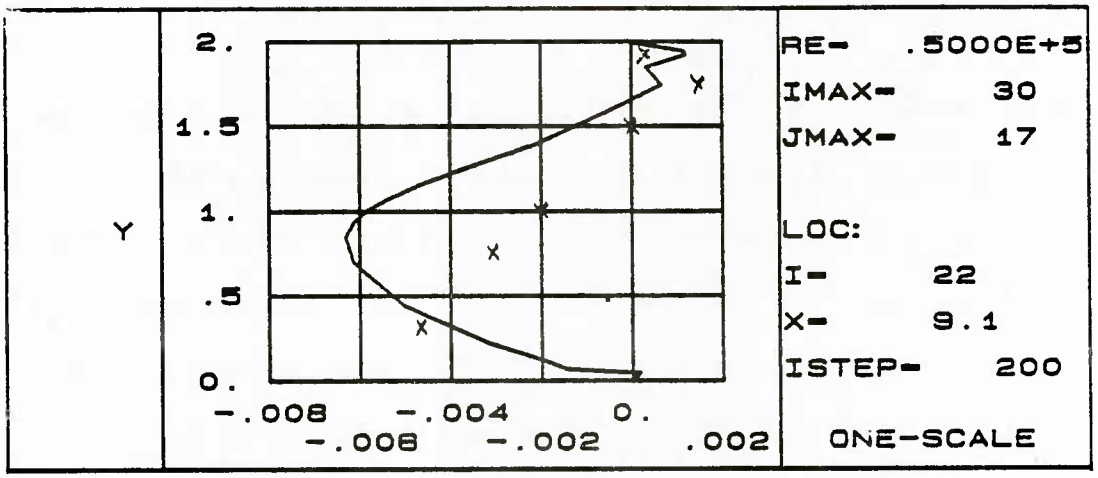

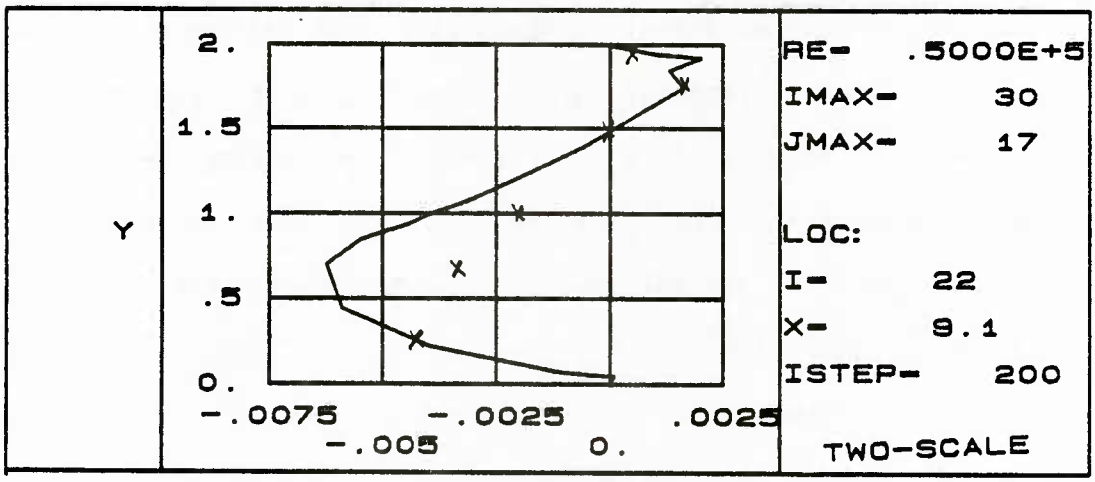

Figure 7.7. Turbulent shear stress profile at x/H=9.1

the experimental data of Durst et al. [65]. The dissipation at the inlet is specified using the relation

$$\varepsilon = \nu_t \left(\partial U/\partial y\right)^2$$

At the outlet, the fully developed profiles for k and ε are assumed. A portion of the streamline contour near the obstacle predicted by the one-scale and the two-scale model for Reynolds number of 17,000 based on H and mean velocity U is shown in figure 7.9. The two-scale model predicts a reattachment zone of 10H. The one-scale model, however, predicts a length of 4H. The experimental results of Durst et al. [65] for Re=17,000 show a separation length of about 7H. This is in closer agreement with the 10H predicted by the two-scale model.

Figures 7.10 and 7.11 show the velocity profiles predicted by the two models at x/H=4.1 and x/H=7.1 respectively. The two-scale turbulence model has a general tendency to predict a flatter velocity profile in the separation zone as shown in figure 7.10 which is in better agreement with the experimental data. Figure 7.11 shows that the two-scale model predicts separation as indicated by the experiment where the one-scale predicts no separation. In figures 7.12 and 7.13, the kinetic energy profiles are shown at the locations x/H=4.1 and x/H=7.1. Again, the two-scale turbulence model predicts a smaller kinetic energy profile.

7.3 Concluding remarks

The results presented above are two cases of recirculating flows predicted by the turbulence models. Comparison with experiment shows

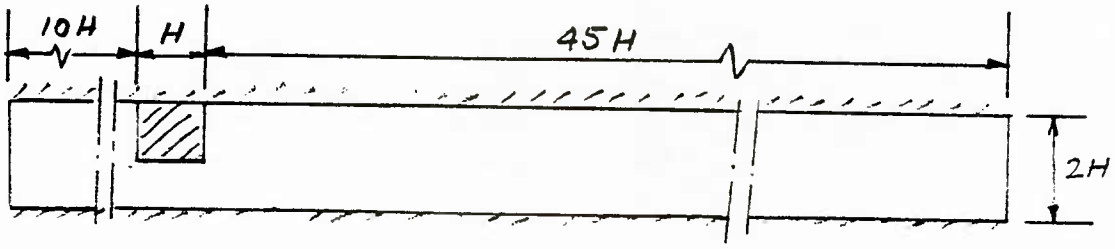

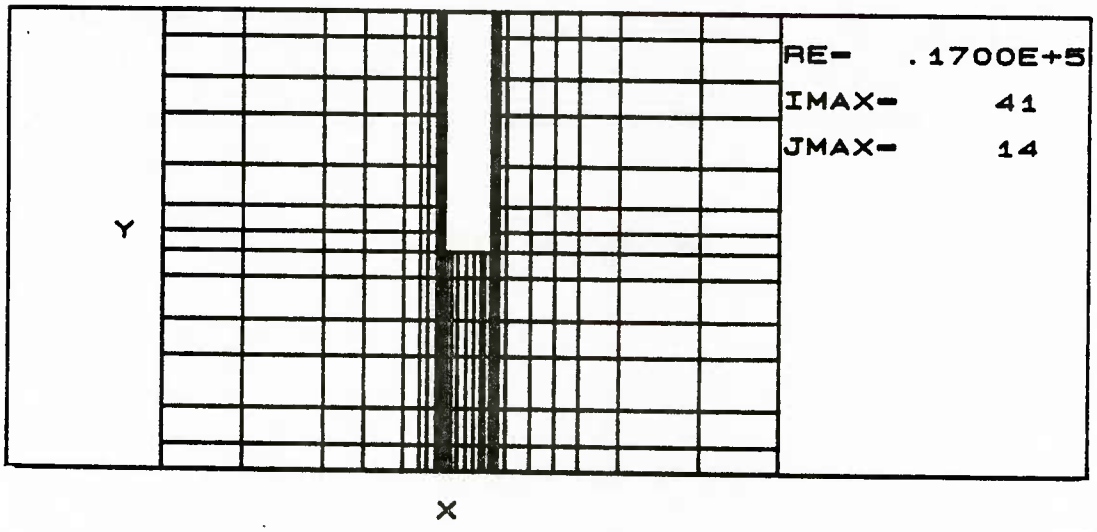

Figure 7.8. Flow geometry and grid distribution

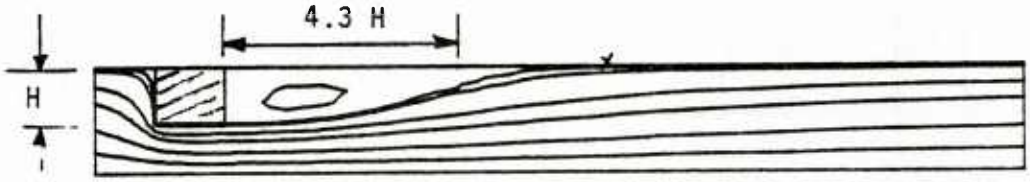

One Scale Model

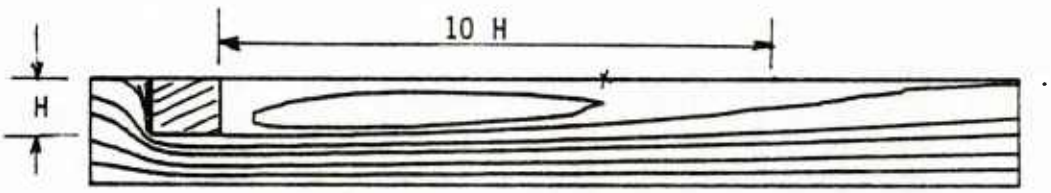

Two Scale Model

x Experimental Reattachment Point

Figure 7.9. Streamlines using both one-scale and two-scale turbulence model

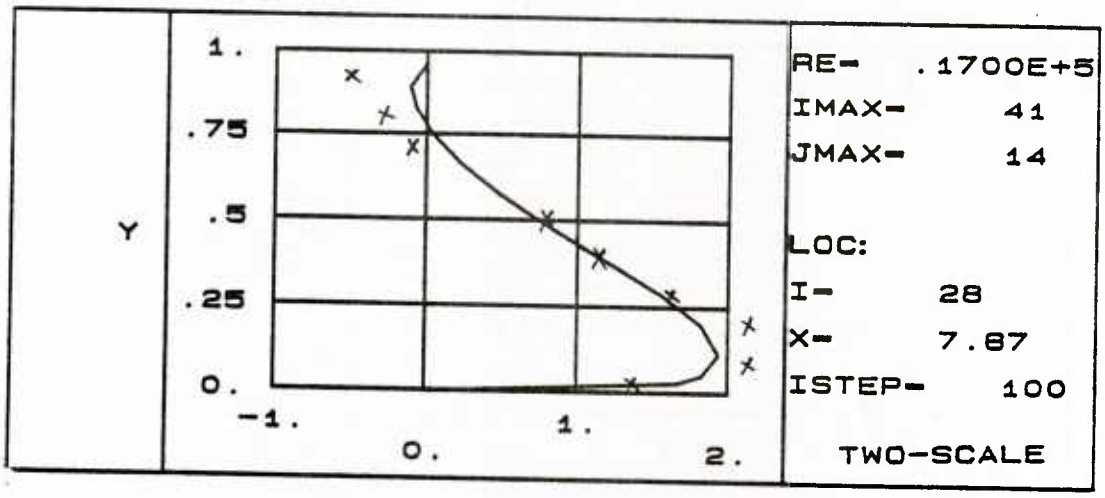

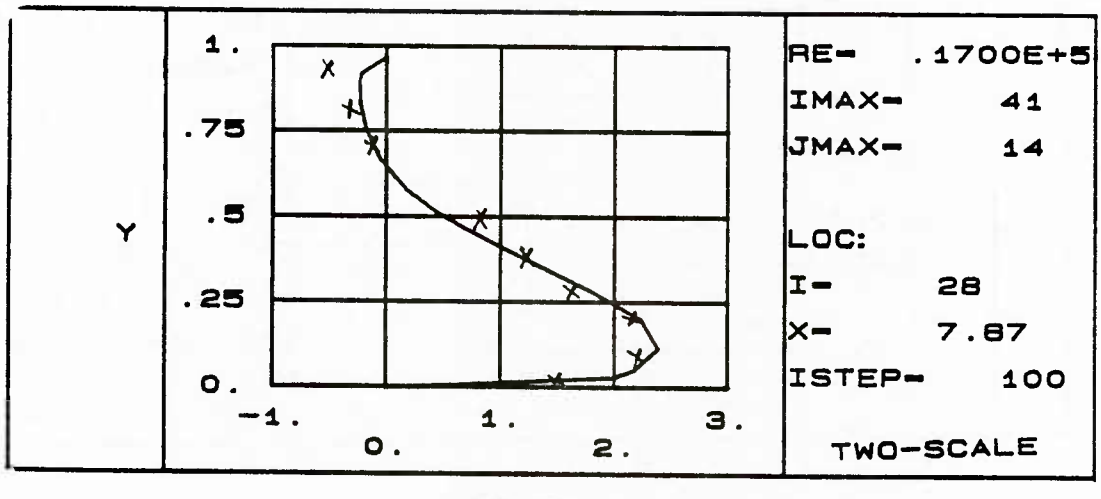

Figure 7.10. Velocity profile
at location x/H=4.1

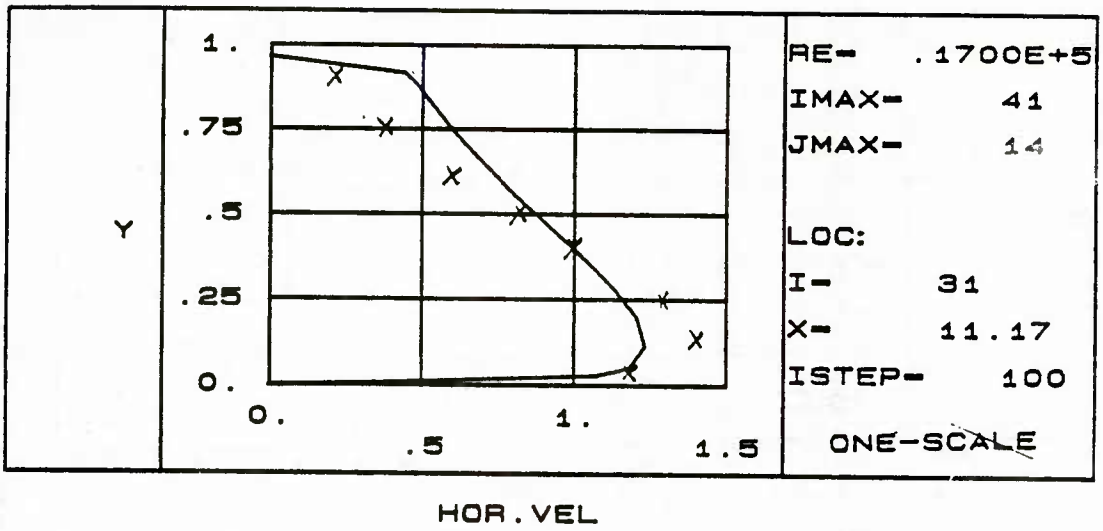

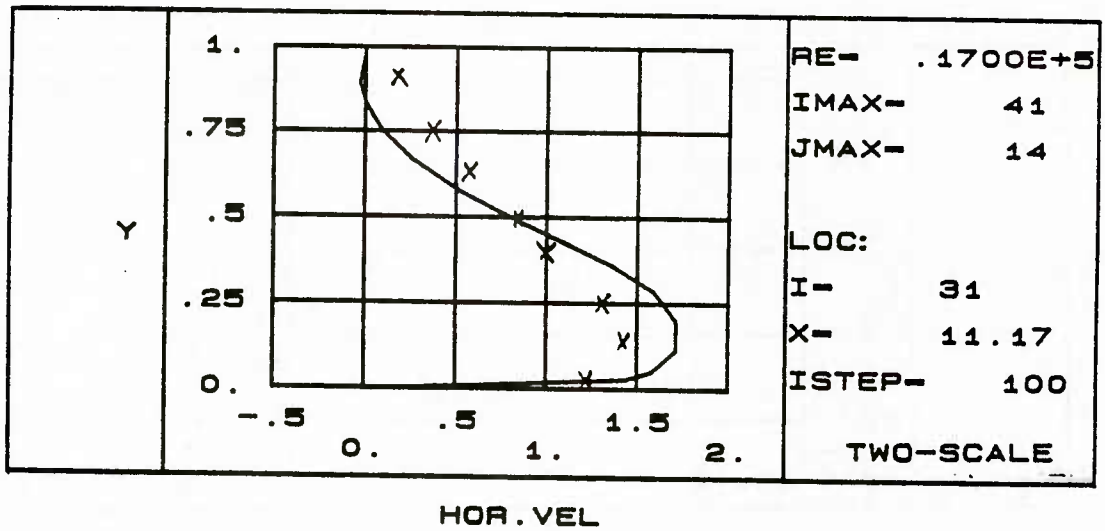

Figure 7.11. Velocity profile
at location x/H=7.1

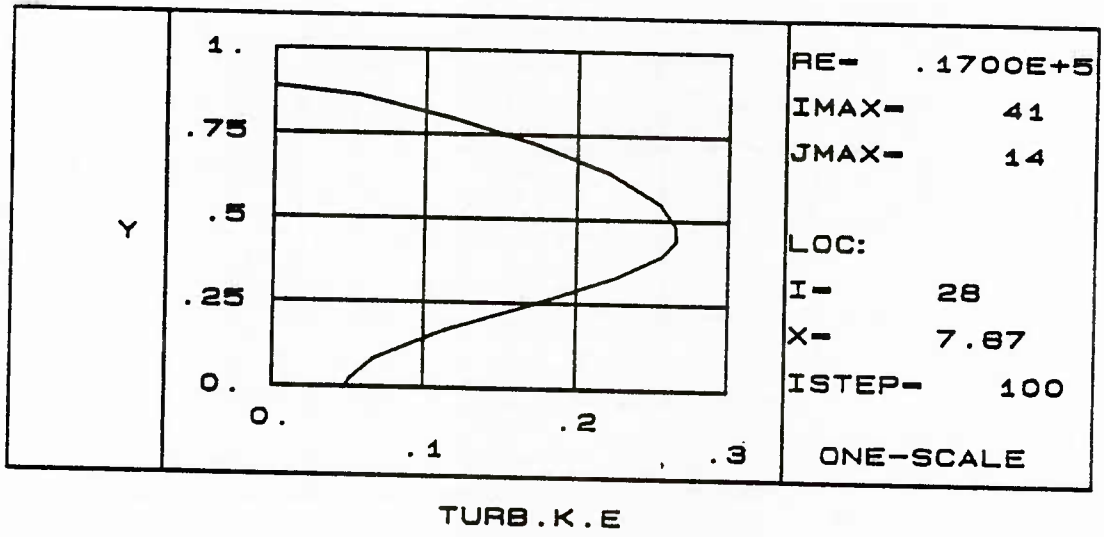

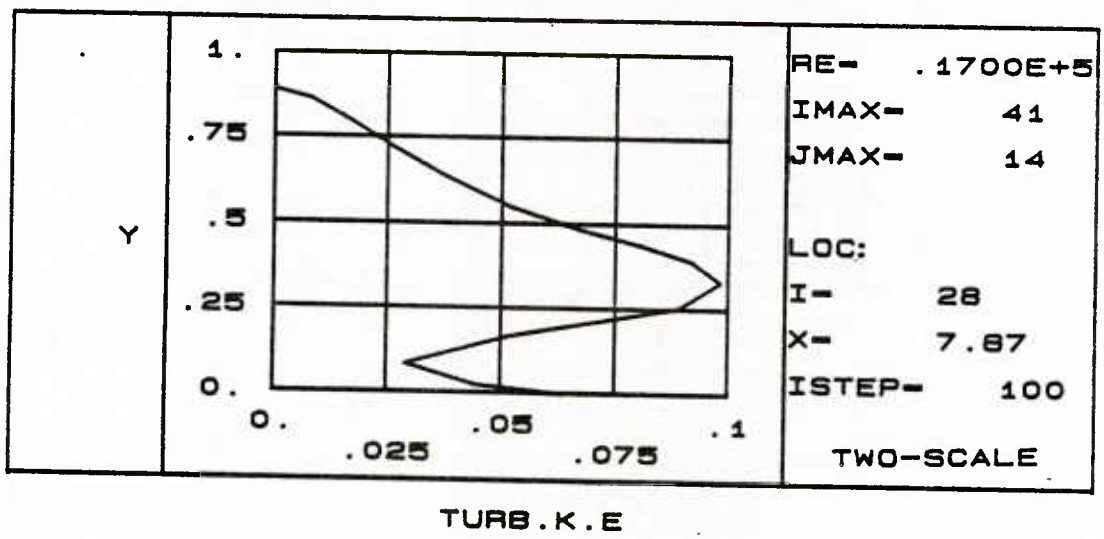

Figure 7.12. Turbulent kinetic energy profile at x/H=4.1

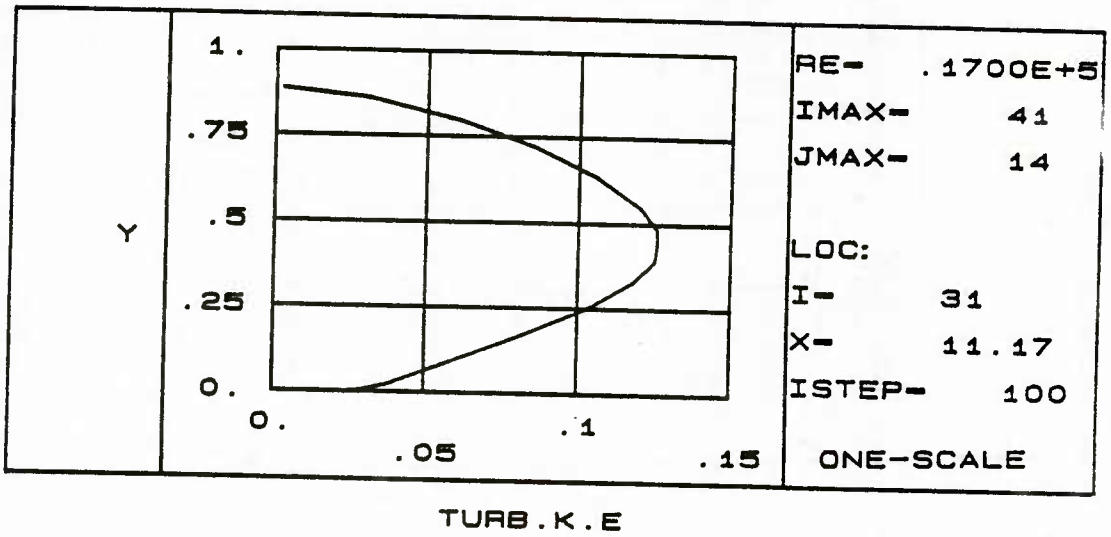

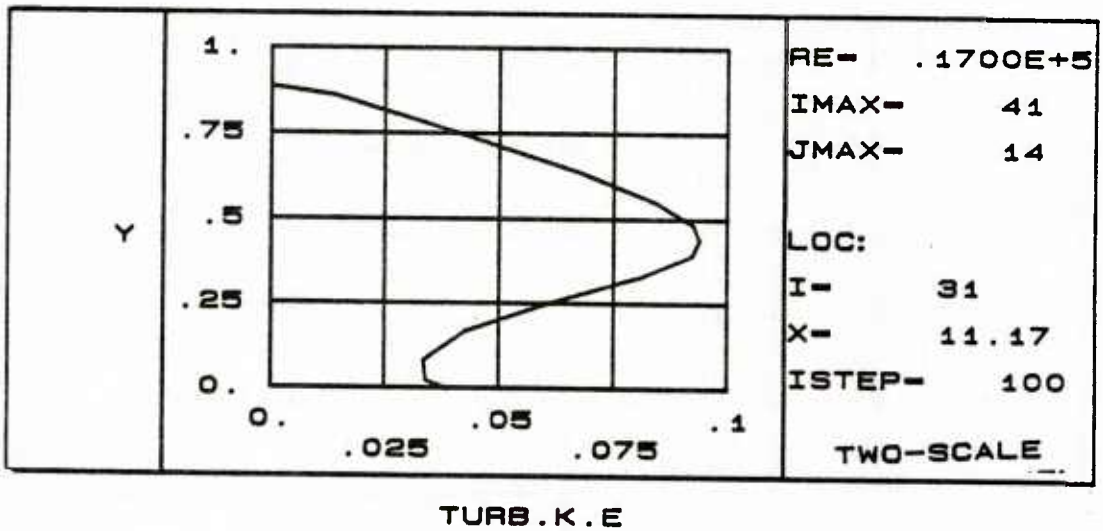

Figure 7.13. Turbulent kinetic energy profile at x/H=7.1

that the two-scale turbulent model indeed predicts better flow field for the two dimensional separation flow than the one-scale model. More work is needed to verify the prediction capability of the two-scale turbulence model in other flow configurations. Grid dependence studies, as well as improvement in the wall function, are necessary for better prediction of turbulent quantities.

CHAPTER VIII

CONCLUSIONS AND RECOMMENDATIONS

8.1 Conclusions

In this investigation, a new two-scale turbulence model is developed. The two turbulent scales are based on a large energy containing scale (k,ε) and a small energy dissipating scale (ν,ε). The (k,ε) scale has been used in previous turbulence models. The (ν,ε) scale, which is known as the Kolmogorov scale, is used in the present investigation to model the destruction term of the ε-equation.

The two-scale turbulence model shows that the ε-equation needs to have the influence of viscosity since viscosity is the main cause of dissipation. In general, the two-scale turbulence model predicts a lower kinetic energy than the one-scale model.

Calculations of free shear flows in Chapters V and VI and recirculating flows in Chapter VII indicate that the two-scale k-ε turbulence model gives significant improvement over the one-scale turbulence model. It is important to point out that unlike the one-scale turbulence model, the two-scale turbulence model does not require modification of turbulent constants in predicting plane or round jets,mixing layer flows, plane and round wakes, buoyant jets, flow past

a backward facing step and flow past a channel obstacle. Therefore, the predictability of the two-scale turbulence model is demonstrated.

Since the present study relied on the existing solution techniques, it should be mentioned that proper understanding of the numerical scheme is important in solving the flow problem. During the study it was found that it is necessary to choose a suitable marching step in the modified Patankar - Spalding algorithm in order to obtain an accurately converged solution. Also, it should be remarked that the initial conditions affect the solution to some extent particularly near the inlet or initial zone. Hence, it was necessary to carefully evaluate experimental data before comparisons between either various experiments or experiment and prediction are made.

Further, during the course of this study, it was found that though experimental data was abundant, many sets of data were not complete for most flows. For example, numerous results were given at various sections of the flow field, but initial conditions particularly for turbulent quantities were not mentioned. In some instances, only one component of normal stress was available for comparison instead of the turbulent kinetic energy and shear stress. Finally, since the main difference between the two-scale and the one-scale turbulence model is in the ε-equation, it would be of interest to compare the dissipation of turbulent kinetic energy predicted by the two models. However, there were almost no experimental measurements of the rate of dissipation of turbulent kinetic energy.

8.2 Recommendation for future study

From the present investigation several issues still require further study or clarification. They are explained below.

1. In chapter II, it was mentioned that the turbulent structure in a flow is a function of the Reynolds number, which is normally based on the characteristic velocity and length of the problem. However, in most experimental investigations it is the turbulent Reynolds number based on the Taylor microscale that is used. The correlation between the problem or mean Reynolds number and Taylor microscale Reynolds numbers is not known. Further study is necessary in turbulent spectral analysis to obtain such a relation. It is worthwhile to see how the turbulent structure changes directly with a change in the Reynolds number of the problem. This may verify the validity of the turbulent model for a range of Reynolds numbers.
2. In chapter II it was mentioned that the spectral analysis was done for isotropic flows only. At present, there is no work available for analysis of nonisotropic flows. Such an investigation, if possible, could help in understanding the energy transfer process and provide a better turbulence model.
3. Various aspects of the computation for turbulent flows need to be considered in order to improve the two-scale turbulence model. For example, most of the results shown in Chapters V, VI and VII are either for mean velocity profile, centerline velocity, turbulent kinetic energy and shear stress. It is desirable to

further investigate the prediction of the two-scale model for other flow parameters such as entrainment, normal stresses and for flows involving secondary motion and three dimensional configuration.

4. Further, the model needs to be extended to compressible flows and other flows with strong curvature.

APPENDIX A

COMPUTER PROGRAM GENMIX

```
INSERT SYSCOM>ERRD.INS.FTN
INSERT SYSCOM>KEYS.INS.FTN
INSERT SYSCOM>KEYS.INS.FTN
      IMPLICIT DOUBLE PRECISION (A-H,O-Z)
      REAL*8 LAB
      DIMENSION OUT(83),DIFK(83),DIST(83),CONK(83),F4V(83)
     1,DXRME(40),XUU(40),YYH(40),YYHT(40),XLONG(100),FLONG(8,100)
     2 ,FEI(100)
      DIMENSION XPLOT(100),YPLOT(10,100),YAXES(20),SYMBOL(20)
      DIMENSION FLUX(7),DFI(7),DFE(7),AJID(7),AJED(7)
      DIMENSION YDT(83),UDT(83),TDT(83),CDT(83),FKDT(83),FEMDT(83)
      DIMENSION FBI(7),FBE(7),EPS(83),FK3E2(83),FK4E3(83)
      DIMENSION SYMBL1(5),SYMBL2(4)
      COMMON/COMA/A(83),AJE(7),AJI(7),B(83),C(83),CSALFA,D(83),DPDX(83),
     1 DX,EMU(83),F(7,83),FS(5,83),IAX,IEND,IFIN,INDE(7),INDI(7),IOUT,
     2 ISTEP,ITEST,IUTRAP,JS,JSW,JV,JY,KEX,KIN,KRAD,N,ND2,NF,NOVEL,NP1,
     3 NP2,NP3,OM(83),OMD(83),P(83),PEI,PR(7),PREF(7,83),PSIE,PSII,R(83)
     4,RHO(83),RME,RMI,RU(83),SD(7,83),SU(7,83),TAUE,TAUI,U(83),XD,XU,
     5Y(83),YE,YI,ENU(83),NDEQ,BPI,BPE,DK1(83),DK2(83),EDK1(83),EDK2(83)
     6,US(83),FACTOR
      COMMON/COMB/ARRCON,EWALL,H,HFU,INERT,MASSTR,MODEL,OXDFU,PREEXP,
     1 PRESS,UBAR,AK,RE,FR,ALMG,UFAC
      COMMON/COMC/ENUT(83),ENUTDN(83),DUDY(83),DUDDY(83),DTDY(83),
     1 DTDDY(83),PROK(83),BUPROK(83),ENUPR(83),PREFI(7)
     2,CDFN(83),PKDEP(83),CVFN(83),UV(83),VV(83),UT(83),
     3 VT(83),TT(83),PTDET(83),PROT(83),DIFTT(83),SUUK(83),SUUE(83)
     4 ,SUUT(83),FUUK(83),FUUE(83),FUUT(83)
      COMMON/CONST/IZT,CMUF,GDM,CDIS,C1,C2,NCM,AL1,ALD,CR1,CRD,BUOY,
     1 C1T,C1K,C2K,NIB,ENULIM,NBUPRO,CT,CE1,CE2,CT1,CC1,CC2,C2T,CSP,CE
     2 ,NPKDE,NPTDE,NALG,CAXIAL,PCLINR,LINEAR,LESSON,CE3,CM2,C2TM
      COMMON/AUXL/RENO,VISMIX,RHOA,TA,COEFEP,COEFED,EPSPK,EPSDT
      DATA V1/'TEST 1'/,V2/'U'/,V3/'F(1,I)'/,V4/'F(2,I)'/,V5/'F(3,I)'/
      DATA V6,V7,V8,V9,V10/'TEST2','FS(1,I)','FS(2,I)','FS(3,I)','RHO(I)
     1  '/
      DATA V11,V12,V13,V14,V15/'TEST3','Y(I)','R(I)','RU(I)','TEST4'/
      DATA V16,V17,V18,V19,V20/'EMU(I)','OMEGA','TEST5','R1 YS','VEL'/
      DATA V21,V22,V23,V24,V25 /'TEMP','T','RHO','KENGY','K'/
      DATA V26,V27,V28,V29,V30/'DISSK','D','SU(I)','ENUTDN','ENU'/
      DATA V31,V32,V33,V34,V35/'ENUT','UV','VV','DIFTT','DIST'/
      DATA V36,V37,V38,V39,V40/'UT','VT','DKDEP','PTDET','CD FN'/
      DATA V41,V42,V43,V44,V45/'CV FN','TT-AGL','TT-DEQ','TT','E'/
```

```
      DATA V46,V47,V48,V49,V50/'DUDDY','DTDDY','CONK','DIFK','PROK'/
      DATA V51,V52,V53,V54,V55/'BUPROK','PREFTT','PREFEP'
     1,'PREF-K','PREF-T'/
      DATA SYMBL1/1HU,1HT,1HK,1HD,1HE/
      DATA SYMBL2/1HU,1HT,1HA,1HF/
C
      CALL SR(READ,'INP1',4,7,TYPE,CODE)
      CALL SR(WRIT,'PSP1',4,2,TYPE,CODE)
      CALL SR(WRIT,'PSP3',4,3,TYPE,CODE)
C
C     ------------------------------------------------------------------
CHAPTER11111111111111111  PARAMETERS AND CONTROL INDICES  11111111111111
C     ----- NSTAT= NO. OF STEPS BETWEEN OUTPUT OF SINGLE VARIABLES.
C     ----- NPROF= NO. OF STEPS BETWEEN OUTPUT OF ARRAY VARIABLES.
C     ----- NPLOT= NO. OF STEPS BETWEEN OUTPUT OF PLOT.
C     ----- IN THIS EXAMPLE, PLOT IS CALLED AT END OF INTEGRATION ONLY.
      NSTAT=100
      NPROF=1000
      NPLOT=20000
C     ----- MODEL=1 ONE-SCALE K-E MODEL
C     ----- MODEL=2 TWO-SCALE K-E MODEL
      MODEL=1
C     ----- IDAT=0=NO DATA READ IN,   =1= BUILT IN PROFILE
      IDAT=0
C----- ILONG =NO  OF  STEPS  BETWEEN  OUTPUT  IN  LONGITUDINAL DIRECTION
       ILONG=300
C     -------   ISTTRAT=1=STRATIFCATION,=0=NO STRATIFICATION
        ISTRAT=0
C     -------   RATTD=RATE OF TD VARIATION IN X DIRECTION (DEG.C/METER)--
       RATTD=2.0
C------  LESSON = 1 = CE1*TOTAL PROK IN EP EQ.-------------
C------  LESSON = 2 = CE1*SHEAR PROK AND CE3 * BUOY PROD.IN EP EQ. -----
       LESSON=2
C-------NBY=1 WHEN BUOYANT FORCE IS INCLUDED-----
  2   NBY=1
 7    KRAD=0
C  ------------------------------------------------------------------
CHAPTER22222222222222222222222  GRID AND GEOMETRY  22222222222222222222
C-------------------------------------------------
C               S. I. UNITS
       L=1
C----N=NO  OF  GRID  POINTS
      N=40
      YNOZ=1.
      XULAST=10.0E+0
      LASTEP=20000
C     IF(KRAD.EQ.1)LASTEP=3500
C     IF(KRAD.EQ.0)LASTEP=2100
      XU=1.E-30
      XP=.99*XU
      XOUT=0.
```

```
      XEND=0.
C-----  FRA = PERCENTAGE OF FORWARD MARCHING, _X = FRA * _Y
      FRA=0.005
C----- FACTOR FOR LINEARIZATION OF SOURCE TERM IN E-EQUATION
      FACTOR=1.0
      ULIM=.01
      ENULIM=1.E+30
      TAN=0.01
      PEILIM=0.01
      KIN=3
      KEX=2
      CSALFA=1.
C     ----- R(1) ADJUSTMENT MADE JUST BEFORE CALL STRIDE(1).
C     ----------STRIDE4----------STRIDE4----------STRIDE4-------STRIDE4
      CALL STRIDE(4)
      IAX=0
      IF(XEND.LE.0.) IEND=0
      IF (XOUT.LE.0.) IOUT=0
C     -------------------- CHANGE IEND, IAX AND IOUT, IF NECESSARY.
C
C  ---------------------------------------------------------------------
CHAPTER33333333333333333333333  DEPENDENT VARIABLES SELECTION  33333333
C     U(I)=VELOCITY
C     F(1,I)=STAGNATION ENTHALPY
C     F(2,I)=CONCENTRATION OF FUEL
C     F(3,I)=CONCENTRATION OF OXIDANT-OXDFU*F(2,I)=PHI
C     FS(1,I)=CONCENTRATION OF OXIDANT
C     FS(2,I)=TEMPERATURE
C     FS(3,I)=CONCENTRATION OF PRODUCT
C     F(4,I)=KINETIC ENERGY OF TURBULENCE
C     F(5,I)=DISSIPATION RATE OF KINETIC ENERGY
C     F(6.I)= THERMAL ENERGY OF TURBULENCE TT
C     F(7.I)= DISS.RATE OF THERMAL ENERGY
C---- FLONG(1,L)=MAXIMUM VELOCITY
C---- FLONG(2,L)=AXIAL  TEMPERATURE
C---- FLONG(3,L)=ENTRAINMENT  COEFFICIENT
C---- FEI(L)=BOUYANT  FLUX  INTEGRAL
C     -----NDEQ=0=ENTHALPY AND CONCENTRATION EQUATION NOT SOLVED
C     -----NDEQ=1=ENTHALPY EQUATION SOLVED
C     -----NDEQ=2=ENTHALPY AND CONCENTRATION EQUATION SOLVED
      NDEQ=1
      NDEQP1=NDEQ+1
      NEQ=3+NDEQ
C     ----NF=NO OF DEPENDENT VARIABLES TO BE SOLVED
      NF=6
C----NDX=NO OF X INTERVAL USED IN CALCULATE ENTRAINMENT COEFF.
      NDX=40
      NDXM1=NDX-1
C  ---------------------------------------------------------------------
CHAPTER4444444444444444444444444444444444444CONSTANTS  4444444444444444
C     CHAPTER 4A--------------MATERIAL CONSTANTS
```

```
C                                                    S.I. UNITS
C------GAS CONSTAT IN JOULE/KILOMOLE/DEG. K ----------
      GASCON=8300.
C------SPECIFIC HEAT AT CONST. PRESS. IN JOULE/KG/DEG.K----
      CMIX=1100.
C------MOLECULAR WEIGHT IN KG/KILOMOLE---------
      WMIX=29.
      WA=29.
      WD=29.
      GAMMA=CMIX/(CMIX-GASCON/WMIX)
      WDGSCN=WMIX/GASCON
      VISMIX=1.0E-7
      PREEXP=1.
C
      IZT=20
C
C     --------------CONSTANTS FOR TURBULENCE MODEL
      CV=.475
C-------- CONSTANTS FOR UT VT EQS ------
      C1T=3.2
      C2T=.5
      C2TM=C2T
C-------- CONSTANTS FOR UV UU VV EQS --------
      CC1=2.8
      CC2=0.47
      CM2=CC2
      CSP=0.9
      IF(MODEL.EQ.1) CSP=0.225
      CST=1.6
C------ CONSTANT FOR TT EQUATION --------
      CT1=0.13
      CT=1.25
C-----CONSTANTS FOR TURBULENT KINEMATIC VISCOSITY -------
      CD=(1.-CC2)*CV/CC1
      PREFI(4)=1.
      PREFI(5)=1.3
      PREFI(6)=CD/CT1
      PREFI(7)=1.
      CDIS=CD
   42 DO 40 J=1,3
      PR(J)=.7
 40   PREFI(J)=(1.-CC2)*C1T/CC1
      BUOY=FLOAT(NBY)*9.81
C
C-------- CONSTANTS FOR EP EQ --------
      CE=2.00
      CE1=17.50
      CE2=18.90
      CE3=CE1
      IF(MODEL.EQ.1) CE=0.15
      IF(MODEL.EQ.1) CE1=1.435
```

```
      IF(MODEL.EQ.1) CE2=1.92
      COEFEP=CE1
      COEFED=CE2
      WRITE(6,45)
      WRITE(6,43) CSP,CC1,CC2,C1T,C2T,CM2,CE1,CE2,CE3,CE,CT1,CT,
     1 FRA,C2TM
 45   FORMAT(20X,'------  CONSTANTS  FOR  TURBULENCE  MODEL ---'/)
 43   FORMAT(4X,'CSP =',F10.5,5X,'CC1 =',F10.5,5X,'CC2 =',F10.5,/
     1       4X,'C1T =',F10.5,5X,'C2T =',F10.5,5X,'CM2 =',F10.5,/
     2       4X,'CE1 =',F10.5,5X,'CE2 =',F10.5,5X,'CE3 =',F10.5,/
     3       4X,'CE  =',F10.5,5X,'CT1 =',F10.5,5X,'CT  =',F10.5,/
     4       4X,'FRA =',F10.5,5X,'C2TM=',F10.5,5X/)
C  ------------------------------------------------------------------------
CHAPTER5555555555555555555555555555555555  INITIAL CONDITIONS  5555555555
C----  SPECIFY  RADIUS ,VELOCITY ,TEMP. ETC
      RA=0.
      RB=0.
      RC=0.
      RD=0.065
      DIAD=2.*RD
      UA=1.5
      UB=UA
      UC=UA
      UD=0.0
      TA=315.
      TD=300.5
      TDD=TD
      TB=TA
      TC=TA
      NEMU=1
      EMUI=1.
      UREF=1.
      YIN=RB
      TWALL=299.
      PRESS=1.E5
      PDGSCN=PRESS/GASCON
      RHOA=PDGSCN*WA/TA
      RHOD=PDGSCN*WD/TD
C------   INITIAL  LONGITUDINAL  CONDITIONS  --------
       DD=2.*RD
       XLONG(1)=XU/DD
       FLONG(1,1)=1.
       FLONG(2,1)=1.
       FLONG(3,1)=0.5
       FEI(1)=0.
C------- CALCULATE RE.FR GR RI NUMBERS --------
C
      SBG=9.81*RATTD/TD
      BGDGD=RD*SBG/(9.81*(TA-TD)/TD)
      GUDGD=SBG*UA**2./((9.81*(TA-TD)/TD)**2.)
      RENO=(RHOA*UA*2*RD)/(VISMIX*DSQRT(TA))
```

```
      FRNOS=(UA**2*TA)/(9.81*2*RD*(TA-TD))
      FRNO=DSQRT(FRNOS)
      GRNO=(9.81*(TA-TD)*(2*RD)**3)/(TA*(VISMIX*DSQRT(TA)/RHOA)**2)
      RICHN=DSQRT(GRNO)/RENO
C
      WRITE(6,48) RENO,FRNOS,FRNO,GRNO,RICHN,BGDGD,GUDGD,SBG
 48   FORMAT(/4X,'RENO =',E13.6,2X,'FRNOS=',E13.6,2X,'FRNO =',E13.6,/
     1        4X,'GRNO =',E13.6,2X,'RICHN=',E13.6,2X,'BGDGD=',E13.6,/
     2        4X,'GUDGD=',E13.6,2X,'SBG  =',E13.6/)
C
C     --------------CREATION OF INTIAL PROFILES
      Y(NP3)=RD-RB
      EXPY=1.
      UIN=UA
      UEN=UD
      TMPI=TA
      TMPE=TD
      C1I=1.
      C1E=0.
      FATT=0.10
      FAET=0.10
      FA1=FATT
      FA2=FAET
      DO 52 J=4,NF
      FBI(J)=0.
   52 FBE(J)=0.
C     ------------------------------------------------------------------
C     INITIALIZE SOME OF THE PARAMETERS
C
      DO 53 I=1,NP3
      UT(I)=0.0
      VT(I)=0.0
      UV(I)=0.0
      VV(I)=0.0
      F4V(I)=0.0
 53   CONTINUE
      Y(1)=0.
      Y(2)=0.
      YEPLS=0.0
      RME=0.0
      U1DUOL=0.0
      T1DTOL=0.0
      SB=1.0
      SA=1.0
      F(3,1)=1.0
      FE=1.0
      Y(NP2)=Y(NP3)
      U(1)=UIN
      U(2)=UIN
      U(NP3)=UEN
      U(NP2)=UEN+1.0E-6
```

```
      UHB=U(1)-U(NP3)
      UHBS=UHB**2
      FS(2,1)=TMPI
      FS(2,2)=TMPI
      FS(2,NP3)=TMPE
      FS(2,NP2)=TMPE
      F(2,1)=C1I
      F(2,2)=C1I
      F(2,NP3)=C1E
      F(2,NP2)=C1E
      DO 513 J=4,NF
  513 F(J,NP3)=FBE(J)
      IF(KIN.NE.2) GO TO 510
      DO 514 J=4,NF
  514 F(J,1)=FBI(J)
      GO TO 503
  510 F(4,1)=FA1*UHBS
      F(5,1)=0.10*F(4,1)**1.5/(0.09*Y(NP3))
      F(6,1)=FATT*(FS(2,1)-FS(2,NP3))**2.
      F(7,1)=0.10*F(6,1)**1.5/(0.09*Y(NP3))
  503 DO 516 J=4,NF
      F(J,2)=F(J,1)
  516 F(J,NP2)=F(J,NP3)
C
C     --------------PROFILES
C
      DYAF=1./FLOAT(N)**EXPY
      DO 520 I=2,NP2
      Y(I)=(1.-DYAF*FLOAT(NP2-I)**EXPY)*Y(NP3)
      YP2=Y(I)**2.
      U(I)=U(NP3)+(U(1)-U(NP3))*DEXP(-2.8*YP2)
      FS(2,I)=TMPE+(TMPI-TMPE)*DEXP(-2.8*YP2/1.44)
      F(2,I)=C1E+(C1I-C1E)*DEXP(-2.8*YP2)
      F(3,I)=1.-F(2,I)
      F(4,I)=UHBS*FA1*DEXP(-1.7*YP2)
      IF(KIN.EQ.2.AND.KEX.EQ.2) F(4,I)=FA1*UHBS*(1.-((Y(I)-Y(NP3)/2.)
     1 /(Y(NP3)/2.))**2)
      F(5,I)=0.10*F(4,I)**1.5/(0.09*Y(NP3))
      F(6,I)=F(6,1)*DEXP(-1.7*YP2)
      F(7,I)=0.10*F(6,I)**1.5/(0.09*Y(NP3))
  520 CONTINUE
      DO 521 I=1,NP3
      RHO(I)=PDGSCN/FS(2,I)*WMIX
  521 F(1,I)=CMIX*FS(2,I)+.5*U(I)*U(I)+F(4,I)
      IF(KIN.EQ.3) YNOZ=2.*Y(NP3)
      IF(KIN.EQ.2) YNOZ=2.*YIN
C------ CALCULATE INITIAL CD FUNCTION FOR ENU(I) ------
      DO 525 I=1,NP3
      CDFN(I)=0.07
  525 CVFN(I)=0.47
      WRITE(6,526) PKDEP(3),CDFN(3),CVFN(3),N
```

```
 526  FORMAT(/'PKDEP=',E13.6,1X,'CDFN =',E13.6,1X,'CVFN =',E13.6,1X,
     1'N    =',I5)
       DO 527 J=1,NF
       DO 527 I=1,NP3
 527  PREF(J,I)=1.
C     CALCULATE OMEGA AND STREAM QUANTITIES AND WRITE
  501 YMDP=1.
      DO 540 I=3,NP2
      IF(KRAD.EQ.1) YMDP=.5*(Y(I-1)+Y(I))+YIN
      RUA=.5*(RHO(I)*U(I)+RHO(I-1)*U(I-1))
  540 OM(I)=OM(I-1)+YMDP*RUA*(Y(I)-Y(I-1))
      PEI=OM(NP2)
C-----OMEGA,OM(I),IS MADE DIMENSIONLESS HERE -------
      DO 541 I=3,NP2
  541 OM(I)=OM(I)/PEI
      PSII=YIN*U(1)*RHO(1)
      IF(KRAD.EQ.1) PSII=PSII*YIN/2.
      PSIE=PSII+PEI
C---------SET UP INITIAL SPREAD PARAMETER FOR U AND T
      F1A=CMIX*TA+.5*UA**2
      F1D=CMIX*TD+.5*UD**2
      F2A=1.
      F2D=0.
      F3A=1.-F2A
      F3D=1.-F3A
      DYHA=0.
      UBARDL=1.
      DYHAV=1.
      YHA=0.
      YHALS=0.25
      YELS=0.
      DYHAT=0.
      TBARDL=1.
      DYHAVT=1.
      YHAT=0.
      YHATLS=0.25
      DO 549 K=1,NDX
      YYH(K)=0.
      YYHT(K)=0.
      XUU(K)=0.
 549  CONTINUE
      XUU(NDX)=XU
C-----SET UP INITIAL ENTRAINMENT VELOCITY-----
C ----- RTBDVB IS RATIO OF TEMP. TO VEL.LAYER AT BOUNDY,USE IN
C ------------------------------------------- ENTRAIN.CONTROL
      RTBDVB=1.4
      ENTV=0.
      ENTVLS=0.
      DENTV=0.
      YELS=RD
      IF(KIN.EQ.3) U1V=U(1)
```

```
      FLOA=PSII
      IF(RC.LE.RB) GO TO 560
      DO 550 I=1,NP3
      YAB=Y(I)+YIN
      IF(YAB.LT.RC) GO TO 550
      IC=I
      GO TO 551
  550 CONTINUE
  551 FLOB=PEI*OM(IC)
      FLOC=PEI-FLOB
      ICM1=IC-1
      F2B=0.
      DO 552 I=2,ICM1
      OMDP=OM(I+1)-OM(I)
      TB=TB+(FS(2,I)+FS(2,I+1))*OMDP
  552 F2B=F2B+(F(2,I)+F(2,I+1))*OMDP
      TB=.5*TB
      F2B=.5*F2B
      F3B=1.-F2B
      F2C=0.
      DO 553 I=IC,NP1
      OMDP=OM(I+1)-OM(I)
      TC=TC+(FS(2,I)+FS(2,I+1))*OMDP
  553 F2C=F2C+(F(2,I)+F(2,I+1))*OMDP
      TC=.5*TC
      F2C=.5*F2C
      F3C=1.-F2C
      GO TO 570
  560 FLOB=0.
      F2B=0.
      F3B=0.
      FLOC=PEI
      F2C=0.
      DO 561 I=2,NP1
      OMDP=OM(I+1)-OM(I)
      TC=TC+(FS(2,I)+FS(2,I+1))*OMDP
  561 F2C=F2C+(F(2,I)+F(2,I+1))*OMDP
      TC=.5*TC
      F2C=.5*F2C
      F3C=1.-F2C
  570 FLOTOT=PEI
C
C     ------------------------------------------------------------------
CHAPTER666666666666666666666666666666  THERMODYNAMIC PROPERTIES  666666
C  ********************  START OF MAIN LOOP  **********************
   60 CONTINUE
C
  603 CONTINUE
C     ------------------------------ ADJUST R(1) AND YIN
      IF(KIN.NE.2) GO TO 630
      IF(KRAD.EQ.1) GO TO 631
```

```
      YIN=PSII/(U(1)*RHO(1))
      GO TO 630
  631 YIN=DSQRT(DABS(2.*PSII/(RHO(1)*U(1))))
      R(1)=YIN
  630 CONTINUE
C
C     ----------STRIDE1----------STRIDE1----------STRIDE1-------STRIDE1
      CALL STRIDE(1)
C
C     --------RHO*U   R  AND  Y  ARE  CALCULATED
C     --------------CALCULATION OF CHARACTERISTIC FLOW WIDTH AND UGL
      UHB=U(1)-U(NP3)
      UHB2=1./(UHB**2)
      UHA=.5*UHB
      UHC=DABS(UHA)
      UHA=UHA+U(NP3)
      UHE=DABS(UHB)/(DEXP(1.))
      IHE=3
C
C----  YEP= Y AT U= UMAX/EXP ---------------
C----  YHA= Y AT U= UMAX/2   ---------------
C----  YHAT= Y AT T= TMAX/2. ---------------
C
      DO 619 I=3,NP2
      IF(DABS(U(I)-U(NP3)).GT.UHE) GO TO 619
      IHE=I-1
      GO TO 618
  619 CONTINUE
  618 YEP=Y(IHE)+(UHE-U(IHE))*(Y(IHE+1)-Y(IHE))/(U(IHE+1)-U(IHE))
      IHA=2
      DO 620 I=3,NP2
      IF(DABS(U(I)-U(NP3)).GT.UHC) GO TO 620
      IHA=I-1
      GO TO 621
  620 CONTINUE
C
C----------CALCULATE Y HALF (YHA) -------
C
  621 YHA=Y(IHA)+(UHA-U(IHA))*(Y(IHA+1)-Y(IHA))/(U(IHA+1)-U(IHA))
      YHR=YHA+YIN
      THB=FS(2,1)-FS(2,NP3)
      THB2=1./(THB**2)
      THA=.5*THB
      THC=DABS(THA)
      THA=THA+FS(2,NP3)
      IHT=1
      DO 626 I=3,NP2
      IF(DABS(FS(2,I)-FS(2,NP3)).GT.THC)GO TO 626
      IHT=I-1
      IF(IHT .GT. 0) GOTO 627
  626 CONTINUE
```

```
 627  YHAT=Y(IHT)+(THA-FS(2,IHT))*(Y(IHT+1)-Y(IHT))/
     1 (FS(2,IHT+1)-FS(2,IHT)+.1E-5)
       DYHAT=(YHAT-YYHT(1))/(XUU(NDX)-XUU(1))
       DYHA=(YHA-YYH(1))/(XUU(NDX)-XUU(1))
       DYHATL=(YHAT-YHATLS)/(XU-XP)
       YHDYHT=YHA/YHAT
       DYEP=(YEP-YEPLS)/(XU-XP)
C
C------CALCULTE ENTRAINMENT COEFFICINT--------
C
      DYE=-(YELS2-YE)/(XUU(NDX-2)-XP)
      ANG=ATAN(DYHA)
      ANG=COS(ANG)
      ENTV=RME*ANG/(RHO(NP3)*R(NP3))/RTBDVB
      ALFA=ENTV/U(1)
      ALFALO=RME*ANG/(RHO(NP3)*R(NP3)*U(1))/RTBDVB
      ALFAAX=RME*ANG/(RHO(NP3)*U(1)*(Y(IHE)**KRAD))/RTBDVB
      DENTV=(ENTV-ENTVLS)/(XU-XP)
      IF(KIN.NE.2) GO TO 610
C
C-----------IF FLOW IS OF SHEAR LAYER  -------
C
      YHM=YHA
      UDI=.9*UHB
      UDIC=DABS(UDI)
      UDI=UDI+U(NP3)
      UDE=.1*UHB
      UDEC=DABS(UDE)
      UDE=UDE+U(NP3)
      YDI=0.
      IDI=2
      DO 622 I=3,NP1
      IF(DABS(U(I)-U(NP3)).GT.UDIC)GO TO 622
      IDI=I-1
      IF(IDI .GT. 0) GO TO 623
 622  CONTINUE
 623  YDI=Y(IDI)+(UDI-U(IDI))*(Y(IDI+1)-Y(IDI))/(U(IDI+1)-U(IDI))
      IDE=1
      DO 624 I=3,NP1
      IREAL=NP3-I+1
      IF(DABS(U(IREAL)-U(NP3)).LT.UDEC) GO TO 624
      IDE=IREAL
      IF(IDE.GT.0) GO TO 625
 624  CONTINUE
  625 YDE=Y(IDE)+(UDE-U(IDE))*(Y(IDE+1)-Y(IDE))/ (U(IDE+1)-U(IDE))
      YHA=YDE-YDI
C
C-------CALCULATE RATE OF SPREAD--------
C
  610 CONTINUE
      IF(U(NP3).LE.0.) GO TO 640
```

```
      IF(DABS(UHB/U(NP3)).LT..02) DYHA=DYHA*U(NP3)/UHB
  640 DYHALO=(YHA-YHALS)/DX
      YHALS=YHA
      YHATLS=YHAT
      YELS=YE
      YEPLS=YEP
      ENTVLS=ENTV
      YYH(NDX)=YHA
      YYHT(NDX)=YHAT
      XUU(NDX)=XP
      DO 650 K=1,NDXM1
      YYH(K)=YYH(K+1)
      YYHT(K)=YYHT(K+1)
      XUU(K)=XUU(K+1)
  650 CONTINUE
C
CHAPTER777777777777777777777777777777777777  FORWARD STEP  777777777
      DX=FRA*Y(NP3)
      IF(ISTEP.LT.50) DX=DX/FLOAT(51-ISTEP)
C
      IF(ISTEP.GE.IEND) GO TO 70
      IF(DX.LT.XEND-XU) GO TO 70
      DX=XEND-XU
      IEND=ISTEP+1
   70 IF(ISTEP.GE.IOUT) GO TO 71
      IF(DX.LT.XOUT-XU) GO TO 71
      DX=XOUT-XU
      IOUT=ISTEP+1
   71 IF(DX.GT.XULAST-XU) DX=XULAST-XU
      IF(DX.GT.0.) GO TO 73
      IFIN=1
      GO TO 1011
C
   73 XD=XU+DX
C     -------THIS IS JUST INITIAL GENERAL SETUP
C     ----- FURTHER ADJUSTMENTS TO DX ARE MADE IN CHAPTERS 8 AND 9.
C
C  ------------------------------------------------------------------------
CHAPTER88888888888888888888888  ADJUST LONGITUDINAL CONDITIONS  8888888
C
C     CHAPTER8A ------------------------------BOUNDARY CONDITIONS
C     ---------------- I BOUNDARY
C     ------------------- SYMMETRY AXIS
   80 KIN=3
      RMI=0.
      YIN=0.
      R(1)=0.
      PSII=0.
C     ----------------------------------------FREE
   85 KEX=2
C     ----------------------UBAR
```

```
   89 UBAR=0.
      TBAR=0.
      DO 820 I=2,NP1
      TBAR=TBAR+(FS(2,I)+FS(2,I+1))*OMD(I)
  820 UBAR=UBAR+(U(I)+U(I+1))*OMD(I)
      TBAR=.5*TBAR
      UBAR=.5*UBAR
      IF(KIN.EQ.2) UBAR=(UBAR-UA)*PEI/PSIE+UA
      IF(KIN.EQ.2)TBAR=(TBAR-FS(2,NP3))*PEI/PSIE+FS(2,NP3)
C
C  ---------------------------------------------------------------------
CHAPTER99999999999999999999  TRANSPORT AND ENTRAINMENT PROPERTIES  9999
C     ---------- LAMINAR VISCOSITY ACCORDING TO SQUARE-ROOT FORMULA,
C                       WITH WEIGHTING ACCORDING TO MASS FRACTION.
      DO 98 I=1,NP3
      FSAB=DABS(FS(2,I))
   98 EMU(I)=VISMIX*DSQRT(FSAB)
      CONTINUE
      EMU(2)=EMU(1)
      EMU(NP2)=EMU(NP3)
C
C     ----------AUX----------AUX----------AUX----------AUX----------AUX
      CALL AUX
C---- SOURCE TERM FOR K AND EP ALSO UV,VV,VT,UT,TT,ARE CALCULATED
C     ------------------------------ ENTRAINMENT CONTROL.
      IF(KIN.NE.2) GO TO 94
      RAT=DABS((U(3)-U(1))/(U(NP3)-U(1)+1.E-30))
      IF(RAT.LT.ULIM) EM U(2)=EM U(2)*RAT/ULIM
      RMI=2.*EM U(2)
   94 CONTINUE
      IF(KEX.NE.2) GO TO 97
      RAT=DABS((U(NP1)-U(NP3))/(U(NP3)-U(1)+1.E-30))
      RME=-2.*EM U(NP1)*RTBDVB
      IF(RAT.LT.ULIM) RME=RME*(RAT/ULIM)**2
      IF(RAT.LT.ULIM*.5) RME=0.
   97 IF(XD.EQ.XEND.OR.XD.EQ.XOUT.OR.XD.EQ.XULAST.OR.IAX.EQ.ISTEP+1)
     1            GO TO 96
C     ---------- LIMIT ON INCREMENT IN PEI.
      IF((DABS(RMI)+DABS(RME))*DX.LT.PEI*PEILIM) GO TO 96
      DX=PEI*PEILIM/(DABS(RMI)+DABS(RME))
      XD=XU+DX
   96 CONTINUE
C
C     ----------STRIDE2----------STRIDE2----------STRIDE2-------STRIDE2
   95 CALL STRIDE(2)
C
C------ SET UP A B C D ARRAY ---------
C  ---------------------------------------------------------------------
CHAPTER 10 10 10 10 10 10 10 10 10 10 10 10 10 10 10 10   OUTPUT   10 10 10
C------- SET UP OUTPUT FORMAT ---------
 1000 ANSTAT=NSTAT
```

```
      ANPROF=NPROF
      ANPLOT=NPLOT
      IF(ISTEP.GT.0) GO TO 106
CHAPTER 10A  ----------------------------------  HEADINGS
      REY=2.*R(NP3)*RHO(1)*UBAR/EMU(1)
      EQRAT=0.0
C
      WRITE(6,1013) KRAD,LESSON
C
 1013 FORMAT(/'KRAD  =',I3,10X,'LESSON=',I3,10X/)
      WRITE(6,1010) UA,UB,UC,UD,TA,TB,TC,TD,RA,RB,RC,RD,
     1 XULAST,PRESS,PREEXP
C
 1010 FORMAT(/4X,'UA    =',E13.6,5X,'UB    =',E13.6,5X,'UC    =',E13.6/
     1       ,4X,'UD    =',E13.6,5X,'TA    =',E13.6,5X,'TB    =',E13.6/
     2       ,4X,'TC    =',E13.6,5X,'TD    =',E13.6,5X,'RA    =',E13.6/
     3       ,4X,'RB    =',E13.6,5X,'RC    =',E13.6,5X,'RD    =',E13.6/
     4       ,4X,'XULAST=',E13.6,5X,'PRESS =',E13.6,5X,'PREEXP=',E13.6/)
      LAB=V17
      WRITE(6,100) LAB,(OM(I),I=1,NP3)
      PRESS1=PRESS
  106 CONTINUE
C
C     ----- IPRINT=0 GIVES NO OUTPUT,  =1 GIVES SINGLE VARIABLES ONLY,
C                 =2 GIVES BOTH SINGLE AND ARRAY (PROFILE) VARIABLES.
 1011 IPRINT=0
      IF(FLOAT(ISTEP/NSTAT).EQ.FLOAT(ISTEP)/ANSTAT) IPRINT=1
      IF(FLOAT(ISTEP/NPROF).EQ.FLOAT(ISTEP)/ANPROF) IPRINT=2
      IF(ISTEP.EQ.IEND.OR.ISTEP.EQ.IAX.OR.ISTEP.EQ.IOUT) IPRINT=2
      IF(ITEST.NE.0.OR.IFIN.NE.0) IPRINT=2
C     ----- THE NEXT STATEMENT WOULD BE USED FOR A TYPICAL PLOT CONTROL
      IF(FLOAT(ISTEP/NPLOT).EQ.FLOAT(ISTEP)/ANPLOT) IPRINT=3
C     ----- THE NEXT STATEMENT PROVIDES A PLOT JUST PRIOR TO TERMINATION
      IF(XU.GE.XULAST.OR.IFIN.NE.0.OR.ISTEP.EQ.LASTEP) IPRINT=3
C
 1015 ALFAX=RME*ANG/(RHO(IHE)*UBAR*(YEPLS**KRAD))
C
CHAPTER 10C     ----------------------------SINGLE STATION VARIABLES.
 1200 IF(IPRINT.EQ.0) GO TO 110
      UBAR=0.
      DO 1021 I=2,NP1
 1021 UBAR=UBAR+OMD(I)*(U(I)+U(I+1))
      UBAR=.5*UBAR
      UBARLS=UBARDL
      UBARDL=(UBAR-U(NP3))/UHB
      DUBAR=DABS(UBARDL-UBARLS)/UBARDL
      DDYHA=DABS((DYHA-DYHAV))
      DYHAV=DYHA
      U1DUO=U(1)/(UA-U(NP3))
      T1DTO=(FS(2,1)-TDD)/(TA-TDD)
C-------  TEST  FOR  DEVELOPED  FLOW  --------------
```

```
      IF(DUBAR.LT.1.E-3.AND.DDYHA.LT.1.E-4.AND.ISTEP.GT.4000) IFIN=2
      IF(IFIN.EQ.2) IPRINT=3
      WRITE(6,1030) ISTEP,KRAD,KIN,KEX,FRNOS,PSII,PSIE,U1DUO,
     1 RMI,RME,PEI,U(1),YHA,DYHA,UBARDL,T1DTO
C
 1030 FORMAT(////'ISTEP ='I9,5X,'KRAD  =',I9,5X,
     1        'KIN   =',I9,5X,'KEX   =',I9,5X,/
     1        'FRNOS =',E9.3,5X,'PSII  =',E9.3,5X,'PSIE  =',E9.3,/
     2        'U1DUO =',E9.3,5X,'RMI   =',E9.3,5X,'RME   =',E9.3,/
     3        'PEI   =',E9.3,5X,'U(1)  =',E9.3,5X,'YHA   =',E9.3,/
     4        'DYHA  =',E9.3,5X,'UBARDL=',E9.3,5X,'T1DTO =',E9.3,/)
       XDD=XU/DIAD
       DU1DUO=(U1DUOL-U1DUO)/(XU-XP)/DIAD
       DT1DTO=(T1DTOL-T1DTO)/(XU-XP)/DIAD
       WRITE(6,1014) XDD,DU1DUO,DT1DTO,DYEP
 1014  FORMAT('XDD   ='E9.3,5X,'DU1DUO=',E9.3,5X,'DT1DTO=',E9.3,
     1        5X,'DYEP  =',E9.3,/)
       U1DUOL=U1DUO
       T1DTOL=T1DTO
      WRITE(6,1036) DUBAR,DDYHA,BPE,FS(2,1),FS(2,NP3),YHAT,DYHAT,RATTD
 1036 FORMAT('DUBAR =',E9.3,5X,'DDYHA =',E9.3,5X,'BPE   =',E9.3,5X,
     1 'FS2I  =',E9.3,5X,/'FS2E  =',E9.3,5X,'YHAT  =',E9.3,5X,
     2 'DYHAT =',E9.3,5X,'RATTD =',E9.3,/)
      WRITE (6,1037) ALFA,ENTV,DENTV,DYE,CE1,CE2
     1,ALFALO,DYHALO,ALFAX,DYHATL,YHDYHT
 1037 FORMAT('ALFA  =',E9.3,5X,'ENTV  =',E9.3,5X,'DENTV =',E9.3,5X,
     1 'DYE   =',E9.3,5X,/'CE1   =',E9.3,5X,'CE2   =',E9.3,5X,
     2 'ALFALO=',E9.3,5X,'DYHALO=',E9.3,5X,/'ALFAX =',E9.3,5X,
     3 'DYHATL=',E9.3,5X,'YHDYHT=',E9.3,/)
      DO 1020 J=1,NF
 1020 FLUX(J)=0.
      DO 1035 I=2,NP1
      DO 1035 J=1,NF
 1035 FLUX(J)=FLUX(J)+OMD(I)*(F(J,I)+F(J,I+1))
      UFLUX=PEI*UBAR
      DO 1022 J=1,NF
 1022 FLUX(J)=.5*PEI*FLUX(J)
C
      UREF=U(NP3)+1.E-30
      RUREF=UREF*RHO(NP3)
      AEXD=0.
      DO 1023 J=1,NF
      DFI(J)=F(J,1)-F(J,NP3)+1.E-30
 1023 DFE(J)=DFI(J)+F(J,1)-F(J,NP3)
      UFLUX=UFLUX-PEI*U(NP3)+U(1)*PSII
      GO TO (1041,1042,1043), NDEQP1
 1043 FLUX(3)=FLUX(3)-PSIE*F3D+F3A*PSII
 1042 FLUX(2)=FLUX(2)-PSIE*F2D+F2A*PSII
 1041 FLUX(1)=FLUX(1)-PSIE*F1D+F1A*PSII
      PRESSD=PRESS/PRESS1-1.
      RELO=U(1)*2.*YHA*RHO(1)/(VISMIX*DSQRT(FS(2,1)))
```

```
C
      WRITE(6,1031)XU,DX,UFLUX,RELO
 1031 FORMAT('XU    =',E9.3,5X,'DX    =',E9.3,5X,'UFLUX =',E9.3,5X,
     1  'RELO  =',E9.3,/)
C
      TK25=.5*(F(4,2)+F(4,3))
      E25=.5*(F(5,2)+F(5,3))
C
 1026 CONTINUE
C
CHAPTER 10D     ----------------------------PROFILES AND OTHER ARRAYS.
      IF(IPRINT.EQ.1) GO TO 110
C
CHAPTER 10DD    ------------------KINETIC ENERGY BALANCE
C
      DO 1087 I=3,NP1
      FK3E2(I)=F(4,I)**3/F(5,I)**2
      FK4E3(I)=F(4,I)**4/F(5,I)**3
      DIV=U(1)**3/YHA
      PROK(I)=PROK(I)/RHO(I)/DIV
      BUPROK(I)=BUPROK(I)/RHO(I)/DIV
      DIFK(I)=(ENU(I)*(R(I)+R(I+1))*(F(4,I+1)-F(4,I))/
     1 ((Y(I+1)-Y(I))*PREF(4,I))-ENU(I-1)*(R(I-1)+R(I))*(F(4,I)-F(4,I-1)
     2 )/((Y(I)-Y(I-1))*PREF(4,I)))/((Y(I+1)-Y(I-1))*R(I))
      DIFK(I)=DIFK(I)/RHO(I)/DIV
      CONK(I)=-(RHO(I)*U(I)*(F(4,I)-F4V(I))/(XU-XP)+PEI*(SA+SB*OM(I))
     1 *(F(4,I+1)-F(4,I-1))/((Y(I+1)-Y(I-1))*R(I)))
      CONK(I)=CONK(I)/RHO(I)/DIV
      DIVT=FS(2,1)**2.*U(1)/YHAT
      PROT(I)=PROT(I)/RHO(I)/DIVT
      DIFTT(I)=(ENU(I)*(R(I)+R(I+1))*(F(6,I+1)-F(6,I))/
     1 ((Y(I+1)-Y(I))*PREF(6,I))-ENU(I-1)*(R(I-1)+R(I))*(F(6,I)-F(6,I-1)
     2 )/((Y(I)-Y(I-1))*PREF(6,I)))/((Y(I+1)-Y(I-1))*R(I))
      DIFTT(I)=DIFTT(I)/RHO(I)/DIVT
      DIST(I)=CT*F(5,I)*F(6,I)/F(4,I)/DIVT
 1087 CONTINUE
C------  10E  ---------  10E  ---------  10E  --------
CHAPTER  10E  OUTPUT  TRAVERSE  PROFILES
 1086 CONTINUE
      LAB=V19
      DIV=YHA
      DO 1095 I=1,NP3
 1095 OUT(I)=Y(I)/DIV
      WRITE(6,100) LAB,R(1),(OUT(I),I=2,NP3),Y(NP3),YHA
      XAXIS=V12
      DO 1085 I=1,NP3
 1085 XPLOT(I)=OUT(I)
      LAB=V2
      SUB=0.
      DIV=1.
      IF(KIN.EQ.3) SUB=U(NP3)
```

```
      IF(KIN.EQ.3) DIV=U(1)-U(NP3)+1.E-30
      DO 1094 I=1,NP3
 1094 OUT(I)=(U(I)-SUB)/DIV
      WRITE(6,100) LAB,U(1),(OUT(I),I=2,NP3),U(NP3),DIV
      NY=1
      YAXES(NY)=V20
      SYMBOL(NY)=SYMBL1(NY)
      DO 1084 I=1,NP3
 1084 YPLOT(NY,I)=OUT(I)
      IF(NDEQ.EQ.0) GO TO 1091
C
      LAB=V21
      SUB=FS(2,NP3)
      DIV=1.E-30+FS(2,1)-FS(2,NP3)
      DO 1093 I=1,NP3
 1093 OUT(I)=(FS(2,I)-SUB)/DIV
      WRITE(6,100) LAB,FS(2,1),(OUT(I),I=2,NP3),FS(2,NP3),DIV
      NY=NY+1
      YAXES(NY)=V21
      SYMBOL(NY)=SYMBL1(NY)
      DO 1083 I=1,NP3
 1083 YPLOT(NY,I)=OUT(I)
C
      LAB=V23
      WRITE(6,100) LAB,(RHO(I),I=1,NP3)
C
 1091 CONTINUE
 9999 LAB=V24
      DIV=(U(1)-U(NP3))**2
      DO 1097 I=1,NP3
 1097 OUT(I)=F(4,I)/DIV
      WRITE(6,100) LAB,(OUT(I),I=1,NP3),DIV
      NY=NY+1
      YAXES(NY)=V24
      SYMBOL(NY)=SYMBL1(NY)
      DO 1098 I=1,NP3
 1098 YPLOT(NY,I)=OUT(I)
C
      LAB=V26
      DIV=(U(1)-U(NP3))**3/YHA
      DO 1096 I=1,NP3
 1096 OUT(I)=F(5,I)/DIV
      WRITE(6,100) LAB,(OUT(I),I=1,NP3),DIV
      NY=NY+1
      YAXES(NY)=V26
      SYMBOL(NY)=SYMBL1(NY)
      DO 1099 I=1,NP3
 1099 YPLOT(NY,I)=OUT(I)
      DITT=(FS(2,1)-FS(2,NP3))**2.
      IF(ISTEP.EQ.0) GO TO 1114
      LAB=V28
```

```
      WRITE(6,100) LAB,(US(I),I=1,NP3)
      LAB=V29
      WRITE(6,100) LAB,(ENUTDN(I),I=1,NP3)
      LAB=V30
      WRITE(6,100) LAB,(ENU(I),I=1,NP3)
      LAB=V31
      WRITE(6,100) LAB,(ENUT(I),I=1,NP3)
      LAB=V32
      DIV=(U(1)-U(NP3))**2
      DO 1071 I=1,NP3
 1071 OUT(I)=UV(I)/DIV
      WRITE(6,100) LAB,(OUT(I),I=1,NP3),DIV
      IF(MODEL.NE.4) GO TO 1120
      LAB=V33
      DO 1100 I=1,NP3
1100  OUT(I)=VV(I)/DIV
      WRITE (6,100) LAB,(OUT(I), I=1,NP3),DIV
      LAB=V34
      WRITE(6,100)LAB,(DIFTT(I),I=1,NP3)
      LAB=V35
      WRITE(6,100)LAB,(DIST(I),I=1,NP3),DIVT
      DIUT=U(1)*(FS(2,1)-FS(2,NP3))
      LAB=V36
      DO 1105 I=1,NP3
1105  OUT(I)=UT(I)/DIUT
      WRITE(6,100)LAB,(OUT(I),I=1,NP3),DIUT
      LAB=V37
      DO 1110 I=1,NP3
1110  OUT(I)=VT(I)/DIUT
      WRITE(6,100)LAB,(OUT(I);I=1,NP3),DIUT
      LAB=V38
      WRITE(6,100)LAB,(PKDEP(I),I=1,NP3)
      LAB=V39
      WRITE(6,100)LAB,(PTDET(I),I=1,NP3)
      LAB=V40
      WRITE(6,100) LAB,(CDFN(I),I=1,NP3)
      LAB=V41
      WRITE(6,100) LAB,(CVFN(I),I=1,NP3)
      LAB=V42
      DO 1115 I=1,NP3
 1115 OUT(I)=TT(I)/DITT
      WRITE(6,100)LAB,(OUT(I),I=1,NP3),DITT
 1114 LAB=V43
      DO 1111 I=1,NP3
 1111 OUT(I)=F(6,I)/DITT
      WRITE(6,100)LAB, (OUT(I),I=1,NP3),DITT
       IF(ISTEP.EQ.0) GO TO 110
      NY=NY+1
      YAXES(NY)=V44
      SYMBOL(NY)=SYMBL1(NY)
      DO 1113 I=1,NP3
```

```
 1113 YPLOT(NY,I)=OUT(I)
 1120 CONTINUE
      LAB=V46
      WRITE(6,100) LAB,(DUDDY(I),I=1,NP3)
      LAB=V47
      WRITE(6,100) LAB,(DTDDY(I),I=1,NP3)
      LAB=V48
      WRITE(6,100) LAB,(CONK(I),I=1,NP3)
      LAB=V49
      WRITE(6,100) LAB,(DIFK(I),I=1,NP3)
      LAB=V50
      WRITE(6,100) LAB,(PROK(I),I=1,NP3)
      LAB=V51
      WRITE(6,100) LAB,(BUPROK(I),I=1,NP3)
      LAB=V52
      WRITE(6,100)LAB,(PREF(6,I),I=1,NP3)
      LAB=V53
      WRITE(6,100)LAB,(PREF(5,I),I=1,NP3)
      LAB=V54
      WRITE(6,100) LAB,(PREF(4,I),I=1,NP3)
      LAB=V55
      WRITE(6,100) LAB,(PREF(1,I),I=1,NP3)
C
 1009 CONTINUE
      IF(IPRINT.EQ.2) GO TO 110
       IF(ISTEP.EQ.0) GO TO 110
      WRITE(6,1070) XU,ISTEP,KRAD,FRNOS,DYHALO,DYHATL
 1070 FORMAT('PLOT AT XU=',E9.3,1X,'ISTEP=',I5,1X,'KRAD=',I5,1X,
     1 'FRNOS=',E9.3,1X,'DYHALO=',E9.3,1X,'DYHATL=',E9.3/)
      CALL PLOTS(XPLOT,43,NP3,XAXIS,YPLOT,10,NY,YAXES,SYMBOL)
         NPLOT2=2
      IF(NPLOT2.NE.1) GO TO 110
      NY=1
      YAXES(NY)=V32
      SYMBOL(NY)=V64
      DO 1201 I=1,NP3
 1201 YPLOT(NY,I)=UV(I)
      NY=NY+1
      YAXES(NY)=V33
      SYMBOL(NY)=V65
      DO 1210 I=1,NP3
 1210 YPLOT(NY,I)=VV(I)
      NY=NY+1
      YAXES(NY)=V36
      SYMBOL(NY)=V66
      DO 1220 I=1,NP3
 1220 YPLOT(NY,I)=UT(I)
      NY=NY+1
      YAXES(NY)=V37
      LAB=V67
      DO 1230 I=1,NP3
```

```
 1230 YPLOT(NY,I)=VT(I)
      CALL PLOTS(XPLOT,43,NP3,XAXIS,YPLOT,10,NY,YAXES,SYMBOL)
C  ---------------------------------------------------------------------
CHAPTER 11  11  11  11  11  11  11  11  11  11  11  END OF MAIN LOOP
  110 IF(ISTEP.GE.LASTEP.OR.XU.GE.XULAST.OR.IFIN.NE.0) GO TO 111
      XP=XU
      SA=RMI/PEI
      SB=(RME-RMI)/PEI
      DO 113 I=1,NP3
  113 F4V(I)=F(4,I)
C
       LX=L*ILONG
       IF(ISTEP.NE.LX)GO TO 114
       L=L+1
       XLONG(L)=XU/DD
       FLONG(1,L)=(U(1)-U(NP3))
       FLONG(2,L)=(FS(2,1)-FS(2,NP3))/(TA-TD)
       FLONG(3,L)=-ALFAX
       AFDTT=DABS(F(6,1)/DITT)
       FLONG(4,L)=DSQRT(AFDTT)
       IF(NBY.EQ.0) GO TO 104
       FLONG(5,L)=FLONG(1,L)*XLONG(L)**(KRAD/3.)
       FLONG(6,L)=FLONG(2,L)*XLONG(L)**((3.+2.*KRAD)/3.)
       GO TO 105
  104  CONTINUE
       FLONG(5,L)=FLONG(1,L)*XLONG(L)**((1.+KRAD)/2.)
       FLONG(6,L)=FLONG(2,L)*XLONG(L)**((1.+KRAD)/2.)
 105  FEI(L)=FE
       FLONG(7,L)=F(4,1)/((U(1)-U(NP3))**2)
C     ----------STRIDE3----------STRIDE3----------STRIDE3-------STRIDE3
 114  CALL STRIDE(3)
      IF(IFIN) 1011,60,111
C
C     ------------------------------------------ TERMINATION
  111 WRITE(6,112) ISTEP,LASTEP,XU,XULAST,IFIN,DDYHA
  112 FORMAT(23H TERMINATED WITH ISTEP=,I5,8H LASTEP=,I5,
     1 4H XU=,1PE11.3,8H XULAST=,E11.3,6H IFIN=,I3,7H DDYHA=,E11.3)
C------   11A   ------  11A  --------   11A   ----------   11A  -----
C-----  CHAPTER  11A  OUTPUT  LONGITUDINAL  PROFILES
       NLONG=1
       IF(NLONG.EQ.0)GO TO 120
       WRITE(6,103)
       DO 115 I=1,L
 115   WRITE(6,102)I,XLONG(I),FLONG(1,I),FLONG(2,I),FLONG(3,I),FEI(I)
     1 ,FLONG(4,I),FLONG(5,I),FLONG(6,I),FLONG(7,I)
 102   FORMAT(I4,1P11E11.3)
 103   FORMAT(3X,'L',4X,'X/D',4X,'U(1)/UA',2X,'(TC-TD)/(TA-TD)',
     1  2X,'-ALFAX',3X,'FE INTGL',1X,'DSQRT(TT)/(TC-TA)',1X,'UAXIAL*X'
     2 ,1X,'TAXIAL*X',1X,'KENG')
      XAXIS=V68
      IF(L.GT.65) L=65
```

```
      IF(L .EQ. 65) GO TO 120
       DO 1310 I=1,L
 1310  XPLOT(I)=XLONG(I)
       NY=1
       DO 1330 J=1,3
      YAXES(NY)=V69
       DO 1320 I=1,L
 1320  YPLOT(NY,I)=FLONG(J,I)
 1330  NY=NY+1
      SYMBOL(1)=SYMBL2(1)
      SYMBOL(2)=SYMBL2(2)
      SYMBOL(3)=SYMBL2(3)
      SYMBOL(4)=SYMBL2(4)
      YAXES(NY)=V72
       DO 1340 I=1,L
 1340  YPLOT(NY,I)=FEI(I)
 1350  FORMAT(1H1,35H PLOT LONGITUDINAL VARIABLES AT Y=0)
         CALL PLOTS(XPLOT,65,L,XAXIS,YPLOT,10,NY,YAXES,SYMBOL)
C  ------------------------------------------------------------------
C------ CHAPTER 11B CONTROL FOR CASES CALCULATION ---------
  120 CONTINUE
 150  DO 119 I=1,NP3
      YY=Y(I)/YHA
      UU=(U(I)-U(NP3))/(U(1)-U(NP3)+1.E-30)
       WRITE(7,8888) YY,UU
 119   CONTINUE
      DO 129 I=1,NP3
      YY=Y(I)/YHA
      FF=F(4,I)/(U(1)-U(NP3))**2
C     FF=F(4,I)/(U(1)**2)
       WRITE(7,8888) YY,FF
 129  CONTINUE
      DO 139 I=1,NP3
      YY=Y(I)/YHA
      FUV=UV(I)/(U(1)-U(NP3))**2
C     FUV=UV(I)/(U(1)**2)
       WRITE(7,8888) YY,FUV
 139  CONTINUE
      DO 149 I=1,NP3
      YY=Y(I)/YHA
      FT=(FS(2,I)-FS(2,NP3))/(FS(2,1)-FS(2,NP3))
      WRITE(7,8888) YY,FT
 149  CONTINUE
      DO 159 I=1,L
      UUU=FLONG(1,I)/(DSQRT(UA*(UA-UD)))
      WRITE(7,8888) XLONG(I),UUU
 159  CONTINUE
 8888 FORMAT( 2E20.7)
       CALL EXIT
C 100 FORMAT(1H ,A8,1P11E10.3,8(/9X,11E10.3))
 100  FORMAT(//1H ,A8,1P5E14.7,8(/9X,5E14.7))
```

```
C 100 FORMAT(1H ,A8,1P11E10.3/(9X,11E10.3)/(9X,12E10.3))
  101 FORMAT(1H ,A8,11I11)
      END
      SUBROUTINE AUX
C/-------- SUBROUTINE FOR PROGRAM GENMIX 4A
      IMPLICIT DOUBLE PRECISION(A-H,O-Z)
      REAL*8 LAB
      DIMENSION YMPI(83),UAV(83),Z(83),FLAV(83),RAVE(83)
      DIMENSION DUDO(83),SC(83),SCV(83),GD(83),DS(2,43),YEDGE(6)
      COMMON/COMA/A(83),AJE(7),AJI(7),B(83),C(83),CSALFA,D(83),DPDX(83),
     1 DX,EMU(83),F(7,83),FS(5,83),IAX,IEND,IFIN,INDE(7),INDI(7),IOUT,
     2 ISTEP,ITEST,IUTRAP,JS,JSW,JV,JY,KEX,KIN,KRAD,N,ND2,NF,NOVEL,NP1,
     3 NP2,NP3,OM(83),OMD(83),P(83),PEI,PR(7),PREF(7,83),PSIE,PSII,R(83)
     4,RHO(83),RME,RMI,RU(83),SD(7,83),SU(7,83),TAUE,TAUI,U(83),XD,XU,
     5Y(83),YE,YI,ENU(83),NDEQ,BPI,BPE,DK1(83),DK2(83),EDK1(83),EDK2(83)
     6,US(83),FACTOR
      COMMON/COMB/ARRCON,EWALL,H,HFU,INERT,MASSTR,MODEL,OXDFU,PREEXP,
     1 PRESS,UBAR,AK,RE,FR,ALMG,UFAC
      COMMON/COMC/ENUT(83),ENUTDN(83),DUDY(83),DUDDY(83),DTDY(83),
     1 DTDDY(83),PROK(83),BUPROK(83),ENUPR(83),PREFI(7)
     2,CDFN(83),PKDEP(83),CVFN(83),UV(83),VV(83),UT(83),
     3 VT(83),TT(83),PTDET(83),PROT(83),DIFTT(83),SUUK(83),SUUE(83),
     1 SUUT(83),FUUK(83),FUUE(83),FUUT(83)
      COMMON/CONST/IZT,CMUF,GDM,CDIS,C1,C2,NCM,AL1,ALD,CR1,CRD,BUOY,
     1 C1T,C1K,C2K,NIB,ENULIM,NBUPRO,CT,CE1,CE2,CT1,CC1,CC2,C2T,CSP,CE
     2 ,NPKDE,NPTDE,NALG,CAXIAL,PCLINR,LINEAR,LESSON,CE3,CM2,C2TM
      COMMON/AUXL/RENO,VISMIX,RHOA,TA,COEFEP,COEFED,EPSPK,EPSDT
      DATA V1/'TEST 1'/,V2/'U'/,V3/'F(1,I)'/,V4/'F(2,I)'/,V5/'F(3,I)'/
      DATA V6,V7,V8,V9,V10/'TEST2','FS(1,I)','FS(2,I)','FS(3,I)','RHO(I)
     1  '/
      DATA V11,V12,V13,V14,V15/'TEST3','Y(I)','R(I)','RU(I)','TEST4'/
      DATA V16,V17,V18,V19,V20/'EMU(I)','OMEGA','TEST5','R1 YS','VEL'/
      DATA V21,V22,V23,V24,V25 /'TEMP','T','RHO','KENGY','K'/
      DATA V26,V27,V28,V29,V30/'DISSK','D','SU(I)','ENUTDN','ENU'/
      DATA V31,V32,V33,V34,V35/'ENUT','UV','VV','DIFTT','DIST'/
      DATA V36,V37,V38,V39,V40/'UT','VT','DKDEP','PTDET','CD FN'/
      DATA V41,V42,V43,V44,V45/'CV FN','TT-AGL','TT-DEQ','TT','E'/
      DATA V46,V47,V48,V49,V50/'DUDDY','DTDDY','CONK','DIFK','PROK'/
      DATA V51,V52,V53,V54,V55/'BUPROK','PREFTT','PREFEP'
     1,'PREF-K','PREF-T'/
C
C  SD(3,I) IS USED FOR R(I)*(Y(I+1)-Y(I-1))
C-----------------------------------
C-----  K  E  MODEL  -----------
C------- CALCULATE  V  AND  T  GRADIENT
  500 DO 550 I=2,NP2
      CDFN(I)=0.07
  550 CVFN(I)=0.47
  600 DO 601 I=2,NP1
      YMPI(I)=Y(I+1)-Y(I)
      DUPI=U(I+1)-U(I)
```

```
      DUDY(I)=DUPI/YMPI(I)
      DTDY(I)=(FS(2,I+1)-FS(2,I))/YMPI(I)
      UAV(I)=.5*(U(I)+U(I+1))
      CDFN(I)=.5*(CDFN(I+1)+CDFN(I))
  601 DUDO(I)=DUPI/OMD(I)
      DUDY(1)=0.
      DTDY(1)=0.
      DUDY(NP2)=DUDY(NP1)
      DTDY(NP2)=DTDY(NP1)
      CVFN(NP3)=CVFN(NP2)
      CDFN(NP3)=CDFN(NP2)
      DO 630 I =2,NP1
C--------CALCULATE ,K=Z(I), EPSILON=FLAV(I),RAVE=R AVERAG----
      Z(I)=.5*(F(4,I)+F(4,I+1))
      FLAV(I)=.5*(F(5,I)+F(5,I+1))
      RAVE(I)=.5*(R(I)+R(I+1))
C--------CALCULATE TURBULNT VISCOSITY
  628 ENUT(I)=0.5*(RHO(I)+RHO(I+1))*CDFN(I)*Z(I)**2/FLAV(I)
      ENUTDN(I)=1.+(2./(2.*C1T-1.+PKDAVE+CT*(PTDAVE-1.))*Z(I)
     1/FLAV(I))*(BUOY/FS(2,NP3))*(DTDY(I)/DUDY(I))*((1.-CM2)/(1.-CC2))
      IF(ENUTDN(I).GT.ENULIM) ENUTDN(I)=ENULIM
  630 ENU(I)=ENUT(I)*ENUTDN(I)
C------ CALCULATE REY. STRESS UV -------
      ENU(1)=ENU(2)
      ENU(NP2)=ENU(NP1)
      ENU(NP3)=ENU(NP2)
      ENUT(1)=ENUT(2)
      ENUT(NP2)=ENUT(NP1)
      ENUT(NP3)=ENUT(NP2)
      FLAV(1)=FLAV(2)
      FLAV(NP2)=FLAV(NP1)
      Z(1)=Z(2)
      Z(NP2)=Z(NP1)
      ENUTDN(1)=1.
      ENUTDN(NP2)=ENUTDN(NP1)
      ENUTDN(NP3)=ENUTDN(NP2)
      UV(NP3)=0.
      UV(1)=0.
      UV(NP2)=(UV(NP1)+UV(NP3))*.5
C     ---------------------------------------------------
C     2 2 2 2 2 2 2 2 2 2 2 2 2 2 2 2 2 2 2 2 2 2 2 2 2 VISCOSITIES
C     --------------------  LAMINAR VISCOSITIES FOR CELL BOUNDARIES
  200 DO 23 I=2,NP1
   23 EMU(I)=.5*(EMU(I)+EMU(I+1))
C  ---------------------------------------  TURBULENT CONTRIBUTION
      DO 20 I=2,NP1
      EMU(I)=EMU(I)+ENU(I)
   20 CONTINUE
C     ----------------  MODIFICATION OF EMU ARRAY
   29 DO 24 I=2,NP1
   24 EM U(I)=EMU(I)/(Y(I+1)-Y(I))
```

```
      IF(KRAD.EQ.0) GO TO 25
      DO 26 I=2,NP1
   26 EM U(I)=EM U(I)*.5*(R(I)+R(I+1))
   25 CONTINUE
C     ------------------------------------ INITIAL PREF S.
      DO 230 I=1,NP2
      PREF(1,I)=(1.-CC2)*C1T/CC1*ENUTDN(I)
      PREF(2,I)=1.
      PREF(3,I)=1.
      PREF(4,I)=1.0*(1-CC2)/(CSP*CC1)
      PREF(5,I)=1.0*(1-CC2)/(CE*CC1)
      PREF(6,I)=2.*ENU(I)*FLAV(I)/(CT1*(RHO(I)+RHO(I+1))*Z(I)*Z(I))
  230 PREF(7,I)=1.
      DO 231 J=1,NF
  231 PREF(J,NP3)=PREF(J,NP1)
      DO 227 I=1,NP3
  227 ENUPR(I)=ENU(I)/PREF(1,I)
C  3  3  3  3  3  3  3  3  3  3  3  3  3  3  3  3  3   SOURCES
C     ----- VELOCITY U
C------CALCULATE  SOURCE TERM IN M EQ ------
      DO 308 I=3,NP1
  308 US(I)=S D(3,I)*(DPDX(I)-BUOY*RHO(I)*(FS(2,I)-FS(2,NP3))/FS(2,NP3))
      US(2)=S D(3,2)*(DPDX(2)-BUOY*RHO(1)*(.25*(2.*FS(2,1)+
     1 FS(2,2)+FS(2,3))/FS(2,NP3)-1.))
      US(NP2)=S D(3,NP2)*(DPDX(NP2)-BUOY*RHO(NP3)*(.25*(2.*FS(2,NP3)+
     1 FS(2,NP2)+FS(2,NP1))/FS(2,NP3)-1.))
C------ TO CALCULATE SOURCE TERM FOR K AND EPS EQS ----
C------ FIRST COMPUTE VV,VT,TT,UT,UV,ETC-IN CENTRAL DIFFERENCE-----
C     ---------------------K AND EPS
  800 DO 801 I=2,NP2
      DTDDY(I)=.5*(DTDY(I)+DTDY(I-1))
  801 DUDDY(I)=.5*(DUDY(I)+DUDY(I-1))
      DTDDY(1)=0.
      DUDDY(1)=0.
      F4KIN=.5*(.5*(F(4,3)+F(4,2))+F(4,1))
      F5KIN=.5*(.5*(F(5,3)+F(5,2))+F(5,1))
      F(4,2)=F4KIN
      F6KIN=.5*(.5*(F(6,3)+F(6,2))+F(6,1))
      F(5,2)=F5KIN
      F(6,2)=F6KIN
      F(4,NP2)=0.5*(.5*(F(4,NP1)+F(4,NP2))+F(4,NP3))
      F(5,NP2)=.5*(.5*(F(5,NP1)+F(5,NP2))+F(5,NP3))
      F(6,NP2)=.5*(.5*(F(6,NP1)+F(6,NP2))+F(6,NP3))
  810 UV(1)=-.5*ENU(1)*DUDDY(1)/RHO(1)
      VISCOS=VISMIX*DSQRT(TA)/RHOA
      IF(MODEL.EQ.1) GO TO 812
      CE1=COEFEP/DSQRT(RENO)
      CE2=COEFED/DSQRT(RENO)
  812 CE3=CE1
      DO 850 I=2,NP2
      UV(I)=-.5*(ENU(I)+ENU(I-1))*DUDDY(I)/RHO(I)*1.0
```

```
      VV(I)=2.*(CC2-1.+CC1+(CM2/CC2-CC2)*BUOY*UT(I)/FS(2,NP3)
     1 /F(5,I))*F(4,I)/(3.*CC1)
      VT(I)=-2.*F(4,I)*VV(I)*DTDDY(I)/(F(5,I)*(2.*C1T
     1 +CT))
        IF(NALG.EQ.0) GO TO 820
C----TT(I) HERE IS ALG - TT   ------------
      TT(I)=-2.*F(4,I)*VT(I)*DTDDY(I)/(F(5,I)*CT)
       F(6,I)=TT(I)
 820   CONTINUE
      UT(I)=(-UV(I)*DTDDY(I)-VT(I)*DUDDY(I)*(1.+C2T)+BUOY*F(6,I)
     1 *(1.-C2TM)/FS(2,NP3))*F(4,I)/(.5*F(5,I)*(2*C1T
     2 +0.5*CT))
      PROK(I)=RHO(I)*(-UV(I)*DUDDY(I)+BUOY*UT(I)/FS(2,NP3))
      RDY=.5*R(I)*(Y(I+1)-Y(I-1))
      IF (I.EQ.2) RDY=YI*R(2)
      IF (I.EQ.NP2) RDY=YE*R(NP2)
      BUPROK(I)=RHO(I)*BUOY*UT(I)/FS(2,NP3)
      SU(4,I)=(PROK(I)-RHO(I)*1.00*F(5,I))*RDY
      PROKM=PROK(I)
      IF (LESSON.EQ.2) PROKM=RHO(I)*(-UV(I)*DUDDY(I)+BUOY*UT(I)
     1 /FS(2,NP3)*(CE3/CE1))
      FFF=DABS(F(5,I))
      IF(MODEL.EQ.1) GO TO 830
      EPSPK=RDY*DSQRT(FFF/VISCOS)*(CE1*PROKM)
      EPSDT=RDY*DSQRT(FFF/VISCOS)*(CE2*F(5,I)*RHO(I))
      GO TO 840
 830  EPSPK=RDY*FFF/F(4,I)*(CE1*PROKM)
      EPSDT=RDY*FFF*(CE2*FFF)/F(4,I)*RHO(I)
 840  SU(5,I)=EPSPK-EPSDT
      SU(5,I)=FACTOR*SU(5,I)
      PROT(I)=RHO(I)*(-2.*VT(I)*DTDDY(I))
 850  SU(6,I)=(PROT(I)-RHO(I)*CT*F(5,I)*F(6,I)/F(4,I))*RDY
      F(4,2)=2.*(2.*F4KIN-F(4,1))-F(4,3)
      F(5,2)=2.*(2.*F5KIN-F(5,1))-F(5,3)
      F(6,2)=2.*(2.*F6KIN-F(6,1))-F(6,3)
      F(6,NP2)=2.*(2.*F(6,NP2)-F(6,NP3))-F(6,NP1)
      F(5,NP2)=2.*(2.*F(5,NP2)-F(5,NP3))-F(5,NP1)
      F(4,NP2)=2.*(2.*F(4,NP2)-F(4,NP3))-F(4,NP1)
C-------------------------------------------------------------
      RETURN
  100 FORMAT(1H,A8,1P11E11.3/(9X,11E11.3))
      END
      SUBROUTINE STRIDE(ISW)
C/-------- SUBROUTINE FOR PROGRAM GENMIX 4A
C/---------------- D.B.SPALDING, IMPERIAL COLLEGE, 1972 --------------
C/ THIS SUBROUTINE PERFORMS THE SAME OPERATIONS AS THE ONE IN GENMIX4A
C  BUT MORE ECONOMICALLY. THE A,B,C ARRAYS ARE ONE-DIMENSIONAL. SOME
C  OFTEN USED FUNCTIONS OF OM ARE STORED, AND A D ARRAY SAVES
C  UNNECESSARY ARITHMETIC IN THE TDMA OPERATION.
C-------------------------------------------------------------------
      IMPLICIT DOUBLE PRECISION(A-H,O-Z)
```

```
      DIMENSION A2(7),ANP2(7),B2(7),BNP2(7),C2(7),CNP2(7),D2(7),DNP2(7),
     1 AHLPT(83),BOMT3(83),FDIFE(7),
     2 FDIFI(7),GE(7),GI(7),PBOM(83),PGOM(83),THLPT(83),TTPF(7)
      DIMENSION BOM(83),OMPOM(83)
      COMMON/COMA/A(83),AJE(7),AJI(7),B(83),C(83),CSALFA,D(83),DPDX(83),
     1 DX,EMU(83),F(7,83),FS(5,83),IAX,IEND,IFIN,INDE(7),INDI(7),IOUT,
     2 ISTEP,ITEST,IUTRAP,JS,JSW,JV,JY,KEX,KIN,KRAD,N,ND2,NF,NOVEL,NP1,
     3 NP2,NP3,OM(83),OMD(83),P(83),PEI,PR(7),PREF(7,83),PSIE,PSII,R(83)
     4,RHO(83),RME,RMI,RU(83),SD(7,83),SU(7,83),TAUE,TAUI,U(83),XD,XU,
     5Y(83),YE,YI,ENU(83),NDEQ,BPI,BPE,DK1(83),DK2(83),EDK1(83),EDK2(83)
     6,US(83),FACTOR
C
      GO TO (1000,2000,3000,4000), ISW
C
C*********************************************  S T R I D E 1  ******************
 1000 IF(ISTEP) 1003,1003,1100
 1003 OMI=.5*OM(3)
      OME=.5*(1.-OM(NP1))
      DO 1002 I=2,NP2
      BOM(I)=OM(I+1)-OM(I-1)
      BOMT3(I)=3.*BOM(I)
      OMPOM(I)=OM(I)+OM(I+1)
 1002 OMD(I)=OM(I+1)-OM(I)
      OMD(1)=BOM(2)
      BPE=1.
      BPI=1.


      Y(1)=0.
      IF(KRAD.EQ.1) GO TO 1100
      DO 1001 I=1,NP3
 1001 R(I)=1.
      R25=1.
      RN15=1.
      IF(ITEST.NE.0) WRITE(6,9010) (R(I),I=1,NP3),R25,RN15
C---------------------------  CALCULATION OF RHO*U 'S  ---------------
 1100 DO 1101 I=1,NP3
      IF(RHO(I).GT.0.) GO TO 1101
      WRITE(6,1108) RHO(I),I,RHO(1)
 1108 FORMAT(36H ********** NEGATIVE OR ZERO RHO(I)=,1PE11.3,6H AT I=,
     1 I3,6X,21HSET TO ABS OF RHO(1)=,E11.3,17H ******** STRIDE1)
      RHO(I)=DABS(RHO(1))
 1101 RU(I)=RHO(I)*U(I)
      RU3=RU(3)
      RUN1=RU(NP1)
      DO 1102 I=2,NP1
 1102 RU(I)=.5*(RU(I)+RU(I+1))
      IF(ITEST.NE.0) WRITE(6,9010) (RU(I),I=1,NP3),RUN1,RU3,PEI
C---------------------------  CALCULATION OF Y 'S AND R 'S  ----------
C  ---------------------------------------  Y'S FOR PLANE GEOMETRY
      YI=PEI*OMI/(BPI*RU(2))
```

```
      Y(3)=YI+PEI*OM(3)/(RU(2)+RU3)
      Y(2)=2.*YI-Y(3)
      DO 1103 I=4,NP1
 1103 Y(I)=Y(I-1)+PEI*OMD(I-1)/RU(I-1)
      YN15=Y(NP1)+PEI*OMD(NP1)/(RU(NP1)+RUN1)
      YE=PEI*OME/(BPE*RU(NP1))
      Y(NP3)=YN15+YE
      Y(NP2)=2.*YN15-Y(NP1)
      IF(KRAD.EQ.0) RETURN
C  ----------------------  Y'S AND R'S FOR AXISYMMETRICAL GEOMETRY
      IF(CSALFA.EQ.0.) GO TO 1110
C  ---------------------------------------  CSALFA NE ZERO
      COSD2=.5*CSALFA
      IF(R(1).NE.0.) GO TO 1105
C---------------------------------------  R(1)=0.
      DO 1106 I=2,NP3
      Y(I)=DSQRT(DABS(Y(I)/COSD2))
 1106 R(I)=Y(I)*CSALFA
      YI=DSQRT(DABS(YI/COSD2))
      YN15=DSQRT(DABS(YN15/COSD2))
      GO TO 1107
C  ---------------------------------------   R(1) NE 0.
 1105 R1D2=.5*R(1)
      R1D2SQ=R1D2*R1D2
      DO 1104 I=2,NP3
      Y(I)=Y(I)/(R1D2+DSQRT(DABS(R1D2SQ+COSD2*Y(I))))
 1104 R(I)=R(1)+Y(I)*CSALFA
      YI=YI/(R1D2+DSQRT(DABS(R1D2SQ+COSD2*YI)))
      YN15=YN15/(R1D2+DSQRT(DABS(R1D2SQ+COSD2*YN15)))
 1107 R25=R(1)+YI*CSALFA
      RN15=R(1)+YN15*CSALFA
      YE=Y(NP3)-YN15
      RETURN
C  ---------------------------------------  CSALFA EQ ZERO
 1110 DO 1111 I=2,NP3
      Y(I)=Y(I)/R(1)
 1111 R(I)=R(1)
      YI=YI/R(1)
      YN15=YN15/R(1)
      R25=R(1)
      RN15=R(1)
      YE=Y(NP3)-YN15
      RETURN
C*****************************************  S T R I D E 2  ****************
C  ----------------------------  PRELIMINARIES FOR COEFFICIENTS
 2000 PX=PEI/DX
      PD8=.125*PX
      PD4=PD8+PD8
      G=RMI-RME
      ARMI=DABS(RMI)
      ARME=DABS(RME)
```

```
      GD4=.25*G
      PG=PX+G
      PGD8=.125*PG
      PGD4=PGD8+PGD8
      RMID2=.5*RMI
      DO 2004 I=2,NP2
      PBOM(I)=PX*BOM(I)
 2004 PGOM(I)=PGD4*OMD(I)
      P4OMP=PD4*BOM(2)
C  ---------------------------------------  GRID POINT 2
C---------------------------------------  TAUI, BPI, T1
      T1=0.
      IF(KRAD.EQ.0) BPI=.33333+.66667*RU(1)/RU(2)
      IF(KRAD.EQ.1) BPI=(R(1)*(5.*RU(1)+RU(2))+3.*R25*
     1                        (RU(1)+RU(2)))/6./(R(1)+R25)/RU(2)
C  ---------------------  BOUNDARY COEFFICIENTS FOR VELOCITY
 2002 HLP=RMID2-GD4*OMPOM(2)
      AHLP=DABS(HLP)
      THLP=HLP+HLP
      THLPT(2)=THLP
      TP=EM U(2)
      TTP=TP+AHLP+DABS(TP-AHLP)
      A(2)=TTP-THLP-T1-PGOM(2)
      B(2)=2.*T1+RMI+ARMI
      C(2)=P4OMP*(3.*U(2)+U(3))-US(2)
      D(2)=A(2)+B(2)+PBOM(2)
C  ------------------------------  BOUNDARY COEFFICIENTS FOR F'S
      IF(NF.EQ.0) GO TO 2304
      DO 2300 J=1,NF
      IF(J.GE.NDEQ+1.AND.J.LT.4) GO TO 2300
      TPF2=TP/PREF(J,2)
      TTPF(J)=TPF2+AHLP+DABS(TPF2-AHLP)
      T1F=0.
      FDIFI(J)=0.
 2302 A2(J)=TTPF(J)-THLP-T1F-PGOM(2)+.5*SD(J,2)
      B2(J)=2.*T1F+RMI+ARMI
      SIMP=0.
      IF(J.EQ.5) SIMP=SU(5,2)*(1.-FACTOR)/FACTOR
      D2(J)=A2(J)+B2(J)+PBOM(2)-2.*SD(J,2)-SIMP
      T=-T1F*FDIFI(J)
      TT=3.*F(J,2)+F(J,3)
      C2(J)=P4OMP*TT+2.*(T+SU(J,2))
      IF(J.EQ.5)C2(J)=P4OMP*TT+2.*(T+SU(J,2))
 2300 CONTINUE
C  ---------------------------------------  GRID POINT NP2
C---------------------------------------  TAUE, BPE, TNP3
 2304 TNP3=0.
      IF(KRAD.EQ.0) BPE=.33333+.66667*RU(NP3)/RU(NP1)
      IF(KRAD.EQ.1) BPE=(R(NP3)*(5.*RU(NP3)+RU(NP1))+3.*RN15*
     1            (RU(NP3)+RU(NP1)))/6./(R(NP3)+ RN15)/RU(NP1)
C  -------------------  BOUNDARY COEFFICIENTS FOR VELOCITY
```

```
 2310 HLM=RMID2-GD4*OMPOM(NP1)
      AHLM=DABS(HLM)
      THLM=HLM+HLM
      TM=EM U(NP1)
      TTM=TM+AHLM+DABS(TM-AHLM)
      P4OMM=PD4*BOM(NP2)
      A(NP2)=2.*TNP3-RME+ARME
      B(NP2)=TTM+THLM-TNP3-PGOM(NP1)
      C(NP2)=P4OMM*(3.*U(NP2)+U(NP1))-US(NP2)
      D(NP2)=A(NP2)+B(NP2)+PBOM(NP2)
      IF(NF.EQ.0) RETURN
C  ---------------------  BOUNDARY COEFFICIENTS FOR F'S
      DO 2320 J=1,NF
      IF(J.GE.NDEQ+1.AND.J.LT.4) GO TO 2320
      TMF=TM/PREF(J,NP1)
      TTMF=TMF+AHLM+DABS(TMF-AHLM)
      TNP3F=0.
      FDIFE(J)=0.
 2312 ANP2(J)=2.*TNP3F-RME+ARME
      BNP2(J)=TTMF+THLM-TNP3F-PGOM(NP1)+.5*SD(J,NP2)
      SIMP=0.
      IF(J.EQ.5) SIMP=SU(5,NP2)*(1.-FACTOR)/FACTOR
      DNP2(J)=ANP2(J)+BNP2(J)+PBOM(NP2)-2.*SD(J,NP2)-SIMP
      T=-TNP3F*FDIFE(J)
      TT=3.*F(J,NP2)+F(J,NP1)
      CNP2(J)=P4OMM*TT+2.*(T+SU(J,NP2))
      IF(J.EQ.5) CNP2(J)=P4OMM*TT+2.*(T+SU(J,NP2))
 2320 CONTINUE
      RETURN
C*****************************************  S T R I D E 3  ****************
 3000 DO 3005 I=3,NP1
      THLM=THLP
      HLP=RMID2-GD4*OMPOM(I)
      THLP=HLP+HLP
      THLPT(I)=THLP
      AHLP=DABS(HLP)
      AHLPT(I)=AHLP
      TTM=TTP
      TP=EM U(I)
      TTP=TP+AHLP+DABS(TP-AHLP)
      A(I)=TTP-THLP-PGOM(I)
      B(I)=TTM+THLM-PGOM(I-1)
      C(I)=PD4*(BOMT3(I)*U(I)+OMD(I)*U(I+1)+OMD(I-1)*U(I-1))-US(I)
      D(I)=A(I)+B(I)+PBOM(I)
      D(I)=A(I)+B(I)+PBOM(I)
 3005 CONTINUE
C---------------------------                          -----------------
      IF(KIN.EQ.2.AND.RU(1).NE.0.) U(1)=U(1)-DPDX(1)*DX/RU(1)
      IF(KEX.EQ.2.AND.RU(NP3).NE.0.) U(NP3)=U(NP3)-DPDX(NP3)*DX/RU(NP3)
C---------------------------  SOLVE FOR DOWNSTREAM U 'S  -------------
      B(2)=(B(2)*U(1)+C(2))/D(2)
```

```
      A(2)=A(2)/D(2)
      DO 3048 I=3,NP2
      T=D(I)-B(I)*A(I-1)
      A(I)=A(I)/T
 3048 B(I)=(B(I)*B(I-1)+C(I))/T
      DO 3050 IDASH=2,NP2
      I=N+4-IDASH
      U(I)=A(I)*U(I+1)+B(I)
 3050 CONTINUE
C     ------------------------------------------------
      IF(KIN.EQ.3) U(1)=.5*(U(2)+U(3))
      IF(KEX.EQ.3)U(NP3)=.5*(U(NP1)+U(NP2))
C     ------------------------------------------
 3013 IF(NF) 3060,3060,3014
 3014 DO 3320 J=1,NF
      IF(J.GE.NDEQ+1.AND.J.LT.4) GO TO 3320
C---------------------------   SOLVE FOR DOWNSTREAM F 'S  ------------
      A(2)=A2(J)
      B(2)=B2(J)
      C(2)=C2(J)
      D(2)=D2(J)
      A(NP2)=ANP2(J)
      B(NP2)=BNP2(J)
      C(NP2)=CNP2(J)
      D(NP2)=DNP2(J)
      DO 3002 I=3,NP1
      TTMF=TTPF(J)
      TPF=EM U(I)/PREF(J,I)
      TTPF(J)=TPF+AHLPT(I)+DABS(TPF-AHLPT(I))
      A(I)=TTPF(J)-THLPT(I)-PGOM(I)
      B(I)=TTMF+THLPT(I-1)-PGOM(I-1)
      C(I)=PD4*(BOMT3(I)*F(J,I)+OMD(I)*F(J,I+1)+OMD(I-1)*F(J,I-1))+
     1                                                    2.*SU(J,I)
      SIMP=0.
      IF(J.EQ.5) SIMP=SU(5,I)*(1.-FACTOR)/FACTOR
 3002 D(I)=A(I)+B(I)+PBOM(I)-2.*SD(J,I)-SIMP
C     ----------------------------------------
      B(2)=(B(2)*F(J,1)+C(2))/D(2)
      A(2)=A(2)/D(2)
      DO 3148 I=3,NP2
      T=D(I)-B(I)*A(I-1)
      A(I)=A(I)/T
 3148 B(I)=(B(I)*B(I-1)+C(I))/T
      DO 3150 IDASH=2,NP2
      I=N+4-IDASH
 3150 F(J,I)=A(I)*F(J,I+1)+B(I)
C---------------------------  ADJUST F(J,1) AND F(J,NP3)  ------------
      GO TO (3220,3220,3230),KIN
 3230 F(J,1)=.5*(F(J,2)+F(J,3))
 3220 GO TO (3320,3320,3330),KEX
 3330 F(J,NP3)=.5*(F(J,NP1)+F(J,NP2))
```

```
 3320 CONTINUE
C     ----------------------------------------
 3060 XU=XD
C     ITEST=0
      PSII=PSII-RMI*DX
      PSIE=PSIE-RME*DX
      PEI=PSIE-PSII
      ISTEP=ISTEP+1
      RETURN
C********************************  S T R I D E 4  ********************************
 4000 CONTINUE
      ND2=N/2
      NP1=N+1
      NP2=N+2
      NP3=N+3
      OM(1)=0.
      OM(2)=0.
      OM(NP3)=1.
      ISTEP=0
      IEND=10000
      IAX=10000
      IOUT=10000
      DX=1.E-30
      IFIN=0
      DO 4001 J=1,7
      DO 4001 I=1,NP3
      SU(J,I)=0.
 4001 SD(J,I)=0.
      RETURN
 9010 FORMAT(1H ,1P11E11.3)
      END
      SUBROUTINE PLOTS (X,IDIM,IMAX,XAXIS,Y,JDIM,JMAX,YAXES,SYMBOL)
C*****14.8.72*************************************************************************
C                                                                                     *
C  SUBROUTINE FOR PLOTTING J CURVES OF Y(J,I) AGAINST X(I).
C                                                                                     *
C  X AND Y ARE ASSUMED TO BE IN ANY RANGE EXCEPT THAT NEGATIVE VALUES  *
C   ARE PLOTTED AS ZERO.                                                              *
C  X AND Y ARE SCALED TO THE RANGE 0. TO 1. BY DIVISION BY THE MAXIMA, *
C   WHICH ARE ALSO PRINTED.                                                           *
C  IDIM IS THE VARIABLE DIMENSION FOR X.                                              *
C  IMAX IS THE NUMBER OF X VALUES.                                                    *
C  XAXIS STORES THE NAME OF THE X-AXIS.                                               *
C  JDIM IS THE VARIABLE DIMENSION FOR Y.                                              *
C  JMAX IS THE NUMBER OF CURVES TO BE PLOTTED, (UP TO 10).                            *
C  THE ARRAY YAXES(J) STORES THE NAMES OF THE CURVES.                                 *
C  THE ARRAY SYMBOL(J) STORES THE SINGLE CHARACTERS USED FOR PLOTTING. *
C                                                                                     *
C*************************************************************************************
      IMPLICIT DOUBLE PRECISION (A-H,O-Z)
      DIMENSION X(IDIM),Y(JDIM,IDIM),YAXES(JDIM),SYMBOL(JDIM),
```

```
     1 A(101),YMAX(20)
       DATA  DOT,CROSS,BLANK/1H.,1H+,1H /
C******  SCALING X ARRAY TO THE RANGE 0 TO 50
       XMAX=1.E-30
       DO 1 I=1,IMAX
     1 IF(X(I).GT.XMAX) XMAX=X(I)
       DO 2 I=1,IMAX
       X(I)=X(I)/XMAX*50.
     2 IF(X(I).LT.0.) X(I)=0.
C******  SCALING Y ARRAY TO THE RANGE 0 TO 100
       DO 3 J=1,JMAX
       YMAX(J)=1.E-30
       DO 4 I=1,IMAX
     4 IF(Y(J,I).GT.YMAX(J)) YMAX(J)=Y(J,I)
       DO 3 I=1,IMAX
       Y(J,I)=Y(J,I)/YMAX(J)*100.
     3 IF(Y(J,I).LT.0.) Y(J,I)=0.
C******  IDENTIFYING THE VARIOUS CURVES TO BE PLOTTED
       WRITE(6,103) XAXIS,XMAX
       WRITE(6,100) (YAXES(I),I=1,JMAX)
       WRITE(6,106) (SYMBOL(I),I=1,JMAX)
       WRITE(6,102) (YMAX(I),I=1,JMAX)
       DO 5 I=1,11
     5 A(I)=0.1*FLOAT(I-1)
       WRITE(6,101) (A(I),I=1,11)
C******  MAIN LOOP.  EACH PASS PRODUCES AN X-CONSTANT LINE.
       DO 40 I=1,51
       IF(I.EQ.1.OR.I.EQ.51) GO TO 32
       GO TO 33
C******  ALLOCATE . OR + AS MARKER ON THE Y-AXIS
    32 DO 30 K=1,101
    30 A(K)=DOT
       DO 31 K=11,101,10
    31 A(K)=CROSS
C******  ALLOCATE . OR + MARK ON THE X-AXIS, ALSO THE APPROPRIATE X VALUE
    33 A(1)=DOT
       A(101)=DOT
       K=I-1
    46 K=K-5
       IF(K)48,47,46
    47 A(1)=CROSS
       A(101)=CROSS
    48 XL=0.02*FLOAT(I-1)
C******  CHECK IF ANY Y( X(I) ) VALUE LIES ON THIS X-CONSTANT LINE
C******  IF YES GO TO 41, OTHERWISE GO TO 42
       DO 43 K=1,IMAX
       IF(IFIX(X(K)+1.5)-I) 43,41,43
C******  LOCATE  Y(  X(I)  )
    41 DO 44 J=1,JMAX
       NY=Y(J,K)+1.5
       A(NY)=SYMBOL(J)
```

```
   44 CONTINUE
      GO TO 42
   43 CONTINUE
C******  PRINT X-CONSTANT LINE
   42 WRITE(6,105) XL,(A(K),K=1,101),XL
C******  PUTTING BLANKS INTO X-CONSTANT LINE
      DO 49 K=1,101
   49 A(K)=BLANK
   40 CONTINUE
      DO 50 I=1,11
   50 A(I)=.1*FLOAT(I-1)
      WRITE(6,104) (A(I),I=1,11)
      RETURN
  100 FORMAT(11H Y-AXES ARE,5X,10(1X,A10))
  101 FORMAT(1H0,2X,11F10.1)
  102 FORMAT(15H MAXIMUM VALUES,1P10E11.3)
  103 FORMAT(11H0X-AXIS IS ,A8,17H ,MAXIMUM VALUE =,1PE10.3)
  104 FORMAT(3X,11F10.1/1H1)
  105 FORMAT(2H X,F6.2,3X,101A1,F6.2)
  106 FORMAT(7H SYMBOL,11X,10(1X,A10))
      END
```

REFERENCES

1. Reynolds,O.,'On the dynamical theory of incompressible viscous fluids and the determination of the criterion', Phil. Trans. R. Soc.,186,123-164,1895.

2. Phillips,O.M.,'The dynamics of the upper ocean', Cambridge University Press, Cambridge, England,1969.

3. Prandtl,L.,'Bericht uber Untersuchungen zue ausgebildeten Turbulenz',Z. Angew. Math. Mech.,5,136-139,1925.

4. Rodi,W.,'The prediction of free turbulent boundary layers by use of a two-equation model of turbulence',Ph.D. thesis, University of London,1972.

5. Von Karman,T.H.,'Mechanische Ahnilichkeit und Turbulenz',Proc. 3rd Int. Congress Appl. Mech.,Stokholm, pt. 1,pp 85,1930.

6. Clauser,F.H.,'The turbulent boundary layer',Adv. in App. Mech. IV,pt. 1,New York,Academic Press,1956.

7. Chou,P.Y.,'On velocity correlations and solution of the equations of turbulent fluctuations',Quart.Appl.Math., 3,pg 38,1945.

8. Rotta,J.C.,'Statistische Theorie nichthomogeners Turbulenz',(English translation), Imperial College,Dept. of Mech. Engg. Reports TWF/TN/38-39,1968.

9. Bradshaw,P.,Ferriss,D.H., and Atwell,N.P.,'Calculation of boundary-layer development using the turbulent energy equation',JFM,28,pp 593-616,1967.

10. Kolmogorov,A.N.,'Equations of turbulent motion in an incompressible fluid',(English translation), Imperial College,Mech. Engg. Report ON/6,1968.

11. Jones,W.P. and Launder,B.E.,'The prediction of Laminarization with a two-equation model of turbulence',Int. J. Heat and Mass Transfer,15,pp 301,1972.

12. Hinze,J.O.,'Turbulence: An introduction to its mechanism and theory',McGraw-Hill,New York,1975.

13. Frieche,C.A., van Atta,C.W. and Gibson,C.H.,AGARD Conference Proceedings, 93, 18.1, 1971.

14. Driscoll,R.J. and Kennedy,L.A., 'A model for the turbulent energy spectrum', Phys. Fluids, 26(5), pp 1228-1233, 1983.

15. Tenekes,H. and Lumley,J.L.,'A first course in turbulence',MIT Press,Cambridge,pg 270,1972.

16. Hanjalic,K.,Launder,B.E., and Schiestel,R.,'Multiple-time scale concepts in turbulence transport modelling', Turbulent Shear Flow 2,Springer-Verlag,Berlin,pp. 36-49, 1979.

17. Lumley,J.,'Prediction methods for turbulent flows',von Karman Institute for Fluid Dynamics, Lecture series 76,March 1975.

18. Chen,C.J.,'Prediction of turbulent flows', Central Research Institute of Electric Power Industry,Japan,1984.

19. Launder,B.E.,Reece,G.J. and Rodi,W.,'Progress in the development of a Reynolds stress turbulence closure',JFM,68,pp 537-566,1975.

20. Launder,B.E.,'On the effects of a gravitational field on the turbulent transport of heat and momentum',JFM,67,pp. 569-581,1975.

21. Uberoi,M.S., 'Energy transfer in isotropic turbulence', Physics of Fluids, vol 6, p.1048, 1963.

22. Webster,C.A.G., 'An experimental study of turbulence in a density stratified shear flow', JFM, 19, pp.221-245, 1964.

23. Chen,C.J. and Nikitopoulos,C., 'On the near field characteristics of axisymmetric turbulent buoyant jets in a uniform environment',Int. J. Heat Mass transfer,22, no. 1, pp.1-10,1979.

24. Gibson,C.H. and Schwarz,W.H.'The universal equilibrium spectra of turbulent velocity and scalar fields',JFM,16,pp. 365-384,1963.

25. Bradbury,L.J.S.,'The structure of self preserving plane jet',JFM,23,pp.31-64,1965.

26. Heskestad,G.,'Hot wire measurements in a plane turbulent jet',J. of App. Mech.,p.1, Dec. 1965.

27. Patel,R.P.,'A study of two-dimensional symmetric and asymmetric turbulent shear flows',Ph.D. thesis,McGill University,1970.

28. Gutmark,E.,'The two-dimensional turbulent jet', M.Sc. thesis,Technion-Israel Institute of Technology,Israel,1970.

29. Robins,A.,'The structure and development of a plane turbulent free jet',Ph.D. thesis, University of London,England,1971.

30. Bradbury,L.J.S. and Riley,J.,'The spread of a turbulent plane jet issuing into a parallel moving air stream', JFM,27,pp. 381-394,1967.

31. Vander Hegge Zijnen,B.G.,'Measurements of the velocity distribution in a plane turbulent jet of air', Appl. Sci. Res., Section A, 7, pp 256-276, 1958.

32. Hetsroni,G. and Sokolov,M.'Distribution of mass,velocity and intensity of turbulence in a two-phase turbulent jet',Trans. ASME, J. of App. Mech.,38,pp.314-327,1971.

33. Wygnanski,I. and Fiedler,H.E.,'Some measurements in the self preserving jet',JFM, 38,pp.577-612,1969.

34. Shearer,A.J. and Faeth,G.M.'Evaluation of a locally homogeneous model of spray evaporation', NASA Contract Report 3198,Oct. 1979.

35. Corsin,S. and Uberoi,M.S., 'Further experiments on the flow and heat transfer in a heated turbulent air jet', NACA Rept. No. 998, 1950.

36. Chevray,R. and Kovasznay,L.S.G.,'Turbulence measurements in the wake of a thin flat plate', AIAA,7,pp.1641-1642,1969.

37. Patel,V.C. and Scheuerer,G.,'Calculation of two-dimensional near and far wakes',AIAA,20, pp.901-907,1982.

38. Andreopoulos,J.,'Symmetric and Asymmetric near wake of a flat plate',JFM,100,pp.639-668, 1980.

39. Pot,P.J.,'measurements in a 2D wake and in a 2D wake merging into a boundary layer', Data report,NLR TR-19063 U,1979.

40. Ramaprian,B.R.,Patel,V.C. and Sastry,M.S.,'Turbulent wake development behind streamlined bodies', Iowa Institute of Hydraulic Research,Iowa City, IIHR rept. 231,1981.

41. Wygnanski,I. and Fiedler,H.E.,'The two-dimensional mixing region',JFM,41,pp.327-363,1970.

42. Liepman,H.P. and Laufer,J.,'Investigations of free turbulent mixing',NACA TN 1257,1947.

43. Sunyach,M. and Mathiew,J.,'Zone de melange d'un jet plan; fluctuations induities dans le cone a potential -- intermittence',Int. J. Heat Mass Transfer,12,pp. 1679-1697, 1969.

44. Sami,S.,Carmody,T. and Rouse,H.,'Jet diffusion in the region of flow establishment',JFM,27,pp. 231-252,1967.

45. Bradshaw,P.,Ferriss,D.H. and Johnson,R.F.,'Turbulence in the noise-producing region of a circular jet',JFM,19, pp. 591-624,1964.

46. Birch,S.,'Planar mixing layer',1980-81 AFORS-HTTM Stanford Conference on Complex Turbulent Flows, pp. 170-177,1980.

47. Husain,Z.D. and Hussain,A.K.M.F., 'Axisymmetric mixing layer: influence of the initial and boundary conditions', AIAA J., vol 17, no. 1, pp.48-55, 1979.

48. Hill,P.G.,'Turbulent jets in ducted streams',JFM,22, pp. 161,1965.

49. Antonio,R.A. and Bilger,R.W.,'An experimental investigation of an axisymmetric jet in a co-flowing air stream',JFM,61,pp. 805-822,1973.

50. Chen,C.J. and Rodi,W.,'Vertical turbulent buoyant jets; A review of experimental data',vol 4,Pergamon Press,1976.

51. Rouse,H.,Yih,C.S. and Humphreys,H.W.,'Gravitational Convection from a Boundary Source', Tellus, vol 4, pp. 201-210, 1952.

52. Ramaprian,B.R. and Chandrasekhara,'Study of vertical plane turbulent jets and plumes', Iowa Institute of Hydraulic Research, IIHR Report No. 257,Univ. of Iowa,Iowa City,1984.

53. Kotsovinos,N.E.,'A study of the entrainment and turbulence in a plane buoyant jet',Ph.D. theisi, California Institute of Technology,Pasadena,1975.

54. George,W.K.,Alpert,R.L. and Tamanini,F.,'Turbulence measurements in an axisymmetric buoyant plume',Int. J. Heat Mass Transfer,vol. 20,pp. 1145-1154,1977.

55. Patankar.S.V., 'Numerical heat transfer and Fluid flow', Hemisphere Publishing Corporation, Washington, 1975.

56. Chen,C.J. and Chen,C.H.,'On the prediction and unified correlation for the decay of vertical buoyant jets', J. of Heat Transfer,vol. 101,no.3, pp. 532-537, 1979.

57. Pope,S.B.,'An explanation of the turbulent round jet/plane jet anamoly', Rep. No. FS/77/12, Imperial college,London,1977.

58. Morse,A.P.,'Axisymmetric turbulent shear flows with and without swirl', Ph.D. Thesis,London Univ.,England, 1977.

59. McGuirk,J.J. and Rodi,W. 'The calculation of three dimensional free jets', Symposium on Turbulent Shear Flows, Pennsylvania State Univ., April 1977.

60. Eaton,J.K and Johnston,J.P., 'Backward facing step flow', 1980-81 AFORS-HTTM Stanford Conference on Complex Turbulent Flows, pp.275-278, 1980.

61. Stevenson,W.H.,Thompson,H.D. and Craig,R.C., 'Laser velocimeter measurements in highly turbulent recirculating flows', Engg. Applications of Laser velocimetry, ASME, pp. 163-170, 1982.

62. Chen,C.J.,Naseri-Neshat,H. and Li,P. 'The Finite Analytic Method', Iowa Institute of Hydraulic Research, IIHR report 232, University of Iowa, Iowa City, 1980.

63. Chen,C.J. and Chen,H.C., 'Finite analytic numerical method for unsteady two-dimensional Navier-Stokes equations', J. of Computational Physics, vol 53, no. 2, pp.209-226, February 1984.

64. Sheikholeslami,M.Z., 'Finite analytic solution of turbulent two-dimensional Navier-Stokes equations in Internal flows', Ph.D. thesis, Department of Mechanical Engineering, University of Iowa, Iowa City, 1985.

65. Durst,F. and Rastogi,A.K., 'Theoretical and experimental investigations of turbulent flows with separation', Turbulent Shear Flows I, pp. 208-219, 1977.